Advances in Polymer Science 250

Wim H. de Jeu *Editor*

Liquid Crystal Elastomers: Materials and Applications

Springer

250
Advances in Polymer Science

For further volumes:
http://www.springer.com/series/12

Aims and Scope

The series presents critical reviews of the present and future trends in polymer and biopolymer science including chemistry, physical chemistry, physics and material science. It is addressed to all scientists at universities and in industry who wish to keep abreast of advances in the topics covered.

Review articles for the topical volumes are invited by the volume editors. As a rule, single contributions are also specially commissioned. The editors and publishers will, however, always be pleased to receive suggestions and supplementary information. Papers are accepted for *Advances in Polymer Science* in English.

In references *Advances in Polymer Sciences* is abbreviated as *Adv Polym Sci* and is cited as a journal.

Special volumes are edited by well known guest editors who invite reputed authors for the review articles in their volumes.

Impact Factor in 2010: 6.723; Section “Polymer Science”: Rank 3 of 79

Wim H. de Jeu
Editor

Liquid Crystal Elastomers: Materials and Applications

With contributions by

M. Brehmer · F. Brömmel · G. Cordoyiannis · W.H. de Jeu · H. Finkelmann · D. Kramer · Z. Kutnjak · A. Lebar · C. Ohm · B.I. Ostrovskii · P. Palffy-Muhoray · K. Urayama · B. Zalar · R. Zentel

Springer

Editor
Wim H. de Jeu
DWI at RWTH Aachen University
Aachen
Germany

ISSN 0065-3195 ISSN 1436-5030 (electronic)
ISBN 978-3-642-31581-7 ISBN 978-3-642-31582-4 (eBook)
DOI 10.1007/978-3-642-31582-4
Springer Heidelberg New York Dordrecht London

Library Control Congress Number: 2012943862

Printed on acid-free paper

Springer is part of Springer Science+Business Media (www.springer.com)

Preface

The quest for responsive materials with the ability to mimic living systems is one of the major challenges for future polymeric materials. This requires a high level of mobility combined with shape retention. Both properties can be found in liquid-crystalline (LC) elastomers, in which crosslinks keep the shape and the liquid state guarantees mobility. These remarkable materials consist of polymeric liquid crystals in which mesogenic molecules are attached to a polymer backbone, which —in turn—is weakly cross-linked to form the elastomer. Like in other LC systems, their phase structure as well as functionality is found in a defined temperature range. The collective molecular organisation of LC elastomers requires new chemistry and physics. In addition, these materials provide new possibilities to study fundamental aspects of ordering and phase transitions in general.

The idea of the present volume came up at the International Liquid Crystal Elastomer Conference in 2005 in Cambridge (UK), but only became concrete at the 2009 conference at Kent (OH, USA). The motivation to start this project was threefold: (1) No comprehensive overview exists of the chemistry, material properties and experimental physics of LC elastomers. Such an overview would be a welcome addition to the existing literature. (2) The field of LC elastomers could be better imbedded in polymer science in general. A volume in the series *Advances in Polymer Science* might help to promote the field in a broader context. (3) Applications are gradually evolving, and reviewing the state of the art could stimulate further developments in this direction. Though several fascinating possibilities for applications have been proposed, a "smashing" one is still missing. Yet, in combination with novel preparation techniques like lithography, ink-jet printing and microfluidics, one can imagine new possibilities for applications of LC elastomers that would be difficult to achieve otherwise.

The book attempts to cover many of the aspects mentioned above. The first two chapters have a strong background in chemistry. In the first one by Felicitas Brömmel, Dominic Kramer and Heino Finkelmann (Freiburg, Germany), the preparation of LC elastomers is discussed. It treats the synthesis of LC polymer networks, mechanical orientation behaviour and liquid single-crystal elastomers. Coming from the late Freiburg group that had such an important impact in the field,

I expect it to be very welcome. The second chapter by Christian Ohm, Martin Brehmer and Rudolf Zentel (University of Mainz, Germany) treats applications of LC elastomers, mainly from a chemical point of view. The introduction on preconditions for selecting LC elastomers is followed by sections on actuators powered by a phase transition and on LC elastomers in electric fields. The following two chapters cover applications of LC elastomers, mainly from a physical point of view. Peter Palffy-Muhoray (Kent State University, Kent, OH, USA) discusses in a complementary way the effects of LC elastomers on light and of light on LC elastomers. In the next chapter Kenji Urayama (Kyoto University, Kyoto, Japan) treats electro-opto-mechanical effects in swollen nematic elastomers, including both static and dynamic aspects. The last two chapters cover some fundamental aspects of LC elastomers. Andrija Lebar, George Cordoyinassis, Zdravko Kutnyak and Boštjan Zalar (Jožef Stefan Institute, Ljubljana, Slovenia) discuss the isotropic to nematic conversion in LC elastomers on the basis of their extensive work using differential scanning calorimetry and nuclear magnetic resonance. Finally, Wim de Jeu (at that time University of Massachusetts, Amherst, MA, USA) and Boris Ostrovskii (Institute of Crystallography, Moscow, Russia) discuss order and disorder in relation to cross-linking in LC elastomers.

Editing a volume of reviews like the present one turned out to be not an easy task. I want to thank the various authors for the constructive interaction. I am grateful to some of them for delivering their contribution so timely, and to the others for not giving up during the process.

Aachen, Germany Wim H. de Jeu
January 2012

Contents

Adv Polym Sci (2012) 250:1–48
DOI: 10.1007/12_2012_168

Published online: 3 July 2012

Preparation of Liquid Crystalline Elastomers

F. Brömmel, D. Kramer, and H. Finkelmann

Abstract The combination of rubber elasticity and anisotropic liquid crystalline order of liquid crystalline elastomers (LCEs) gives rise to exceptional physical properties, unknown for conventional solid-state materials. By selecting suitable chemistry of the liquid crystalline moieties, the liquid crystalline phase structure, and the chemistry of the macromolecular network structure, these physical properties can be optimized for specific applications like mechanics, optics, diffusional or electronic transport, etc. In this chapter we outline basic aspects to be considered when synthesizing LCEs, including some basic characterization techniques. We give an overview of the chemistry involved in synthesizing LCEs and the different techniques of chemical crosslinking developed for this purpose. The unique coupling of the polymer chain conformation and the anisotropic LC order in LCEs can be exploited to induce a macroscopic orientation of the LC phase structure by applying mechanical fields. By performing chemical crosslinking in the aligned state, the uniform macroscopic orientation can be fixed permanently. Different strategies are introduced to synthesize such liquid single-crystal elastomers (LSCEs), and illustrated by a wide range of examples. Orientation techniques based on external magnetic and electric fields or surface treatment are also included. We emphasize practical aspects and give advice for successful preparation of this fascinating class of materials. A promising future for LSCEs is expected because of their unique and as yet largely unexplored abilities to mimic living systems.

Keywords Chain conformation · Cholesteric · Elastomer · Liquid crystal · Liquid crystal polymer · Nematic · Polymer networks · Smectic

F. Brömmel (✉), D. Kramer, and H. Finkelmann
Institut für Makromolekulare Chemie, Albert-Ludwigs-Universität Freiburg, Freiburg i. Br., Germany
e-mail: felicitas.broemmel@bristol.ac.uk

Contents

Abbreviations

3D	Three-dimensional
EO	Ethylene oxide
k	Smectic layer normal
LC	Liquid crystal
LCE	Liquid crystalline elastomer
LCP	Liquid crystalline polymer
LSCE	Liquid single crystal elastomer
n	Nematic director
S_A	Smectic-A
SANS	Small-angle neutron scattering
S_C	Smectic-C
T_g	Glass transition temperature
$T_{LC,\,i}$	Clearing temperature, i.e., LC – isotropic phase transformation temperature

1 Introduction

Understanding the chemistry and physics of macromolecules is a prerequisite for the development and application of new materials in the present age of plastics. One of the major challenges will be the development of responsive materials with the ability to mimic biological systems. Such properties require a high level of mobility combined with shape retention that cannot be found in the glassy or (semi-) crystalline state of conventional polymers.

As early as 1908 Otto Lehmann [1] speculated in his article on “Scheinbar lebende Kristalle, Pseudopodien, Cilien und Muskeln” that liquid crystals might be the origin of the tension in natural muscles. However, liquid crystals are fluids and any internal or external tension is usually eliminated by flow. The same holds

for linear and branched macromolecules in the liquid crystalline state. In three-dimensional networks of macromolecules (elastomers), on the contrary, the macro-Brownian motions of the polymer chains are prevented and a form-retaining material results. Because the micro-Brownian motions of the chain segments are hardly influenced by the network structure of the polymer chains, a liquid crystalline state of order of the chain segments can exist [2].

In 1975 P.G. de Gennes recognized that the interplay between liquid crystalline order and the macromolecular network structure generates new physical properties that also resemble those of biological systems and muscles [3]. In the following years Otto Lehmann's early ideas were actually demonstrated with liquid crystalline elastomers although at that time the basic concepts of macromolecular chemistry were still unknown.

Just as for biological beings, the liquid crystalline phase structure and simultaneously the functionality of liquid crystalline elastomers are strictly limited to a defined temperature regime. Similar to low molar mass liquid crystals and LC polymers this temperature regime is determined by the chemical constitution of the polymer networks. For the synthesis and investigation of liquid crystalline elastomers the basic concepts of liquid crystals, LC polymers, and polymer networks have to be brought together.

Research on liquid crystal elastomers has attracted scientists from very different fields, such as theoretical and experimental physics, organic and physical chemistry, biology, material science, and engineering. Theories and experiments have always gone hand in hand and there are several examples where theoretical predictions have actually led to the development of new materials.

In this chapter we outline the basic aspects to be considered when working with liquid crystal elastomers (LCEs), including techniques for their synthesis and characterization. For readers new to the field – who may not have a strong background in macromolecular chemistry – we shall introduce strategies for a successful approach. We start with an introduction to the synthesis of LC polymer networks and their basic characterization (Sect. 2). Subsequently their mechanical orientation behavior will be discussed (Sect. 3). Techniques to prepare elastomers that are permanently oriented to form a single crystal are the subject of Sect. 4. Finally a brief outlook is given in Sect. 5.

2 Synthesis of LC Polymer Networks

To obtain the liquid crystalline state in a polymer network, several strategies are conceivable. They are all based on well known principles evaluated during the last few decades for linear liquid crystalline polymers. The monomer units of the network have to consist of mesogenic moieties, which are either rigid rods or discs in the case of thermotropic polymorphism or amphiphiles in the case of lyotropic polymorphism. The mesogenic units can be attached either as side chains to the monomer units yielding "side chain elastomers" (Fig. 1a, b) or directly linked

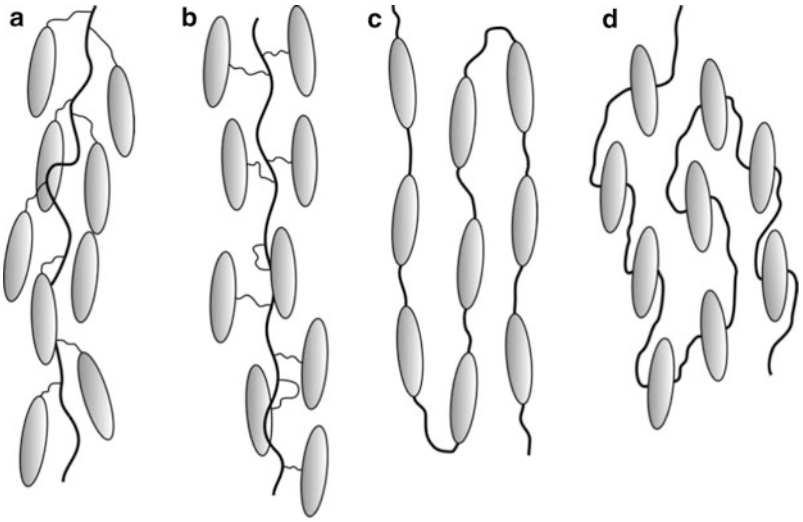

Fig. 1 Different attachment geometries for the synthesis of LCEs: side chain elastomers with end-on (**a**) or side-on (**b**) attached mesogenic side chains and main chain elastomers with mesogenic units incorporated end-on (**c**) or side-on (**d**) into the polymer main chain

together within the polymer backbone yielding "main chain elastomers" (Fig. 1c, d). An additional variation of the architecture of the network is given by connecting the mesogenic groups via different geometries, e.g., for rods via their long axis ("end-on") as shown in Fig. 1a, c or via their short axis ("side-on") (Fig. 1b, d). All these different geometries directly and specifically affect the liquid crystalline state of order and the polymorphism.

Compared to low molar mass liquid crystals having a similar chemical constitution as the monomer units of the networks, two principal tendencies have to be considered that determine the LC phase regime. First, the specific volume of the mesogenic monomers normally exceeds the specific volume of the network. This reduction of the free volume shifts the liquid crystalline phase regime of the networks towards higher temperatures and may modify the polymorphic liquid crystalline variants. The second fact concerns the translational diffusion and the degree of rotational freedom of the mesogenic monomer units incorporated into or attached to the polymer backbone. Compared to low molar mass liquid crystals, both are elementary restricted and determine the liquid crystalline state and order. While, for example, end-on side chain polymers (or elastomers) (Fig. 1a) tend towards the formation of smectic phases, the lateral linkage of the mesogenic units (Fig. 1b) often prevents long range positional ordering and favors the formation of nematic phases. Furthermore, side-on linkage directly restricts the rotation of the mesogenic unit along their long molecular axis and may convert a uniaxial nematic or smectic phase into the corresponding biaxial phase [4–9].

Bearing in mind these basic aspects, the synthesis of LCEs is straightforward and offers two strategies. The first strategy is to start the synthesis of a network

with a polymerization process of a new mesogenic monomer. Here all the factors mentioned above have to be considered and the knowledge of the liquid crystalline phase behavior of the corresponding linear polymer has to be elucidated. The consolidated findings of intensive research on linear LC polymers will help to evaluate a chemical constitution of a new monomer that successfully yields an LCE. The second strategy avoids all these problems by already starting with a linear LC polymer with known LC phase behavior. A crosslinking process – either via suitable functionalization of the linear polymer or by γ-irradiation – hardly modifies the LC phase behavior.

For the synthesis as well as for the usability of the networks the transition temperatures are most important. They determine the regime of use and hence the functionality of the LC structure. These are the liquid crystalline to isotropic phase transformation temperature $T_{LC,i}$ and the glass transition temperature T_g, where the material transfers from the glassy state into the LC state. A transformation from the LC into the crystalline phase at $T_{c,LC}$ is mainly suppressed due to the complex structure of LCEs and should be avoided as it might destroy the network.

$T_{LC,i}$ should be above the temperature-regime of interest in cases where the physical properties of the elastomers within the LC phase, such as ferroelectricity or optical properties, are to be used. If changes in the physical properties are to be exploited, such as length changes at the phase transition, $T_{LC,i}$ must be adjusted to the desired transition temperature. For polymers with discotic or calamitic mesogenic groups, the phase transition temperatures are determined by the structure of the mesogenic monomer and of the main chain. The principles of their manipulation are well known from work on linear LC polymers. Additionally $T_{LC,i}$ can be systematically modified by copolymerization with different mesogenic or non-mesogenic co-monomers.

T_g of LC elastomers is determined by the flexibility of the main chain, by interactions between the mesogens and the main chain, as well as by interactions between the mesogens. In the case of elastomers, the crosslinking density also plays an important role for the glass transition. This is rather different depending on the flexibility of the crosslinker used. If a flexible crosslinker is used, T_g decreases with respect to the linear polymer for low crosslinking densities. Here the crosslinker acts as softening agent. If the crosslinking density is further increased, T_g rises due to increasing immobilization of the network strands. For a rigid, mesogenic crosslinker, T_g increases continuously with the concentration of the crosslinker. A high crosslinking density offers the chance to freeze-in the LC structures into anisotropic glasses, yielding duromers with highly interesting properties. Those materials have been investigated, for example, in the work of Broer (for a review, see [10]). For systems where dynamic processes such as electromechanical behavior or photo-mechanics are of interest, a T_g below 20 °C is favorable. Strategies to obtain such low T_g will be described below.

Another very important aspect for the synthesis of LC elastomers is the functionality Φ of the crosslink. Φ determines the number of chains that meet at a junction. The local topology of the crosslink determines the properties of the

network and may be considered as a local defect within the LC phase structure of the network. This topology is not only determined by the chemical constitution of the multifunctional molecule, e.g., rod-like or flexible, but it is also affected by the local order imprinted during the crosslinking procedure. A network synthesized in the liquid crystalline state differs from a network with the same chemistry that was synthesized within the isotropic state. To minimize the effect of crosslinking molecules, their concentration has to be minimized. The influence of Φ can be shown using an elementary molecular theory of amorphous polymeric networks introduced by Flory in 1953. This ideal network theory does not consider dangling chain ends (i.e., a network chain that is connected to a junction of the network at only one end) or loops (i.e., a network chain, both ends of which are attached to the same polymer chain) and assumes that all junctions of the network have a functionality of $\Phi > 2$. Such an ideal network can of course not be achieved in reality. In the ideal network the number of network chains is denoted as v and the number of junctions as μ. The formation of a perfect network can then be imagined as a process of end-linking of network chains with a crosslink. Herby, the number of chain-ends $2v$ has to be equal to the number of functional groups $\Phi\mu$, so that $\mu = 2v/\phi$. Fewer junctions are needed when the functionality of the crosslink is higher [11, 12]. A higher functionality thus leads to fewer local defects in LC elastomers.

In the following sections some selected examples of the chemistry of LC networks will be summarized. While the synthesis of LC side chain elastomers mainly follows the radical polymerization technique and the polymer analogous addition reaction, LC main chain elastomers are exclusively synthesized by polycondensation or polyaddition reactions.

2.1 Side Chain Elastomers

In side chain elastomers, the mesogenic moieties, which can be rods, discs, or amphiphiles, are attached as side-groups to a polymer main chain via a flexible, aliphatic spacer. The existence of this spacer is crucial for the formation of LC phases as it lowers the tendency for crystallization and allows for a sufficient decoupling of the mesogenic units from the polymer backbone. This partial decoupling is necessary to allow the polymer chains to gain some entropy while the mesogenic side chains can exhibit orientational (and positional) long-range order of the LC phase. Concepts to change the LC phase behavior by modifying the chemical constitution are well known from linear polymers and crosslinking usually does not change the phase behavior dramatically. Rod-like mesogenic units are typically composed of two aromatic rings which are linearly connected via ester or ether bonds. For short aliphatic spacers and short tails of the mesogenic units, nematic phases are observed. However, with increasing spacer or tail length the stability of smectic phases increases. Mesogens based on three aromatic rings show preferably nematic phases but suffer from high transition temperatures. For the preparation of cholesteric elastomers part of the nematogenic side chains is

replaced by chiral dopands, e.g., cholesteryl derivatives that exhibit high helical twisting power. In such co-elastomers of chiral and non-chiral side chains, the phase behavior and the helical pitch which define the optical properties of the material can easily be tuned. Smectic-A phase behavior can be induced reliably by using perfluorinated tails, which are much stiffer compared to alkyl chains and may further promote the segregation into a lamellar phase structure. The incorporation of polar ethylene oxide (EO) side chains or of mesogenic units carrying EO tails can cause lyotropic phase behavior when the elastomer is swollen with water.

In the following we will outline two basic methods to synthesize LC side chain elastomers. As a starting point for the synthesis of LC elastomers a mixture of mesogenic monomers and bi- or multi-functional crosslinker molecules may serve. This will be discussed in the first part of the section. Alternatively, polymer analogous reactions, where the mesogenic moieties are attached to a polymer backbone, can be employed, which will be discussed in the second part of the section.

If LC monomers are used as starting materials, it is very important to consider that monomer and polymer networks can differ in their phase behavior as previously mentioned. This is a particular issue for nematic elastomers. Only very few examples are known in which the temperature regime of a nematic phase of a monomer overlaps with the nematic temperature regime of the polymer. The systematic that was hereby obtained for the LC phase behavior of linear polymers also holds for LC polymer networks because for elastomers the concentration of the mesogens is much higher than that of the crosslink. The chemistry that can be used for the crosslink is determined by the chemistry of the polymerization technique.

The only practicable chemical reaction to prepare LC elastomers from functional monomers is *radical polymerization*. Acrylates or methacrylates are mainly used as starting materials. It has to be ensured that the mesogenic group and the crosslinker have the same reactivity, so that a statistical arrangement along the chains can be achieved and a change in concentration ratio with advancing reaction is avoided. In principal, radical polymerization can be carried out in bulk. However, only if the polymerization temperature is within the overlapping temperature regime where monomer and polymer exhibit the same LC phase a homogeneous reaction can take place. Otherwise de-mixing occurs, which causes an uncontrolled network formation. Furthermore, the large reaction enthalpy of the polymerization restricts this method to the preparation of thin films only, in which a suitable heat transfer and control is guaranteed. To avoid these problems, the reaction can be carried out in solution. When the reaction is completed, the solvent has to be carefully removed in a de-swelling process. In some cases, especially if macroscopically ordered LCE are to be synthesized (see Sect. 4), low molar mass LCs of appropriate phase behavior can also serve as a solvent and have to be removed in an extraction process after synthesis [13].

An example for the synthesis of a side chain elastomer using radical polymerization of acrylates is presented in Scheme 1 and was demonstrated by Thomsen and co-workers [14]. Here, the mesogenic groups are attached side-on to the polymer-backbone. This attachment geometry is useful for a number of applications, because

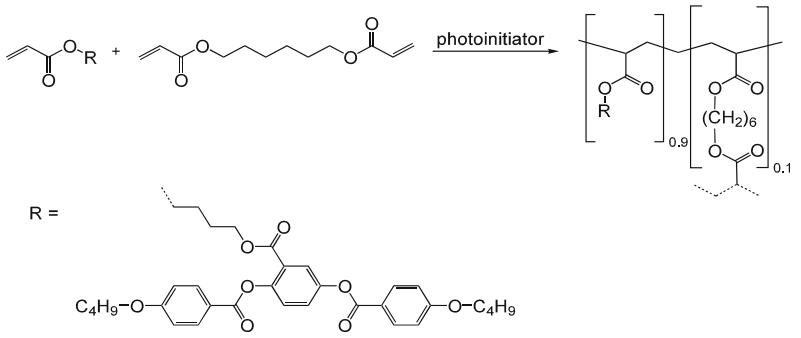

Scheme 1 Synthesis of poly(acrylate) LC elastomers with side-on attached mesogenic moieties [14]

it offers larger length changes at $T_{LC,i}$ as compared to elastomers with end-on attached mesogens. In this example, a bifunctional, flexible crosslinker was used and the elastomer can thus be synthesized in a one-pot reaction.

Another method is based on the synthesis of functional linear prepolymers. This can be achieved by copolymerization of the mesogenic monomer with a functional co-monomer, e.g., co-monomers containing a reactive hydroxy group. In a second reaction step, these functional linear polymers can be crosslinked, e.g., with a diisocyanate crosslinker [15].

Ionic polymerization and especially anionic polymerization offers the opportunity to achieve a very narrow molar mass distribution of the polymer chains and would therefore be ideal for the synthesis of well-defined polymer networks. However, the method is strongly limited due to the sensitive chemistry of this reaction. Most LC side chain polymers synthesized so far are based on acrylates and methacrylates as the involved chemistry works well for most of the commonly used mesogenic building blocks. In contrast, many mesogens are sensitive to nucleophilic attack, e.g., phenyl benzoate moieties. Ionic polymerization works rather reliably for mesogens with azo-groups and when a bulky initiator is used [16]. Polymer networks have not yet been synthesized by ionic polymerization techniques, but their properties would certainly be interesting. Stereoregular ionic polymerization using proper initiators could also open up the possibility to analyze the impact of polymer tacticity on the LC phase behavior.

Polymer analogous reactions can be carried out in two general ways: either functionalized linear polymers are crosslinked or the mesogenic monomer, the crosslinker, and a functional prepolymer are reacted in a one-pot synthesis. The first method offers the advantage that the crosslinking process can be performed in the LC state of the linear polymer, e.g., the LC phase structure of the linear polymer can be ordered macroscopically by techniques well known from low molar mass LCs (surface effects, electric or magnetic fields) or the polymer can be brought into a casting mold [17].

Functionalized linear polymers were synthesized by Schuring et al. [18]. With linear poly(siloxanes) obtained by a hydrosilylation reaction of a

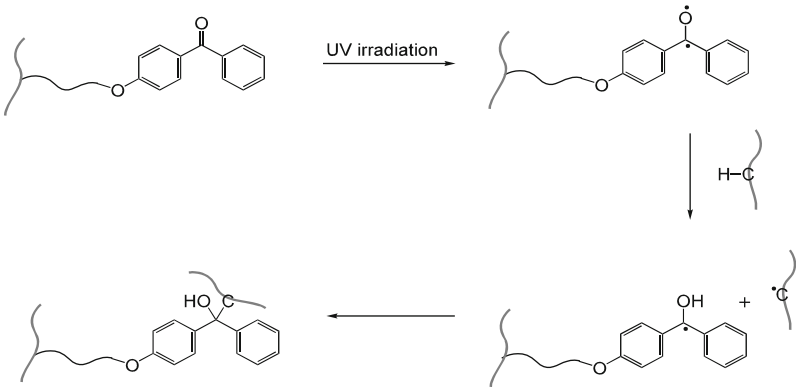

Scheme 2 Mechanism of photo-crosslinking of a benzophenone unit via a diradical state [19]

poly(hydrogenmethylsiloxane) and olefinic mesogenic side-groups and side-groups with additional acrylate functionality as crosslinker they were able to produce free-standing films. The crosslinkers can be activated by UV-irradiation that causes degradation of dissolved initiator molecules. A drawback of this procedure is the rather complex synthesis of the functional, linear polymers and spontaneous crosslinking reactions that can occur at elevated temperatures.

Another very useful approach was introduced by Komp et al., who attached a photo-crosslinkable benzophenone side-group to a polymer-backbone. This system can be crosslinked with UV-light via a diradical state (Scheme 2). The linear polymers are thermally stable and can be processed in the liquid state at elevated temperatures without undergoing a crosslinking reaction. The photophore absorbs a photon and promotes one electron from a non-bonding sp^2-orbital on the oxygen in the carbonyl group to an antibonding π^*-orbital. The electrophilic oxygen n-orbital can interact with any weak C–H σ-bond, abstracting an H-atom. The residual ketyl radical recombines with the C-radical. If this reaction occurs between two different polymer chains a crosslinking reaction takes place [19]. Hence, it should be considered that the benzophenone unit needs to be separated from neighboring mesogens. This can be done via a long flexible spacer or by inserting a long mesogen-like moiety between the photophore and the polymer backbone.

Without the use of functional side-groups, the network formation can also be realized by γ-irradiation as demonstrated by Vazilets and co-workers. A benefit of this method is that good control of the crosslink distribution can be achieved and that the crosslinking works with non-functionalized and thus thermally stable polymers that are not light sensitive. However, for this method an irradiation source is required that is not usually readily available [20, 21].

More recently, ring opening metathesis polymerization (ROMP) has been used to prepare telechelic liquid crystalline polymers that carry azide end groups which can be crosslinked with a triacetylene species using the well known copper catalyzed click chemistry [22].

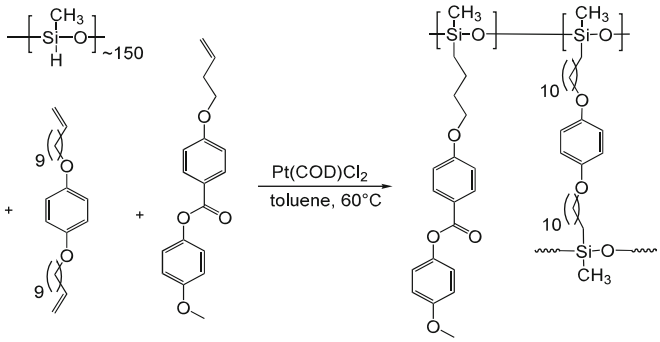

Scheme 3 LC elastomer prepared by using a Pt-catalyzed hydrosilylation reaction following Küpfer's method; COD: cyclooctadiene [92, 120]

Carrying out the synthesis of LC elastomers in a polymer-analogous one-pot reaction is chemically much simpler. Poly(hydrogenmethylsiloxanes) have been proven to be very useful prepolymers as the Si–H bond can be easily functionalized in a platinum catalyzed hydrosilylation reaction with vinyl terminated mesogens and crosslinkers, respectively. Moreover, the resulting elastomers show low glass transition temperatures. In contrast to polyacrylates or polymethacrylates, LCEs are accessible which are liquid crystalline at room temperature. Furthermore, this reaction can be easily interrupted at a certain point, yielding a lightly crosslinked polymer gel that can be oriented before the reaction is completed (see Sect. 4). Typical components are shown in Scheme 3. An advantage of this method is that the components can be easily synthesized and are stable towards light and air. What is more, statistical copolymers can be easily obtained to modify phase transformation temperatures or induce the desired phase behavior of the final network. The crosslinking molecules can be bi- or multi-functional, they can be isotropic or mesogenic rods, and can even be light-sensitive. In earlier works the crosslinker was often functionalized with a vinyl group at one end and a methacrylate group at the other. These groups exhibit very different reaction speeds toward the hydrosilylation reaction, so that the synthesis of the elastomers can be carried out in two relatively well-defined steps. The length of the spacer that links the mesogen to the polymer backbone can be varied to induce different polymer chain conformations (see Sect. 3). The mesogens can also be attached side-on when they carry a vinyl-terminated lateral spacer.

2.2 Main Chain Elastomers

The chemistry of main chain elastomers is limited to step-growth reactions, i.e., polycondensation and polyaddition reactions, which demand the highest purity of the starting materials and experimental conditions which exclude side reactions.

Compared to side chain elastomers the preparation of main chain elastomers with suitable transition temperatures is rather challenging. What is more, due to the rigid rod-like mesogenic moieties in the polymer main chain, most linear main chain liquid crystalline polymers exhibit high clearing temperatures and tend to crystallize [23], making them unfavorable for many LC elastomer applications.

Due to the regular arrangement of the mesogens along the polymer backbone main chain polymers tend to form smectic or higher ordered mesophases [23], so that, especially if nematic phase behavior is required, strategies to overcome these problems have to be employed. The ability to do this is well known from linear LC polymers and has been discussed extensively in the literature [24, 25]: kinks can be incorporated in the mesogens, laterally attached side chains can act as plasticizers, or flexible spacers can be introduced, separating the rigid mesogenic moieties.

Despite their more complex chemistry, main chain LC elastomers have gained much interest in recent years due to the direct coupling of the liquid crystalline order and the polymer backbone conformation. The ground breaking predications of de Gennes were also based on main chain elastomers [3].

The chemistry used for the synthesis of main chain elastomers is usually based on poly-esterification, hydrosilylation reactions or epoxy resins. Here we shall discuss the possibilities for realizing main chain elastomers depending on three well-established preparation techniques. These include: (1) crosslinking of terminally functionalized LC polymers with a suitable multifunctional crosslinker, (2) photo-crosslinking of LC main chain polymers containing a photo-crosslinkable group, and (3) one-pot synthesis of main chain LC elastomers, usually starting from a mesogen, a flexible chain-extender, and a crosslinker.

Crosslinking of terminally functionalized LC polymers with a suitable multifunctional crosslinker was introduced by Zentel et al. [26]. They crosslinked allyl side-groups of a liquid crystalline polyester with an oligo-siloxane crosslinker, yielding elastomers with S_A and S_B phase behavior and rather high transition temperatures.

Bergmann [27] was able to synthesize nematic elastomers following a similar approach. As precursor, a main chain polyether with a comparatively low LC-isotropic phase transformation temperature of about 120 °C developed by Percec et al. [28] was used (Scheme 4). The free rotation around the C–C bond between the biphenyl unit and the phenyl ring of the mesogenic moiety allows for the formation of two different conformations of the mesogen, which not only lowers T_{ni} but also suppresses the formation of smectic phases. The ethyl-substituent creates chirality within the repeating units causing four different constitutional possibilities. This additionally hinders crystallization, improves solubility in organic solvents, and decreases both T_g and T_{ni}. The mesogenic moieties are separated from each other by a rather long C_{10} spacer to allow for the formation of a low-temperature nematic phase. For the synthesis of the elastomer, a prepolymer with vinyl end groups was prepared and successively crosslinked with a cyclo-siloxane crosslinker in a hydrosilylation reaction (Scheme 4). This approach offers the advantage that the phase behavior of the prepolymer is only slightly changed by the crosslinking so that the properties of the resulting elastomer can be easily predicted.

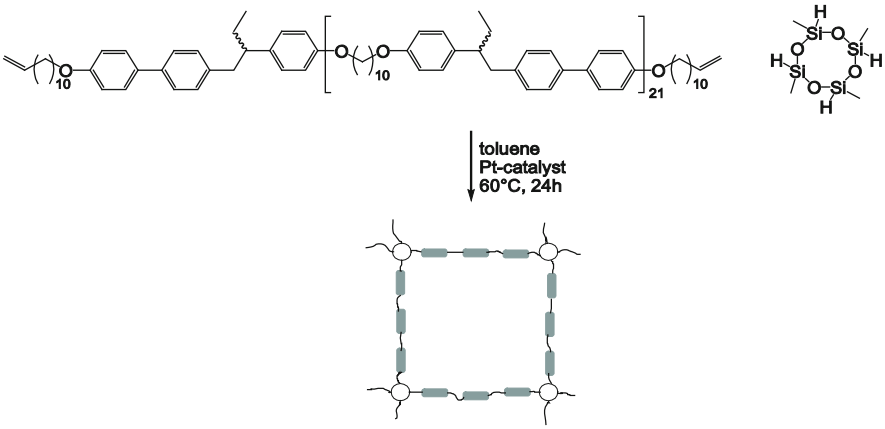

Scheme 4 Elastomer synthesized by Bergmann [27] on the basis of a LC polyether published by Percec [28]

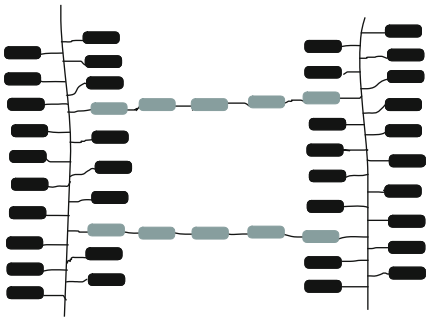

Scheme 5 Combined main chain side chain elastomer synthesized by Wermter et al. [29]

One of the difficulties of this method is that both the content of end-groups of the polymer and the amount of volatile crosslinker is hard to measure and weigh, respectively, so that it is extremely difficult to keep to the exact stoichiometry. This often results in high soluble contents of the elastomers and imperfect comparability of the samples.

It is also possible to use the vinyl-terminated pre-polymer to crosslink a side chain LC polymer. This was demonstrated by Wermter et al. [29] who crosslinked a side chain end-on polymer similar to that shown in Scheme 3 with a main chain polymer carrying vinyl end-groups (Scheme 5). The side chain component can be understood as a multifunctional crosslinker for the main chain elastomer and also acts as a plasticizer, further decreasing the transition temperature to about 90 °C. Such combined main chain/side chain elastomers show, if oriented to a permanent monodomain (Sect. 4) extremely high length changes at the phase transformation to

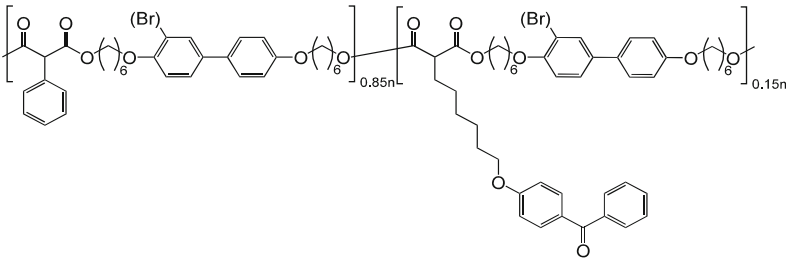

Scheme 6 Photo-crosslinkable main chain polymer with S_A phase behavior [31]

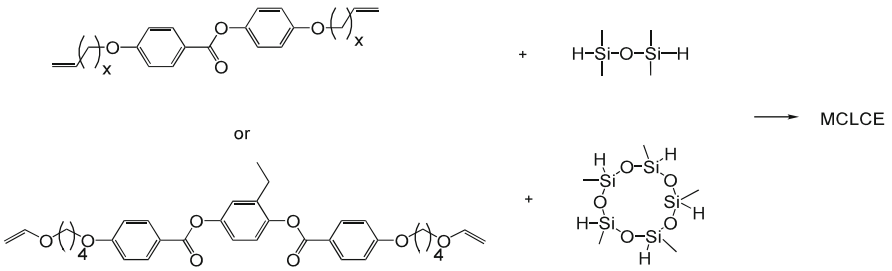

Scheme 7 Components for the synthesis of main chain elastomers (MCLCEs) in a one-pot reaction. The two-ring mesogen yields smectic and nematic phases, depending on the spacer-length; the three-ring mesogen yields broad nematic phases with low transition temperatures [30]

the isotropic phase and have been very useful in examining the influence of the elastomers chemical constitution on its physical properties [30].

Photo-crosslinking of LC main chain polymers containing photo-crosslinkable groups was successfully performed by Beyer et al. [31]. They synthesized S_A elastomers with an LC polyester as a precursor (Scheme 6). By introducing photo-crosslinkable side chains, they were able to crosslink thin prepolymer films in bulk using UV-irradiation. Compared to the elastomers synthesized by Bergmann, this approach allows much better control of the crosslinking reaction. This is a rare example of main chain elastomers showing S_A phase behavior. Usually main chain polymers tend to form nematic or smectic-C phases, the latter especially when the mesogenic units are based on aromatic esters or ethers. In most cases S_A phase behavior can only be induced by using biphenyl derivatives which, however, suffer from high transition temperatures and a tendency to crystallize. Here an LC polymer where 50 mol% of the biphenyl units are laterally substituted with bromine to suppress crystallization was developed, yielding an S_A elastomer with suitable transition temperatures ($T_{S,I} \approx 60$ °C). Krause et al. [32] used a similar concept with photo-crosslinkable units introduced into the main chain of an LC polymer containing flexible poly(ethyleneoxide) spacers and two-ring mesogens to yield nematic elastomer films and fibers.

The one-pot synthesis of main chain LC elastomers is a less complicated approach for the synthesis of main chain LC elastomers and was introduced by Donnio [33] based on the chemistry of linear polymers investigated by Aguilera

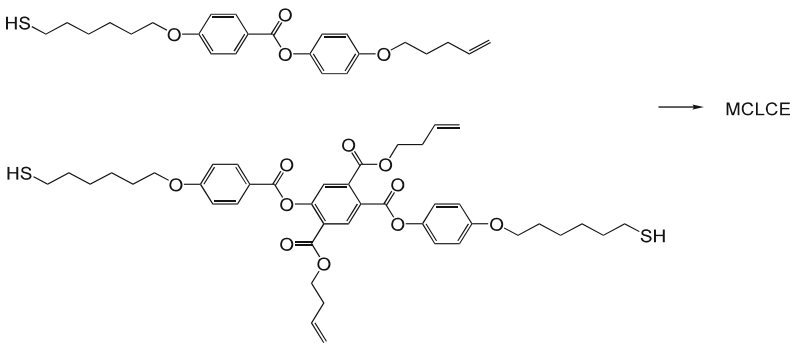

Scheme 8 Components for the synthesis of main chain elastomers (MCLCEs) in a solvent-free one-pot reaction employing a photo-initialized thio-ene polycondensation [39]

et al. [34]. Instead of starting from pre-synthesized main chain polymers, this synthetic approach is based on a polyaddition reaction in solution via hydrosilylation of a divinyl substituted mesogen with tetramethyl dihydro disiloxane as additional flexible spacer to lower the phase-transition temperatures. As a crosslinker a cyclic pentasiloxane was used (Scheme 7) which is less volatile than the cyclic tetrasiloxane used by Bergmann.

Brandt and Krause [30] continued these investigations by varying the mesogenic shape and the length of the siloxane units. Using mesogenic units consisting of two aromatic rings lowers the phase transition temperatures significantly. The formation of smectic phases mainly caused by the tendency of the siloxane units to phase-separate can be avoided by using short vinyl-chains and short siloxane units. Copolymerization of mesogens with different spacer length or the introduction of lateral (alkyl) substituents at the central aromatic core can additionally decrease the tendency for the formation of smectic phases.

In the early stages, main chain elastomers that were synthesized with the one-pot method exhibited a considerable amount of soluble content, caused by an incomplete conversion of the polyaddition reaction. To overcome this problem Krause [30] developed a new mesogenic unit based on Donnio's three-ring core with a laterally attached ethyl-substituent that successfully suppresses smectic phases. The terminal vinyloxy groups (Scheme 7) lead to an exceptionally clean polyaddition reaction and prevent side-reactions such as double-bond migration. This allows for the synthesis of elastomers with very low crosslink content and low elastic moduli. The vinyloxy groups also significantly lower the T_{ni} of the elastomers. However, the vinyloxy chemistry requires a lot of effort, as the end groups are sensitive to acids and not stable towards air. With respect to clean polyaddition reactions one nowadays has recourse to the more robust vinyl spacers as the according precursors can be commercially purchased in excellent purity.

A very similar chemical approach with a trisiloxane co-monomer and a tetracyclic crosslinker was used to realize main chain LCEs with pentaphenyl mesogens incorporated side-on into the polymer main chain [35]. Such elastomers have an S_A phase behavior due to the segregation of the aromatic and the siloxane moieties.

Ishige and co-workers [36–38] produced S_{CA} main chain elastomers with transition temperatures of about 180 °C also utilizing a one-pot method, by a melt trans-

esterification chemistry to obtain polyesters. They did not use a flexible chain-extender like the short tetrasiloxane in the examples discussed above, but started from a flexible dialcohol, an aromatic di-ester as a mesogenic group, and a trifunctional aromatic ester as a crosslinker.

A new and elegant solvent-free approach to main chain LCEs was found by Yang et al. [39] who, based on the work on linear LC polymers by Lub et al. [40–42], made use of the photo-induced addition of thiols and olefins (click-chemistry) to synthesize nematic polymer networks. Starting from a mixture of the mesogen, a tetrafunctional crosslinker and a photo-initiator networks with a T_{ni} around 170 °C were obtained by UV crosslinking (Scheme 8).

2.3 Basic Characterization of LC Networks

The first question that has to be addressed after the synthesis of a polymer network is whether the crosslinking reaction was successful and is reproducible. Therefore, it is advisable to measure the soluble content of the elastomer, that is, the weight loss in percent after the extraction of unreacted monomers, oligomers, or polymers. For the extraction the elastomer is placed in a poor solvent of the linear polymer (e.g., isohexane). Subsequently the solvent quality is increased by slowly adding a good solvent (e.g., toluene). The swelling of the elastomers has to be carried out very carefully as inhomogeneous or too fast swelling can produce local mechanical stress which might cause the sample to break. This is especially important for macroscopically oriented samples (LSCEs) for which the LC-isotropic phase transformation that occurs upon swelling is accompanied with large length-changes of the sample. The extraction is usually done over about 1 day for nematic main chain elastomers; for the less sensitive side chain elastomers or for smectic elastomers this can be done faster. After the extraction of unreacted material is completed the elastomers have to be deswollen again. This is done by the reverse procedure by adding poor solvent. Afterwards the elastomer is dried at elevated temperatures to evaporate any remaining solvent. This extraction procedure is crucial to obtain samples with reproducible properties.

Information on the crosslinking density of the synthesized elastomer can be obtained using various methods. Mechanical characterization, especially stress–strain measurements, thermoelastic measurements in the isotropic phase, and swelling experiments yield information about the molecular weight of the network chains M_c. In a first approach, the affine network model, introduced by Kuhn, may be used to correlate the experimental results with the chemical constitution of the networks. This network model assumes that the average squared distance of the chain ends of a network chain is the same as for an uncrosslinked polymer of the same length. Furthermore, a deformation of the network does not change the sample's volume so that two polymer segments are separated about the same factor λ that is determined by the macroscopic deformation. Finally, the enthalpy of network chains does not change under deformation. Network defects like loops or dangling chain ends are not

considered in this theoretical description. Nevertheless, within a homologous series of networks that only differ with respect to the crosslinking density, some relative quantities can be obtained that help to control the chemistry of the network formation.

The E-modulus in the isotropic phase can be determined from both stress–strain and thermoelastic measurements and M_c can be calculated according to $M_C = 3\frac{\rho \cdot R \cdot T}{E}$ when the density ρ of the elastomer is known. The degree of swelling Q in a certain solvent can yield M_c according to

$$Q = \left(\frac{M_C}{\rho \cdot V}\left(\chi - \frac{1}{2}\right)\right)^{\frac{3}{5}}$$

The second virial coefficient χ can be determined for the linear, uncrosslinked polymer, for example, in osmosis measurements [11, 12, 43].

The LC phase behavior of the elastomers can be analyzed with conventional techniques also used for low molar mass LCs. Polarizing optical microscopy as well as X-ray scattering provide information about the phase structure of the networks and about $T_{LC,i}$ and $T_{c,LC}$. In addition to the determination of phase transformation temperatures, DSC experiments can be used to measure the glass transition temperature T_g. To obtain reliable DSC results, it is necessary to measure at various heating and cooling rates (usually about four heating and cooling runs, with heating and cooling rates between ~10 and ~40 K min^{-1}) and to plot the obtained transition temperatures as a function of the square-root of the heating and cooling rate. The transition temperatures are then obtained by extrapolating to zero heating rates.

3 Mechanical Orientation Behavior

When LCEs are synthesized in the absence of external fields, so-called polydomain LC elastomers are obtained, which show macroscopically isotropic properties similar to polycrystalline materials. This resembles, e.g., bulk material of a low molar mass liquid crystal, where thermal fluctuations prevent a uniform director orientation over the whole sample. For nematic elastomers the overall isotropic behavior also indicates an overall isotropic conformation of the polymer chains, which is the consequence of the maximization of the chain entropy.

However, it is well known that a mechanical deformation of a conventional, isotropic polymer network causes anisotropy. Under deformation the chain segments become oriented according to the symmetry of the external field and the state of order of the network can be characterized by an order parameter similar to that of nematic liquid crystals. Very early mechanical experiments on nematic polydomain elastomers actually demonstrate that a uniaxial deformation of a nematic elastomer converts the polydomain structure into a macroscopically uniformly ordered monodomain network [44]. This is shown in Fig. 2, where the opaque polydomain becomes optically transparent and converts into a monodomain

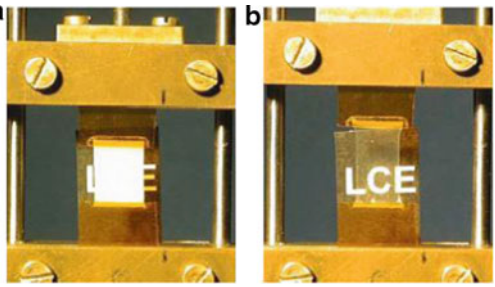

Fig. 2 Nematic polydomain elastomer with locally prolate chain conformation in the undeformed state (**a**) and upon mechanical stretching above a critical stress (**b**)

network by stretching. The experiment unambiguously indicates that the state of order of the network chains is directly connected with the liquid crystalline state of order. Obviously, with respect to the orientation of the LC phase structure of the elastomer, a mechanical field acts very similar to an electric or magnetic field on low molar mass LCs. This opens new perspectives for macroscopically uniformly ordered LC networks.

To get a systematic insight into the interplay between mechanical deformation of an LC elastomer and the orientation behavior of the LC phase structure, the knowledge of the chain conformation of a polymer backbone in the liquid crystalline state is necessary. This chain conformation has been investigated in detail on linear LC polymers in the past and will be briefly summarized in Sect. 3.1. In Sect. 3.2 it will be described how the global state of order of polydomain elastomers can easily be manipulated using mechanical fields. We will hereby only focus on some principal aspects and concentrate on symmetry arguments between the local and the global chain conformation. While the local chain conformation of the network strands originates from the chemical constitution of the monomer units and their interaction with the anisotropic LC order, the global chain conformation is induced by the external mechanical field. These considerations are the basis for many synthetic concepts to prepare liquid single crystal elastomers (LSCEs). A more detailed description of various orientation strategies is given in Sect. 4.1.

3.1 Chain Conformation of Linear Polymers

In the isotropic melt of macromolecules the undisturbed dimensions of the chains can be well described with random flight statistics. On average the chains form a statistical coil with spherical shape (Fig. 3a) [11]. The radius of gyration of the coil is given by $\overline{R_0^2} = NP$. N is the number and P the length of the statistical chain segments. In the LC state, however, the monomer units become spontaneously aligned due to their mesogenic character. This can cause a significant deformation of the statistical coil towards a prolate or oblate shape and has been directly proven by small-angle neutron scattering (SANS) on deuterated polymers (Fig. 3b, c) [45]. It is obvious that the chemical constitution of the mesogenic monomer units as well

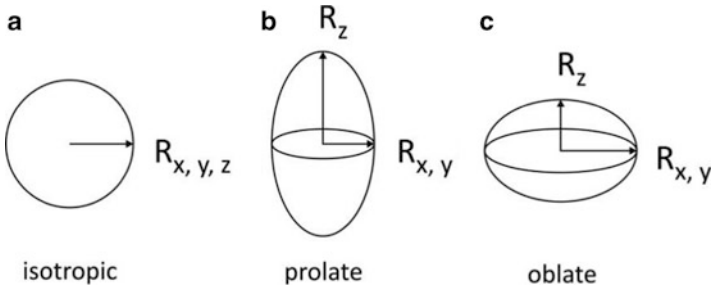

Fig. 3 Schematic representation of the polymer chain conformation: spherical with $R_x = R_y = R_z$ (**a**), prolate with $R_z > R_x$, R_y (**b**), and oblate with $R_z < R_x$, R_y (**c**). R_z and R_x, R_y are the radii of gyration parallel and perpendicular to the axis of highest priority (nematic director, smectic layer normal, or helix axis), respectively

as their position and linkage within the polymer chain play an important role. The knowledge of the chemical constitution of the polymer chain and the corresponding chain conformation is the key to the understanding of the orientation behavior of LC elastomers. In the following we restrict the discussion to polymers having rod like mesogens.

For main chain polymers in the LC state the coil is strongly extended along the director (prolate chain conformation) showing an anisotropy of the radii of gyration parallel and perpendicular to the director of up to $R_{\parallel}/R_{\perp} \approx 5$ [46–53]. On a local scale the polymer chain is fully extended which is in agreement with ^{2}H-NMR experiments [54] as well as theoretical predictions of Yoon and Flory [55]. For large flexible spacers separating the mesogenic groups the existence of hairpins, i.e., local backfolding of the polymer main chain, has been proven by SANS experiments [50, 51, 53, 56]. Investigations on smectic-C fluctuations existing in the nematic phase showed a strong orientational coupling of the mesogenic units and the global chain conformation, so that the whole polymer chain becomes inclined in the layers of the S_C short-range order [53]. Prolate chain conformations also exist for smectic main chain polymers. However, the tendency of backbone backfolding might be stronger in lamellar mesophases [36–38].

For side chain polymers with side-on attached mesogenic units (Fig. 1b) very similar results are obtained. For short flexible linkages between the polymer backbone and the mesogenic units, prolate chain conformations comparable to main chain polymers are found ($R_{\parallel}/R_{\perp} \approx 5$). However, with increasing spacer length the chain anisotropy decreases. The limit is reached using a spacer length of $x = 11$ (x is the number of spacer atoms), where a nearly spherical coil is obtained ($R_{\parallel}/R_{\perp} \approx 1$) [57–62]. This can be explained by the so-called "jacketed effect": as a consequence of the lateral attachment to the polymer chain, the rod-like units and the polymer backbone are oriented parallel to each other on a local scale. For short spacers lengths the polymer backbone is stretched significantly parallel to the mesogenic rods. Although the polymer main chain, e.g., a polysiloxane or polyacrylate, is intrinsically flexible, it forms a highly elongated polymer coil. As the spacer length increases this effect becomes less pronounced until these steric

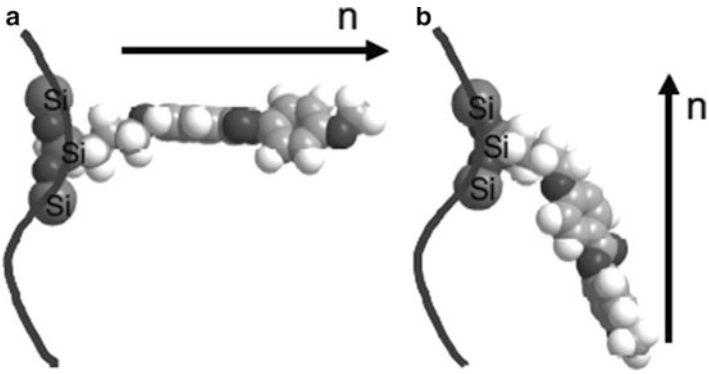

Fig. 4 Molecular model of the local chain conformation of LC end-on side chain polymers depending on the length of the flexible spacer: oblate conformation for an even number of spacer atoms (**a**) and prolate chain conformation for odd numbered spacers (**b**)

interactions between side-groups and the polymer backbone are completely decoupled [45].

Side chain polymers with end-on attached mesogenic units (Fig. 1a) show a more complex behavior, as the coupling between the LC order and the polymer backbone depends on the chemical constitution of the flexible spacer and the phase structure [2, 63–68]. Nematic polymers having an odd number x of atoms in the spacer have the tendency to adopt a weak globally prolate shape with $R_{\parallel}/R_{\perp} \approx 1.5$. Here the polymer backbone and the mesogenic units are oriented parallel on average (Fig. 4b). Slightly oblate chain conformations, where the polymer backbone and nematic director are oriented perpendicular to each other, have been observed for nematic polymers having a short spacer with an even number of atoms of $x < 7$ (Fig. 4a). Oblate chain conformations are also observed for nematic polymers that exhibit smectic short-range order. Here the chain conformation results from the local confinement of the polymer backbone between the layers of the smectic fluctuations (see below).

Smectic side chain polymers show an oblate equilibrium conformation of the polymer melt where the polymer backbone is partially confined between the smectic layers independent of the attachment geometry. For S_A polymers the confinement depends not only on the smectic order parameter but also on the type of S_A phase structure. For the monolayer phase structure S_{A1} the anisotropy of the radii of gyration is $R_{\parallel}/R_{\perp} \approx 0.3$ while for the less densely packed partially bilayer structure S_{Ad} the confinement of the backbone is less pronounced ($R_{\parallel}/R_{\perp} \approx 0.7$) [63, 64, 69–71].

Simple mechanical experiments can provide information about the local orientation of the mesogenic units and the polymer chain and can give some indications about the existing chain anisotropy [2, 65–68]. If a polymeric fiber is drawn from the isotropic melt, the polymer chains are expanded in the stretching direction. The mechanical deformation induces an orientation of the LC phase structure which can easily be analyzed using X-ray scattering. When the mesogens are aligned

along the stretching direction, locally a prolate chain exists. In the opposite case the mesogenic units and the stretching direction are aligned perpendicular to each other, indicating locally an oblate chain conformation. In order to obtain conclusive information about the local orientation of mesogenic units with respect to the stretching direction, equilibrium conditions have to be ensured. Sometimes this can be problematic, as for high drawing speeds and high cooling rates non-equilibrium orientations or non-uniform orientations within the fiber cross-section may be frozen-in.

3.2 Orientation of Polydomain Networks

As a direct consequence of the interaction between LC order and polymer chain conformation, the global state of order in polydomain LCEs can be manipulated by mechanical stretching. It is well known from conventional rubbers that mechanical deformation induces changes in the macroscopic chain conformation of the network strands. Uniaxial elongation causes the formation of prolate chain conformations while biaxial stretching, which is equivalent to uniaxial compression, establishes global oblate chain conformations. This has important consequences for LC elastomers. By changing the macroscopic chain conformation so that it is consistent with the phase symmetry of the LC state, macroscopic alignment can be induced. Uniaxial stretching a polydomain nematic elastomer with locally prolate chain conformation, e.g., a main chain polymer, a side chain side-on polymer or a side chain end-on polymer with an odd number of spacer atoms, produces a transparent polymer network with uniform orientation of the nematic director along the stress axis above a characteristic strain. We shall refer to this alignment of the director in the film plane as homogeneous orientation. The formation of a monodomain is shown for a nematic side chain elastomer in Fig. 2. Above the characteristic threshold strain, the directors of the individual domains rotate towards the mechanical stress axis. The resulting macroscopic orientation of the director can be easily proven by X-ray scattering or IR dichroism. This process is completely reversible. When the mechanical stress is released, the sample relaxes back into the polydomain equilibrium state.

The concept of mechanical field induced orientation can easily be transferred to nematic elastomers with oblate chain conformation, i.e., side chain end-on elastomers with an even number of spacer atoms. In order to achieve a monodomain structure, a globally oblate chain conformation has to be established. This can be achieved by uniaxial compression or biaxial stretching of the polydomain elastomer which induces a uniform homeotropic alignment of the nematic director perpendicular to the film plane. Up to now, this orientation technique has only been realized experimentally for chiral nematic elastomers [72].

Mechanical fields can also be deployed to achieve a macroscopic orientation of the helicoidal z-axis of cholesteric elastomers. As discussed above, nematic side chain polymers with odd spacer length exhibit a locally prolate chain conformation

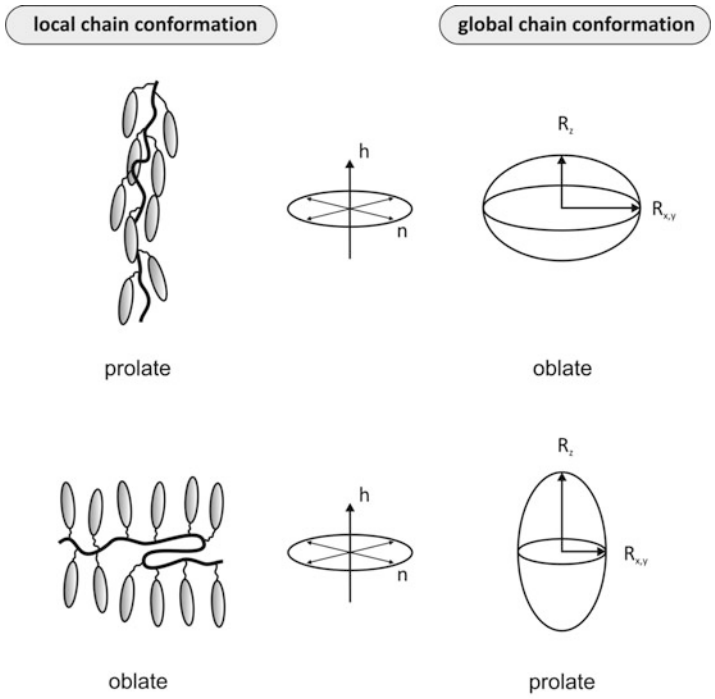

Fig. 5 Local polymer chain conformation of nematic side chain elastomers (with respect to the nematic director *n*) and resulting global chain conformation in the cholesteric phase structure (with respect to the cholesteric helix axis *h*)

with respect to the local director. In the helicoidal phase structure of chiral nematic elastomers, however, this orientation corresponds to an overall oblate chain conformation with respect to the helix axis as the local director rotates continuously along this axis (Fig. 5). Therefore a globally oblate chain conformation has to be established in order to achieve a cholesteric monodomain. Using biaxial stretching or uniaxial compression, elastomers with homeotropically aligned helix axes can be obtained [72]. In the case of a chiral nematic polymer with even spacer length and thus locally oblate chain conformation with respect to the local director, a prolate chain conformation exists with respect to the helix axis. Uniaxial mechanical stretching induces a macroscopic orientation of the helix axis along the stretching direction in the film plane [73].

Smectic side-chain polymers prefer locally oblate chain conformations, independent of the spacer length or attachment geometry. Analogous to oblate nematic polydomain elastomers, biaxial mechanical stretching or uniaxial compression can be used to orient S_A polydomain elastomers. This achieves a simultaneous orientation of the director and the smectic layer normal in a uniform homeotropic fashion [74].

Upon uniaxial stretching a polydomain elastomer in the smectic-A phase, the layer planes usually couple to the mechanical field. This process does not

produce a monodomain but causes a reorientation of the polydomain structure consistent with the induced globally prolate chain conformation. The layer normals align perpendicular to the stretching direction (z-direction) but are randomly distributed in the xy-plane [75]. The orientational behavior of smectic elastomers can change drastically if a uniaxial mechanical field is applied in the isotropic state followed by slowly cooling into the LC phase. If an intermediate nematic phase occurs before reaching the smectic state, a uniaxial mechanical field can be sufficient to induce a macroscopic orientation [75–77]. This will be discussed in more detail in Sect. 4.1.1 when we will address the synthesis of S_A LSCEs.

While the partial decoupling of the LC order and the polymer backbone in side chain elastomers allows for some flexibility in their relative orientation, the much stronger coupling in S_A main chain elastomers induces only prolate chain conformations [31, 36–38]. Therefore, uniaxial mechanical stretching macroscopically aligns the director, which has also been observed for main chain elastomers with laterally attached mesogenic units [35, 78]. However, the stretching speed can have an impact on the induced orientation. For high stretching rates a coupling of the layer planes has been observed which should lead to a polydomain structure similar to that discussed above for side chain elastomers under uniaxial mechanical stress [79].

For smectic-C polydomain elastomers the situation becomes more complex as the director is inclined at an angle theta from the layer normal. A simultaneous orientation of both is usually not possible when simple mechanical deformations are deployed. This can only be achieved using more complex deformations in a multi-step procedure which will be discussed in Sect. 4.2.2. Uniaxial mechanical fields only cause reorientations of the LC phase structure yielding a polydomain which is consistent with the induced macroscopic chain conformation. This usually induces a macroscopic orientation of the director and leaves a conical distribution of the layer normal around the stress axis. The attendant angle θ between n and k corresponds to the tilt angle of the smectic-C phase (Fig. 6). The formation of this special polydomain structure has been observed for side chain elastomers [80–84] as well as for main chain elastomers [33, 79, 85–88]. For side chain elastomers the orientation can be strongly influenced by the crosslinking topology. Upon cooling from the S_A phase to the S_C phase under uniaxial mechanical stress, elastomers with rod-like crosslinkers form a conical layer distribution, while for more flexible crosslinkers the mesogenic side-chains tilt at an angle of $\pm\theta$ with respect to the layer normal which is oriented parallel to the mechanical stress [89].

In conclusion, simple symmetry considerations allow for a successful orientation of polydomain elastomers using mechanical fields. In principle knowledge is only needed of the local chain conformation of the LC polymer on which the elastomer is based, and the consistent mechanical deformation must be applied. Nevertheless, the chemical constitution of the whole polymer network has to be considered. Often, the orientational behavior is strongly influenced by the crosslinking topology. As a rule of thumb, prolate chain conformations are increasingly preferred when the crosslinker concentration is increased and when the crosslinker molecules are more rod-shaped [90, 91].

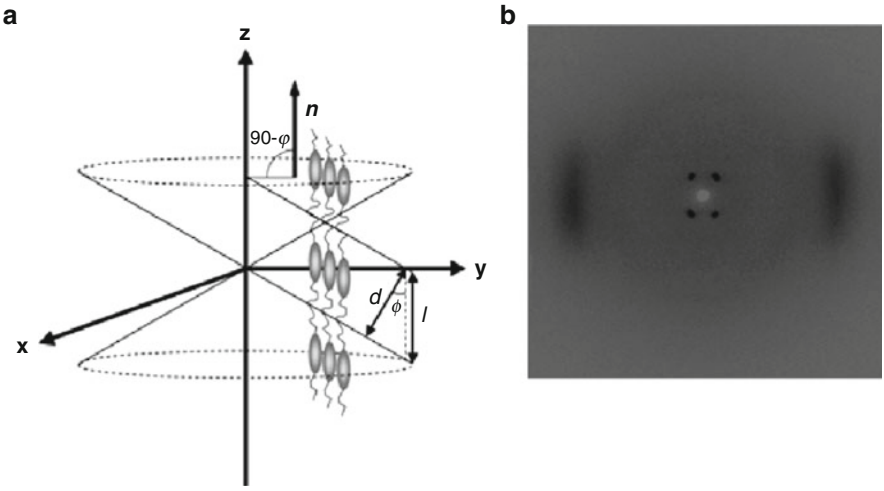

Fig. 6 Schematic representation of the conical layer distribution of polydomain S_C elastomers exposed to uniaxial mechanical deformation (**a**) and corresponding X-ray pattern (**b**). θ (denoted ϕ in this figure) is the S_C tilt angle, d the smectic layer spacing, and l the length of the mesogenic units. The layer normal k is conically distributed around the stress axis z. Reprinted with permission from [87]. Copyright (2008) American Chemical Society

4 Liquid Single Crystal Elastomers

For a detailed understanding of the desired physical properties of liquid crystalline elastomers as well as for many applications, elastomers are desired with a permanently stable macroscopic orientation of the LC phase structure. Such monodomain polymer networks show anisotropic physical properties comparable to single crystals and the term "LSCEs" has been coined. As discussed in Sect. 3.2, the synthesis of LCEs basically leads to polydomain samples, analogous to polycrystalline materials. However, the presence of external fields, e.g., magnetic, electric, and mechanical fields, or surface effects, can induce a macroscopic orientation of the LC phase structure. As a direct consequence of the coupling of the liquid crystalline order and the chain conformation of the network strands, macroscopic orientation of the LC phase structure leads to a macroscopically anisotropic chain conformation and vice versa. As demonstrated by Küpfer et al. in 1991, a suitable synthetic concept to fix this global orientation and chain conformation permanently yielding LSCEs, is a chemical crosslinking reaction in the aligned state (Fig. 7) [92].

In the first part of this section we will discuss several strategies developed in the last decades to prepare LSCEs with a permanently stable orientation of the main axis, i.e., the director n for nematic elastomers, the helix axis for cholesteric elastomers, and the layer normal k for smectic polymer networks, respectively (Sect. 4.1). In some cases, however, alignment of the main axes is not sufficient to achieve a uniform orientation of the whole phase structure and more complex

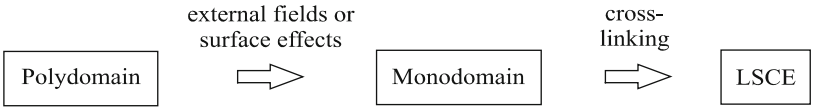

Fig. 7 Principal route to liquid single crystal elastomers (LSCEs)

procedures have to be applied. This is the case for the mechanical field induced orientation of S_C elastomers where two separate steps are necessary to orient both the layer normal and the director. For biaxial nematic and biaxial S_A phases the mesogens exhibit orientational long range order in all three spatial directions, and the minor director *m* is used in addition to the major director *n* to denote the orientation of the minor molecular axes. Here, a second orientation step is necessary to produce monodomains with a macroscopic 3D orientation of the LC phase structure. These two cases will be discussed in Sect. 4.2.

4.1 Permanent Orientation of the Main Axis

For the preparation of monodomains with respect to the main axis, two principal strategies can be deployed (Fig. 8). The first approach takes advantage of the anisotropy of the polymer chain conformation of the network strands and is based on considerations discussed in Sect. 3.2. Mechanical deformation of polydomain LCEs leads to a globally anisotropic chain conformation and can induce a macroscopic orientation of the LC phase structure above a certain threshold stress. By introducing a globally anisotropic chain conformation a priori during synthesis, LSCEs are accessible. This can be realized by chemical crosslinking after or during orientation by means of mechanical or viscous flow fields and will be discussed in detail in Sect. 4.1.1.

Following the second route, the anisotropic physical properties of the LC phase structure, such as the anisotropy of the diamagnetic or dielectric susceptibility, can be utilized to orient the mesogenic units in a magnetic or electric field, respectively. Macroscopic alignment can also be achieved by surface effects, a technique well known from low molar weight LCs. As the mesogenic units are covalently linked to the polymer chains, the orientation of the LC phase structure leads directly to the formation of a globally anisotropic chain conformation. Both are fixed permanently by chemical crosslinking in the aligned state, which will be discussed in Sect. 4.1.2.

If the first route is chosen, large-area elastomers can be produced with a wide variety of film thicknesses. As precursors, only polymeric materials, for example, photo-crosslinkable polymers or lightly crosslinked polymer gels, can be used. The second route is usually limited by the available field strength to thin film geometries. Typically photo-crosslinkable LC polymers or monomer/crosslinker mixtures (usually containing additional photo-initiators and/or inert LCs as solvents) can serve as starting materials. The latter offer the advantage that molding techniques can be applied and elastomeric materials of more complex geometries can be realized.

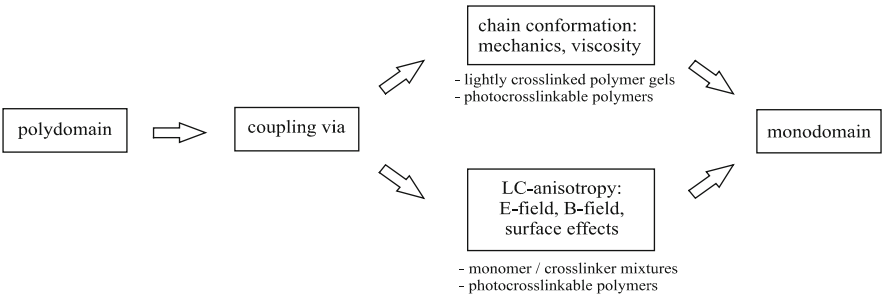

Fig. 8 Two principal routes for the formation of monodomain LC elastomers and applicable starting materials

Before synthesizing LSCEs, it has to be considered that the preparation routes can have significant impact on the material properties as it influences the crosslinking topology as well as the global chain conformation. The application of strong mechanical fields during synthesis that are used when employing the first route leads to a strong deformation of the polymer backbone. This results in a non-Gaussian chain conformation as stated recently by Martinoty et al. In contrast, elastomers that have been prepared employing the second route show a lower anisotropy of polymer chain conformation and can be described well with the Gaussian rubber elasticity theory. Both LSCEs will therefore differ strongly, e.g., in their mechanical properties, their swelling behavior, and their spontaneous length change at the LC-isotropic phase transformation [93, 94].

4.1.1 Coupling to the Chain Anisotropy

The orientation of polydomain polymers by mechanical or viscous flow fields can be achieved easiest if a macroscopic chain anisotropy that coincides with the local symmetry of the LC phase structure is induced and fixed by chemical crosslinking. For nematic or S_A main chain polymers which locally show a prolate (see Sect. 3) chain anisotropy, a uniaxial deformation leads to a globally prolate chain conformation. If the chain conformation of the LC polymer is locally oblate, a globally oblate chain conformation can be induced by either uniaxial compression or – equivalently – biaxial stretching of the sample (Fig. 9).

In some cases it is also possible to induce a global chain conformation of the LSCE opposite to the local chain conformation of the polymeric starting material which will be discussed for cholesteric and smectic-A side chain elastomers.

In the following, several examples of the preparation of LSCEs will be given. For selected preparation techniques we will also discuss some practical aspects which are important to produce high quality elastomer samples. The examples are ordered according to their different phase structures.

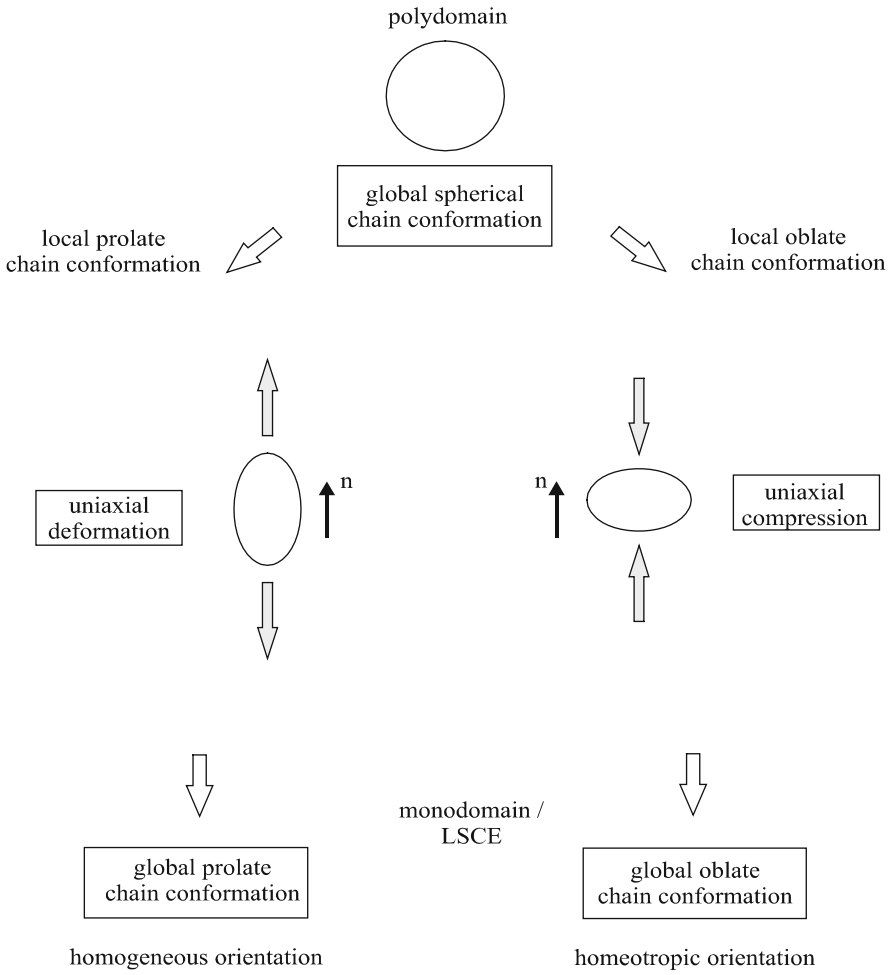

Fig. 9 Formation of monodomains from LC elastomers by using mechanical fields for the case of locally prolate (*left*) and locally oblate (*right*) chain conformation of the polymers

Nematic LSCEs

The simplest way to prepare nematic LSCEs from locally prolate polymers which bear, e.g., photo-crosslinkable side-groups, is to draw manually a fiber from the polymer melt and to photo-crosslink afterwards [95]. A more sophisticated version of this approach is, for example, the electrospinning of LC fibers from a polymer solution with subsequent crosslinking [32]. A one-step network formation during the spinning process has so far only been reported for thermoplastic LC elastomers, in which the fast occurring phase separation of crystalline segments drives the physical crosslinking [96]. LSCEs that can be obtained from fiber spinning/drawing methods

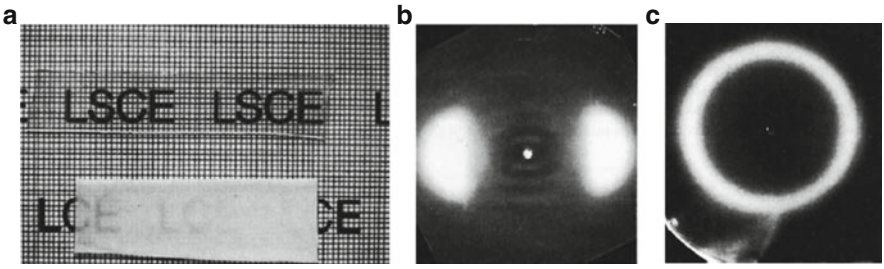

Fig. 10 Photographs of oriented and unoriented nematic elastomers (**a**) and corresponding X-ray patterns of the monodomain (**b**) and the polydomain (**c**) sample [92]

are usually restricted in their dimensions. Larger elastomer samples have only been described for uniaxially drawn films of a very viscous and robust photo-crosslinkable main chain polymer [32]. However, comparatively thin samples can be well obtained with the described methods and can be useful for some applications.

A reliable route to globally prolate, large-area LSCEs of variable film thickness provides the two-step crosslinking procedure introduced by Küpfer et al. [92], in which a lightly crosslinked gel is oriented in the nematic state by applying a uniaxial mechanical field followed by a second crosslinking step in order to fix the induced orientation. Figure 10 shows a stretched monodomain elastomer prepared with the Küpfer method and an unoriented polydomain elastomer as well as the corresponding X-ray patterns.

This robust synthetic approach has frequently been used to produce LSCEs in the last few years as it works well for side chain as well as main chain elastomers. It is also applicable for polymer networks of different LC phase structures (smectic, cholesteric, lyotropic hexagonal) as long as they exhibit prolate chain conformations. We will therefore give a more detailed description in the following paragraphs.

In the first step a lightly crosslinked polymer gel is prepared using a one-pot reaction in isotropic solution, e.g., a hydrosilylation reaction to yield side chain or main chain elastomers (see Sects. 2.1 and 2.2). A spin-casting technique can be deployed in order to prepare elastomer films of homogenous thickness. This is necessary for detailed investigations of the mechanical properties of LSCEs as local variations in the film thickness can lead to non-uniform stress distributions and the formation of neckings or ruptures. Such uniform films cannot usually be obtained by simply casting the reaction mixture into a mold (early attempts to cast elastomers on the very flat surface of liquid mercury were discarded for obvious reasons). With a typical spin-casting setup, films of about 15 cm length, 1–2 cm width, and 80–900 mm thickness are accessible.

In order to produce LSCEs, the crosslinking/casting reaction is interrupted before completion. At that time a lightly crosslinked gel is obtained which is swollen with organic solvent and thus isotropic. A macroscopic orientation can now be induced by deswelling the gel under uniaxial mechanical load at room temperature. The gel is removed from the casting setup, hung vertically, and has a

load attached (Fig. 11). Upon deswelling the elastomer slowly becomes liquid crystalline and the uniaxial mechanical stress induces a macroscopic orientation of the nematic director. After complete alignment, the crosslinking reaction is finished at elevated temperatures. This "second crosslinking step" has to be carried out deeply enough in the nematic phase, as the crosslinking temperature has significant impact on the crosslink topology and in the vicinity of $T_{n,i}$ a more disordered state is fixed.

Compared to approaches based on crosslinking of aligned LC prepolymers (Sect. 4.1.2), LSCEs with rather complex crosslinking histories are obtained. This is important to consider when discussing chain anisotropies, effects of random disorder, or pretransformational effects.

In the following, a detailed description of the two-step crosslinking procedure, including many practical details that proved to be useful in order to obtain high quality samples will be presented. Readers not interested in experimental details can proceed below.

The spin casting process can be carried out in a heatable centrifuge using a spinning cell of the desired sample dimensions. It is advisable to cover the inner wall of the cell with a strip of poly(tetrafluoroethylene) foil (Teflon) in order to avoid adherence between the casted elastomer film and the wall and allow for easy removal. The ends of the strip should not overlap and they should be marked so that they can be recognized easily after synthesis.

For side chain elastomers, the reactants – mesogens, crosslinker, and prepolymer – are dissolved in a minimum of solvent. Toluene is a good choice as it evaporates slowly at room temperature and thus leaves enough time for the orientation of the swollen polymer gel. For a hydrosilylation reaction the solvent needs to be thiophene-free because otherwise the platinum catalyst is inhibited. Before use, toluene has to be washed with concentrated sulfuric acid and distilled several times. If one of the components is insoluble in toluene, dichloromethane, or tetrahydrofuran also give good results. Both can be used at analytical purity without prior distillation. However, the orientation process usually becomes more difficult for solvents with low vapor pressure. If polymeric crosslinkers are used, it is advisable to dissolve the mixtures overnight. To start the hydrosilylation reaction, the catalyst is added to the clear solution of the starting materials. Next, the mixture is transferred into the centrifuge cell through a millipore filter in order to remove dust particles or other insoluble impurities. As a catalyst, a solution of dichloro(1,5-cyclooctadiene)platinum-II in dichloromethane (5–15 μL, 1.0 wt%) is used. The catalyst has been developed for the insertion of terminal C=C double bonds into the Si–H bond for vinylic spacers (except for allylic spacers). It provides a fast conversion at moderate temperatures ($T = 60$ °C) with a minimum of side reactions. Higher quantities of catalyst or aged catalyst solutions result in a brown color of the elastomers. If a catalyst with a higher reactivity is required, solutions of hexachloroplatinum acid can be used.

For main chain elastomers, a proper preparation of the reaction mixture is crucial as volatile reactants are often involved and the exact stoichiometry has to

be kept in order to obtain high molecular weight products. Therefore, non-volatile reactants are weighed first before adding more volatile starting materials. For the synthesis of main chain elastomers based on a hydrosilylation reaction, 1,2-dihydrotetramethyldisiloxane has often been used as co-monomer, as it acts as flexible chain extender. Owing to its very low vapor pressure it should be added quickly to the glass vessel after the mesogen and crosslinker. It is used in slight excess and then left to evaporate until the excess to stoichiometric conditions is about 2%. Then the solvent is added and after all components are dissolved the mixture is quickly transferred to the centrifuge cell (it is often better to do that without prior filtration). The slight excess of the chain extender is needed to compensate for the loss due to evaporation during the transfer of the solution. If there are problems in dissolving the mesogen quickly in the solvent used, it is advisable to recrystallize it in an appropriate solvent and cooling rapidly using an ice-bath so that small, fluffy crystals are obtained.

After the reaction mixture has been transferred into the centrifuge cell, it is spun at 5,000 rpm and an interior cell temperature of 60 °C. For the reaction time of the first crosslinking step, the minimum time to obtain a stable gel film at the cell's wall is chosen. This minimizes the number of crosslinks formed in the isotropic state. The film has to be mechanically stable enough to be removed from the Teflon support and to be loaded with a small weight, e.g., a paper clip. It should not be too sticky and it should not be possible to draw fibers from the elastomer film. The reaction time usually has to be optimized for each system and can range from 45 min to 24 h. At a given temperature it basically depends on the purity of the starting materials and the crosslinker concentration used. Especially after longer storage times it is advisable to recrystallize mesogens and crosslinkers followed by drying in vacuo in order to remove impurities and humidity.

In order to interrupt the crosslinking/casting reaction the cell is removed from the centrifuge and cooled for about 30 s in liquid nitrogen to room temperature. This is preferable to water cooling since traces of water can prevent the proceeding of the reaction when they happen to get into the gel. If no stable gel is obtained the crosslinking reaction under spinning is continued. One has to be very careful to add more catalyst to the reaction mixture, as close to the gel state this can cause heterogeneous reactions.

Once the reaction is successful, the elastomer strip is loosened from the centrifuge wall with the non-cutting side of a thin lancet. The elastomer film is carefully removed from the cell together with the Teflon support and cut into smaller (usually two or three) pieces. For cutting the swollen polymer gel the best method is to use a carpet knife and a hammer. That way, a clean cut of both the gel and the Teflon band is achieved. It is useful, especially if working with sticky side chain elastomers, to keep some toluene at the preparation table to clean the tools before reuse. If possible, both long rims of the film should also be cut with a carpet knife, because small defects at the rim can

(continued)

cause the elastomer to break when later a mechanical load is applied during the orientation process.

In order to remove the cast elastomer film from the Teflon support, a strip of Kapton based adhesive tape is fixed at one end of the swollen gel. Kapton is used as it can withstand high temperatures and is stable towards organic solvents. The film is now removed from the support by slowly pulling the tape. In some cases it is useful to rinse the space between the elastomer film and the Teflon foil with toluene. The elastomer film is fixed at a metal holder and hung vertically. At the lower end of the film a small load, e.g., a paper clip, is attached and held steady with Kapton tape from both sides (Fig. 10).

Some elastomers cannot be prepared as described above because they are too sticky or mechanically not stable enough. This often holds for side chain side-on elastomers, for elastomers with mesogens carrying ethylene oxide or fluorinated chains, or for very low crosslinking densities. In that case the gels can be prepared over a liquid nitrogen bath. The gel is frozen to the glassy state while the Teflon still remains flexible at this temperature, allowing for an easier removal. For this procedure, a small Dewar is filled with liquid nitrogen and a cork ring is placed inside. On the cork ring a PVC Petri dish is placed with the rim facing downwards. The elastomer film is put on the Petri dish with the Teflon foil facing the Petri dish. After the gel is frozen (test with tweezers) the sample ist turned over and the Teflon foil is removed using a pair of tweezers. In the case where the electrostatic interaction is too strong, one can earth oneself during preparation. Then two strips of Kapton are attached to the ends of the film and thereby warmed with one's thumbs, because they are not sticky in the cold. One of the Kapton strips should already have a paper clip attached because the Kapton tends to curl in the cold and it is difficult to attach the clip afterwards. The film is then attached to the holder and fixed with additional Kapton strips as described above.

For the orientation process, the load is increased successively. For nematic elastomers one typically waits until the gel becomes slightly turbid before more load is applied. For nematic side chain elastomers the load needed to orient the film ranges between 300 mg and about 4 g. For nematic main chain elastomers, loads of about 100 g are often used. It is useful to leave nematic elastomers under load overnight so that they become stable enough for further crosslinking in the oven. Before putting the elastomers in an oven to perform the second crosslinking step, the load should be reduced to the minimum necessary to induce a uniform orientation. The elastomers are typically crosslinked in an oven at $T = 60\ ^{\circ}\mathrm{C}$, the optimum temperature for the catalyst. However, one should be careful not to crosslink at temperatures too close to T_{ni} because this leads to disorder in the elastomer. The elastomers are usually left in the oven for 1 week to ensure complete reaction and good reproducibility.

After complete crosslinking, the elastomer is carefully extracted with a good solvent as described in Sect. 2.3.

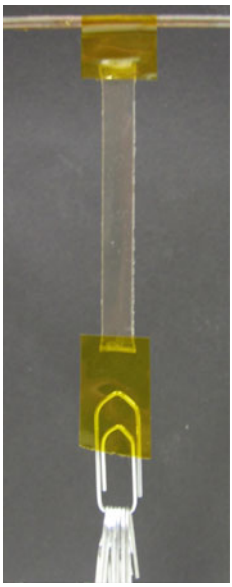

Fig. 11 Photograph of the LSCE preparation according to the two-step crosslinking procedure under mechanical load after Küpfer. The elastomer strip is fixed using Kapton adhesive tape

To orient nematic elastomers showing locally an oblate chain conformation, the same basic ideas presented above can be applied. In order to produce a monodomain, a global chain conformation consistent with the local phase symmetry has to be induced. Therefore, a biaxial mechanical deformation is deployed, which causes uniaxial compression of the film thickness and produces a homeotropically aligned sample with a globally oblate chain conformation. Biaxial mechanical stretching is, however, experimentally very complicated. It is difficult to stretch an elastomer strip uniformly in two directions. Only small sample sizes are accessible as quadratic elastomer sheets have to be deformed. Moreover, the strong boundary conditions at the edges allow for a uniform orientation only in the very center of the sample. Not to mention that it is a very delicate operation to clamp a swollen elastomer sample for such a procedure. A more accessible technique to realize uniaxial compression based on anisotropic deswelling has been introduced for cholesteric elastomers and will be discussed in the next section (Fig. 12).

Cholesteric LSCEs

Since a cholesteric phase is a twisted nematic phase, the local director n is not constant in space but helically arranged perpendicular to an axis, usually referred to as the z-axis. For a nematic polymer with locally a prolate chain conformation, the helicoidal arrangement of n in the z-direction will cause an overall oblate network conformation. As described above for nematic elastomers, a uniaxial compression of the elastomer film can be used to achieve a global network conformation that is

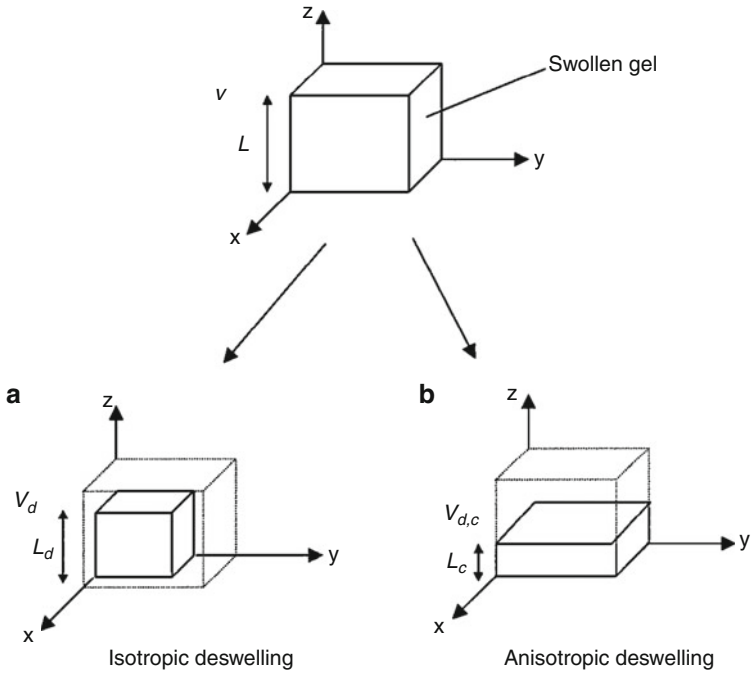

Fig. 12 Schematic representation of deswelling processes of LC gels. Figure taken from [72]

consistent with the helicoidal structure of the cholesteric phase. This deformation can be realized experimentally by using an anisotropic deswelling technique as described by Kim et al. (Fig. 12) [72]. Analogous to the classical two-step crosslinking procedure, a lightly crosslinked elastomer film swollen with a solvent is produced by a spin-casting technique. In a second step the solvent is slowly evaporated under centrifugation. Ordinarily, such a deswelling process would be isotropic. The network deswells simultaneously in all dimensions and the spherical shape of the chain conformation of the network strands is not affected. However, during centrifugation in a confined cell the film can only deswell in one direction – the film thickness (z-direction) – while the other two dimensions are defined by the experimental setup and remain unchanged. This anisotropic deswelling effectively exposes the elastomer film to a uniaxial compression and induces a uniform homeotropic orientation of the cholesteric helix, while finishing the crosslinking process.

In the following box a detailed description of this preparation technique is presented, including some practical details.

In the first step a lightly crosslinked gel is prepared according to the spin-casting procedure described above for nematic elastomers. Instead of removing the elastomer strip from the centrifuge cell and applying a uniaxial load, two screws in the cover plate of the cell are removed after 2 h of reaction time in order to create small windows through which the solvent can slowly

evaporate. The spinning is continued at elevated temperatures ($T = 65$ °C) and the crosslinking process proceeds during the deswelling of the elastomer film for more than 5 h. Afterwards the film is removed from the centrifuge cell and cured at elevated temperature in the LC state for several days to complete the crosslinking reaction. Usually the dry polymer networks stick strongly to the Teflon support foil but can be removed carefully when cooled below the glass transition temperature above a liquid nitrogen bath (see above).

A significant drawback of this procedure is that the orientation process strongly depends on the swelling properties of the polymer networks. Usually the experimental conditions have to be varied when the chemical constitution of the elastomer is changed. A precondition for a successful orientation is a sufficiently high degree of swelling ($q = q_x \cdot q_y \cdot q_z > 3$) in the used solvent. Toluene has been shown to be a good solvent for most LC polymers and it is especially useful for the anisotropic deswelling procedure as it possesses a high vapor pressure. However, using this technique for some LC polymers, e.g., smectic side chain polymers carrying perfluorinated tails, the degree of swelling in toluene appears to be too low to obtain a good orientation. In those cases the utilization of more polar solvents ($CHCl_3$ or THF) might be reasonable. Besides the solvent, the temperature used for the deswelling process plays a crucial role. On one hand the evaporation of the solvent has to be sufficiently slow in order to achieve a uniform orientation over the whole sample. Especially at high reaction temperatures ($T > 70$ °C) gradients in the orientation become more severe. On the other hand the crosslinking reaction speeds up upon deswelling and the swelling capacity of the gel decreases. If the solvent does not evaporate fast enough to match the equilibrium degree of swelling, the uniformly formed elastomer film may collapse under the mechanical stress. This becomes an issue especially for the synthesis of elastomers with high crosslinking densities. Finding the right reaction parameters can therefore be a time-consuming and challenging task.

Cholesteric polymers with locally oblate chain conformation can be obtained when a short flexible spacer between backbone and rigid mesogenic moiety consists of an even number of atoms. In this case, an allyloxy-substituted mesogenic group is normally used for the hydrosilylation reaction. To get a uniform orientation of the helicoidal z-axis of the cholesteric structure, an overall prolate chain conformation is necessary. This can easily be achieved by applying a uniaxial mechanical field in direct analogy to the preparation of nematic LSCEs having a locally prolate chain conformation. Cholesteric LSCEs are obtained with the helix axis parallel to the stretching direction, as directly observable by the selective reflection of the elastomer's cross-section (Fig. 13).

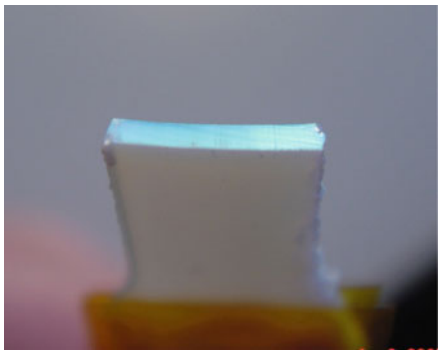

Fig. 13 Cholesteric LSCE having a locally oblate chain conformation. The helicoidal *z*-axis is ordered parallel to the elongation axis [73].

Smectic-A LSCEs

In the smectic-A phase, classical side chain polymers with end-on attached mesogenic units prefer an oblate chain conformation, where the polymer chains are on average located between the smectic layers. Consequently a uniaxial stretching is usually insufficient to achieve a simultaneous orientation of the director and the layer normal (see Sect. 3). Nishikawa et al. demonstrated that the anisotropic deswelling technique can be used to synthesize S_A LSCEs with homeotropic alignment, i.e., a uniform orientation of the layer normal and the director perpendicular to the film plane [74]. A detailed description of this preparation technique as well as some experimental remarks have been given in the previous section. It should be pointed out that this orientation procedure is rather complicated and involves a lot of work in optimizing the experimental conditions. However, it allows the synthesis of rather thick bulk samples (up to 600 μm) whereas conventional strategies to prepare homeotropically aligned elastomers are limited to thin film geometries.

As already discussed for nematic elastomers in Sect. 3.2, for a successful orientation using mechanical fields it is important to consider the chemical constitution of the whole polymer network. While the equilibrium conformation of smectic side-chain elastomers is oblate, this local symmetry and therefore the orientational behavior can change drastically for high crosslinking densities. If the length of the crosslinking unit exceeds the length of the siloxane backbone between two network junctions, the crosslinker itself becomes part of the polymer main chain. This changes the local orientation between polymer main chain and mesogenic units, and uniaxial mechanical fields become sufficient to induce a macroscopic orientation.

The alignment of S_A side chain elastomers with end-on attached mesogenic units becomes much simpler if a nematic phase exists in a temperature range between the smectic and the isotropic state. Nishikawa et al. reported the synthesis of an S_A LSCE by applying a uniaxial mechanical deformation to a coelastomer, which showed a narrow nematic phase region at high temperature [76]. Upon deswelling under uniaxial load analogous to Küpfer's procedure, the elastomer becomes initially nematic and the deformation induces a macroscopic orientation of the

director. Subsequently, transition to the smectic state occurs and uniformly aligned layers are built up. By deploying a second crosslinking step this macroscopic orientation can be fixed permanently. In contrast to the anisotropic deswelling technique, this subsequent orientation of the director and the layer normal induces globally a prolate chain conformation, which is inconsistent with the equilibrium conformation of the smectic polymer melt. By variation of the composition in coelastomers of smectogenic and nematogenic side-chains, it is possible to induce systematically this specific phase behavior. With increasing fraction of nematogenic side chains, the stability of the smectic phase decreases and for a certain composition range the phase sequence smectic-A, nematic, isotropic is observed. Inducing a macroscopic orientation then becomes easy by applying uniaxial mechanical stretching. Of course, the mesogenic side chains must possess a flexible spacer with an odd number of spacer atoms or a long spacer ($x > 7$) to give locally a prolate chain conformation in the nematic state. This synthetic concept is very robust and works for a wide range of chemical constitutions, including smectogenic side chains carrying perfluorinated tails [75, 77].

In contrast to classical side chain elastomers, smectic-A main chain elastomers exhibit prolate chain conformations. Consequently, macroscopically oriented samples can be prepared according to the method of Küpfer et al. utilizing a second crosslinking step under uniaxial deformation [31]. Analogous, S_A LSCEs based on side chain elastomers with side-on attached mesogenic units can be prepared [97].

In general the practical aspects presented in detail for nematic elastomers can be used for the synthesis of S_A LSCEs as well. However, a few additional remarks will be given in the following box.

While deswelling under uniaxial mechanical load is performed at room temperature for nematic elastomers, this procedure is usually not applicable for smectic side-chain elastomers. Especially for elastomers carrying partially fluorinated mesogenic side-chains, the deswelling occurs too fast to allow for a good orientation of the layer normal and the director. As soon as the smectic state is reached the layer planes can couple to the mechanical field and a uniaxial mechanical deformation becomes insufficient to produce a monodomain elastomer (see Sect. 3.2). It is therefore advisable to perform the deswelling at elevated temperature. The elastomer is heated to the isotropic state under uniaxial load until most of the solvent is evaporated. Afterwards it is slowly cooled to a temperature slightly below $T_{n,i}$, detectable by a spontaneous length change. The load is successively increased until a perfectly transparent sample is obtained. After 2 h of crosslinking in the nematic state, the elastomer is cooled to the smectic state and the crosslinking reaction is completed over several days. In the smectic phase the load can be further increased if necessary, as the elastomers can now stand much higher mechanical stress.

Alternatively, the orientation can be carried out at room temperature in a chamber saturated with toluene vapor. This is achieved by placing a few drops of toluene in a chamber of suitable size. After the chamber is filled with

(continued)

toluene vapor the loaded elastomer samples are placed inside. By slightly opening the chamber the deswelling time can easily be controlled. After the orientation is completed, the second crosslinking step is performed at elevated temperature, preferably in the smectic phase.

Lyotropic Elastomers

For the macroscopic orientation of lyotropic elastomers in mechanical fields the same principles as for thermotropic elastomers can be applied. In some ways the situation is even simpler as the rod-like micelles of the hexagonal phase are compatible with an overall prolate network chain conformation. In addition, the lamellar phase built up from disk-like micelles requires an overall oblate chain conformation to form a liquid single-crystal hydrogel (LSCH) [98].

Locally oblate lyotropic elastomers with lamellar phase structure (L_α-phase) can be oriented by uniaxial compression, as outlined above for thermotropic smectic-A elastomers. Fischer et al. synthesized crosslinked polysiloxane elastomers carrying non-ionic amphiphilic side-groups attached with their hydrophobic end to the polymer backbone. They were able to compress elastomer samples between Teflon half-cylinders to about half of their original thickness. The orientation of the phase structure – except for some unoriented domains – was demonstrated by means of ^{2}H-NMR spectroscopy on the directly deuterated samples as well as by X-ray scattering. The preferred orientation of the director, and hence the amphiphilic side chains, was found to be parallel to the axis of compression with the amphiphilic bilayers aligned perpendicularly [98, 99].

Permanently aligned lamellar networks were prepared by fixing the ordered structure in a second crosslinking step employing the anisotropic deswelling technique. The globally oblate orientation of the polymer chains was fixed in the isotropic state in the two-step crosslinking procedure. Subsequent swelling of the fully crosslinked elastomer with water allowed for the formation of well-ordered disc-like micelles as proven by X-ray scattering [100].

Lyotropic elastomers with an H_1 phase exhibit locally a prolate chain conformation in which cylindrical micelles are hexagonally packed. They can be oriented, for example, by placing a strip of the dry elastomer in a cylindrical glass tube and adding a defined amount of water from both sides. The capillary is then sealed and annealed for several days to achieve equilibrium conditions. The elastomer strip can only swell in one direction. As this uniaxial deformation is consistent with the uniaxial phase structure of the hexagonal phase a uniform orientation of the long micellar axis in the direction of the applied field (parallel to the glass walls) can be achieved. This has been directly proven by X-ray scattering as presented by Löffler et al. [101].

Weiss et al. were able to orient a hexagonal epoxy-amine elastomer by applying uniaxial strain yielding high degrees of order. The elastomer was crosslinked in the isotropic state and successively swollen with water to give a hexagonal phase [102].

4.1.2 Coupling to LC Properties

In this section some selected examples for the orientation due to surface effects and magnetic and electric fields will be presented. Elastomers oriented using the anisotropic physical properties of the liquid crystalline phase structure are usually restricted to thin films, except for lyotropic samples and when extremely high fields are available. Typically, a thin film of a linear LC polymer or a reactive mixture of low molar mass LC and crosslinker is aligned by using surface effects, magnetic fields, or electric fields and subsequently photo-crosslinked. This method has been widely used for side chain polymers, which show low viscosities, allowing good orientation at moderate field strengths. Main chain polymers exhibit much higher viscosities and thus it is usually very difficult to achieve good alignment.

An advantage with respect to the methods discussed in Sect. 4.1.1 is that a homogeneous or homeotropic orientation of the mesogens can be chosen independently of the chain conformation. For the orientation in an electric or magnetic field it has to be considered that the mesogens must have a suitable anisotropy of the dielectric constant and the diamagnetic susceptibility, respectively.

The orientation achieved by the methods discussed in this section is sometimes, especially in the case of cholesteric elastomers, much better than for the thick films prepared by coupling to a mechanical field.

The orientation of the LC polymer films is usually carried out between treated glass slides. Consequently the orientation process, the existence of defect structures and variations in orientation, as well as boundary effects can be directly visualized by means of polarizing optical microscopy.

Orientation Due to Surface Effects

In order to minimize the energy at its surface, thin films of monomeric and polymeric material often form nicely ordered liquid crystalline monodomains on surfaces. This happens spontaneously especially for smectic-A and cholesteric films and can be promoted by coating of the surfaces and by annealing the sample. Annealing is usually done a few Kelvin below $T_{LC,i}$, often after slowly cooling from the isotropic phase, so that the mesogens are mobile enough to organize themselves at the surface.

Urayama et al. were able to synthesize a nematic elastomer with homeotropic orientation of the mesogens employing surface effects. They started from a mixture of a reactive acrylate-monomer, the crosslinker 1,6-hexanediol diacrylate, a photoinitiator, and a non-reactive nematogen that is necessary to broaden the temperature range of the nematic phase. This mixture was sandwiched between two polyimide coated glass plates that were separated by spacers and induce a normal alignment of the mesogens. After photo-polymerization the resulting film was detached from the glass substrate by immersing the cell in dichloromethane. The swelling in dichloromethane also washes out unreacted and nonreactive

material. To deswell the film, methanol was gradually added and the film was subsequently dried in air [13].

Homogeneously planar oriented nematic elastomers have been prepared using a procedure very similar to that presented above. As alignment layers, unidirectionally rubbed polyimide or rubbed poly(vinyl alcohol) were used [14].

Cholesteric films that were prepared using surface interactions show substantially improved optical properties in comparison with samples obtained by the anisotropic deswelling method (Sect. 4.1.1). This is indicated by much lower threshold intensities in lasing experiments [103].

A widely used preparation method has been introduced by Komp et al. and consists in annealing a photo-crosslinkable polymer in the vicinity of the cholesteric to isotropic phase transition temperature T_{ci} between glass plates coated with a sacrificial layer of water-soluble polymer over two days. Thereafter a well-ordered Grandjean texture is obtained [19]. The content of mesogens with odd and even spacers can be changed to vary systematically the main chain conformation from prolate to oblate [104]. The orientation via surface effects is especially suitable for S_A elastomers. In very thin films the lamellar phase structure prefers homeotropic alignment with the layer planes parallel to the solid substrates. In early experiments, linear side chain polymers were spin-coated onto a sodium chloride substrate and were found to align spontaneously. Photo-initiated radical crosslinking in the smectic-A phase and subsequent dissolving of the substrate in water produced thin free-standing elastomer films of 2–3 μm thickness [105]. Subsequently, films with locally varying film thickness in the sub-micron range were drawn from the isotropic melt on a metal frame, followed by UV crosslinking in the smectic phase. Complex sample geometries have also been realized, e.g., free-standing elastomer balloons by expanding thin smectic polymer films (2–3 μm) from a glass capillary [106].

A rather different approach to utilize surface effects for the orientation of smectic elastomers is radical crosslinking of liquid crystalline polymers using a dispersion or miniemulsion technique in a mixture of solvent and surfactants. Crosslinked smectic-A colloids were prepared in sizes of 100–200 nm showing highly oriented phase structures that could be visualized directly in transmission electron microscopy [107].

Orientation in a Magnetic Field

Nematic photo-crosslinkable polymers [108] and reactive monomer mixtures [109] can be easily oriented in a magnetic field. Due to their diamagnetism the mesogens usually orient parallel to the magnetic field in the LC phase.

Figure 14 shows an example of the preparation of a homogeneously oriented free-standing polymer film. A microscope slide is coated with a water-soluble sacrificial layer such as poly(2-ethyl-3-oxazolin) (PEOx) from an ethanol solution. The polymer and two spacers of the desired thickness are placed on the glass slide and successively covered with a second glass slide that is also coated with PEOx. In that state, it is a bit

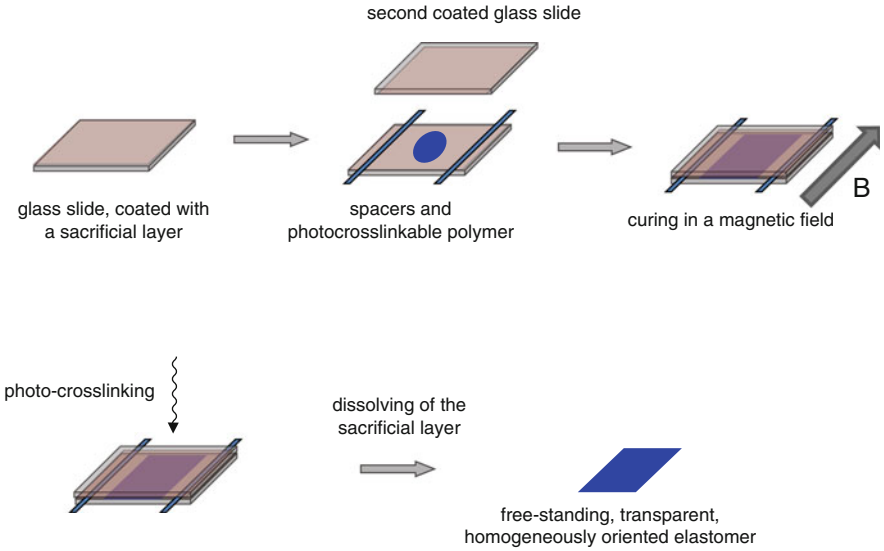

Fig. 14 Schematic representation of the preparation of thin free-standing elastomer films by orienting in a magnetic field

delicate to avoid the formation of air-bubbles, which of course complicate measurements on the films later. It usually helps to lower the second glass slide from one side of the film and to keep the temperature rather high so that the polymer is relatively fluent. It is also advisable to heat the LC polymer for one night in vacuo prior to preparation in order to remove solute gases. However, this should not be done too often as the photo-crosslinker is sensitive to thermal degradation. The sandwiched polymer is placed in a magnetic field (1.8 T, produced by an electromagnet; for a reactive monomer mixture a strong permanent magnet can be sufficient) and slowly cooled from the isotropic to the nematic phase. Subsequent annealing in the magnetic field for several days minimizes surface defects that usually occur.

After removing the sample from the magnetic field the polymer is photo-crosslinked from both sides (a few minutes are sufficient) using a UV-lamp. If T_g is relatively low it can be helpful to photo-crosslink under cooling with an ice-bath so that the mesogens do not reorient due to the heat produced by the UV-lamp. The sandwiched film should now be transparent and can be removed from the glass slide after dissolving the sacrificial layer in water.

Lyotropic liquid crystalline elastomers can be oriented in a magnetic field when they contain rod-like amphiphiles with an aromatic core. This structural element is usually needed to achieve a sufficiently large diamagnetic anisotropy. It has been demonstrated that reactive mixtures of methacrylate monomers, bifunctional crosslinkers, and (deuterated) water in the strong field of an NMR-magnet (7–11 T) can be oriented by slowly cooling from the isotropic phase to the lamellar mesophase and subsequent annealing in the biphasic region. The process of orientation can thereby be nicely followed by NMR spectroscopy [110, 111].

Orientation in an Electric Field

Free-standing nematic LSCE films can be prepared analogous to the procedure shown in Fig. 14 utilizing electric fields. Glass substrates covered with translucent indium tin oxide (ITO) are used to apply alternating electric fields (3 V/μm, 1 kHz). This is sufficient to induce homeotropic alignment of the LC phase structure in elastomer films of thicknesses up to 50 μm. A precondition for this method is the availability of photo-crosslinkable polymers that contain mesogens with a positive anisotropy of the dielectric constant, e.g., with terminal cyano groups. It is important to use relatively long spacers for these polar mesogens in order to achieve sufficient decoupling from the polymer backbone, allowing them to follow the electric field [93].

Electric fields have also been used to prepare freestanding chiral smectic-A* LSCEs with homogeneous alignment of the layer normal and the director in the film plane. An ITO covered glass cell was coated with rubbed polyimide and rubbed polyvinyl alcohol as sacrificial layer and filled with a eutectic mixture of smectic acrylate monomers and bifunctional acrylate crosslinker. The mixture was heated to the isotropic state and cooled to the S_A^* phase, while applying an alternating electric field (6 V/μm, 0.5 Hz, square wave). After successful alignment, the electric field was turned off followed by UV photo-polymerization. Dissolving the sacrificial layer in water yielded a free-standing film of 60 μm thickness [112].

Orientation in electric fields is in particular useful for S_C* elastomers as their mesogenic units usually possess a strong dipole moment. LC polymers with crosslinkable acrylate side-groups were filled into commercially available ITO cells with 10 μm electrode separation and heated into the S_C* phase. A macroscopic orientation was induced by applying an alternating electric field (100–200 V, 1–5 Hz) and performing several heating and cooling cycles around the S_C^*–S_A^* phase transformation. In order to fix the monodomain structure permanently, a DC electric field was applied before UV-initiated radical crosslinking of the sample [113]. Using this method, ferroelectric elastomers have been prepared with a nearly perfect homogeneous orientation and a polar axis perpendicular to the glass substrate [15, 22].

4.2 More Complex Orientation Methods

If LSCEs are prepared using one of the methods described in Sect. 4.1, a monodomain may be obtained with respect to the main director but not necessarily for the whole phase structure. In the case of S_C elastomers an orientation of the director by mechanical stretching or by external fields yields a polydomain with respect to the layer normal. The additional orientation steps that are necessary for a full orientation of this phase are outlined in Sect. 4.2.2.

Biaxial nematic or S_A elastomers lack rotational symmetry around their molecular long axes and the orientation of the three axes is described by the additional minor director *m*. A third director *l* is thereby automatically defined. Figure 15 gives a schematic representation of a uniaxial and biaxial nematic phase. The orientation methods discussed in the previous section yield polydomains with respect to the

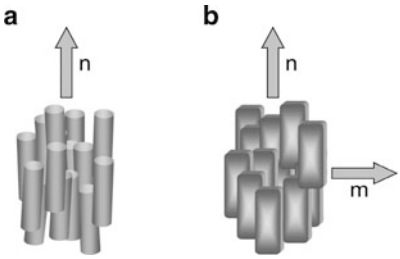

Fig. 15 Schematic representation of the uniaxial (**a**) and biaxial (**b**) nematic phase [4]

minor director. Additional orientation steps are necessary to obtain elastomers with a 3D orientation of the mesogenic axes. Such a 3D monodomain of a biaxial elastomer has not yet been reported, but some potential strategies to obtain such an elastomer will be outlined in Sect. 4.2.1.

4.2.1 Orientation of the Second Director

Over the last few years, significant evidence has been obtained that nematic [4] as well as S_A [9] elastomers can show phase biaxiality over a broad temperature range. A biaxial-nematic phase from 15 °C to about 70 °C was found by means of ^{2}H-NMR spectroscopy on a directly deuterated side chain end-on elastomer prepared by the Küpfer-procedure [4].

After preparation, the minor directors form a polydomain, which can be oriented in the magnetic field of the NMR-experiment. A reorientation of the major director does not occur because this orientation is fixed in the polymer network. If a nematic or S_A elastomer is prepared to yield a homeotropic film, the differently oriented domains can be directly observed by optical methods. Strain-dependent optical investigations give evidence that the minor director can be oriented using a mechanical field.

To produce a monodomain with respect to the orientation of all three molecular axes, an additional orientation step is required. If the elastomer is prepared by orienting the major director of a photocrosslinkable polymer in an electric field, one could think about simultaneously orienting the second director by surface effects, e.g., with a rubbed PI-surface. For orientation by biaxial deswelling an S_A elastomer, an additional crosslinking step under uniaxial strain on the not yet completely crosslinked elastomer could also lead to the orientation of the minor director.

Such a monodomain has as yet not been produced and it is also not clear whether the orientation of the minor director could be permanently fixed in the polymer network or whether it would relax to a polydomain state after some time. Another question is the behavior after heating to the isotropic phase.

4.2.2 Orientation of the Layer Normal in S_C LSCEs

Smectic-C elastomers and especially chiral S_C* elastomers have attracted a lot of interest as they can respond to electric stimuli or transfer mechanical stress into electrical signals. Owing to the C_2-symmetry, chiral smectic-C* phases show

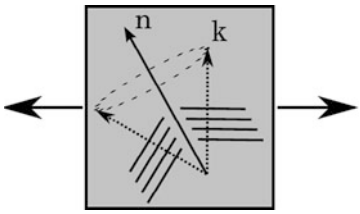

Fig. 16 Smectic-C elastomer with uniform director orientation but conical layer distribution subjected to a second uniaxial mechanical deformation under an angle of θ ±90° with respect to the first deformation axis (θ is the S_C tilt angle) [80, 116]

effects like ferroelectricity, piezoelectricity, pyroelectricity, and second harmonic generation [114]. However, a macroscopic polarization represents a high energy state, which – in the absence of external fields – is cancelled out by the formation of helical superstructure. During the external field induced orientation process of S_C elastomers this helix can easily be unwound. With the preparation of S_C LSCEs the macroscopic C_2-symmetry can be fixed permanently and materials are obtained that can be used as electro-mechanical actuators or sensors.

As shown in the previous section, S_C elastomers can be well aligned in electric fields. These preparation techniques are limited to thin film geometries, while mechanical orientation offers the possibility to prepare uniformly oriented bulk samples.

In Sect. 3.2 it was shown that uniaxial stretching or compression of S_C elastomers does not produce macroscopically oriented samples. Due to the S_C symmetry, uniaxial deformation only induces a uniform orientation of the director but leaves the smectic layer normals conically distributed around the stress axis. Usually such elastomers remain opaque. For the preparation of S_C LSCEs a more complex orientation strategy is necessary which can be realized by deploying two successive orientation processes.

In a first step a monodomain sample with respect to the director is produced. This can be done completely analogous to Küpfer's procedure described for nematic elastomers in Sect. 4.1.1. For this a lightly crosslinked elastomer gel that is swollen with solvent is slowly deswollen under uniaxial mechanical load for several hours. Then in the second orientation step a mechanical field has to be applied that induces a reorientation of the smectic layer structure in order to produce a uniform orientation of both the director and the layer normal.

Semmler et al. have shown for S_C* side chain elastomers that a second uniaxial stretching under an angle of θ ±90° with respect to the first deformation axis (θ is the S_C tilt angle) produces a layer reorientation towards the uniform C_2 symmetry of the S_C* phase (Fig. 16). The tilt angle of uniaxially elongated S_C elastomers can easily be analyzed by using X-ray scattering. The smectic layer normals reorient and take up a position more or less perpendicular to the second deformation: Layers which enclose large angles with the mechanical stress axis realign towards orientations enclosing small angles with the axis. However, by this method no real monodomain elastomers have been obtained. The mechanical deformation only

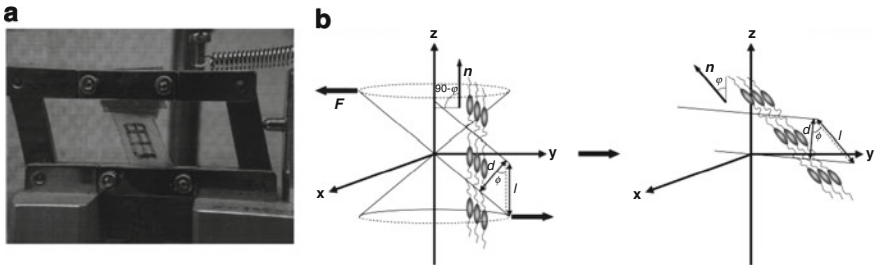

Fig. 17 Smectic-C elastomer with uniformly aligned director but conical layer distribution subjected to shear strain perpendicular to the director [117] (**a**) and corresponding reorientation process that produces an S_C monodomain (**b**). Reprinted with permission from [87]. Copyright (2008) American Chemical Society

leads to an anisotropic distribution of the layer normals on the cone causing a non-centrosymmetric phase structure but cannot induce a completely uniform orientation of both the layer normal and the director. Nevertheless, the partially oriented phase structure can be fixed permanently by chemical crosslinking, yielding highly transparent elastomers which show piezoelectric properties and second harmonic generation [80–83, 115]. The same orientation procedure has also been deployed to align main chain S_C elastomers [116].

A mechanical deformation that is consistent with the biaxial S_C phase symmetry and that is able to induce a macroscopic orientation of the layer normal and the director is a shear mechanical field. Hiraoka et al. prepared side chain S_C* LSCEs by applying a shear deformation perpendicular to the director followed by chemical crosslinking [117, 118]. For this, the uniaxially aligned elastomer with uniformly oriented director but conical layer distribution is mounted into a mechanical shear setup (Fig. 17a). The elastomer is sheared stepwise at room temperature until the shear angle is consistent with the tilt angle of the S_C phase structure. Between each shear step a sufficiently high relaxation time should be maintained to avoid damaging the sample. The mechanical field induces a continuous reorientation of the S_C phase structure where the director rotates towards the shear diagonal, while the layer normal takes up the position perpendicular to the shear mechanical field (Fig. 17b). This multi-step orientation process can take up to several hours. It must be avoided that the chemical crosslinking reaction is completed before a macroscopic orientation is induced. If a hydrosilylation reaction is used, the reaction speed is rather slow at ambient temperature. However, it might be advisable to cool the sample during the orientation process to slow down the crosslinking process and to provide enough time for a successful alignment. The sheared state which corresponds to an S_C monodomain structure can be fixed permanently by completing the chemical crosslinking reaction at elevated temperatures – completely analogous to nematic elastomers. Following this procedure, main chain LSCEs showing S_C and chiral S_C* phase structures have also been realized by Sanchez et al. and Heinze et al., respectively [86, 87, 119].

5 Conclusions and Outlook

The preparation of LCEs comprises sophisticated chemistry that brings together the broad areas of research on macromolecular networks and on liquid crystals. For a successful synthesis it is not sufficient to combine only conventional principles and methods of both fields. In addition specific new features emerge that have to be considered.

Conventional principles and methods concern the synthetic routes for macromolecular networks and the realization of the liquid crystalline state by mesogenic monomer units. Network chemistry has to consider the reactivity and functionality of the monomer units. In most cases, this excludes ionic polymerization techniques and reduces utilizable methods to radical polymerization and polymer analog reactions for side chain networks, and to polycondensation or polyaddition reactions for main chain elastomers. The chemistry of the crosslinking process and the chemical constitution of the crosslinker have to be adapted to the polymerization process. Applying photo-chemistry of suitable functional monomer units opens an additional, versatile pathway to build up the network structure.

The liquid crystalline state can be systematically introduced by rigid anisometric building blocks or by amphiphilic moieties. According to their chemical constitution and basically following the same systematic as known from low-molar-mass liquid crystals, all types of LC phase structure are accessible. Additional aspects to be considered arise from modification of the state of order due to the decreased specific volume of the macromolecules (compared to that of the monomers) and the reduced translational and rotational mobility of the mesogenic units due to their linkage within the macromolecule.

New features to be taken into account for the synthesis of LCEs are (1) the interaction between the LC order and the conformation of the polymer backbone, and (2) the effect of the chemical constitution of the crosslinker on both the local topology of the network and the LC order. The interaction between the LC order and the conformation of the polymer backbone causes a deviation from a conventional statistical spherical coil to an oblate or prolate chain conformation. Without any precautions during the synthesis, LCEs are obtained in a polydomain structure due to maximization of the entropy of the overall chain conformation. The crucial interplay of LC order and conformation of the polymer backbone, however, offers the chance to induce macroscopically an overall anisotropic chain conformation by an external mechanical field. If the symmetry of the mechanical field is consistent with the symmetry of the LC phase structure, a uniform orientation is produced. Introducing an additional chemical crosslinking process, the macroscopic uniform alignment becomes locked-in permanently and a liquid single-crystal elastomer (LSCE) is realized. Alternatively, uniform alignment of LC monomers or linear pre-polymers can be induced by electric or magnetic fields or surface effects. Subsequently, a chemical crosslinking reaction performed in the aligned state yields LSCEs. However, these conventional orientation techniques are limited to very small sample thicknesses.

The macroscopically aligned state of LSCEs is imprinted to the network structure during chemical crosslinking. After heating to the isotropic state and subsequently cooling down to the LC state again, the monodomain structure turns out to be completely reversible. Furthermore, even complex LC structures like biaxial, untwisted, and thus ferroelectric smectic-C LSCEs are accessible if a suitable shear deformation is performed before the final crosslinking step.

The effect of the chemical constitution of the crosslinker on the local topology of the network is the second new feature to be considered. If the crosslinker molecule is flexible it can behave like an isotropic solvent. In that case, essentially only the phase transition and phase transformation temperatures of the LC phase are affected [90]. If, however, the chemical constitution resembles that of a mesogen of the constituent polymer backbone, the history of the crosslinking process becomes important. Under these conditions the crosslinker adopts the state of order in which the final crosslink process of the network occurs and thus determines the local topology of the crosslink [120, 121]. The mechanical properties and the reorientational behavior are considerably modified for networks with the same chemical constitution but crosslinked either in the isotropic or in the liquid crystalline state [122–124]. Other important aspects of the local topology at the crosslink concern the phase transformation behavior [125] as well as the positional ordering in smectic systems [126].

LSCEs offer numerous new aspects to the field of polymer science due to their exceptional physical properties. With respect to mechanical behavior, LSCEs are unique "soft crystals." Mechanical fields not only bias the state of LC order but also cause exceptional reorientation behavior, which impressively modifies the mechanical response. If the LC phase structure additionally exhibits one-dimensional positional long-range order, conventional entropic elasticity exists solely in two dimensions, while the third dimension is determined by the enthalpic elasticity of the LC order.

It is not only the mechanical properties of LSCEs that offer new perspectives for their application and basic research. In fact, all physical properties directly related to the LC order can be influenced by the interaction between mechanics and the state of order of the LC networks. A completely open field is to mimic biological systems in which collective molecular order is responsible for functionality. Lyotropic LSCEs provide one step in this direction. These networks enable ion conductivity [127], which opens the possibility to perform chemical reactions within the network. If, e.g., for a redox reaction, reactants and products modify the LC order differently, a mechanical response will be directly connected. It remains a challenging task for chemists to synthesize new LSCEs that are adapted for such problems.

References

1. Lehmann O (1908) Biologisches Centralblatt 28:31
2. Schätzle J, Finkelmann H (1987) Mol Cryst Liq Cryst 142:85
3. de Gennes PG (1975) C R Acad Sci B Phys 281:101
4. Brömmel F, Stille W, Finkelmann H, Hoffmann A (2011) Soft Matter 7:2387

5. Leube HF, Finkelmann H (1990) Makromol Chem 191:2707
6. Leube HF, Finkelmann H (1991) Makromol Chem 192:1317
7. Severing K, Saalwächter K (2004) Phys Rev Lett 92:125501
8. Severing K, Stibal-Fischer E, Hasenhindl A, Finkelmann H, Saalwächter K (2006) J Phys Chem B 110:15680
9. Storz R, Komp A, Hoffmann A, Finkelmann H (2009) Macromol Rapid Commun 30:615
10. Crawford GP, Broer D, Zumer S (2011) Cross-Linked Liquid Crystalline Systems: From Rigid Polymer Networks to Elastomers. CRC Press
11. Flory PJ (1953) Principles of polymer chemistry. Cornell University Press, Ithaca, p 399
12. Treloar LRG (1975) The physics of rubber elasticity. Clarendon, Oxford
13. Urayama K, Mashita R, Kobayashi I, Toshikazu T (2007) Macromolecules 40:7665
14. Thomsen DL, Keller PN, Pink JR, Jeon H, Senoy D, Ratna BR (2001) Macromolecules 34: 5868
15. Gebhard E, Zentel R (2000) Macromol Chem Phys 201:902
16. Bohnert R, Finkelmann H (1994) Macromol Chem Phys 195:689
17. Amigó-Melchior A, Finkelmann H (2002) Colloid Polym Sci 280:207
18. Schuring H, Stannarius R, Tolksdorf C, Zentel R (2001) Macromolecules 34:3962
19. Komp A, Rühe J, Finkelmann H (2005) Macromol Rapid Commun 26:813
20. Vasilets VN, Kovalchuk AV, Yuranova TI, Ponomarev AN, Talroze RV, Zubarev ER, Plate NA (1996) Polym Adv Technol 7:173
21. Vasilets VN, Kovalchuk AV, Yuranova TI, Ponomarev AN, Talroze RV, Plate NA (2000) Polym Adv Technol 11:330
22. Xia Y, Verduzco R, Grubbs RH, Kornfield JA (2008) J Am Chem Soc 130:1735
23. Ober CK, Jin J-I, Lenz WR (1998) Adv Polym Sci 68:387
24. Greiner A, Schmidt HW (1998) Aromatic Main Chain Liquid Crystalline Polymers. In: Demus D, Goodby J, Grey GW, Spiess H-W, Vill V (eds). Handbook of Liquid Crystals, Wiley-VCH, Weinheim, p 1
25. Sirigu A (1991) In: Ciferri A (ed) Liquid crystallinity in polymers. VCH Publishers, New York, p 261
26. Zentel R, Reckert G (1986) Macromol Chem Phys 187:1915
27. Bergmann GHF, Finkelmann H, Percec V, Zhao MY (1997) Macromol Rapid Commun 18:353
28. Percec V, Asandei AD (1997) Macromolecules 30:7701
29. Wermter H, Finkelmann H (2001) e-Polymers 13:1
30. Krause S, Zander F, Bergmann G, Brandt H, Wertmer H, Finkelmann H (2008) C R Chimie 12:85
31. Beyer P, Terentjev EM, Zentel R (2007) Macromol Rapid Commun 28:1485
32. Krause S, Dersch R, Wendorff JH, Finkelmann H (2007) Macromol Rapid Commun 28:2062
33. Donnio B, Wermter H, Finkelmann H (2000) Macromolecules 33:7724
34. Aguilera C, Bartulin J, Hisgen B, Ringsdorf H (1983) Makromol Chem 184:253
35. Ren W, McMullan PJ, Griffin AC (2008) Macromol Chem Phys 209:1896
36. Ishige R, Osada K, Tagawa H, Niwano H, Tokita M, Watanabe J (2008) Macromolecules 41:7566
37. Ishige R, Tokita M, Funaoka S, Kang S, Watanabe J (2011) Macromol Chem Phys 212:48
38. Ishige R, Tokita M, Naito Y, Zhang CY, Watanabe J (2008) Macromolecules 41:2671
39. Yang H, Buguin A, Taulemesse J-M, Kaneko K, Méry S, Bergeret A, Keller P (2009) J Am Chem Soc 131:15000
40. Lub J, Broer DJ, Van Den Broek N (1997) Liebigs Ann 2281
41. Lub J, Broer DJ, Martinez Antonio ME, Mol GN (1998) Liq Cryst 24:375
42. Lub J, Broer DJ, Allan JF (1999) Mol Cryst Liq Cryst 332:259
43. Kuhn W (1936) Kolloid Zeitschrift 76:258
44. Finkelmann H, Kock HJ, Gleim W, Rehage G (1985) Makromol Chem Rapid Commun 5:287
45. Cotton JP, Hardouin F (1997) Prog Polym Sci 22:795

46. D'Allest JF, Maissa P, ten Bosch A, Sixou P, Blumstein A, Blumstein RB, Teixera J, Noirez L (1988) Phys Rev Lett 61:2562
47. D'Allest JF, Sixou P, Blumstein A, Blumstein RB, Teixera J, Noirez L (1988) Mol Cryst Liq Cryst 155:581
48. Arrighi V, Higgins JS, Weiss RA, Cimecioglu AL (1992) Macromolecules 25:5297
49. Abis J, Arrighi V, Cimecioglu AL, Higgins JS, Weiss RA (1993) Eur Polym J 29:175
50. Li MH, Bralet A, Keller P, Strazielle C, Cotton JP (1993) Macromolecules 26:119
51. Li MH, Brûlet A, Cotton JP, Davidson P, Strazielle C, Keller P (1994) J Phys II 4:1843
52. Li MH, Brûlet A, Keller P, Cotton JP (1996) J Mol Struct 383:11
53. Hardouin F, Sigaud G, Achard MF, Brulet A, Cotton JP, Yoon DY, Percec V, Kawasumi M (1995) Macromolecules 28:5427
54. Sherwood HH, Sigaud G, Yoon DY, Wade CG, Kawasumi M, Percec V (1994) Mol Cryst Liq Cryst 254:455
55. Yoon DY, Flory PJ (1989) MRS Symp Proc 134:11
56. Li J, Brulet A, Davidson P, Keller P, Cotton JP (1993) Phys Rev Lett 70:2297
57. Hardouin F, Leroux N, Mery S, Noirez L (1992) J Phys II 2:271
58. Leroux N, Keller P, Achard MF, Noirez L, Hardouin F (1993) J Phys II 3:1289
59. Hardouin F, Leroux N, Noirez L, Keller P, Mauzac M, Achard MF (1994) Mol Cryst Liq Cryst 254:267
60. Noirez L, Hardouin F, Lecommandoux S, Richard H, Achard MF, Strazielle C (1996) J Phys II 6:225
61. Lecommandoux S, Achard MF, Hardouin F, Brulet A, Cotton JP (1997) Liq Cryst 22:549
62. Lecommandoux S, Noirez L, Achard MF, Brulet A, Cotton JP, Hardouin F (1997) Physica B 234:250
63. Noirez L, Keller P, Cotton JP (1995) Liq Cryst 18:129
64. Noirez L, Cotton JP, Hardouin F, Keller P, Moussa F, Pépy G, Strazielle C (1988) Macromolecules 21:2889
65. Finkelmann H, Kock HJ, Gleim W, Rehage G (1984) Makromol Chem Rapid Commun 5:287
66. Finkelmann H, Gleim W, Hammerschmidt K, Schätzle J (1989) Makromol Chem Macromol Symp 26:67
67. Hammerschmidt K, Finkelmann H (1989) Makromol Chem Macromol Chem Phys 190:1089
68. Mitchell GR, Coulter M, Davis FJ, Guo W (1992) Journal de Physique II 2:1121
69. Noirez L, Davidson P, Schwarz W, Pépy G (1994) Liq Cryst 16:1081
70. Noirez L, Boeffel C, Daoud-Aladine A (1998) Phys Rev Lett 80:1453
71. Lecommandoux S, Noirez L, Achard MF, Hardouin F (2000) Macromolecules 33:67
72. Kim ST, Finkelmann H (2001) Macromol Rapid Commun 22:429
73. Potdevin A (2003) Diploma Thesis, University of Freiburg
74. Nishikawa E, Yamamoto J, Yokoyama H, Finkelmann H (2004) Macromol Rapid Commun 25:611
75. Kramer D (2010) PhD thesis, University of Freiburg
76. Nishikawa E, Finkelmann H, Brand HR (1997) Macromol Rapid Commun 18:65
77. Kramer D, Finkelmann H (in preparation)
78. Lu XH, He CB, Liu PW, Griffin AC (2005) J Polym Sci A Polym Chem 43:3394
79. Patil HP, Liao J, Hedden RC (2007) Macromolecules 40:6206
80. Semmler K, Finkelmann H (1994) Polym Adv Technol 5:231
81. Benné I, Semmler K, Finkelmann H (1994) Macromol Rapid Commun 15:295
82. Semmler K, Finkelmann H (1995) Macromol Chem Phys 196:3197
83. Benné I, Semmler K, Finkelmann H (1995) Macromolecules 28:1854
84. Eckert T, Finkelmann H, Keck M, Lehmann W, Kremer F (1996) Macromol Rapid Commun 17:767
85. Rousseau IA, Mather PT (2003) J Am Chem Soc 125:15300
86. Sánchez-Ferrer A, Finkelmann H (2009) Mol Cryst Liq Cryst 508:357
87. Sanchez-Ferrer A, Finkelmann H (2008) Macromolecules 41:970

88. Sánchez-Ferrer A, Finkelmann H (2011) Macromol Rapid Commun 32:309
89. Hiraoka K, Tagawa N, Baba K (2008) Macromol Chem Phys 209:298
90. Greve A, Finkelmann H (2001) Macromol Chem Phys 202:2926
91. Kramer D, Finkelmann H (2007) Macromol Rapid Commun 28:2318
92. Küpfer J, Finkelmann H (1991) Makromol Chem Rapid Commun 12:717
93. Rogez D, Martinoty P (2011) Eur Phys J E 34:69
94. Rogez D, Brömmel F, Finkelmann H, Martinoty P (2011) Macromol Chem Phys 212:2667
95. Naciri J, Srinivasan A, Jeon H, Nikolov N, Keller P, Ratna BR (2003) Macromolecules 36:8499
96. Ahir S, Tajbakhsh AR, Terentjev EM (2006) Adv Funct Mater 16:556
97. Komp A, Finkelmann H (2007) Macromol Rapid Commun 28:55
98. Fischer P, Schmidt C, Finkelmann H (1994) Macromol Rapid Commun 16:435
99. Fischer P, Finkelmann H (1998) Prog Colloid Polym Sci 111:127
100. Brillault J (2009) PhD thesis, University of Freiburg
101. Löffler R, Finkelmann H (1990) Macromol Rapid Commun 11:321
102. Weiss F, Finkelmann H (2004) Macromolecules 37:6587
103. Schmidtke J, Kniesel S, Finkelmann H (2005) Macromolecules 38:1357
104. Bourgerette C, Chen B, Finkelmann H, Mitov M, Schmidtke J, Stille W (2006) Macromolecules 39:8163
105. Gebhard E, Zentel R (1998) Macromol Rapid Commun 19:341
106. Schüring H, Stannarius R, Tolksdorf C, Zentel R (2001) Macromolecules 34:3962
107. Vennes M, Zentel R, Rossle M, Stepputat M, Kolb U (2005) Adv Mater 17:2123
108. Müller S (2006) PhD thesis, University of Freiburg
109. Buguin A, Li MH, Silberzan P, Ladoux B, Keller P (2006) J Am Chem Soc 128:1088
110. Kleinschmidt F, Hickl M, Saalwächter K, Schmidt C, Finkelmann H (2005) Macromolecules 38:9772
111. Amigó-Melchior A, Finkelmann H (2002) Polym Adv Technol 13:363
112. Spillmann CM, Ratna BR, Naciri J (2007) Appl Phys Lett 90:021911
113. Brehmer M, Zentel R, Wagenblast G, Siemensmeyer K (1994) Macromol Chem Phys 195:1891
114. Meyer RB, Liebert L, Strzelecki L, Keller P (1975) J Phys Lett Paris 36:69
115. Hiraoka K, Stein P, Finkelmann H (2004) Macromol Chem Phys 205:48
116. Heinze P (2010) PhD thesis, University of Freiburg
117. Hiraoka K, Finkelmann H (2001) Macromol Rapid Commun 22:456
118. Hiraoka K, Sagano W, Nose T, Finkelmann H (2005) Macromolecules 38:7352
119. Heinze P, Finkelmann H (2010) Macromolecules 43:6655
120. Küpfer J, Finkelmann H (1994) Macromol Chem Phys 195:1353
121. Zander F, Finkelmann H (2010) Macromol Chem Phys 211:1167
122. Finkelmann H, Kundler I, Terentjev EM, Warner M (1997) J Phys II France 7:1059
123. Kundler I, Finkelmann H (1998) Macromol Chem Phys 199:677
124. Urayama K, Kohmon E, Kojima M, Takigawa T (2009) Macromolecules 42:4084
125. Lebar A, Cordoyiannis G, Kutnjak Z, Zalar B (2012) Adv Polym Sci. doi: 10.1007/12_2010_103
126. de Jeu WH, Ostrovskii BI (2012) Adv Polym Sci. doi: 10.1007/12_2010_105
127. Ramón-Gimenez L, Storz R, Haberl J, Finkelmann H, Hoffmann A (2012) Macromol Rapid Commun 33:353

Adv Polym Sci (2012) 250: 49–94
DOI: 10.1007/12_2011_164

Published online: 3 March 2012

Applications of Liquid Crystalline Elastomers

C. Ohm, M. Brehmer, and R. Zentel

Abstract This chapter focuses on recent developments in the field of liquid crystalline elastomers (LCEs) that bring these materials closer to the world of real applications, concentrating on their actuation properties. First, we briefly introduce different LCE materials that show actuation behavior and explain how they can be synthesized. In the second part, we focus on materials in which a shape change is triggered by a phase transition. In particular, we discuss how the chemistry of the polymeric material influences the strength and direction of the shape change. We review the efforts made to trigger the actuation event by stimuli other than temperature variation. Subsequently, we summarize preparation techniques for various sample geometries of aligned LCEs that all show actuation properties and assign them to particular applications. A short summary is given of devices that have been built in this way. In the third part, we concentrate on actuators that show deformation in an electric field without any phase transition. We start with a short introduction to ferroelectric liquid crystalline elastomers (FLCEs) and discuss molecules exhibiting these phases. Subsequently, we show how the electroclinic effect of FLCEs can be utilized to induce macroscopic deformations by an electric field.

Keywords Actuators · Ferroelectric liquid crystalline elastomers · Liquid crystalline elastomers · Miniaturization · Photoisomerization

C. Ohm, M. Brehmer, and R. Zentel (✉)
Institute of Organic Chemistry, Johannes Gutenberg University, Duesberg Weg 10-14, 55099 Mainz, Germany
e-mail: zentel@uni-mainz.de

Contents

Abbreviations

a	electrostriction coefficient
BCFLCE	Bent-core ferroelectric liquid crystalline elastomer
BCLC	Bent-core liquid crystal
c-director	Projection of the director on the smectic layer
d_{33}	Piezoelectric constant
e	Flexoelectric coefficient
FLC	Ferroelectric liquid crystal
FLCE	Ferroelectric liquid crystalline elastomer
LC	Liquid crystal
LCE	Liquid crystalline elastomer
NI	Nematic–isotropic
P_s	Spontaneous polarization
R	Radius of gyration
S	Order parameter
s_A	Smectic-A phase
s_A*	Chiral smectic-A phase
s_C	Smectic-C phase
s_C*	Chiral smectic-C phase
S_x	unidentified smectic phase of higher order
T	Temperature

1 Introduction

Liquid crystalline elastomers (LCEs) are materials that combine the properties of polymeric elastomers (entropy elasticity) with those of liquid crystals (self-organization). They are the subject of several reviews and books [1–10]. Their most interesting property is the ability to change their shape reversibly after the application of a certain external stimulus. This feature was predicted by de Gennes as early

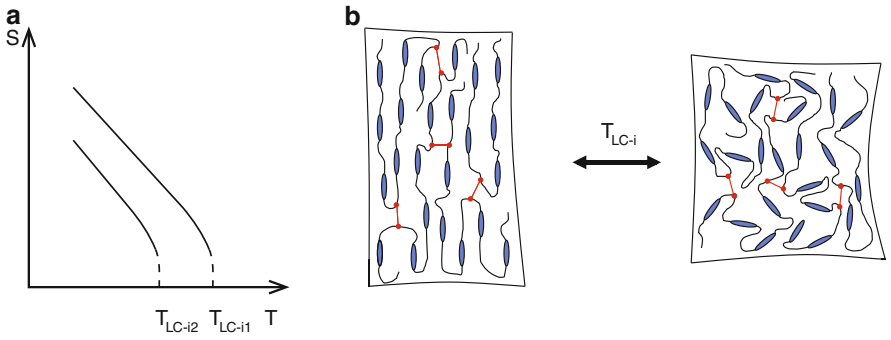

Fig. 1 (**a**) Anisotropy of the LC phase as expressed in the order parameter *S*, leads to an anisotropic conformation of the polymer backbone. The magnitude of chain anisotropy is generally assumed to have the same temperature dependence as *S*. It decreases with increasing temperature and jumps to zero at the clearing temperature ($T_{\text{LC-i1}}$). By a photoisomerization of suitable dyes (mostly azobenzene dyes) it is possible to shift the clearing temperature ($T_{\text{LC-i2}}$) and thus the order parameter and the chain anisotropy at constant temperature. (**b**) Visualization of the change of the order at the clearing temperature. In the isotropic phase the polymer chains adopt a random coil conformation, leading to a macroscopic deformation of the sample

as 1975 [11, 12]. Since then, LCEs have been extensively discussed as materials for actuators. They offer an alternative to piezoelectrics, hydrogels, and various other types of polymer systems (see [13] for an overview). The possible applications are wide, and range from micromechanical systems [14] (in atomic force microscopy , as valves in microfluidic systems, as artificial muscles in robots) to propulsion systems [15] (inspired by cilia in nature), and active smart surfaces that can change their properties according to the environment [16].

The basic idea behind the shape variation of LCEs is straightforward [184]. Imagine a network swollen with an LC material. The polymer chains experience an anisotropic environment and deviate from the isotropic conformation. As a result, the coil dimension (the radius of gyration R_G) will be different parallel and perpendicular to the LC director. Such an elastomer loses its anisotropy when heated to the isotropic phase. As a consequence, an isotropic chain conformation will be regained and the sample as a whole will change its shape (Fig. 1) [10, 11, 17, 18, 184]. This scenario, which relies on the change of the order parameter *S* and the resulting anisotropy of the polymer chains, is used most often. Thereby, the change of the order parameter is either directly induced by a temperature variation or by an "isothermal" shift of the phase transition temperatures, which can be achieved by a photochemical isomerization of dyes [19, 20] (see Fig. 1).

Alternatively, an external (electric) field can be used to change the orientation of the LC director inside the network. The network will then reorient and produce a shape change. This effect can be observed either in LC actuators made from highly swollen nematic systems [7, 9, 21, 22, 185] or in bulk LCEs with ferroelectric phases (see Sect. 3). In LCEs with ferroelectric phases, the electroclinic effect

[23–25] can lead to a change of the tilt angle of the mesogens in chiral smectic-C (smectic-C*) or chiral smectic A (smectic-A*) systems. This causes a change of the smectic layer thickness, which in turn induces the actuation (see Sect. 3). The polymer network serves here mostly as a matrix, which transforms a "liquid-like" ferroelectric phase into a "soft solid-like" ferroelectric, which can exert permanent stress. The magnitude of the shape change achievable in this way is smaller than for systems that rely on a nematic–isotropic (NI) phase transition. But, this actuation principle has the advantage that shape variations happen in direct response to an electric field (in fact it is a piezoelectric effect) and does not require heating.

LCEs can have different topologies depending on the attachment of the mesogenic units (see Fig. 2), which is important for the magnitude of the chain anisotropy. If they are incorporated into the main chain, a large interaction between LC phase and mechanical properties is expected. If the mesogens are attached as side groups (LC side-chain polymers), their orientation is decoupled from that of the polymer chains [26]. Thus orientational correlations will be smaller than in LC main-chain polymers [10, 27].

In this chapter, we will focus on the application of LCEs that can change their shape in response to temperature, to irradiation with light, or to electric fields (either by resistive heating or by a direct piezo-like response). Compared to inorganic piezoelectric materials, LCEs show a much larger shape variation but smaller forces. Compared to gels working by reversible swelling and deswelling, they have the advantage that the shape variation does not require mass transport of solvent.

The basic principles of preparation and operation of LCEs – especially with regard to the route shown in Fig. 3a – have been described in [184]. Still, some

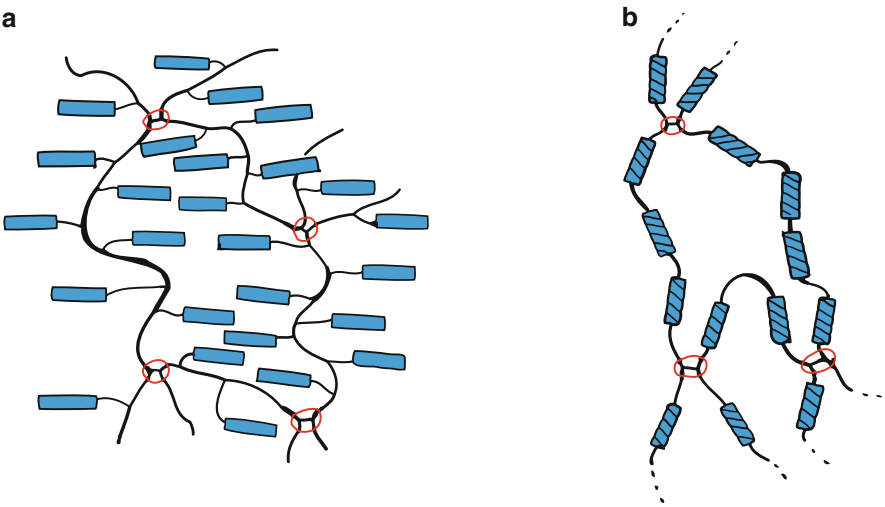

Fig. 2 (**a**) Network containing side-chain mesogens; (**b**) network containing main-chain mesogens

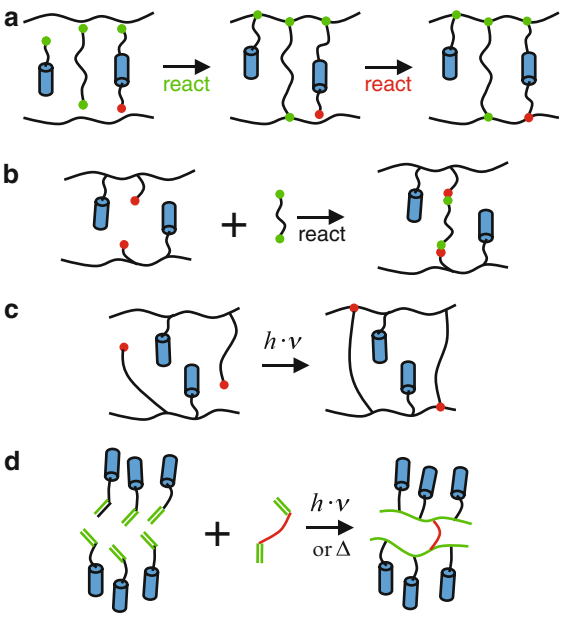

Fig. 3 Different reaction paths for the preparation of LCEs: (**a**) "One-pot" synthesis, usually via hydrosilylation; (**b**) reaction of LC polymer with a crosslinker; (**c**) LC polymer containing a reactive group that is activated by UV irradiation; (**d**) mono- and bifunctional low-molecular-mass LCs that are polymerized

remarks concerning crosslinked liquid crystalline polymers seem appropriate in the present context. We will discriminate between LCEs and liquid crystalline thermosets. LCEs are a subclass of chemically (or physically) crosslinked polymers with a low crosslinking density, resulting in long polymer chains between the netpoints. Thus, they can be deformed easily to high strains and they swell strongly in good solvents. Typical elastic moduli (bulk state, above the glass transition temperature T_g) are in the range of megapascals [28–31]. By contrast, highly crosslinked systems, so-called thermosets, are hard materials with little deformability that hardly swell. Their elastic moduli lie in the range of gigapascals [32]. Both types of networks can be made from LC polymers, depending on the amount of crosslinking agent incorporated. In addition, LCEs can be made by covalent crosslinking or by physical crosslinking due to the (reversible) segregation of hard or ionic blocks [33, 34]. Typical LCEs (low crosslink density) show NI phase transitions (e.g., clearing points) and a temperature-dependent LC order parameter. In LC thermosets (high crosslink density) the LC order is "frozen-in" and is nearly temperature independent, although photoisomerization can slightly change the order.

LCEs and thermosets offer differing potential applications. LCEs give rise to large deformations, which require a phase transition and strong deformability. The more densely crosslinked LC networks show small deformations, but their macroscopic shape variation can often be "boosted" by using bending deformations (see Sect. 2.3). In that case, tiny deformations at one side of an object can lead to huge bending deformations.

Additionally, it is important to realize that deformations at an NI phase transition occur locally, on the level of a small volume of the material in the micrometer range. To observe the unique properties of LCEs on a macroscopic scale, the mesogens have to be aligned uniformly over the whole sample, yielding an LC monodomain or, at least, a sample with a well-defined overall director pattern (see Chap. 1). Thus, the use of LCEs as actuators always requires a step to orient the sample prior to final crosslinking [184]. Consequently, we will discuss first the influence of different preparation strategies on the orientation step, focusing on materials for actuator applications (Sect. 1.1). This section will be followed by a discussion of properties needed for application. We will examine temperature-driven actuators (Sect. 2) and electrically driven systems (Sect. 3).

1.1 Preconditions for Selecting LC Elastomers

Generally, crosslinking can be done in various ways, as summarized in Fig. 3 and outlined in [5]. This includes a one-pot process, in which crosslinking and the build-up of the LC polymer are done simultaneously (Fig. 3a); the crosslinking of functional LC polymers with a bifunctional crosslinking agent (Fig. 3b); the photochemical crosslinking of a properly functionalized LC polymer (Fig. 3c); or the (photo)polymerization of a mixture from a liquid crystalline monomer and a crosslinking agent (Fig. 3d). For chemical crosslinking of a multicomponent mixture a solvent is needed to ensure miscibility of all components. This applies to routes (a) and (b) but it is especially important for route (a), in which the miscibility of various low-molar-mass compounds with a polymer must be ensured [184]. However, the solvent needed for this purpose will destroy the LC phase. Thus, the orientation must be accomplished in a second step, after most of the chemical reactions and a preliminary crosslinking have taken place in concentrated solution. Thereafter, the dried, solvent-free sample (now in its LC phase) is finally crosslinked in a strongly stretched state. By this method, nice macroscopic films of LCEs can be made (centimeter size), which have been the basis for most investigations in this field [184]. However, the samples made by route (a) show non-Gaussian behavior [35]. Additionally, small micrometer-sized samples with complex director patterns are difficult to make by this technique.

Orienting small samples and creating complex director patterns can be accomplished more easily by either using the orientability of the LC phase from the beginning or using electric (magnetic) fields or surface forces. This requires orienting and photocrosslinking of multifunctional LC polymers [36–39] or monomers in the neat (solvent-free) LC state [32, 40] (see Fig. 3c, d). In this case, it is either necessary to incorporate photocrosslinkable groups (route c) into the LC polymer or to establish (route d) a mixed system of (photo)polymerizable LC monomers. Route (c) has the advantage that the crosslinking of a small amount of crosslinkable groups has only a minor influence on the phase type and phase transition temperature. However, in this case the relatively high viscosity can create problems.

Route (d) has the advantage of a low viscosity of the monomer mixture. However, it is not trivial to obtain a system in which phase type and temperature range of the LC phase of polymer and monomer overlap well. From the synthetic side, either acrylate groups (photoinitiated radical polymerization) can be incorporated into an LC polymer by a polymer-analogous reaction [23, 36, 39, 41] or groups leading to direct photocrosslinking can be used, like benzophenone units [42, 43]. As a result of these efforts, neat (i.e., solvent-free) LC materials have become available, in which a complex director pattern can be created by the methods known from low-molar-mass LC systems. The resulting director patterns can afterwards be stabilized by photoinitiated crosslinking. As photocrosslinking can be done in a spatially resolved manner, this route allows the creation of different director patterns in different parts of the sample.

An interesting alternative to covalent crosslinking is the use of secondary interactions like ionic interactions [34] or complex formation [44–46]. Redox reactions that change the valence of the center ion can be used for reversible crosslinking. Also, block copolymers have been used for the formation of supramolecular networks [33, 47]. In this case, the crosslinks are formed by hard polymer segments that are in the glassy state surrounded by LC polymer segments. If such a block copolymer is heated above the T_g of the hard segments, it becomes melt-processable. As with ionic systems, the crosslinking of the block copolymers is reversible and reuse becomes possible. In the case of the covalent networks mostly investigated, recycling is not an option, as there is no way to selectively break the chemical bonds formed during preparation.

2 Actuators Powered by a Phase Transition

2.1 Designing Actuators with Defined Specifications

In this section, we will discuss LCEs in which shape variation is induced by a change of the order parameter S. This is most pronounced in the vicinity of an NI phase transition (see Fig. 1 and Sect. 1). In addition, we will discuss how the size and shape of aligned (and therefore actuating) LCE samples can be controlled in order to meet certain specifications dictated by an application. We will address the question of how the mechanical and actuation properties of the materials are influenced by the chemical nature of the LCE system.

From an application-based point of view, the most important characteristics of an actuator are the stimulus under which actuation occurs, the direction of actuation, the maximum displacement that can be produced, and the maximal force that can be created. The maximum displacement and force that an LCE actuator can produce depend on the chemical structure of the material. This aspect will be discussed in Sect. 2.1.1. Concerning the stimulus leading to the shape change, temperature-driven and UV-driven systems can be distinguished. In both

cases, the transition from the LC phase to the isotropic phase triggers the actuation. UV-driven systems contain photosensitive dyes that allow isothermal isotropization by UV irradiation. Additionally, temperature-driven systems have been coupled with other materials that allow the production of heat, either directly inside the sample by an electric current, by a magnetic field, or by infrared irradiation. The whole concept triggering the actuation will be discussed in Sect. 2.1.2. Finally, the direction in which a deformation occurs depends on the orientation pattern of the LC material. This topic will be addressed in Sect. 2.1.3.

2.1.1 LC Elastomer Structure and Strength of Actuation Properties

LCEs gain their actuation properties from the coupling between the elastomeric network and the LC units. It causes an anisotropic chain conformation of the network polymers if the mesogens exhibit an LC phase. Accordingly, the chains adopt different radii of gyration parallel ($R_{\parallel}$) and perpendicular ($R_{\perp}$) to the director. Depending on the geometrical relation between the director and the long axis of the polymer coil, we distinguish a prolate (parallel, $R_{\parallel} > R_{\perp}$)) and an oblate (perpendicular, $R_{\parallel} < R_{\perp}$)) conformation (see Fig. 4) [10, 48–50].

At the phase transition to the isotropic state, the polymer chain changes into a spherical conformation, which leads to a reversible shape change. The strength of this effect depends directly on the magnitude of chain anisotropy in the LC phase and is therefore a function of the coupling between polymer chains and mesogens. The architecture of the LC polymer (main-chain, side-on, end-on) has a strong impact on this coupling behavior.

Two ways of coupling are possible, namely "through bond" due to the chemical linkage between mesogens and polymer chain, and "through space" [10, 28, 48, 49]

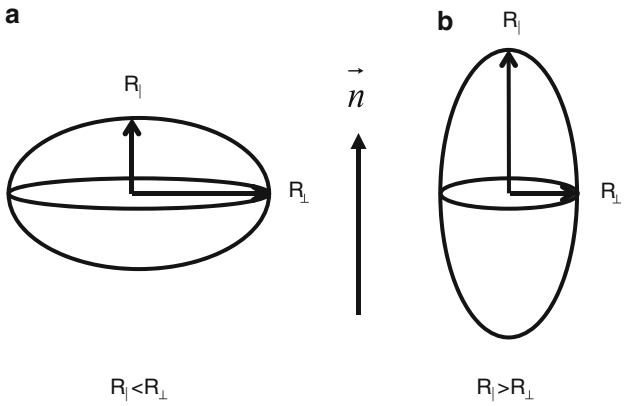

Fig. 4 (**a**) Oblate chain conformation: the long axis of the polymer chain is perpendicular to the director. (**b**) Prolate chain conformation: the long axis of the polymer chain is parallel to the director [5]. Copyright Wiley-VCH Verlag GmbH & Co. KGaA. Reproduced with permission

caused by the anisotropic environment created by the alignment of the mesogens. For LC polymer architectures in which the long axes of the mesogens are parallel to the polymer backbone (main-chain, side-on), both effects act in the same direction and cause a strong elongation of the chains parallel to the director (prolate conformation). Comparing the two systems, we find that main-chain polymers show stronger chain anisotropy than side-on systems. The reason is that the "through bond" coupling in the main-chain architecture is stronger, because the mesogens are directly incorporated into the polymer backbone. Decreasing the spacer length of a side-on system (giving it more main-chain character) increases the coupling between mesogen and backbone and thereby increases the chain anisotropy [28, 51].

In the case of end-on systems, the "through bond" coupling induces an elongation of the polymer chains perpendicular to the director, while the "through space" coupling prefers a parallel extension of the chains. This conflict concerning orientation leads to weaker chain anisotropy in end-on systems than in the two other architectures. The direction in which the backbone elongates depends on many factors, like the nature of the LC phase (nematic or smectic), the spacer length, and the chemical structure of the backbone polymer [28]. Concluding, we expect the strongest backbone anisotropy for main-chain polymers, followed by side-on and then end-on systems. Using D-NMR and small-angle neutron scattering (SANS) [50–58], it was indeed shown that the degree of backbone anisotropy decreases for the three architectures in the order main-chain > side-on > end-on.

Because the shape-changing effect has its origin in the deformed polymer chain conformation, we expect the strongest shape change in main-chain systems, and the weakest one in end-on systems. This prediction has been confirmed by comparing the shape-changing capabilities of three prominent LCE systems with different architectures (see Fig. 5). The main-chain elastomer by Ahir et al. [47] changes its

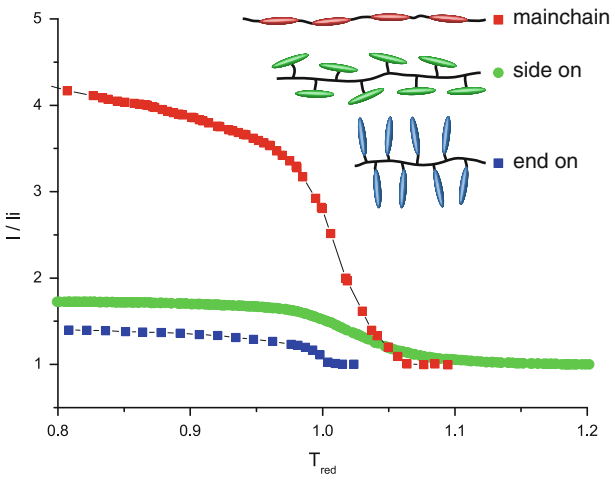

Fig. 5 Comparison of the contraction in the direction of the director for different polymer architectures. Data were taken from [18, 47, 59]

length by roughly 400% during the shape transition. The sample with a side-on architecture by Keller and coworkers deforms by 70% [59], and the end-on system by Wermter and Finkelmann shows an actuation of 40% [59]. Other samples investigated follow this trend. Additionally, the groups of both Finkelmann and Terentjev showed that the shape-change effect can be drastically increased by adding main-chain polymers to side-chain elastomers [60, 61].

Apart from the coupling between backbone and mesogens, the nature of the LC phase also has impact on the shape-changing properties. The examples presented so far were nematic LCEs. The situation in smectic LCEs is much more complex and a clear picture has not yet emerged. In fact, both poorly actuating and strongly actuating systems have been found, depending on the chemical nature of the system. This could be related to the fact that there is little information on the "quality" of the smectic layering. In addition, smectic order might be reduced by the crosslinking reaction [186]. As a first guess, highly ordered (low-temperature) smectic phases should induce a large anisotropy of the chain conformation. However, far too little SANS data exist to verify this assumption. For smectic LCEs, the deformation at the transition to the isotropic phase would be expected to be larger than for nematic ones. However, in most cases smectic LCEs posses weaker actuating properties than their nematic counterparts. Smectic-A main-chain elastomers prepared by Beyer et al. deformed by only 40% [62]. Smectic-A side-on samples by Komp and Finkelmann showed shape changes of 14% [63], and smectic-A end-on elastomers by Nishikawa and Finkelmann deformed by only 12% [64]. On the other hand, Sanchez-Ferrer and Finkelmann recently reported an example that contradicts this general trend [65]. Using two different mesogens, one of them with bulky side groups that destabilize the smectic phase, and the two-step crosslinking process, smectic and nematic main-chain polymers were prepared with nearly identical structures. In this case, the smectics showed a stronger shape variation (210%) than the nematics (80%), which was explained by the higher order parameter of the smectic phase. Finally, some smectic LCEs prepared from "diluted polysiloxanes" [36–38, 66] show no shape change at all at the phase transition to the isotropic phase [67]. The situation is complicated by the fact that in smectic LCEs the relaxation times are often rather large and in some cases the shape-changing effect was irreversible if no retracting force was applied [68].

A third parameter that impacts on the strength of the shape-changing effect is the crosslink concentration of the elastomeric network [184]. An increase in the crosslink density of nematic side-on elastomers decreases their actuation properties [69]. This is mainly due to a stiffening of the elastomeric network, thus making larger forces necessary to deform the sample. Additionally, crosslinking moieties usually produce defects in the LC phase, thereby reducing its order parameter and chain anisotropy [70, 186]. This constraint is especially important in networks from LC-polysiloxanes prepared according to the route shown in Fig. 3a. LC-polysiloxanes are usually prepared from commercially available prepolymers, which have only a modest degree of polymerization (around or below 100). This makes the use of larger amounts of crosslinking agents necessary to obtain properly crosslinked elastomers with low sol content.

2.1.2 Triggering the Actuation

All actuators discussed in this section depend on a transition to the isotropic phase to trigger a deformation. This results from the interest in large deformations, which require a considerable change of the order parameter (exemptions are bending deformations, described in Sect. 2.1.3). The phase transition to the isotropic phase always occurs at a specific temperature that needs to be controlled in order to produce applicable actuating devices. In most cases, a low transition temperature is desired, slightly above ambient conditions, as this is energy efficient and facilitates the construction of devices.

Phase transition temperatures can be influenced by several parameters. The main impact is exerted by the chemical structure of the mesogenic molecules. Stiff and highly symmetric mesogens have high transition temperatures [27, 71] and need to be avoided. For example, Beyer et al. introduced a bulky, lateral bromide group to a main-chain mesogen to suppress crystallization and to reduce the NI phase transition temperature [62]. Also, the flexibility of the polymer backbone has an influence. Highly flexible polymers like polysiloxanes yield LCEs with low glass and phase transitions, which is one reason for their popularity. Another possible way to reduce the transition temperature is by mixing two or more mesogenic molecules within the LCE, yielding a statistic copolymer [59].

Heating the whole device in order to induce actuation is impractical or even impossible for most applications. Accordingly, there is a demand for methods that produce heat directly inside the LCE without affecting its surroundings. Most straightforwardly this can be achieved by integrating a resistive wire into the sample and applying an electric current [72]. The resulting heat leads to a NI phase transition inside the material, triggering a deformation. Evidently this is not a method of choice. A more sophisticated principle was applied by Chambers et al. [73], who incorporated carbon black into the LCE sample, making it conductive by itself. Applying an electric current through the sample creates a temperature increase that initiates a shape change. It is, however, the weak point of these approaches that they require a composite material made from a “shape-changing” compound (LCE) and a “not-shape-changing” compound (the conducting material). Deformations (shape changes) create stress and lead, after repeated actuation, to delamination and a loss of the percolation of the conducting particles.

Alternatively, single-walled carbon nanotubes have been mixed into the LCEs [74]. They were, however, not used for conduction, but because they possess a strong absorption for infrared radiation and the visible spectrum. Thus, irradiating the sample with infrared light can create enough heat to induce the transition to the isotropic phase. Since this process does not require percolation of the carbon nanotubes it is much less sensitive to shape variations.

Magnetic fields have also been used to heat the actuating material directly. For this, Kaiser et al. introduced magnetic iron oxide nanoparticles into an LCE sample [75]. In a quickly changing magnetic field (300 kHz) the continuous reorientation of the magnetization produces heat, which induces a shape change.

For some applications, the production of local heat might be undesirable. In these cases, an isothermal NI phase transition induced by UV irradiation might be a suitable choice. The *cis–trans* isomerization of mesogens containing a photoisomerizable group (mainly azobenzene Ph–N=N–Ph) changes their shape from rod-like to kink-like. This leads to a destabilization of the LC phase [19, 62, 76], reducing the transition temperature to the isotropic phase and thus causing isotropization at a constant temperature [20]. The concept can be transferred to LCEs in two ways. Either an LCE network is swollen with the azo compound [77], or azo-containing mesogens are covalently attached to the polymer backbone [19, 62, 78–80]. Figure 6 shows the actuation properties of an LCE film with covalently incorporated azo-mesogens in different concentrations in dependence of temperature and UV-irradiation state [80]. Both increasing the temperature and irradiating the sample produces a contraction of roughly 20%. After the shape change, irradiating the sample with visible light accelerates the re-isomerization of the azo groups, thus making the actuation reversible. The wavelength under which the isomerization occurs can be influenced by substitution of the azobenzene with functional groups that increase the length of the conjugated π-system. Examples are amino-nitro azobenzene and azotolane, which have absorption maxima close to the wavelength of visible light [81]. For further discussion on this topic see [187].

2.1.3 Modes of Actuation: Contraction, Expansion, and Bending

In Sect. 2.1.1 we pointed out that the direction of actuation relative to the director depends on the architecture of the LC material. Systems with a prolate chain conformation (main-chain and side-on) show a contraction parallel to the director, whereas LCEs with oblate backbones (many end-on systems) expand in this direction. Due to the necessity to retain a constant volume, the LCE sample compensates this deformation by expanding or contracting in the direction perpendicular to the director.

The situation becomes more complex in samples that are not aligned in a classical monodomain (in which the director is uniform over the full sample volume), but in a defective structure. An example is provided by films constrained by two different alignment layers at each side: one that facilitates a planar orientation and one that produces homeotropic alignment. In such films the director is aligned in a splay-defect structure. During the NI phase transition a bending deformation occurs [82]. A similar effect takes place in thick UV-responsive samples if the dye concentration is high enough. Due to the strong absorption, the UV light does not penetrate through the whole film thickness. As a result, the shape change is concentrated at the incident surface. This leads to a bending of the whole film [40, 83].

Complex director field alignment also occurs in very small or strongly curved samples. Nanometer-sized colloids from LC polymers and elastomers prepared by emulsion polymerization can show a bipolar, concentric, axial, or radial director field configuration, depending on their preparation method [84, 85]. During the NI

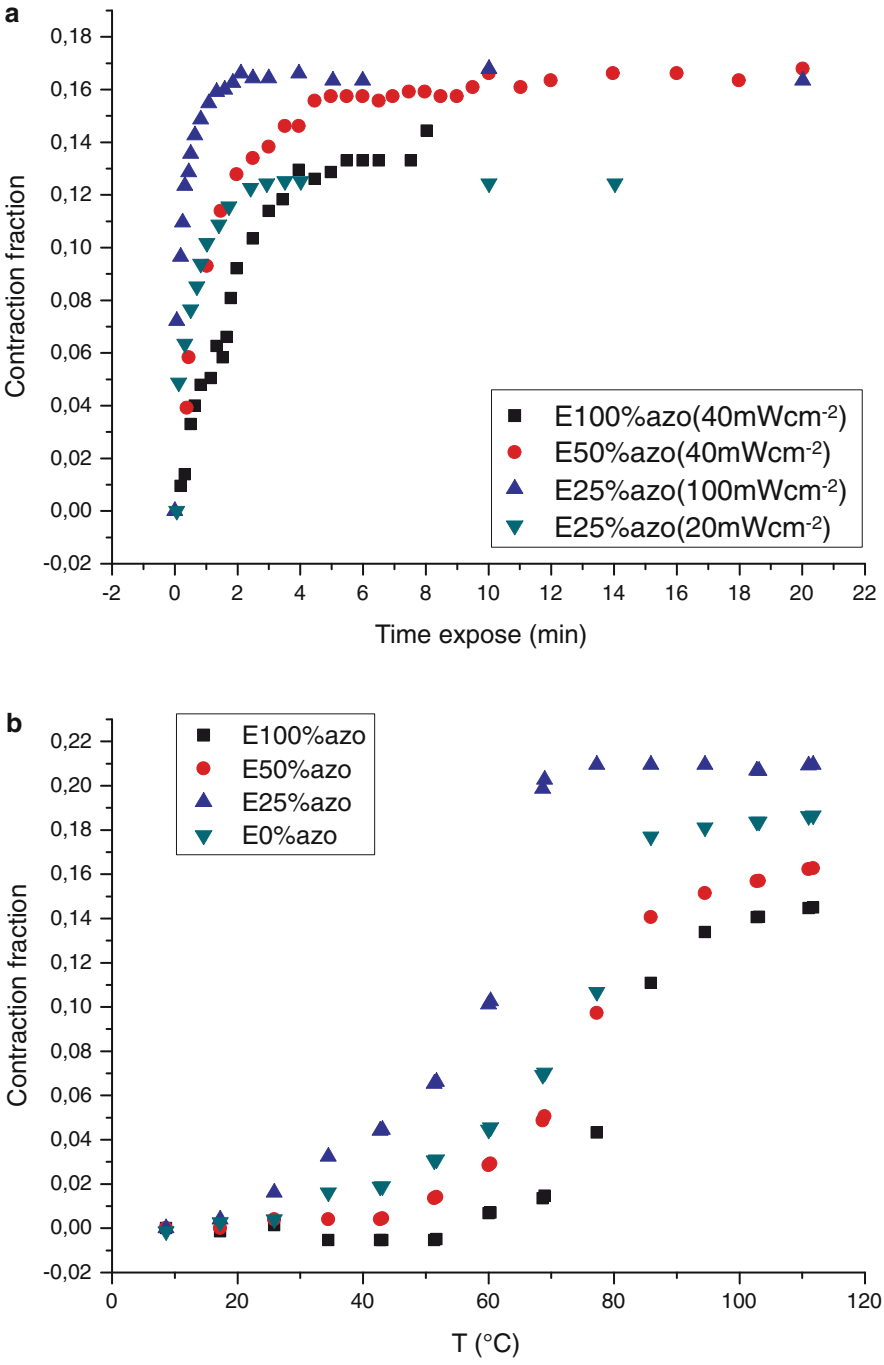

Fig. 6 Shape change of an LCE containing different concentrations of an azobenzene dye: (**a**) by exposition to UV light and (**b**) by changing temperature [80]

phase transition, such samples show different types of deformation [86, 87]. The orientation pattern can be controlled by experimental parameters in larger particles prepared by polymerization in a microfluidic system. Using different amounts of shear during polymerization, Ohm et al. succeeded in preparing two types of particle samples with a concentric and a bipolar orientation, respectively [87]. Upon heating through the NI phase transition, the concentric alignment produces an expansion perpendicular to the symmetry axis while the bipolar samples contract.

2.2 *Introduction of Actuator Systems*

We will discuss several strategies to tether the properties of LCE actuators to certain specifications, and then present examples of actuator systems of different shapes and different domain sizes. We shall differentiate between macroscopic and microscopic LCE actuators. Films (Sect. 2.2.1) and fibers (Sect. 2.2.2) typically have at least one macroscopic dimension. Microscopic actuation systems from LCEs have received much interest lately and have recently been the subject of a specialized review [88]. In Sect. 2.2.3, we will discuss micrometer-sized actuators that are fixed on a solid substrate to yield stimuli-responsive surfaces. In Sect. 2.2.4, we will review several methods for preparation of colloid-like actuators that are freely suspended in air or in a surrounding liquid.

2.2.1 Film Samples from LC Elastomers

The concept of actuation in aligned LCEs was first demonstrated in film samples. Uniform orientation was achieved by mechanical stretching [89] of pre-crosslinked films and subsequent full crosslinking under a load [18, 90, 91]. The shape change of such a film is displayed in Fig. 7a. Subsequently, techniques using magnetic fields [33] and uniform substrate layers [40, 59, 80, 92, 93] were utilized to achieve alignment without the need for the two-step crosslinking procedure. In these cases, the films were usually prepared on solid substrates and released after polymerization by a sacrificial layer. An example of that kind of specimen is given in Fig. 7b. Due to the flat geometry, films allow a defect-free director pattern leading to an LC monodomain with a high value of the order parameter. This results in strong deformations during the NI phase transition.

LCE films typically have lateral dimensions of several centimeters and a thickness of hundreds of micrometers. This large size makes the samples ideally suited for mechanical testing as well as for X-ray investigations. Accordingly, most fundamental studies have been carried out on such films. One disadvantage of film samples is the large amount of LC material often needed. This has been overcome by a technique introduced by Ikeda and coworkers [94]. By laminating a thin layer of aligned LCE material onto a nonresponsive plastic film, a composite

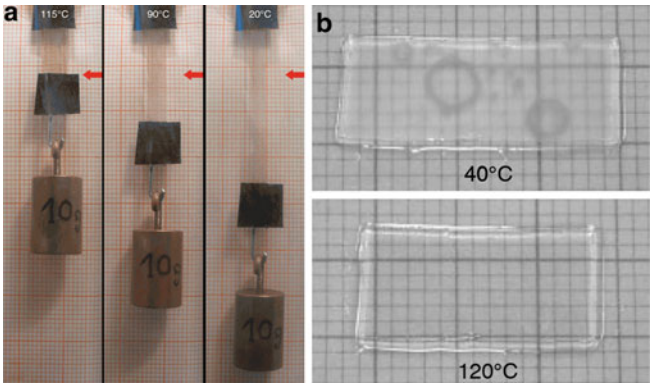

Fig. 7 (**a**) LCE film sample oriented by mechanical stretching with a small weight attached. Increasing the temperature results in a contraction of the film, lifting the weight [60]. (**b**) Film sample orientated by a magnetic field. During the contraction the film shows a deformation [33]. Copyright Wiley-VCH Verlag GmbH & Co. KGaA. Reproduced with permission

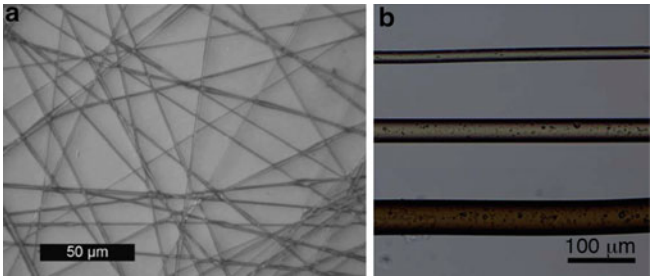

Fig. 8 (**a**) Fibers from a LC elastomer prepared by electrospinning and cast on a substrate [95] . Copyright Wiley-VCH Verlag GmbH & Co. KGaA. Reproduced with permission. (**b**) LCE fibers with different diameters prepared by a wetspinning process [68]. Reproduced by permission of the Royal Society of Chemistry

sample is obtained. At the NI phase transition induced by UV irradiation, a bending deformation occurs due to a shape change in the LCE layer only (compare with a bimetal film with different expansion coefficients). Additionally, the composite sample has superior mechanical stability compared to pure LCE films. (Fig. 8).

2.2.2 Fiber Samples from LC Elastomers

Due to their shape, fibers from LCEs closely resemble “artificial muscles”. They are typically made by extrusion of a reactive LC pre-polymer, either from solution or from the melt, followed by crosslinking. During extrusion, strong shear forces act on the polymer chains and most polymers show alignment under these conditions [96]. For LC polymers the effect is even stronger, resulting in a high degree of

orientational order within the fibers. Usually, the polymer chains are elongated in the direction of the fiber axis. Consequently, the director is aligned parallel to the fiber axis for prolate LCE systems and orthogonal for oblate systems.

The most common way to make fibers is by drawing them manually with tweezers from a polymer melt [41, 97]. The technique is very easy to perform and requires only small amounts of material. Disadvantages are the limited length of the fibers and the poor amount of control over their diameter. Even so, it has developed into a standard method for preparation of samples for X-ray diffraction and thermomechanical experiments. A more sophisticated method is electrospinning [47, 95], whereby a polymer solution is drawn continuously from a thin nozzle by an electric field and is crosslinked at the same time. This results in very thin and highly oriented fibers with diameters of 0.1–5 μm that can be cast onto a substrate. Because of their high tensile strength, there is some similarity between these fibers and natural spider silk. During the NI phase transition the fibers show a contraction. Possible fields of application are microactuation and textiles. A third synthetic technique is wet-spinning in a microfluidic setup, which yields fibers with diameters of 20–50 μm [68]. In this case, the polymer solution is injected into the flow of a second fluid, which mixes with the solvent of the polymer, leading to precipitation. The resulting fiber can be crosslinked continuously by UV light and rolled up. This yields infinitely long oriented fibers with a diameter controlled by the flow rates of the two phases. In a demonstration experiment, a small weight was attached to such a fiber, which was subsequently heated above the NI transition temperature. Across the phase transition a reversible rising of the weight was observed. Hence, the authors concluded that this technique is suitable for preparing specimen for mechanical testing.

2.2.3 Stimuli-Responsive Surfaces

Patterning surfaces with micrometer-sized objects from aligned LCEs is an interesting objective because such stimuli-responsive surfaces allow manipulation of properties like wetting behavior or adhesion on demand. Secondly, creating micrometer-sized structures from LCEs directly on a solid substrate allows their incorporation into micro-electromechanical systems (MEMS) or microfluidic lab-on-chip systems where they can serve as valves, switches, or mixing devices. Due to its simplicity, LCE-based actuation offers strong advantages over conventional motors, if small devices are required.

Keller and coworkers used soft-molding to produce micrometer-sized cylinders attached to a solid substrate [16]. To achieve this, a polydimethylsiloxane (PDMS) mold with a negative of the desired pattern was pressed onto a thin film of a molten, nematic side-on monomer on a solid substrate. After aligning the mesogens in a magnetic field, polymerization and crosslinking were initiated by UV irradiation through the PDMS mold. When the mold was peeled off, a surface consisting of regular cylinders from aligned LCEs was obtained. During the NI phase transition, the cylinders showed a reduction in length. The same procedure has been performed

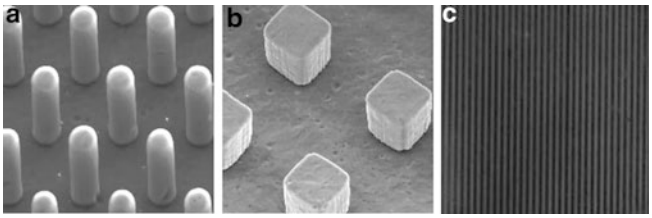

Fig. 9 Micrometer-sized patterns from aligned LCEs on a subsrate: (**a**) cylinders [16], (**b**) cubes [16], (**c**) lines [93]. (a, b) Reprinted with permission; copyright (2009) American Chemical Society. (c) Reproduced by permission of the Royal Society of Chemistry

with another monomer system that yielded main-chain LCEs upon polymerization [16]. Compared to the first example, this drastically increased the strength of the pillar's response at the phase transition up to an impressive value of 400%. Accordingly, smart materials have been obtained that allow manipulation of their surface roughness by an external stimulus. Possible applications of such single pillars are valves and micropumps in microfluidic systems.

Ellias et al. used an approach based on photolithography to produce similar stimuli-responsive surfaces [93]. A layer of a photopolymerizable nematic material was spin-coated on a plasma-treated glass substrate and irradiated through a photomask. After dissolving the unexposed areas, the glass slide was covered with a regular pattern of LCE material. Due to the plasma treatment, the mesogens align homeotropically on the strongly hydrophilic substrate, yielding a director orientation perpendicular to the surface. During the NI phase transition, a reversible contraction of the micrometer-sized features was observed (Fig. 9). Van Oosten et al. applied an ink-jet printing approach to prepare micrometer-sized objects from aligned LCEs on a solid substrate [82]. A polyvinylalcohol (PVA) sacrificial layer was spin-coated on a substrate, followed by an alignment layer from polyimide. Two different LC monomers were ink-jetted on top of this assembly and were polymerized and crosslinked by UV irradiation. Dissolving the PVA yields freestanding cantilevers that are attached to the substrate by only their end. UV irradiation of different wavelengths initiates a reversible bending of these structures in different directions. Mimicking natural celiae, the movement of the cantilevers could be used as a propulsion system for microdevices in a fluid environment. Also, microfluidic devices seem possible in which the bending motion of the cantilevers is utilized to generate a turbulent mixing flow.

2.2.4 Freely Suspended Micro- and Nanometer Particles from LC Elastomers

A different aspect of micro-actuators is their synthesis as freely suspended objects in a fluid environment. The advantage of this concept is that it allows simultaneous application of many actuators with identical size and shape. If the micro-objects are aligned via self-assembly, their sheer number can create strong deformation forces.

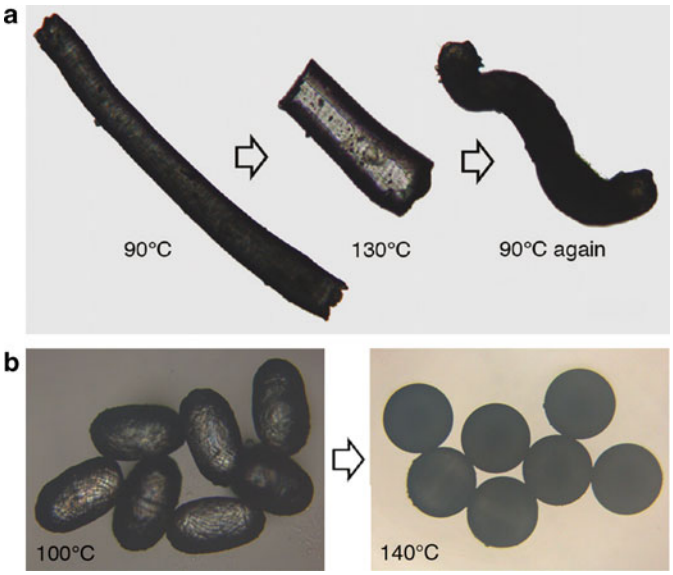

Fig. 10 Thermoactuation of LCE microparticles prepared in a microfluidic setup. *Top*: fiber that shortens during actuation [87]. *Bottom*: spheres that become rods [98]. (**a**) Reprinted with permission; copyright (2011) American Chemical Society. (**b**) Copyright Wiley-VCH Verlag GmbH & Co. KGaA. Reproduced with permission

Ohm et al. used microfluidic techniques to prepare micrometer-sized particles with different shapes from LCEs (Fig. 10) [98]. A molten nematic monomer is injected through a thin needle into a flowing stream of an immiscible carrier fluid. This results in the continuous formation of equally sized monomer droplets. These droplets are flown through thin tubes giving them the shape of spheres, disks, or rods and inducing an ordered director field [87]. By irradiating the droplets with UV light, polymerization and crosslinking is initiated, thus permanently fixing their shape and the internal orientation. When heated, the resulting particles show a reversible deformation. Control could be achieved over different parameters of the micro-actuators, like size, strength of the shape variation, and the direction of actuation (both expansion and contraction). The high level of control over the particle's physical properties allows production of actuators for specialized applications. Possible fields of interest are microlenses, valves on microfluidic chips and displacement devices [69].

Actuators of an even smaller size scale have been prepared by two groups using anodized aluminum oxide (Alox) as a template [99, 100]. In both cases, the regular, cylindrical cavities formed during the anodic oxidation of aluminum were filled with an LC monomer that was subsequently polymerized and crosslinked by UV irradiation. Afterwards, the template was dissolved by wet chemistry and regularly shaped LCE rods with a diameter of hundreds of nanometers and a length of several micrometers were obtained. Due to surface effects within the Alox template, the director was aligned parallel to the long axis of these nanorods. This orientation was

exploited by Cairns et al. to rotate these objects in electric and magnetic fields [99]. Possible applications are rheological fluids. Ohm et al. performed thermomechanical experiments whereby the rods showed reversible actuation on a size scale between the micro- and nanometer region [100].

The smallest defined structures from LCEs have been prepared by miniemulsion polymerization [86]. A main-chain polymer was emulsified by ultrasonication in an immiscible fluid and photocrosslinked in the LC state. The resulting particles were spherical with diameters of 50–300 nm. Upon heating inside an electron microscope the spheres transformed into rods and platelets, thus demonstrating the concept of actuation on a nanometer scale. An interesting question is whether the stimulus-triggered shape change of such suspended colloids also has an impact on the properties of the surrounding medium. If this is the case, fluids with a switchable viscosity might be accessible.

Yang et al. used the same method to prepare particles from noncrosslinked LC polymers [101]. The shape of the obtained nanoparticles was found to deviate from spherical. Such shape-anisotropic colloids are usually very difficult to produce by miniemulsion techniques.

2.3 LC Elastomer Devices

We will now discuss devices based on phase transitions within LCEs. This section will not only deal with weakly crosslinked elastomers, but also with liquid crystalline thermosets. Whereas LCEs are used for linear actuation, more densely crosslinked materials find application in devices that are operated in a bending mode. Due to their higher mechanical stability, the number of examples for materials that show flexure is much larger. Their mechanical properties can be enhanced by coating the LC material on a flexible substrate [94]. The preparation of such devices is easy, as standard procedures for thin film preparation or ink jetting can be used. Another advantage of thin films is the contact-free addressing by light [102]. This is not possible in thicker films, in which an intensity gradient throughout the sample inhibits a uniform deformation.

Light-induced flexing can be used to move objects on surfaces. Finkelmann et al. prepared dye-doped LCE stripes that bend upon irradiation due to a director dislocation [77]. In the dark, the sample relaxes quickly to a flat state. If such LCE rafts float on a water surface, the deformation moves them away from the illuminating beam [77]. Off-center irradiation results in a skew deformation of the LCE allowing directional control of the movement. Directed movement on solid surfaces is also possible in the case of an asymmetric design of the actuator (Fig. 11) [103]. For an LCE covered stripe a change of flexure can be induced. Different edges allow changing the stationary point and enable an inchworm-like movement in one direction. Switching the dye in the sample from the *trans* to the *cis* state and back controls the curvature of the stripes. This shape change is achieved by alternating irradiation with UV and visible light.

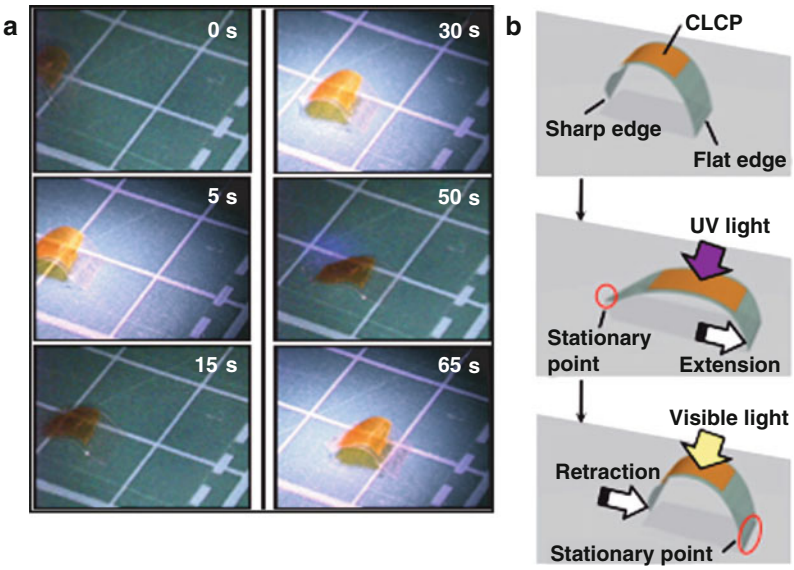

Fig. 11 Moving stripe of a composite of polymer film and LCE. [103]. The photoisomerization of the incorporated azo dyes controls the bending. The direction of the walk depends on the shape of the edges. Reproduced by permission of the Royal Society of Chemistry

Using an LCE-coated ribbon, the group of Ikeda has been able to construct a light-driven motor [94]. The belt is put around two pulleys with different diameters. Upon irradiation on one side with UV light and the other side with visible light, the pulleys is made to rotate due to the consecutive contraction and extension on the two sides. (Fig. 12)

The aforementioned examples of bending devices work digitally with two different states. For other applications it might be necessary to have various different bending angles. Such a variable bending can be achieved by a gradual distortion of the director in the LCE with the help of shape-changing molecules [104]. Consecutive *trans–cis–trans* isomerization of azo compounds induced by polarized light leads to a rotation of the dye out of the polarization direction [105, 106]. In this way, a change of the polarization direction leads to a gradual change of the LCE's order and thus the flexure [104].

Cilia are hair-like objects that work as actuators by flexing. Because of their small size they are used in arrays. They can be prepared easily by inkjet printing [82], which offers the possibility to combine polymers with different absorption wavelengths in one device. If one segment is switched by visible light and the other by UV light, different shapes can be achieved. These fibers have been attached to a surface in order to move objects (Fig. 13). Cilia could also be attached to devices that are propelled autonomically.

Recently, a miniaturized gripper that is propelled by an LCE film has been introduced [107]. Using lithographic methods, an LCE film and the silicon pincers

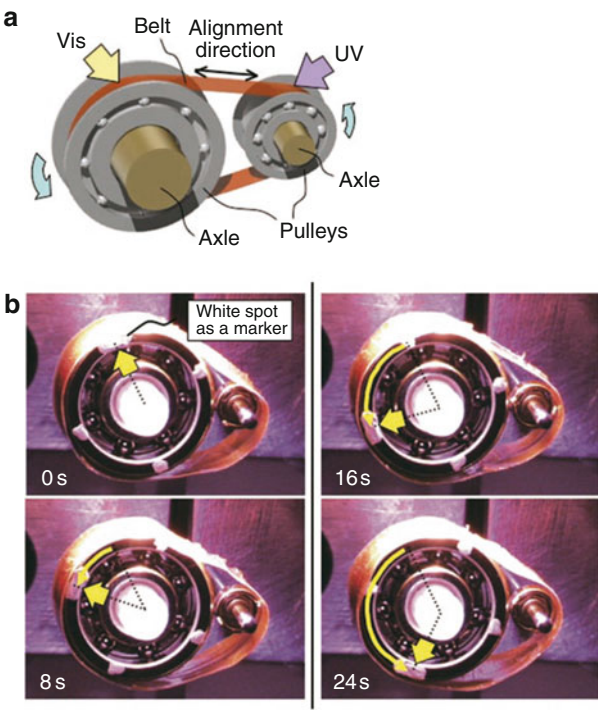

Fig. 12 LCE-covered ribbon moves two pulleys. Simultaneous irradiation with visible and UV light on different areas of the setup leads to contraction and expansion on different sides [94]. Copyright Wiley-VCH Verlag GmbH & Co. KGaA. Reproduced with permission

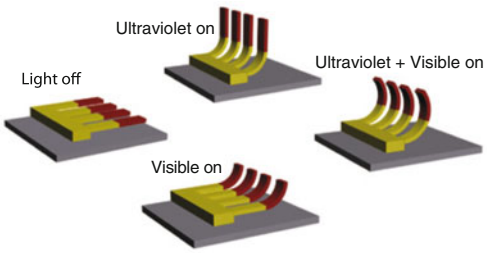

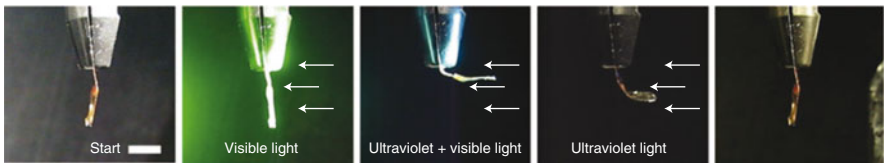

Fig. 13 Fibers containing two different LCEs sensitized to different wavelengths. Different combinations of light sources allow different movements [82]. Reprinted by permission from Macmillan Publishers [Nature Materials]. Copyright (2009)

are integrated into a micromechanical device. A gold wire is wound around the LCE, thus allowing heating of the material with an electric current. If the NI transition temperature is reached, the device can grab an object.

Mechanical deformations can also be used to obtain switchable optical elements. In the first step, lines are written into an oriented polymerizable low-molecular-mass LC by two-photon lithography. After stabilization of the support by polymerization with weak UV light, an optical grating is obtained [108]. If the grating vector is parallel to the nematic director, the distance between the lines shrinks upon heating from the nematic to the isotropic phase. This modifies the step size of the grating and a change of the diffraction pattern is observed. Hence, in this way a tunable grating is generated [109].

Solvent-dependent (chemical) applications of the LCE shape change have also been reported. They are based on a combination of (1) the well-known isotropic swelling of elastomers with (2) a strong anisotropic deformation, when the swollen network becomes isotropic. An LCE containing hydrophilic carboxylate groups changes its shape with water uptake and thus can be used as an indicator of moisture [93, 110]. Starting with an LCE with different director orientations on each side of the sample, the LCE not only increases its volume during water uptake, but also bends strongly because of the anisotropic swelling [69].

3 LCEs in Electric Fields

Reorientation of the LC director in electric fields is the basis of liquid crystal displays (LCDs). Hence, it is straightforward to think of initiation of actuation in an LC elastomer by application of an external electric field that causes reorientation of the LC director inside the elastomer. This should lead to a reorientation of the anisotropic polymer chain (see Fig. 4) which, in turn, induces a shape variation. However, all experiments performed so far demonstrate that it is not possible to transfer enough energy for a shape variation on the nematic director. Because the network topology stabilizes the sample shape and chain anisotropy present during crosslinking [4], the director of nematic LCEs cannot be switched in electric fields if the shape of the elastomer is kept fixed. By contrast, for freely suspended and highly swollen pieces of nematic LCEs, shape variations in electric fields have been observed as a response to the reorientation of the director [14, 15, 185]. However, the interaction with an electric field is much stronger for ferroelectric (chiral smectic) liquid crystals. It is possible to prepare ferroelectric LCEs in which a full switching of the director by external electric fields occurs while, at the same time, the director orientation present during crosslinking is stabilized by the network [23, 36–38].

A second possibility exists for inducing a shape variation in ferroelectric LCEs. It results from the phase transition between a smectic phase with an orientation of the director along the layer normal (s_A) and a smectic phase with tilted mesogens

(s_C*). This transition can be induced by an electric field (electroclinic effect) and leads to a decrease in the thickness of the smectic layers, resulting in a shape variation.

3.1 Ferroelectric Liquid Crystals and Their Networks

We will first describe LC phases with ferroelectric properties and subsequently outline the general properties of the ferroelectric LCEs (FLCEs). The most intensely studied phase is the chiral smectic-C* phase (s_C*) (see Fig. 14). It is the chiral modification of the smectic-C phase, a tilted smectic phase formed from chiral (pure enantiomers) rod-like mesogens. Chirality is essential because it eliminates the mirror plane present in the classical smectic-C phase. This reduces the symmetry of the phase and allows a macroscopic polarization perpendicular to the plane of the layer normal and the director, which now follows the average tilt direction of the mesogens (for an overview see [113–119]). This macroscopic dipole moment (spontaneous polarization) is a consequence of the reduced symmetry and the fact that the lateral dipole moments of individual mesogens no longer cancel each other due to a slightly biased rotation around their long axis. This symmetry argument applies to all tilted smectic phases formed by chiral rod-like mesogens. However, for higher-ordered smectic phases than s_C*, ferroelectric switching (see Fig. 14a), which is the final proof of ferroelectricity, is difficult to perform due to the high viscosity. This problem is even more severe for FLCEs, in which the switching times can be very long [37, 38].

In summary, chiral smectic-C* phases lack a center of symmetry. Hence they can be used as materials for second-order nonlinear optics [120–124], and possess piezoelectric and pyroelectric properties. Pyroelectric measurements have been performed on LC polymers [125] as well as on LCEs [126–128]. Irradiation of an FLCE sample with light usually leads to a temperature increase resulting in a pyroelectric signal [129]. More interesting are systems in which dye molecules like azobenzenes lead to a shift of the phase transition temperature upon isomerization [19].

Furthermore, in FLCEs the macroscopic electric dipole moment provides a handle to apply a strong torque onto the director (see Fig. 14a). The resulting switching occurs on the cone of the so-called **c**-director, the projection of the director on the smectic layer plane (see Fig. 14a). Soon after the discovery of the potential of chiral smectic-C* phases, the search for LC polymers with these phases started [130–132]. However, as ferroelectric switching is the final proof for the assignment of the phase, the more closely studied ferroelectric LC polymers were limited to several LC polysiloxanes, which have a low T_g and a relatively high switching speed [25, 66, 133–136] (see Scheme 1). These polymers form the basis for most of the FLCEs discussed here.

Closely related to the chiral smectic-C* phase is the so-called chiral smectic-A* phase (s_A*, see Fig. 14b) (for an overview see [24, 25, 119, 142, 143]). Without the presence of external electric fields, the s_A* phase is identical to the smectic-A (s_A)

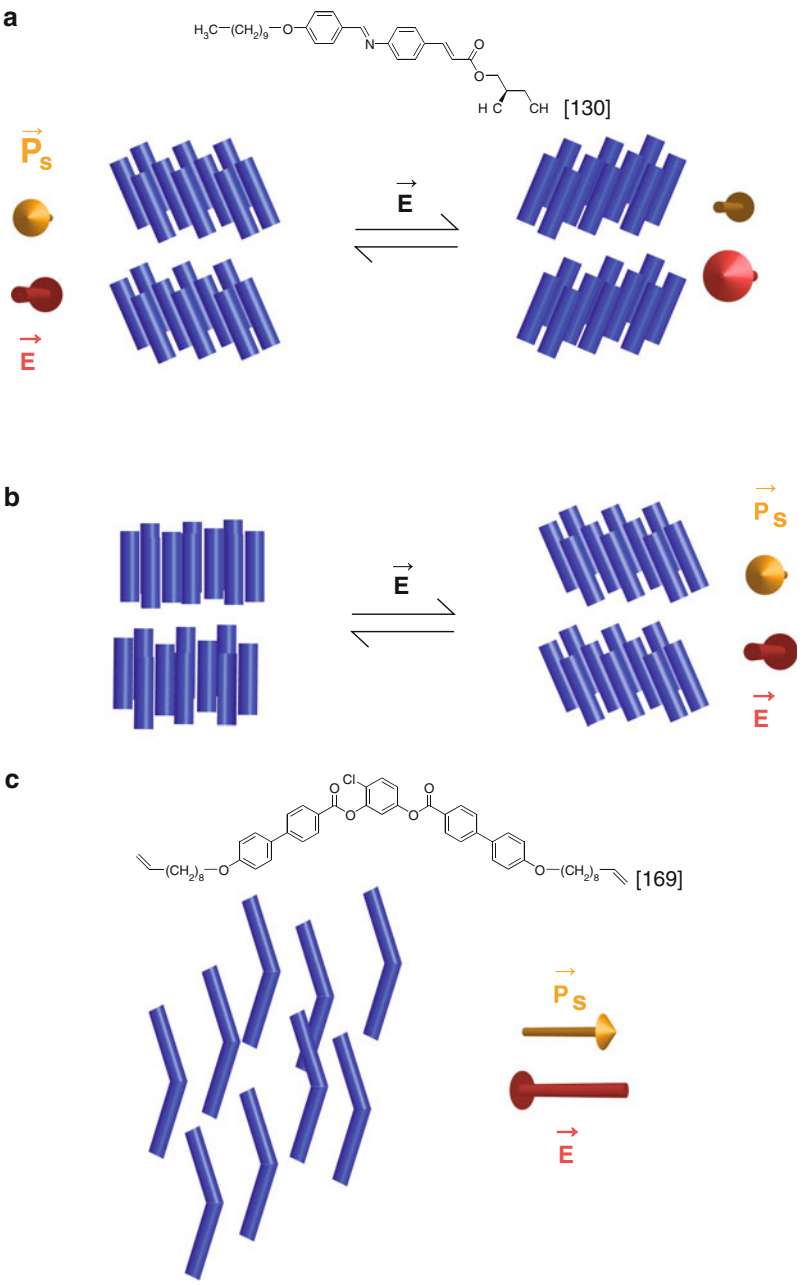

Fig. 14 Ferroelectricity in LCs. (**a**) In the smectic-C* phase an electric field (E) can reverse the tilt and thereby the direction of the polar axis perpendicular to the tilt direction. (**b**) Application of an electric field to a chiral smectic-A* phase induces a tilt of the molecules and thereby a polar structure. (**c**) In an aligned bent-core nematic phase a dipole is present in the direction of the kink. [111, 112]

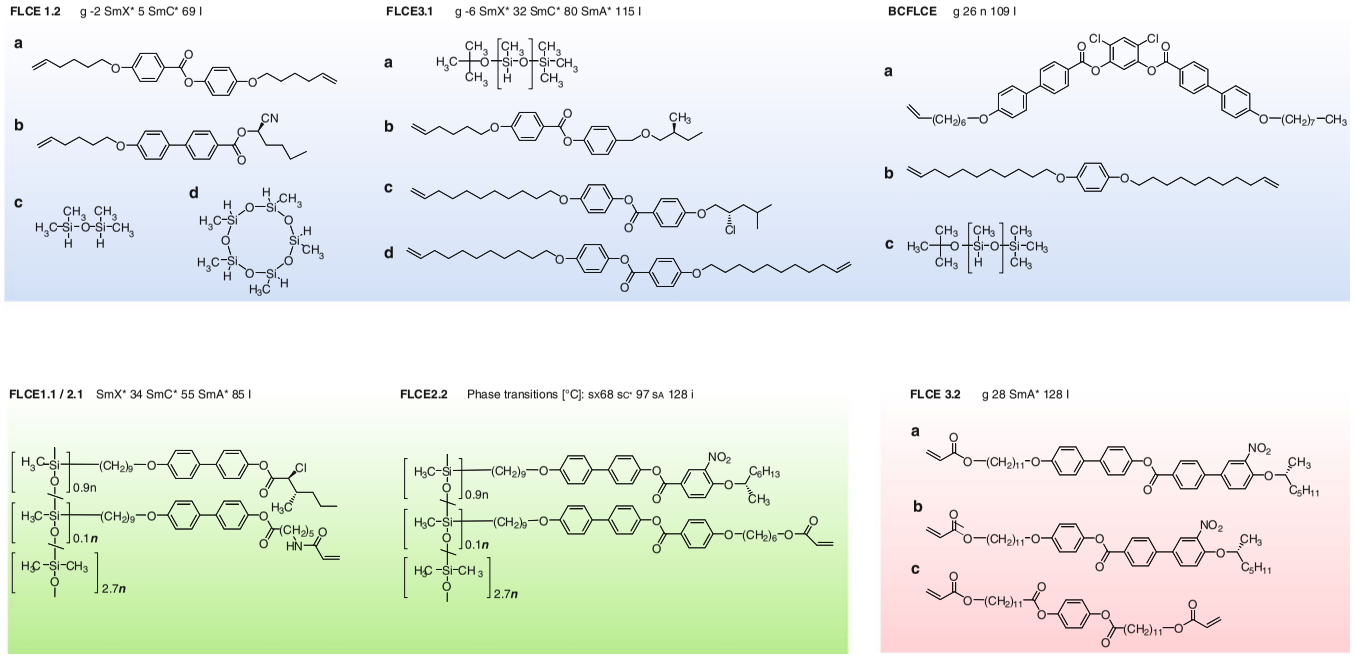

Scheme 1 Starting materials for FLCEs sorted by preparation method. The phase transitions were measured for the elastomers. The data are taken from the following references: FLCE 1.2 [137], FLCE 3.1 [138], BCFLCE [139], FLCE 1.1 and FLCE 2.1 [36, 37], FLCE 2.2 [38], and FLCE 3.2 [140, 141]

phase known from achiral mesogens: the director is oriented parallel to the layer normal, perpendicular to the layer plane. However, if an electric field is applied perpendicular to the layer normal of the s_A* phase, the mesogens tilt perpendicular to the field (see Fig. 14b). Hence the field induces a transition from an orthogonal smectic phase (s_A) to a tilted smectic phase (s_C*). This occurs because the tilting reduces the symmetry and induces a macroscopic polarization, which can interact with the external field. This effect is strongest at the (second-order) phase transition temperature (Curie temperature) between the s_A* and the s_C* phase. In combination with chiral smectic elastomers, this behavior is very effective at inducing shape variation because the sample shrinks parallel to the smectic layer normal (each layer gets thinner by tilting, see Fig. 14b) while it expands in the perpendicular direction.

In addition to chiral rod-like smectics, ferroelectricity has also been observed in LC phases from bent-core mesogens. In the case of these banana-shaped molecules, the core shape, together with their dense packing, biases the rotation around the long molecular axis [144, 145]. This leads to a summation of the molecular dipoles in the direction of the kink [146–148] (see Fig. 14c). Because of their molecular shape, not only smectic phases but also biaxial nematic phases show ferroelectricity [149, 150]. In this context, one has to bear in mind that alignment of the mesogens is essential to obtain devices. Smectic materials with a low viscosity and a low phase transition temperature (like the s_C* phase discussed above) usually meet these prerequisites better than the highly viscous polar phases of banana-shaped mesogens that normally exist at temperatures above 100°C. A recent example of a bent-core elastomer will be discussed at the end of this section.

We will concentrate here on systems in which the LC director is coupled to the network without losing its softness. This means that a rotation of the polar axis is still possible (see Fig. 14a) and real FLCEs can be prepared [23, 36–38]. Densely crosslinked systems that possess a polar axis, but cannot be switched [151–153], will be excluded. Although FLCEs can be switched, the state prior to crosslinking is stored. This is manifested in the optical hysteresis curve (see Fig. 15). The center of the curve is shifted from zero voltage in the direction opposite to that of the polarity of the field applied during crosslinking. This behavior can be explained by an additional internal mechanical field [23] that exhibits a minimum at the switching state in which the sample exists during crosslinking. This asymmetric switching is also observed in the smectic-A* phase. However, in that case the hysteresis is gone. The mesogens do not rotate between two ferroelectric states, but change their induced tilt angle due to the electroclinic effect (see Fig. 14b). Here again, the mechanical field shifts the switching curves to one side [23].

The FLCEs prepared in this way can be used either as sensor components, transforming a mechanical deformation into an electric signal, or as actuators that change their shape on application of an electric field. From the chemical point of view, they can be made by covalently linking the mesogenic groups to form a slightly crosslinked rubbery polymer network structure [3, 5, 8, 10, 154–156] or by dispersing a low-molar-mass liquid crystal in a phase-separated network structure [7, 40, 157–162]. These two systems possess very different structures locally. Macroscopically, however, they show very similar properties.

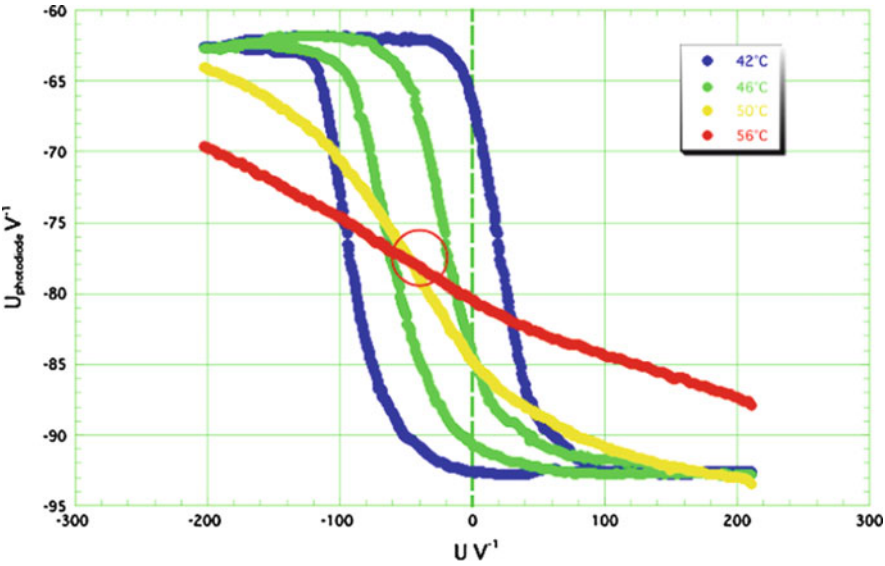

Fig. 15 Electrooptical hysteresis of a ferroelectric elastomer crosslinked in the s_C* phase [23]

3.2 Preparation of FLCEs

The outstanding property of FLCEs being their macroscopic dipole, the preparation must assure uniform alignment of the mesogens. The most direct approach to achieve this goal is application of an electric field during the crosslinking process [36]. Because the material has to be aligned prior to crosslinking at elevated temperatures, thermal reactions are inapplicable and photoinitiation becomes the method of choice. However, some photinitiators can give ionic impurities if irradiated in the presence of an electric field. Such a side reaction renders the sample unsuitable for experiments with electric fields.

Depending on the method of preparation, different orientations of the polar axis can be realized. If the samples are aligned between indium tin oxide (ITO)- and polyimide-coated glass slides, the mesogens align parallel to the surface and the smectic layers are oriented perpendicular to the glass slides [111]. Application of an electric field leads to a polar monodomain by alignment of the director. The polar axis is perpendicular to the film, in the direction of the electrodes (Fig. 16).

In spin-coated or free-standing films, the smectic layers are aligned parallel to the surface [163, 164]. In such a homeotropic arrangement the tilt direction is not defined and the polar axis of different domains is randomly distributed over the film. If the substrate is water-soluble, it can be dissolved and freely suspended films can be obtained [165].

Alternatively, a “two-stage” mechanical orientation can be applied to obtain polar FLCEs (see Fig. 17 and [184]). A first stretching aligns the director. However,

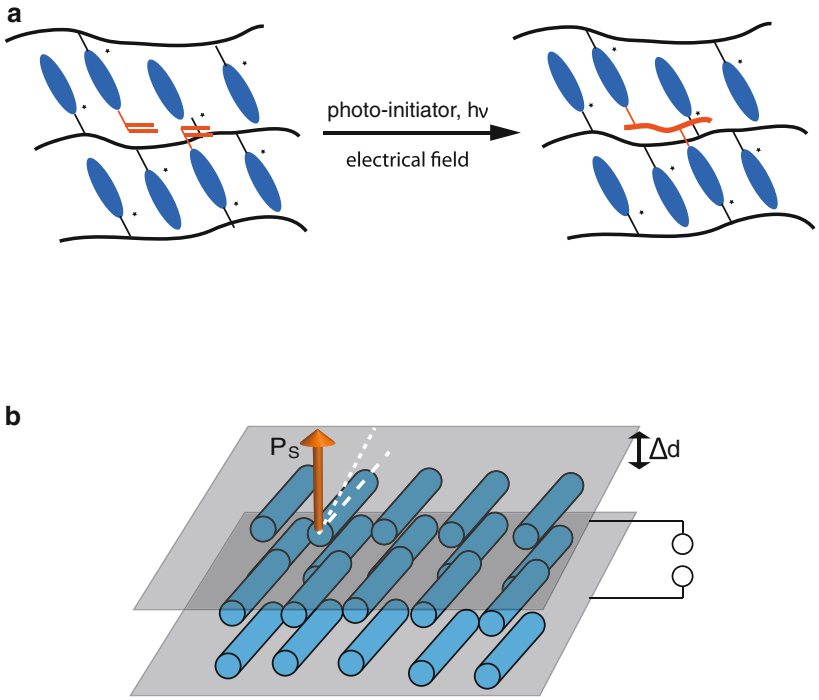

Fig. 16 (**a**) Crosslinking of an FLC polymer in the polar state. (**b**) FLCE in bookshelf configuration. The polar axis is perpendicular to the film. Δd indicates the direction of the thickness change induced by a mechanical field [36]

two orientations of the polar axis are still possible due to different tilt directions of the smectic layers: the sample maintains macroscopically an apolar structure. A second shear deformation applied parallel to the smectic layer planes (see Fig. 17) finally leads to a polar sample [166, 167]. The influence of the second shear process on the polarity of the sample can be determined from the evolution of the piezoelectric constant d_{33} perpendicular to the tilt direction. Initially, areas with opposite polarity exist and the film does not show any signal, but if the mesogens become reoriented by the shear, a signal will be measured [168].

Starting materials for the preparation of FLCEs are depicted in Scheme 1. They include ferroelectric LC polymers with polymerizable groups (FLCE 1.1 and FLCE 2.2), which can be crosslinked as depicted in Fig. 3c; reactive ferroelectric monomer mixtures (FLCE 3.3, see Fig. 3d); and mesogens with vinyl groups that react with silanes to form either side-chain (FLCE 3.1 and BCFLCE) or main-chain polymers (FLCE 1.2) according to Fig. 3a. Although the first three examples (FLCE 1.1, FLCE 2.2, and FLCE 3.3) allow photocrosslinking in the neat s_C^* phase, FLCE 3.1 and BCFLCE require crosslinking in solution and thus a two-stage deformation process.

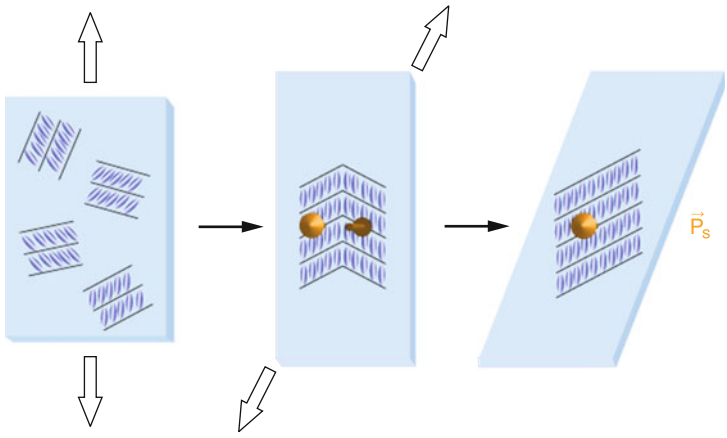

Fig. 17 Mechanical orientation of an FLCE by two stretching steps yields a polar monodomain [166, 167]. Depending on the procedure, the samples have a different thicknesses and director configurations

3.3 Electromechanical Properties of FLCEs

In this section we discuss the properties of FLCEs that are important for applications. Two options are possible: either a mechanical deformation generates a change of size or orientation of the polarization of the FLCE (an electric signal), or an applied electric field generates a deformation. In the case that an electric signal is detected, the piezoelectric constant is obtained. If the sample is deformed, the generated strain is of interest. Some characteristic values are collected in Table 1.

The first effect, piezoelectricity, is in principle well known for many types of polar materials [119]. The asymmetry of the switching observed for photocrosslinked elastomers (see Fig. 15) indicates stabilization of one particular switched state. This means that the sample must have a permanent dipole. If the sample is deformed, the director, and thereby the direction of the polar axis, changes. This effect is detected as an electric signal. Indeed a piezoelectric signal can be measured if the sample is deformed in the direction of the polar axis. As a consequence of the stabilization of the polar state, the sample shows a piezoelectric effect not only in the smectic-C* phase, but also in the smectic-A* phase [36]. The signal vanishes when the sample becomes isotropic (see Fig. 18).

For the measurements presented in Fig. 18, the smectic-C* material FLCE1.1 (see Table 1), was crosslinked inside a commercial EHC glass cell with an electrode gap of 10 μm. Deformation of the cell with a force of 1 N induces a charge of 6 pC/cm^2 [36]. The magnitude of this value should be compared to the macroscopic spontaneous polarization P_s (macroscopic dipole moment) of the FLC under investigation. For the uncrosslinked FLC, P_s values of 40–60 nC/cm^2 have been observed [36]. Thus, if a full reversal of the orientation of P_s could be induced by

Table 1 Properties of different piezoelectric materials

Material	Group	Thickness (mm)	Elastic modulus (Pa)	Strain (%)	Piezoelectriccoefficient (pC/N)	Electric field strength (V/μm)	Flexoelectric constant (nC/m)	Polarization (nC/cm^2)
PVDF	Goodfellow GmbH, Bad Nauheim, Germany	0.005	3.0×10^9	–	20	–	–	12×10^3
PZT	PI Ceramic GmbH, Lederhose, Germany	1.8	1.6×10^{11}	1.0×10^{-3}	150–300	–	–	14×10^3
FLCE1.1	Zentel [36]	0.01	10×10^6	–	5	–	–	80
FLCE1.2	Kremer [168]	0.35	–	0.4	17.5	–	–	–
BCFLCE	Harden [169]	0.3	–	10	–	–	30	10
FLCE2.1	Kremer [170]	7.5×10^{-5}	10×10^6	3	–	1.5	–	80
FLCE2.2	Stannarius [171]	0.280	10×10^6	1	–	3	–	200
FLCE3.1	Hiraoka [172]	0.4	–	0.6	30	3	–	–
FLCE3.2	Ratna and Naciri [140]	0.06	–	5	–	13.3	–	–

PVDF polyvinylidenfluoride; *PZT* lead zirconium titanate; *FLCE1* piezoelectric effect by compression perpendicular to the polar axis, planar alignment; *FLCE2* electroclinic effect in homeotropic films; *FCLCE3* electroclinic effect in stretched film with planar alignment; *BCFLCE* flexoelectric effect on bent-core material

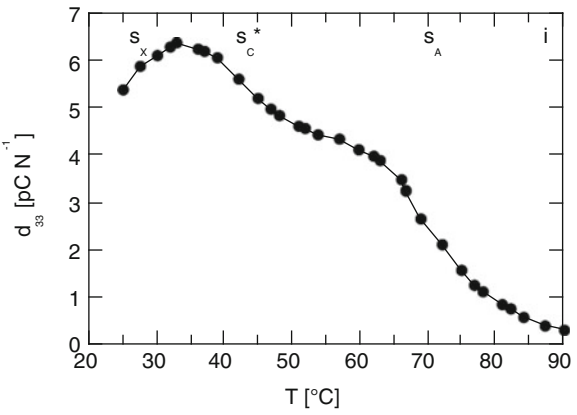

Fig. 18 Piezoelectric coefficient d_{33} of an FLCE crosslinked in the smectic-C* phase. The stabilization of the polar order leads to a smectic-A* phase that is also polar [36]

a mechanical deformation (elastic modulus of about 1 MPa [28–31, 173]), a piezoresponse of similar magnitude would be expected. The observed value of a few pC/cm^2 is about a factor 10,000 smaller. The EHC cell is glued on the sides and some stress is taken up by the deformation of the cell alone. Thus, the resulting piezoelectric coefficient should be somewhat larger if the glass plates are not connected with each other. This has been seen for free-standing films of FLCE1.2 that show a value of 17.5 pC/N [168]. This value is, however, still much smaller than the spontaneous polarization. Obviously, a reorientation of the polar axis could not be achieved, because a mechanical deformation parallel to the polar axis is not very effective at rotating P_s. Shear deformations might be more useful.

To optimize the piezoelectric response, some studies on the structure–property relations are adequate. One would like to work with FLCEs with a strong coupling between the polar axis and the network. Thus ferroelectric main-chain polymers might be attractive (see Fig. 2). However, up to now, there have been only a few reports about ferroelectric switching in main-chain polymers [174–176] and none about switching the corresponding elastomers. Concerning LC side-chain polymers, the position of the netpoints is essential for determining the coupling between the polar axis (and thus the director) and the polymer network. In the experiments described above, the crosslinkable group was attached to the end of the mesogen. This means that the netpoints link the polymer chains via the mesogenic groups [36]. As the mesogens have to move during switching, this is a serious obstacle and long switching times of 1 s are measured at fields up to 500 V. This can be circumvented if the polymer chains are directly attached to each other without including mesogenic units. This leads to much faster switchable ferroelectric polymer networks [37, 177]. In that case, the coupling between polar axis and polymer network is rather weak and the piezoelectric effect should be low.

On an absolute scale, a comparison of FLCEs with crystalline (or semicrystalline) materials like polyvinylidenfluoride (PVDF) and ceramic materials like lead zirconium titanate (PZT) is necessary. These have much larger polarizations (see Table 1). However, their elastic modulus is also much higher (in the gigapascal range).

Accordingly, the piezoelectric coefficients measured for FLCEs and for other ferroelectric materials have a similar magnitude because for similar forces the elastomers are deformed more strongly.

Concerning the shape variations resulting from the application of an external electric field, the consequences of an induced ferroelectric switching will be discussed at first. As evident from Fig. 14a, both polar states are very similar and the deformation resulting from the rotation of the director on the cone can be considered to be rather small. In fact some "vibrations" have been observed during rapid switching of low-molar-mass ferroelectrics; thus the shape variations must be rather small [178, 179]. The electroclinic effect, on the other hand, promises much larger deformations (see Fig. 14b) and most experiments have focused in this direction. In free-standing films, the smectic layers are parallel to the film surface and the polar axis lies in the plane of the film. This arrangement is ideal for observation of the electroclinic effect around the smectic-A* to chiral smectic-C* phase transition (see Fig. 19a). If an electric field is applied parallel to the smectic layers, the chiral mesogens will tilt such that the induced polarity is opposite to the electric field. The tilt of the molecules is accompanied by a decrease in the smectic layer thickness. Due to the stacking of the smectic layers in the film, the thickness variation of the various layers is expected to add up and a reasonable change of the film thickness should be observed.

These considerations have led to several attempts to measure the thickness change of films in dependence on an applied electric field. In a first experiment, a Michelson interferometer was used for the determination of the thickness change in a 75-nm thick free-standing smectic film of FLCE2.1 (Scheme 1). With this method, a strain of 4% at a field of 1.5 V/μm was measured [170], which would correspond to $a = 55 \times 10^{-15}$ m^2/V^2. In a second experiment (with the similar material FLCE2.2) reflection microscopy was used. This allowed simultaneous measurement of the decrease in film thickness and the associated increase in width of the sample (Fig. 20). In this experiment, a strain of only 1% was detected at a field of 3 V/μm [171], corresponding to $a = 1 \times 10^{-15}$ m^2/V^2. Most probably the smaller value is correct [171], because its magnitude is consistent with tilt angle susceptibilities of similar materials [23, 25], for which induced tilt angles of the

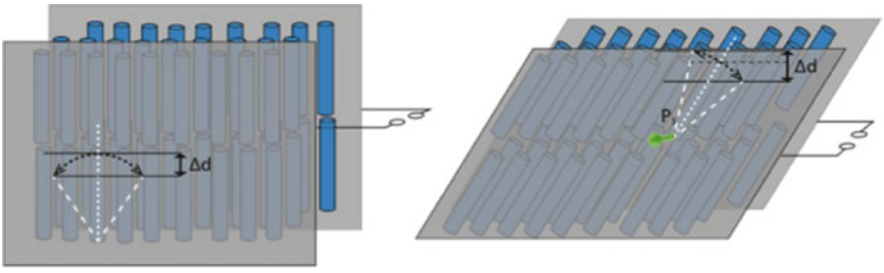

Fig. 19 (**a**) FLCE film crosslinked in the smectic-C* phase. (**b**) FLCE film crosslinked in the smectic-A* phase

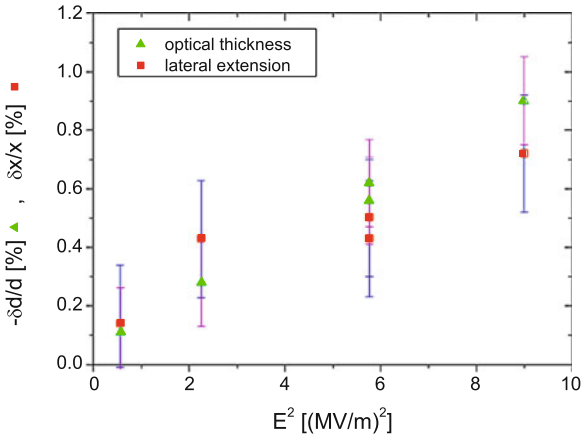

Fig. 20 Change of sample width and thickness, respectively, during electroclinic switching of a free- standing FLCE film [171]

order of 5° are found for comparable electric fields. This explanation is also supported by the findings of other groups (see Table 1) that also give values in the range of $a = 1 \times 10^{-15}$ m^2/V^2. Independent of the exact magnitude of the shape variation accessible with free-standing films, these results belong to the highest values ever reported for piezoelectric materials. Possibly, the shape variation can be increased further using LCEs from main-chain polymers [174], but so far no such measurements have been reported.

Elastomer films oriented by the two-stage stretching process have been used for similar experiments. If the electroclinic effect is measured in such films, it should be realized that the smectic layers are now perpendicular to the film surface. Thus tilting of the mesogens, either by a phase transition or by an electric field, will be seen primarily by a change in the length of the film while the thickness will vary only slightly to conserve the volume. The two-step stretching gives a rhomboedric sample with ferroelectric monodomains (see Fig. 19) if the sample is crosslinked in the s_C* phase. If such a sample is heated from the smectic-C* to the smectic-A* phase, the tilt angle approaches 0°. As a consequence of the crosslinking, a freely movable sample shows a macroscopic shear deformation during which it becomes rectangular and the length increases [138]. In this case, the macroscopic shape reflects the molecular arrangement: the mesogens change their orientation from tilted to perpendicular. With electrodes mounted to the film surface, the electroclinic effect can be observed in the smectic-C* and the smectic-A* phase. In the case of an elastomer crosslinked in the smectic-C* phase (FLCE3.1, see Fig. 19) [180], the mesogens are tilted toward the layer normal. Upon application of an alternating current field the sample extends or shrinks depending on the polarity of the applied field. In one case, the electroclinic effect adds an additional tilt to the existing tilt and the sample shrinks. In the other situation, the electroclinic effect counteracts the tilt of the s_C* phase and the sample becomes more elongated. If the elastomer sample is, however, crosslinked in the smectic-A* phase (FLCE3.2) [140], the mesogens are oriented perpendicular to the smectic layers. After the application of an electric field, a tilt is induced and the film shrinks perpendicular to

the layers. This effect is independent of the polarity (tilting to the left or the right). The shrinking rate perpendicular to the smectic layers is comparable to the shrinking of the homeotropic film mentioned before. As described for the thermal transition, the thickness change that is caused by the electroclinic switching is always accompanied by shear parallel to the smectic layers.

So far we have discussed networks containing calamitic rod-like mesogens. Due to their kinked shape, bent-core LCs (BCLCs) also have ferroelectric properties. Though they have been known for about 15 years, because of their high phase transition temperatures it is hard to obtain oriented samples. As a consequence, low-molar-mass BCLC systems have mainly been investigated so far. In a first experiment, direct measurement of the flexoelectric effect was performed [112]. The mechanical deformation resulted in induced currents of up to 8 nA (at 5 Hz and a 4.8 cm^2 electrode area). This corresponds to a bend flexoelectric coefficient $|e_3|$ of 60 nC/m. In nonaligned samples, smaller values are observed that increase upon mechanical treatment. This is attributed to improvement of the degree of orientational order. In the case of smectic BCLCs, the behavior is even more complicated. These phases are primarily composed of alternating layers that prevent a macroscopic polar orientation. Such samples have to be poled to align the polar axis and to obtain a piezoelectric signal. After poling, a piezoelectric current of up to 20 nA (2 cm^2 sample area) has been measured [181]. This corresponds to a piezoelectric constant of 100 pC/N, a value comparable to PVDF and ceramic materials. However, due to a thermal back-relaxation to the macroscopically apolar state, this value cannot be maintained. At 60°C the half-life time of the measured current is only 50 s.

Crosslinking can be used to overcome the aforementioned obstacles, as in the case of the calamitic networks in which the orientation and polarity are preserved. First experiments were performed by swelling a calamitic LCE with a low-molar-mass BCLC [182, 183]. Up to 35 mol% of this material could be incorporated into the network. The resulting gel had a flexoelectric constant $|e_3|$ of 20 nC/m. This is one-third of the value of the low-molar-mass BCLC, which corresponds to the volume fraction of the BCLC. Only recently has a pure bent-core elastomer (BCFLCE) been made [139, 169]. Following the synthetic route of Finkelmann, an oriented, transparent nematic elastomer sample could be obtained. As a polysiloxane backbone was used, the T_g was close to room temperature. The flexoelectric constant of 40 nC/m is somewhat smaller than for the pure bend-core monomer, but larger than the value obtained for the swollen elastomer.

4 Conclusions and Outlook

LCEs have been under investigation for several years. These systems are unique because of the combination of order and softness. During recent years, several developments have evolved that bring them closer to application. One important achievement is the introduction of various stimuli like electric current and

irradiation with light that can, in addition to heat, trigger the NI phase transition and thereby the actuation process. In addition, FLCEs have been made that can produce a movement in an electric field without any phase transition. These new stimuli allow direct addressing of the actuator without the need to heat the whole device.

As far as synthesis is concerned, photochemistry has become the method of choice for crosslinking reactions. In this way, polymerization and crosslinking of monomeric liquid crystals can be initiated, as well as crosslinking of functional prepolymers on demand. This allows the utilization on LCEs of several orientation techniques known from low-molar-mass liquid crystals, like electric fields and surface forces. Macroscopic machines have been constructed that use either the bending motion or the lateral deformation of an LCE actuator. Among them are locomotion devices that work both on land and in water, grippers, and devices that transform light into rotational energy.

The most important development in LCE research is miniaturization. Novel preparation techniques like lithography, inkjet printing, microfluidics, and electrospinning allow fabrication of aligned LCE samples on micrometer and even nanometer scales.

These advances are the most promising for use in real-world applications, because actuation on these scales is difficult to achieve with traditional methods. Potential applications are stimuli-responsive surfaces, microlenses, propulsion systems for microrobots, and lab-on-a-chip systems. In our opinion, future research in the field of LCEs will focus on these small scales.

References

1. Brand HR, Finkelmann H (1998) Physical properties of liquid crystalline elastomers. In: Demus D, Boodby J, Gray GW, Spiess HW (eds) Handbook of liquid crystals, vol. 3, Chap. 5. Wiley-VCH, Weinheim. doi:10.1002/9783527620593.ch5
2. Brand HR, Pleiner H, Martinoty P (2006) Selected macroscopic properties of liquid crystalline elastomers. Soft Matter 2(3):182–189. doi:10.1039/b512693m
3. Brehmer M, Zentel R (1994) Liquid crystalline elastomers- characterization as networks. Mol Cryst Liq Cryst Sci Technol Sect A-Mol Cryst Liq Cryst 243:353–376. doi:10.1080/10587259408037775
4. Finkelmann H, Brand HR (1994) Liquid crystalline elastomers - a class of materials with novel properties. Trends Polym Sci 2 (7):222–226
5. Ohm C, Brehmer M, Zentel R (2010) Liquid crystalline elastomers as actuators and sensors. Adv Mater 22(31):3366–3387. doi:10.1002/Adma.200904059
6. Terentjev EM (1999) Liquid-crystalline elastomers. J Phys-Condens Matter 11(24): R239–R257. doi:10.1088/0953-8984/11/24/201
7. Urayama K (2007) Selected issues in liquid crystal elastomers and gels. Macromolecules 40 (7):2277–2288. doi:10.1021/ma0623688
8. Warner M, Terentjev EM (2003) Liquid crystal elastomers, vol 120. International series of monographs on physics. Oxford University Press, Oxford. doi:http://ukcatalogue.oup.com/product/9780198527671.doa
9. Xie P, Zhang RB (2005) Liquid crystal elastomers, networks and gels: advanced smart materials. J Mater Chem 15(26):2529–2550. doi:10.1039/b413835j

10. Zentel R (1989) Liquid crystalline elastomers. Angew Chem Int Ed Engl 28(10):1407–1415
11. de Gennes PG (1975) One type of nematic polymers. Comptes Rendus Hebdomadaires Des Seances De L Academie Des Sciences Serie B 281(5–8):101–103
12. de Gennes PG, Hebert M, Kant R (1996) Artificial muscles based on nematic gels. In: 2nd international symposium on molecular order and mobility in polymer systems, St Petersburg, Russia, 21–24 May 1996. Huthig & Wepf Verlag, pp 39–49. doi:10.1002/masy.19971130107
13. Mirfakhrai T, Madden JDW, Baughman RH (2007) Polymer artificial muscles. Mater Today 10(4):30–38. doi:10.1016/S1369-7021(07)70048-2
14. Selinger RLB, Mbanga BL, Selinger JV (2008) Modeling liquid crystal elastomers: actuators, pumps, and robots – art. no. 69110A. In: Chien LC (ed) Conference on emerging liquid crystal technologies III, San Jose, CA, 20–22 Jan 2008. SPIE-int soc optical engineering, p A9110. doi:10.1117/12.768282
15. Madden JDW, Vandesteeg NA, Anquetil PA, Madden PGA, Takshi A, Pytel RZ, Lafontaine SR, Wieringa PA, Hunter IW (2003) Artificial muscle technology: physical principles and naval prospects. In: 13th international symposium on unmanned untethered submersible technology, Durham, NH, 24–27 Aug 2003. IEEE-Inst Electrical Electronics Engineers Inc, pp 706–728. doi:10.1109/joe.2004.833135
16. Yang H, Buguin A, Taulemesse J-M, Kaneko K, Méry S, Bergeret A, Keller P (2009) Micron-sized main-chain liquid crystalline elastomer actuators with ultralarge amplitude contractions. J Am Chem Soc 131(41):15000–15004. doi:10.1021/ja905363f
17. Bualek S, Kapitza H, Meyer J, Schmidt GF, Zentel R (1988) Orientability of crosslinked and of chiral liquid-crystalline polymers. Mol Cryst Liq Cryst 155:47–56. doi:10.1080/00268948808070351
18. Küpfer J, Finkelmann H (1991) Nematic liquid single-crystal elastomers. Makromol Chem-Rapid Commun 12(12):717–726. doi:10.1002/marc.1991.030121211
19. Öge T, Zentel R (1996) Manipulation of the ferroelectricity in LC polymers via photomechanical isomerization of azobenzene moieties. Macromol Chem Phys 197(6):1805–1813
20. de Jeu WH (1980) Physical properties of liquid crystalline materials, vol 1, Liquid crystal monographs. Gordon and Breach, New York
21. Kempe MD, Scruggs NR, Verduzco R, Lal J, Kornfield JA (2004) Self-assembled liquid-crystalline gels designed from the bottom up. Nat Mater 3(3):177–182. doi:10.1038/nmat1074
22. Li JJ, Stannarius R, Tolksdorf C, Zentel R (2003) Hydrogen bonded ferroelectric liquid crystal gels in freely suspended film geometry. Phys Chem Chem Phys 5(5):916–923. doi:10.1039/b205210e
23. Brehmer M, Zentel R, Giesselmann F, Germer R, Zugenmaier P (1996) Coupling of liquid crystalline and polymer network properties in LC-elastomers. Liq Cryst 21(4):589–596. doi:10.1080/02678299608032868
24. Garoff S, Meyer RB (1977) Electro-clinic effect at A/C phase-change in a chiral smectic liquid-crystal. Phys Rev Lett 38(15):848–851. doi:10.1103/PhysRevLett.38.848
25. Poths H, Andersson G, Skarp K, Zentel R (1992) Fast electroclinic switching in a ferroelectric LC-polysiloxane. Adv Mater 4(12):792–794. doi:10.1002/adma.19920041204
26. Finkelmann H, Ringsdorf H, Wendorff JH (1978) Model considerations and examples of enantiotropic liquid-crystalline polymers - polyreactions in ordered systems, 14. Makromol Chem - Macromol Chem Phys 179(1):273–276. doi:10.1002/macp. 1978.021790129
27. Zentel R (1994) Liquid crystalline polymers. In: Stegemeyer H (ed) Liquid crystals. Steinkopff, Darmstadt, pp 103–140
28. Kaufhold W, Finkelmann H, Brand HR (1991) Nematic elastomers. 1. Effect of the spacer length on the mechanical coupling between network anisotropy and nematic order. Makromol Chem - Macromol Chem Phys 192(11):2555–2579. doi:10.1002/macp.1991.021921104
29. Martinoty P, Stein P, Finkelmann H, Pleiner H, Brand HR (2004) Mechanical properties of monodomain side chain nematic elastomers. Eur Phys J E 14(4):311–321. doi:10.1140/epje/i2003-10154-y

30. Pakula T, Zentel R (1991) Mechanical behavior of liquid-crystalline side-group polymers and their networks. Makromol Chem - Macromol Chem Phys 192(10):2401–2410. doi:10.1002/macp.1991.021921018
31. Zentel R, Wu JS (1986) Rheological properties of liquid crystalline side-group polymers in the isotropic, nematic and smectic states. Makromol Chem - Macromol Chem Phys 187(7):1727–1736. doi:10.1002/macp.1986.021870716
32. Hikmet RAM, Lub J, Broer DJ (1991) Anisotropic networks formed by photopolymerization of liquid-crystalline molecules. Adv Mater 3(7–8):392–394. doi:10.1002/adma.19910030713
33. Li MH, Keller P, Yang JY, Albouy PA (2004) An artificial muscle with lamellar structure based on a nematic triblock copolymer. Adv Mater 16(21):1922–1925. doi:10.1002/adma.200400658
34. Wiesemann A, Zentel R, Pakula T (1992) Redox-active liquid-crystalline ionomers.1. Synthesis and rheology. Polymer 33(24):5315–5320. doi:10.1016/0032-3861(92)90818-H
35. Rogez D, Martinoty P (2011) Mechanical properties of monodomain nematic side-chain liquid-crystalline elastomers with homeotropic and in-plane orientation of the director. Eur Phys J E Soft matter 34(7):69. doi:10.1140/epje/i2011-11069-8
36. Brehmer M, Zentel R, Wagenblast G, Siemensmeyer K (1994) Ferroelectric liquid crystalline elastomers. Macromol Chem Phys 195(6):1891–1904. doi:10.1002/macp.1994.021950601
37. Gebhard E, Zentel R (2000) Ferroelectric liquid crystalline elastomers, 1 - Variation of network topology and orientation. Macromol Chem Phys 201(8):902–910. doi:10.1002/(SICI)1521-3935(20000501)201:8<902::AID-MACP902>3.0.CO;2-9
38. Gebhard E, Zentel R (2000) Ferroelectric liquid crystalline elastomers, 2 - Variation of mesogens and network density. Macromol Chem Phys 201(8):911–922. doi:10.1002/(SICI)1521-3935(20000501)201:8<911::AID-MACP911>3.0.CO;2-9
39. Kapitza H, Zentel R (1991) Chiral liquid-crystalline elastomers by polymer-analogous reactions. Makromol Chem - Macromol Chem Phys 192(8):1859–1872. doi:10.1002/macp.1991.021920821
40. Ikeda T, Nakano M, Yu YL, Tsutsumi O, Kanazawa A (2003) Anisotropic bending and unbending behavior of azobenzene liquid-crystalline gels by light exposure. Adv Mater 15(3):201–205. doi:10.1002/adma.200390045
41. Beyer P, Braun L, Zentel R (2007) (Photo)crosslinkable smectic LC main-chain polymers. Macromol Chem Phys 208(22):2439–2448. doi:10.1002/macp.200700292
42. Beyer P, Terentjev EM, Zentel R (2007) Monodomain liquid crystal main chain elastomers by photocrosslinking. Macromol Rapid Commun 28(14):1485–1490. doi:10.1002/marc.200700210
43. Komp A, Ruhe J, Finkelmann H (2005) A versatile preparation route for thin free-standing liquid single crystal elastomers. Macromol Rapid Commun 26(10):813–818. doi:10.1002/marc.200500049
44. McKenzie BM, Wojtecki RJ, Burke KA, Zhang C, Jakli A, Mather PT, Rowan SJ (2011) Metallo-responsive liquid crystalline monomers and polymers. Chem Mater 23(15):3525–3533. doi:10.1021/cm2011617
45. Fox JD, Rowan SJ (2009) Supramolecular polymerizations and main-chain supramolecular polymers. Macromolecules 42(18):6823–6835. doi:10.1021/ma901144t
46. Oriol L, Pinol M, Serrano JL (1997) The state of the art in metallomesogenic polymers. Prog Polym Sci 22(5):873–911. doi:10.1016/s0079-6700(97)00011-7
47. Ahir SV, Tajbakhsh AR, Terentjev EM (2006) Self-assembled shape-memory fibers of triblock liquid-crystal polymers. Adv Funct Mater 16(4):556–560. doi:10.1002/adfm.200500692
48. Finkelmann H (1987) Liquid crystalline polymers. Angew Chem Int Ed Engl 26(9):816–824. doi:10.1002/anie.198708161
49. Boeffel C, Spiess HW, Hisgen B, Ringsdorf H, Ohm H, Kirste RG (1986) Molecular order of spacer and main chain in polymeric side-group liquid-crystals. Makromol Chem Rapid Commun 7(12):777–783

50. Noirez L, Keller P, Cotton JP (1995) On the structure and the chain conformation of side-chain liquid-crystal polymers. Liq Cryst 18(1):129–148. doi:10.1080/02678299508036602
51. Leroux N, Keller P, Achard MF, Noirez L, Hardouin F (1993) Small-angle neutron-scattering experiments on side-on fixed liquid-crystal polyacrylates. J Phys II 3(8):1289–1296. doi:10.1051/jp2:1993199
52. Arrighi V, Higgins JS, Weiss RA, Cimecioglu AL (1992) A small-angle neutron scattering study of a semi-flexible main-chain liquid-crystalline copolyester. Macromolecules 25(20): 5297–5305
53. Dallest JF, Maissa P, Tenbosch A, Sixou P, Blumstein A, Blumstein R, Teixeira J, Noirez L (1988) Experimental evidence of chain extension at the transition-temperature of a nematic polymer. Phys Rev Lett 61(22):2562–2565. doi:10.1103/PhysRevLett.61.2562
54. Hardouin F, Leroux N, Méry S, Noirez L (1992) Small-angle neutron-scattering experiments on side-on fixed liquid-crystal polysiloxanes. J Phys II 2(3):271–278. doi:10.1051/jp2:1992131
55. Keller P, Carvalho B, Cotton JP, Lambert M, Moussa F, Pepy G (1985) Side-chain mesomorphic polymers-studies labeled backbones by neutron-scattering. Journal De Physique Lettres 46(22):1065–1071. doi:10.1051/jphyslet:0198500460220106500
56. Kirste RG, Ohm HG (1985) The conformation of liquid-crystalline polymers as revealed by neutron-scattering. Makromol Chem Rapid Commun 6(3):179–185. doi:10.1002/marc.1985.030060312
57. Ohm HG, Kirste RG, Oberthur RC (1988) The backbone conformation of liquid-crystalline side-chain polymers in the mesophases and in the isotropic phase determined by scattering methods. Makromol Chem Macromol Chem Phys 189(6):1387–1405. doi:10.1002/macp.1988.021890616
58. Pepy G, Noirez L, Keller P, Lambert M, Moussa F, Cotton JP, Strazielle C, Lapp A, Hardouin F, Mauzac M, Richard H (1990) Observation of the conformation and structure of some liquid-crystal polymers by small-angle neutron-scattering. Makromol Chem Macromol Chem Phys 191(6):1383–1392. doi:10.1002/macp.1990.021910617
59. Thomsen DL, Keller P, Naciri J, Pink R, Jeon H, Shenoy D, Ratna BR (2001) Liquid crystal elastomers with mechanical properties of a muscle. Macromolecules 34(17):5868–5875. doi:10.1021/ma001639q
60. Wermter H, Finkelmann H (2001) Liquid crystalline elastomers as artificial muscles. e-Polymers 013. Available at http://www.e-polymers.org/journal/papers/finkelmann_210801.pdf
61. Tajbakhsh AR, Terentjev EM (2001) Spontaneous thermal expansion of nematic elastomers. Eur Phys J E 6(2):181–188. doi:10.1007/s101890170020
62. Beyer P, Krueger M, Giesselmann F, Zentel R (2007) Photoresponsive ferroelectric liquid-crystalline polymers. Adv Funct Mater 17(1):109–114. doi:10.1002/Adfm.200600513
63. Komp A, Finkelmann H (2007) A new type of macroscopically oriented smectic-A liquid crystal elastomer. Macromol Rapid Commun 28(1):55–62. doi:10.1002/marc.200600640
64. Nishikawa E, Finkelmann H (1999) Smectic-A liquid single crystal elastomers – strain induced break-down of smectic layers. Macromol Chem Phys 200(2):312–322. doi:10.1002/(SICI)1521-3935(19990201)200:2<312::AID-MACP312>3.0.CO;2-Y
65. Sanchez-Ferrer A, Finkelmann H (2009) Thermal and mechanical properties of new main-chain liquid-crystalline elastomers. Mol Cryst Liq Cryst 508:348–356. doi:10.1080/15421400903065861
66. Poths H, Zentel R (1994) Structure–property relationships of diluted ferroelectric polysiloxanes. Liq Cryst 16(5):749–767. doi:10.1080/02678299408027848
67. Stannarius R, Schuring H, Tolksdorf C, Zentel R (2001) Elastic properties of liquid crystal elastomer balloons. Mol Cryst Liq Cryst 364:305–312. doi:10.1080/10587250108024999
68. Ohm C, Morys M, Forst FR, Braun L, Eremin A, Serra C, Stannarius R, Zentel R (2011) Preparation of actuating fibres of oriented main-chain liquid crystalline elastomers by a wetspinning process. Soft Matter 7(8):3730–3734. doi:10.1039/c1sm05111c

69. Ohm C, Fleischmann EK, Kraus I, Serra C, Zentel R (2010) Control of the properties of micrometer-sized actuators from liquid crystalline elastomers prepared in a microfluidic setup. Adv Funct Mater 20(24):4314–4322. doi:10.1002/adfm.201001178
70. de Jeu WH, Obraztsov EP, Ostrovskii BI, Ren W, McMullan PJ, Griffin AC, Sanchez-Ferrer A, Finkelmann H (2007) Order and strain in main-chain smectic liquid-crystalline polymers and elastomers. Eur Phys J E 24(4):399–409. doi:10.1140/epje/i2007-10254-8
71. Demus D, Goodby J, Gray GW, Spiess HW (2008) Handbook of liquid crystals set. Wiley-VCH Verlag GmbH, Weinheim. doi:10.1002/9783527619276
72. Spillmann CA, Naciri J, Martin BD, Farahat W, Herr H, Ratna BR (2005) Stacking nematic elastomers for artificial muscle applications. In: 3rd international conference on materials for advanced technologies (ICMAT-2005)/9th international conference on advanced materials (ICAM 2005), Singapore, SINGAPORE, 03–08 July 2005. pp 500–505. doi:10.1016/j.sna.2006.04.045
73. Chambers M, Finkelmann H, Remskar M, Sanchez-Ferrer A, Zalar B, Zumer S (2009) Liquid crystal elastomer-nanoparticle systems for actuation. J Mater Chem 19(11):1524–1531. doi:10.1039/b812423j
74. Yang LQ, Setyowati K, Li A, Gong SQ, Chen J (2008) Reversible infrared actuation of carbon nanotube-liquid crystalline elastomer nanocomposites. Adv Mater 20(12):2271–2275. doi:10.1002/adma.200702953
75. Kaiser A, Winkler M, Krause S, Finkelmann H, Schmidt AM (2009) Magnetoactive liquid crystal elastomer nanocomposites. J Mater Chem 19(4):538–543. doi:10.1039/b813120c
76. Ikeda T, Tsutsumi O (1995) Optical switching and image storage by means of azobenzene liquid-crystal films. Science 268(5219):1873–1875. doi:10.1126/science.268.5219.1873
77. Camacho-Lopez M, Finkelmann H, Palffy-Muhoray P, Shelley M (2004) Fast liquid-crystal elastomer swims into the dark. Nat Mater 3(5):307–310. doi:10.1038/nmat1118
78. Finkelmann H, Nishikawa E, Pereira GG, Warner M (2001) A new opto-mechanical effect in solids. Phys Rev Lett 87(1):4. doi:01550110.1103/PhysRevLett.87.015501
79. Hogan PM, Tajbakhsh AR, Terentjev EM (2002) uv manipulation of order and macroscopic shape in nematic elastomers. Phys Rev E 65(4):10. doi:04172010.1103/PhysRevE.65.041720
80. Li MH, Keller P, Li B, Wang XG, Brunet M (2003) Light-driven side-on nematic elastomer actuators. Adv Mater 15(7–8):569–572. doi:10.1002/adma.200304552
81. Yin RY, Xu WX, Kondo M, Yen CC, Mamiya J, Ikeda T, Yu YL (2009) Can sunlight drive the photoinduced bending of polymer films? J Mater Chem 19(20):3141–3143. doi:10.1039/b904973h
82. van Oosten CL, Bastiaansen CWM, Broer DJ (2009) Printed artificial cilia from liquid-crystal network actuators modularly driven by light. Nat Mater 8(8):677–682. doi:10.1038/nmat2487
83. Yu YL, Nakano M, Ikeda T (2003) Directed bending of a polymer film by light – miniaturizing a simple photomechanical system could expand its range of applications. Nature 425(6954):145. doi:10.1038/425145a
84. Vennes M, Zentel R, Rossle M, Stepputat M, Kolb U (2005) Smectic liquid-crystalline colloids by miniemulsion techniques. Adv Mater 17(17):2123–2127. doi:10.1002/adma.200500310
85. Haseloh S, van der Schoot P, Zentel R (2010) Control of mesogen configuration in colloids of liquid crystalline polymers. Soft Matter 6(17):4112–4119. doi:10.1039/c0sm00125b
86. Haseloh S, Ohm C, Smallwood F, Zentel R (2011) Nanosized shape-changing colloids from liquid crystalline elastomers. Macromol Rapid Commun 32(1):88–93
87. Ohm C, Kapernaum N, Nonnenmacher D, Giesselmann F, Serra C, Zentel R (2011) Microfluidic synthesis of highly shape-anisotropic particles from liquid crystalline elastomers with defined director field configurations. J Am Chem Soc 133(14):5305–5311. doi:10.1021/ja1095254
88. Yang H, Ye G, Wang XG, Keller P (2011) Micron-sized liquid crystalline elastomer actuators. Soft Matter 7(3):815–823. doi:10.1039/c0sm00734j

89. Zentel R, Strobl GR (1984) Structures of liquid crystalline side group polymers oriented by drawing. Makromol Chem - Macromol Chem Phys 185(12):2669–2676. doi:10.1002/macp.1984.021851217
90. Kim ST, Finkelmann H (2001) Cholesteric liquid single-crystal elastomers (LSCE) obtained by the anisotropic deswelling method. Macromol Rapid Commun 22(6):429–433. doi:10.1002/1521-3927(20010301)22:6<429::AID-MARC429>3.0.CO;2-#
91. Nishikawa E, Yamamoto J, Yokoyama H, Finkelmann H (2004) Smectic a elastomers with uniform homeotropic orientation obtained by applying a biaxial mechanical field. Macromol Rapid Commun 25(5):611–617. doi:10.1002/marc.200300183
92. Harris KD, Cuypers R, Scheibe P, van Oosten CL, Bastiaansen CWM, Lub J, Broer DJ (2005) Large amplitude light-induced motion in high elastic modulus polymer actuators. J Mater Chem 15(47):5043–5048. doi:10.1039/b512655j
93. Elias AL, Harris KD, Bastiaansen CWM, Broer DJ, Brett MJ (2006) Photopatterned liquid crystalline polymers for microactuators. J Mater Chem 16(28):2903–2912. doi:10.1039/b605511g
94. Yamada M, Kondo M, Mamiya JI, Yu YL, Kinoshita M, Barrett CJ, Ikeda T (2008) Photomobile polymer materials: towards light-driven plastic motors. Angew Chem Int Ed 47(27):4986–4988. doi:10.1002/anie.200800760
95. Krause S, Dersch R, Wendorff JH, Finkelmann H (2007) Photocrosslinkable liquid crystal main-chain polymers: thin films and electrospinning. Macromol Rapid Commun 28(21):2062–2068. doi:10.1002/marc.200700460
96. Odell JA, Keller A, Mueller AJ (1989) Extensional flow behavior of macromolecules in solution. In: Polymers in aqueous media, vol 223. Advances in Chemistry. American Chemical Society, Washington, pp 193–244. doi:10.1021/ba-1989-0223.ch011
97. Naciri J, Srinivasan A, Jeon H, Nikolov N, Keller P, Ratna BR (2003) Nematic elastomer fiber actuator. Macromolecules 36(22):8499–8505. doi:10.1021/ma034921g
98. Ohm C, Serra C, Zentel R (2009) A continuous flow synthesis of micrometer-sized actuators from liquid crystalline elastomers. Adv Mater 21(47):4859–4862. doi:10.1002/adma.200901522
99. Cairns DR, Shafran MS, Sierros KA, Huebsch WW, Kessrnan AJ (2010) Stimulus-responsive fluidic dispersions of rod shaped liquid crystal polymer colloids. Mater Lett 64(10):1133–1136. doi:10.1016/j.matlet.2010.02.021
100. Ohm C, Haberkorn N, Theato P, Zentel R (2011) Template-based fabrication of nanometer-scaled actuators from liquid-crystalline elastomers. Small 7(2):194–198. doi:10.1002/smll.201001315
101. Yang ZQ, Huck WTS, Clarke SM, Tajbakhsh AR, Terentjev EM (2005) Shape-memory nanoparticles from inherently non-spherical polymer colloids. Nat Mater 4(6):486–490. doi:10.1038/nmat1389
102. Ikeda T, Mamiya J, Yu YL (2007) Photomechanics of liquid-crystalline elastomers and other polymers. Angew Chem Int Ed 46(4):506–528. doi:10.1002/anie.200602372
103. Yamada M, Kondo M, Miyasato R, Naka Y, Mamiya J, Kinoshita M, Shishido A, Yu YL, Barrett CJ, Ikeda T (2009) Photomobile polymer materials-various three-dimensional movements. J Mater Chem 19(1):60–62. doi:10.1039/b815289f
104. White TJ, Serak SV, Tabiryan NV, Vaia RA, Bunning TJ (2009) Polarization-controlled, photodriven bending in monodomain liquid crystal elastomer cantilevers. J Mater Chem 19(8):1080–1085. doi:10.1039/b818457g
105. Anderle K, Birenheide R, Werner MJA, Wendorff JH (1991) Molecular adressing - studies on light-induced reorientation in liquid-crystalline side-chain polymers. Liq Cryst 9(5):691–699. doi:10.1080/02678299108030382
106. Natansohn A, Rochon P, Gosselin J, Xie S (1992) Azo polymers for reversible optical storage. 1. poly[4'-[[2-(acryloyloxy)ethyl]ethylamino]-4-nitroazobenzene]. Macromolecules 25(8):2268–2273. doi:10.1021/ma00034a031

107. Sanchez-Ferrer A, Fischl T, Stubenrauch M, Wurmus H, Hoffmann M, Finkelmann H (2009) Photo-crosslinked side-chain liquid-crystalline elastomers for microsystems. Macromol Chem Phys 210(20):1671–1677. doi:10.1002/macp.200900308
108. Sungur E, Li MH, Taupier G, Boeglin A, Romeo M, Mery S, Keller P, Dorkenoo KD (2007) External stimulus driven variable-step grating in a nematic elastomer. Opt Express 15(11): 6784–6789
109. Sungur E, Mager L, Boeglin A, Li MH, Keller P, Dorkenoo KD (2010) Temperature tunable optical gratings in nematic elastomer. Appl Phys A Mater Sci Process 98(1):119–122. doi:10.1007/s00339-009-5448-z
110. Harris KD, Bastiaansen CWM, Lub J, Broer DJ (2005) Self-assembled polymer films for controlled agent-driven motion. Nano Lett 5(9):1857–1860. doi:10.1021/nl0514590
111. Clark NA, Lagerwall ST (1980) Submicrosecond bistable electro-optic switching in liquid-crystals. Appl Phys Lett 36(11):899–901. doi:10.1063/1.91359
112. Harden J, Mbanga B, Eber N, Fodor-Csorba K, Sprunt S, Gleeson JT, Jakli A (2006) Giant flexoelectricity of bent-core nematic liquid crystals. Phys Rev Lett 97. doi:10.1103/PhysRevLett.97.157802
113. Lagerwall ST (2007) The necessary conditions for macroscopic polarization. In: Ferroelectric and antiferroelectric liquid crystals. Wiley-VCH Verlag GmbH, Weinheim, pp 57–91. doi:10.1002/9783527613588.ch3
114. Ho RM, Chiang YW, Lin SC, Chen CK (2011) Helical architectures from self-assembly of chiral polymers and block copolymers. Prog Polym Sci 36(3):376–453. doi:10.1016/j.progpolymsci.2010.09.001
115. Brochu P, Pei QB (2010) Advances in dielectric elastomers for actuators and artificial muscles. Macromol Rapid Commun 31(1):10–36. doi:10.1002/marc.200900425
116. Lagerwall JPF, Giesselmann F (2006) Current topics in smectic liquid crystal research. ChemPhysChem 7(1):20–45. doi:10.1002/cphc.200500472
117. Zentel R, Gebhard E, Brehmer M (2000) Ferroelectric LC-elastomers. Adv Chem Phys 113:159–182. doi:10.1002/9780470141724.ch4
118. Kremer F, Skupin H, Lehmann W, Hartmann L, Stein P, Finkelmann H (2000) Structure, mobility, and piezoelectricity in ferroelectric liquid crystalline elastomers. Adv Chem Phys 113:183–201. doi:10.1002/9780470141724.ch5
119. Brehmer M, Zentel R (2011) Ferroelectric liquid crystalline elastomers. In: Encyclopedia of polymer science and technology. Wiley. doi:10.1002/0471440264.pst429.pub2
120. Walba DM, Xiao L, Keller P, Shao RF, Link D, Clark NA (1999) Ferroelectric liquid crystals for second order nonlinear optics. Pure Appl Chem 71(11):2117–2123. doi:10.1351/pac199971112117
121. Walba DM, Dyer DJ, Sierra T, Cobben PL, Shao RF, Clark NA (1996) Ferroelectric liquid crystals for nonlinear optics: orientation of the disperse red 1 chromophore along the ferroelectric liquid crystal polar axis. J Am Chem Soc 118(5):1211–1212. doi:10.1021/ja952387p
122. Liu JY, Robinson MG, Johnson KM, Walba DM, Ros MB, Clark NA, Shao RF, Doroski D (1991) The measurement of 2nd-harmonic generation in novel ferroelectric liquid-crystal materials. J Appl Phys 70(7):3426–3430. doi:10.1063/1.350330
123. Kapitza H, Zentel R, Twieg RJ, Nguyen C, Vallerien SU, Kremer F, Willson CG (1990) Ferroelectric liquid-crystalline polysiloxanes with high spontaneous polarization and possible applications in nonlinear optics. Adv Mater 2(11):539–543. doi:10.1002/adma.19900021106
124. Wischerhoff E, Zentel R, Redmond M, Mondainmonval O, Coles H (1994) Ferroelectric liquid-crystalline polysiloxanes designed for high 2nd-order nonlinear susceptibilities. Macromol Chem Phys 195(5):1593–1602. doi:10.1002/macp.1994.021950511
125. Kocot A, Wrzalik R, Vij JK, Brehmer M, Zentel R (1994) Dielectric and electrooptical studies of a ferroelectric copolysiloxane. Phys Rev B 50(22):16346–16356. doi:10.1103/PhysRevB.50.16346
126. Lehmann W, Leister N, Hartmann L, Geschke D, Kremer F, Stein P, Finkelmann H (1999) Piezoelectric and pyroelectric investigations on microtomized sections of single-crystalline

ferroelectric liquid crystalline elastomers (SC-FLCE). Mol Cryst Liq Cryst Sci Technol Sect A Mol Cryst Liq Cryst 328:437–445. doi:10.1080/10587259908026087
127. Leister N, Lehmann W, Weber U, Geschke D, Kremer F, Stein P, Finkelmann H (2000) Measurement of the pyroelectric response and of the thermal diffusivity of microtomized sections of 'single crystalline' ferroelectric liquid crystalline elastomers. Liq Cryst 27(2): 289–297. doi:10.1080/026782900203119
128. Mauzac M, Nuyen HT, Tournilhac FG, Yablonsky SV (1995) Piezoelectric and pyroelectric properties of new polysiloxane smectic C* elastomers. Chem Phys Lett 240(5–6):461–466. doi:10.1016/0009-2614(95)00574-n
129. Ono H, Harato Y (1999) Characteristics of photothermal effects in guest-host liquid crystals by heat-conduction analysis. J Opt Soc Am B Opt Phys 16(12):2195–2201. doi:10.1364/josab.16.002195
130. Shibaev VP, Kozlovsky MV, Beresnev LA, Blinov LM, Plate NA (1984) Thermotropic liquid crystalline polymers. 16. Chiral smectics C with spontaneous polarization. Polym Bull 12(4): 299–301. doi:10.1007/bf00263142
131. Kostromin SG, Sinitzyn VV, Talroze RV, Shibaev VP, Plate NA (1982) Thermotropic liquid crystalline polymers. 12. Smectic C phase in liquid crystalline polyacrylates with CN-containing mesogenic groups. Makromol Chem Rapid Commun 3(11):809–814
132. Vallerien SU, Zentel R, Kremer F, Kapitza H, Fischer EW (1989) Ferroelectric modes in combined side-group main chain liquid-crystalline polymers. Makromol Chem Rapid Commun 10(7):333–338
133. Naciri J, Pfeiffer S, Shashidhar R (1991) Fast switching of ferroelectric side-chain liquid-crystalline polymer and copolymer. Liq Cryst 10(4):585–591. doi:10.1080/02678299108036446
134. Scherowsky G, Fichna U, Wolff D (1995) Ferroelectric liquid-crystalline polymers side-group derived from mesogenic vinyl ether monomers. Liq Cryst 19(5):621–627. doi:10.1080/02678299508031076
135. Cooray NF, Kakimoto M, Imai Y, Suzuki Y (1994) Novel fluorine-containing ferroelectric side-chain liquid-crystalline polysiloxanes showing bistable fast switching. Macromolecules 27(6):1592–1596. doi:10.1021/ma00084a048
136. Poths H, Schonfeld A, Zentel R, Kremer F, Siemensmeyer K (1992) Structure property relationships determining the spontaneous polarization in FLC-polymers. Adv Mater 4(5): 351–354. doi:10.1002/adma.19920040507
137. Heinze P, Finkelmann H (2010) Shear deformation and ferroelectricity in chiral SmC* main-chain elastomers. Macromolecules 43(16):6655–6665. doi:10.1021/ma1002084
138. Hiraoka K, Sagano W, Nose T, Finkelmann H (2005) Biaxial shape memory effect exhibited by monodomain chiral smectic C elastomers. Macromolecules 38(17):7352–7357. doi:10.1021/ma050642c
139. Verduzco R, Luchette P, Hong SH, Harden J, DiMasi E, Palffy-Muhoray P, Kilbey SM, Sprunt S, Gleeson JT, Jakli A (2010) Bent-core liquid crystal elastomers. J Mater Chem 20(39):8488–8495. doi:10.1039/c0jm01920h
140. Spillmann CM, Ratna BR, Naciri J (2007) Anisotropic actuation in electroclinic liquid crystal elastomers. Appl Phys Lett 90(2):3. doi:10.1063/1.2420780
141. Artal C, Ros MB, Serrano JL, Pereda N, Etxebarria J, Folcia CL, Ortega J (2001) SHG characterization of different polar materials obtained by in situ photopolymerization. Macromolecules 34(12):4244–4255. doi:10.1021/ma001928e
142. Shashidhar R, Naciri J, Ratna BR (2000) Large electroclinic effect and associated properties of chiral smectic a liquid crystals. In: Prigogine I, Rice SA and Vij JK (eds) Advances in chemical physics, vol 113, John Wiley & Sons, Inc., Hoboken, NJ, USA. pp 51–76. doi:10.1002/9780470141724.ch2
143. Kapernaum N, Walba DM, Korblova E, Zhu CH, Jones C, Shen YQ, Clark NA, Giesselmann F (2009) On the origin of the "giant" electroclinic effect in a "de Vries"-type ferroelectric liquid crystal material for chirality sensing applications. ChemPhysChem 10(6):890–892. doi:10.1002/cphc.200900065

144. Etxebarria J, Ros MB (2008) Bent-core liquid crystals in the route to functional materials. J Mater Chem 18(25):2919–2926. doi:10.1039/b803507e
145. Ros MB, Serrano JL, de la Fuente MR, Folcia CL (2005) Banana-shaped liquid crystals: a new field to explore. J Mater Chem 15(48):5093–5098. doi:10.1039/B504384k
146. Keith C, Reddy RA, Prehm M, Baumeister U, Kresse H, Chao JL, Hahn H, Lang H, Tschierske C (2007) Layer frustration, polar order and chirality in liquid crystalline phases of silyl-terminated achiral bent-core molecules. Chemistry 13(9):2556–2577. doi:10.1002/chem.200600876
147. Reddy RA, Baumeister U, Keith C, Tschierske C (2007) Influence of the core structure on the development of polar order and superstructural chirality in liquid crystalline phases formed by silylated bent-core molecules: naphthalene derivatives. J Mater Chem 17(1):62–75. doi:10.1039/b614089k
148. Weissflog W, Pelzl G, Kresse H, Baumeister U, Brand K, Schröder MW, Tamba MG, Findeisen-Tandel S, Kornek U, Stern S, Eremin A, Stannarius R, Svoboda J (2010) In search of a new design strategy for solid single-component organic ferroelectrics: polar crystalline phases formed by bent-core molecules. J Mater Chem 20(29):6057–6079. doi:10.1039/c0jm00322k
149. Keith C, Lehmann A, Baumeister U, Prehm M, Tschierske C (2010) Nematic phases of bent-core mesogens. Soft Matter 6(8):1704–1721. doi:10.1039/b923262a
150. Tschierske C, Photinos DJ (2010) Biaxial nematic phases. J Mater Chem 20(21):4263–4294. doi:10.1039/b924810b
151. Hult A, Sahlen F, Trollsas M, Lagerwall ST, Hermann D, Komitov L, Rudquist P, Stebler B (1996) A pyroelectric liquid crystal polymer (PLCP) for second-harmonic generation. Liq Cryst 20(1):23–28. doi:10.1080/02678299608032022
152. Trollsas M, Orrenius C, Sahlen F, Gedde UW, Norin T, Hult A, Hermann D, Rudquist P, Komitov L, Lagerwall ST, Lindstrom J (1996) Preparation of a novel cross-linked polymer for second-order nonlinear optics. J Am Chem Soc 118(36):8542–8548. doi:10.1021/ja961309e
153. Trollsas M, Sahlen F, Gedde UW, Hult A, Hermann D, Rudquist P, Komitov L, Lagerwall ST, Stebler B, Lindstrom J, Rydlund O (1996) Novel thermally stable polymer materials for second-order nonlinear optics. Macromolecules 29(7):2590–2598. doi:10.1021/ma9511154
154. Davis FJ (1993) Liquid-crystalline elastomers. J Mater Chem 3(6):551–562. doi:10.1039/JM9930300551
155. Gleim W, Finkelmann H (1989) Side chain liquid crystalline elastomers. In: McArdle CB (ed) Side chain liquid crystalline polymers. Blackie and Son, Glasgow
156. Finkelmann H (1991) Liquid-crystalline sidechain polymers. In: Ciferri A (ed) Liquid crystallinity in polymers. VCH, Weinheim
157. Hikmet RAM, Boots HMJ, Michielsen M (1995) Ferroelectric liquid-crystal gels - network stabilized ferroelectric displays. Liq Cryst 19(1):65–76. doi:10.1080/02678299508036721
158. Hikmet RAM, Lub J (1996) Anisotropic networks and gels obtained by photopolymerisation in the liquid crystalline state: synthesis and applications. Prog Polym Sci 21(6):1165–1209. doi:10.1016/S0079-6700(96)00017-2
159. Tolksdorf C, Zentel R (2001) Reversible physical network stabilized ferroelectric liquid crystals. Adv Mater 13(17):1307–1310. doi:10.1002/1521-4095(200109)13:17<1307::AID-ADMA1307>3.0.CO;2-7
160. Prigann J, Tolksdorf C, Skupin H, Zentel R, Kremer F (2002) FT-IR spectroscopic studies on reorientation of ferroelectric liquid crystals in a thermoreversible gel network. Macromolecules 35(10):4150–4154. doi:10.1021/ma002065s
161. Deindörfer P, Eremin A, Stannarius R, Davis R, Zentel R (2006) Gelation of smectic liquid crystal phases with photosensitive gel forming agents. Soft Matter 2(8):693–698. doi:10.1039/b603562k
162. Meziane R, Brehmer M, Maschke U, Zentel R (2008) Gelling and the collective dynamics in ferroelectric liquid crystals. Soft Matter 4(6):1237–1241. doi:10.1039/b800737c

163. Skarp K, Uto S, Myojin K, Moritake H, Ozaki M, Helgee B, Yoshino K (1995) Electrooptical and nonlinear-optical effects in free-surface films of polymeric ferroelectric liquid-crystals prepared by spin-coating method. Jpn J Appl Phys Part 1-Regular Papers Short Notes & Review Papers 34(9B):5433–5437. doi:10.1143/JJAP.34.5433
164. Gillberg G, Leube H, McKenzie L, Pruksarnukul L, Reeder L (1994) Self-assembled structures of azobenzene amphiphiles - a new photorecording medium. J Appl Polym Sci 53(5):687–699. doi:10.1002/app.1994.070530519
165. Gebhard E, Zentel R (1998) Freestanding ferroelectric elastomer films. Macromol Rapid Commun 19(7):341–344. doi:10.1002/(SICI)1521-3927(19980701)19:7<341::AID-MARC341>3.0.CO;2-S
166. Benné I, Semmler K, Finkelmann H (1995) Mechanically induced 2nd-harmonic generation in SC* elastomers. Macromolecules 28(6):1854–1858
167. Benné I, Semmler K, Finkelmann H (1994) 2nd-harmonic generation on mechanically oriented S(C)*-elastomers. Macromol Rapid Commun 15(4):295–302
168. Papadopoulos P, Heinze P, Finkelmann H, Kremer F (2010) Electromechanical properties of smectic c* liquid crystal elastomers under shear. Macromolecules 43(16):6666–6670. doi:10.1021/ma1005028
169. Harden J, Chambers M, Verduzco R, Luchette P, Gleeson JT, Sprunt S, Jakli A (2010) Giant flexoelectricity in bent-core nematic liquid crystal elastomers. Appl Phys Lett 96(10):102907. doi:10.1063/1.3358391
170. Lehmann W, Skupin H, Tolksdorf C, Gebhard E, Zentel R, Krüger P, Lösche M, Kremer F (2001) Giant lateral electrostriction in ferroelectric liquid-crystalline elastomers. Nature 410 (6827):447–450. doi:10.1038/35068522
171. Köhler R, Stannarius R, Tolksdorf C, Zentel R (2005) Electroclinic effect in free-standing smectic elastomer films. Appl Phys A-Mater Sci Process 80(2):381–388. doi:10.1007/s00339-003-2267-5
172. Hiraoka K, Kobayasi M, Kazama R, Finkelmann H (2009) Electromechanics of monodomain chiral smectic c elastomer: mechanical response to electric stimulation. Macromolecules 42(15):5600–5604. doi:10.1021/ma900761w
173. Stannarius R, Köhler R, Dietrich U, Lösche M, Tolksdorf C, Zentel R (2002) Structure and elastic properties of smectic liquid crystalline elastomer films. Phys Rev E 65(4):11. doi:04170710.1103/PhysRevE.65.041707
174. Walba DM, Yang H, Shoemaker RK, Keller P, Shao RF, Coleman DA, Jones CD, Nakata M, Clark NA (2006) Main-chain chiral smectic polymers showing a large electroclinic effect in the SmA* phase. Chem Mater 18(19):4576–4584. doi:10.1021/cm0606373
175. Walba DM, Keller P, Shao RF, Clark NA, Hillmyer M, Grubbs RH (1996) Main-chain ferroelectric liquid crystal oligomers by acyclic diene metathesis polymerization. J Am Chem Soc 118(11):2740–2741. doi:10.1021/ja953779z
176. Keller P, Shao RF, Walba DM, Brunet M (1995) The first high polarization ferroelectric main-chain liquid-crystalline polymers. Liq Cryst 18(6):915–918. doi:10.1080/02678299508036710
177. Brehmer M, Zentel R (1995) Ferroelectric liquid-crystalline elastomers with short switching times. Macromol Rapid Commun 16(9):659–662. doi:10.1002/marc.1995.030160904
178. Jakli A, Saupe A (1995) Mechanical vibrations of smectic cells under fast field reversal. Mol Cryst Liq Cryst Sci Technol Sect A Mol Cryst Liq Cryst 263:103–111. doi:10.1080/10587259508033574
179. Jakli A, Saupe A (1996) Field-induced thickness change of ferroelectric liquid crystal films. Phys Rev E 53(6):R5580–R5583
180. Hiraoka K, Toyoda S, Hourai Y, Tokita M, Watanabe J (2010) Influence of DC electric field on soft mode of main-chain ferroelectric liquid-crystalline polyesters: polymeric effect on collective fluctuation. Appl Phys Express 3(1). doi:10.1143/APEX.3.011701

181. Jakli A, Pintre IC, Serrano JL, Ros MB, de la Fuente MR (2009) Piezoelectric and electric-field-induced properties of a ferroelectric bent-core liquid crystal. Adv Mater 21(37): 3784–3788. doi:10.1002/adma.200900131
182. Chambers M, Verduzco R, Gleeson JT, Sprunt S, Jakli A (2009) Calamitic liquid-crystalline elastomers swollen in bent-core liquid-crystal solvents. Adv Mater 21(16):1622–1626. doi:10.1002/adma.200802739
183. Chambers M, Verduzco R, Gleeson JT, Sprunt S, Jakli A (2009) Flexoelectricity of a calamitic liquid crystal elastomer swollen with a bent-core liquid crystal. J Mater Chem 19(42):7909–7913. doi:10.1039/b911652d
184. Kramer D, Brömmel F, Finkelmann H (2012) LC Elastomers – Synthesis and Mechanical Behavior. Adv Polym Sci. Springer, Heidelberg, Berlin (in print)
185. Urayama K (2011) Electro-Opto-Mechanical Effects in Swollen Nematic LC Elastomers. Adv Polym Sci. doi:10.1007/12_2010_107
186. De Jeu WH, Ostrovskii BI (2011) Order and Disorder in Liquid-Crystalline Elastomers. Adv Polym Sci. doi:10.1007/12_2010_105
187. Pallfy-Muhoray P (2012) Liquid Crystal Elastomers and Light. Adv Polym Sci. doi:10.1007/12_2011_165

Adv Polym Sci (2012) 250: 95–118
DOI: 10.1007/12_2011_165

Published online: 1 March 2012

Liquid Crystal Elastomers and Light

Peter Palffy-Muhoray

Abstract Liquid crystal elastomers (LCEs) are solid liquid crystals; they combine elasticity with orientational order. Mechanical strain therefore changes liquid crystalline order and the optical properties of these materials. Conversely, light can change the orientational order, and give rise to mechanical forces and changes in shape. Light–matter interactions in LCEs therefore involve a broad range of unusual phenomena, which raise a number of intriguing questions. There is great potential for device applications, but considerable challenges must first be overcome. The most appealing aspect of light–matter interactions in LCEs, however, is the promise of new physics waiting to be discovered.

Keywords Elastomer · Lasing · Liquid crystal · Orientational order · Photoactuation · Photoisomerization · Strain

Contents

P. Palffy-Muhoray (✉)
Liquid Crystal Institute, Kent State University, Kent, OH, USA
e-mail: mpalffy@cpip.kent.edu

Abbreviations

5CB	4-Cyano-4′-pentylbipheny
CW	Continuous wave
DCM	4-(Dicyanomethylene)-2-methyl-6-(4-dimethylaminostyryl)-4*H*-pyran
DOS	Density of states
LC	Liquid crystal
LCE	Liquid crystal elastomer
UV	Ultraviolet

1 Introduction

Liquid crystal elastomers (LCEs) are fascinating materials; they are "solid" liquid crystals. Initially proposed by de Gennes [1] and first realized by Finkelmann [2], they bring together, for the first time, the key aspect of liquid crystals, orientational order, and the essential aspect of solids, the ability to support shear stress. The new coupling of mechanical stress and orientational order gives rise to a wide variety of fascinating new phenomena and the potential for new applications.

Coupling between orientational order and strain results in two complementary phenomena. In general, mechanical deformations cause changes in orientational order and in the physical properties that depend on this, and similarly, changes in orientational order cause stress in the sample, leading to changes in shape.

In this chapter, we focus on light–matter interactions, and consider the effects of mechanical deformations on the optical properties of LCE samples, and the effects of light on the mechanical properties of LCE samples.

1.1 Orientational Order

Liquid crystals are inherently soft materials. According to Goldstone's theorem [3], systems with broken continuous symmetry show low energy excitations, the so-called Goldstone modes, whose energy goes to zero as their wavelength approaches infinity. Liquid crystals are systems with such spontaneously broken symmetry, and hence they show remarkable responsivity to even modest stimuli. Externally applied fields can therefore easily change the order parameter, and these order parameter changes are readily manifested in the resulting change in anisotropic physical properties.

In nematic liquid crystals, a convenient measure of orientational order is the order parameter tensor, which may be defined in terms of the orientation of the constituent molecules. If $\hat{\mathbf{l}}$ is a unit vector along the symmetry axis of a molecule, then the order parameter tensor is $\mathbf{Q}$ defined as

$$\mathbf{Q} = \left\langle \frac{1}{2}(3\hat{\mathbf{l}}\hat{\mathbf{l}} - \mathbf{I}) \right\rangle, \tag{1}$$

where $\mathbf{I}$ is the identity tensor and the brackets indicate an ensemble average. $\mathbf{Q}$ is symmetric and traceless; the eigenvalues give the degree of orientational order, while the eigenvectors give its principal directions. If two of the eigenvalues are the same, the system is uniaxial and $\mathbf{Q}$ may be written as

$$\mathbf{Q} = S\frac{1}{2}(3\hat{\mathbf{n}}\hat{\mathbf{n}} - \mathbf{I}), \tag{2}$$

where the unique eigenvalue S is the scalar order parameter and the associated eigenvector $\hat{\mathbf{n}}$ is the nematic director. Physical properties, such as the dielectric tensor and the magnetic susceptibility, are linear functions of the order parameter $Q_{a\beta}$. The dielectric tensor is given by

$$\varepsilon_{\alpha\beta} = \bar{\varepsilon}\delta_{\alpha\beta} + \Delta\varepsilon Q_{\alpha\beta}, \tag{3}$$

where $\bar{\varepsilon}$ and $\Delta\varepsilon$ are the average dielectric constant and the dielectric anisotropy, and $\delta_{\alpha\beta}$ is the Kroenecker delta, which takes the value of 1 if $\alpha = \beta$ and is zero otherwise. Orientational order is determined by the interactions of the constituent particles as well as the influence of external fields. The free energy may be written in terms of $\mathbf{Q}$ as

$$\begin{aligned} F_{\text{nem}} = {} & \frac{1}{2}a_{\text{o}}(T/T\text{c} - 1)Q_{\alpha\beta}Q_{\beta\alpha} - \frac{1}{3}BQ_{\alpha\beta}Q_{\beta\gamma}Q_{\gamma\delta} + \frac{1}{4}C(Q_{\alpha\beta}Q_{\beta\alpha})^2 + \cdots \\ & - \frac{1}{2}\Delta\varepsilon Q_{\alpha\beta}E_\alpha E_\beta, \end{aligned} \tag{4}$$

where a_{o}, B, and C are constants, and summation is implied over repeated Greek indices. $T_{\text{c}} = \rho U/5k$ is the critical temperature; ρ is the number density of nematic molecules, U is an interaction strength, and k is Boltzmann's constant. The last term takes into account the effect of an external electric field. If the dielectric anisotropy $\Delta\varepsilon$ is positive, the free energy is minimized if the director is parallel to the electric field.

If the orientational order is spatially inhomogeneous, the free energy cost of order parameter variations is given, to a good approximation, by the Frank elastic energy [4]

$$F_{\text{F}} = \frac{1}{2}K_1(\nabla \cdot \hat{\mathbf{n}})^2 + \frac{1}{2}K_2(\hat{\mathbf{n}} \cdot \nabla \times \mathbf{n} - q_o)^2 + \frac{1}{2}K_3(\hat{\mathbf{n}} \times \nabla \times \mathbf{n})^2, \tag{5}$$

where the K_is (K_1, K_2, K_3) are curvature elastic constants and q_o is a pseudoscalar that gives a measure of the material chirality. Cholesteric liquid crystals consist of chiral molecules, which prefer to align so that the symmetry axes of adjacent molecules are slightly twisted relative to one another. In the absence of fields, the free energy is minimized if the director has the structure

$$\hat{\mathbf{n}} = (\cos(q_o z), \sin(q_o z), 0) \tag{6}$$

that is, the tip of director traces out a helix. Cholesterics thus spontaneously form a periodic dielectric structure, which is responsible for their unusual optical properties.

1.2 Elasticity

The elastic response of materials can be described in terms of the deformation **u** where a material point located at **r** in the undeformed sample, moves to the position

$$\mathbf{r}' = \mathbf{r} + \mathbf{u}(\mathbf{r}) \tag{7}$$

after a deformation. The strain tensor is defined [5] as

$$e_{\alpha\beta} = \frac{1}{2}\left(\frac{\partial u_\alpha}{\partial r_\beta} + \frac{\partial u_\beta}{\partial r_\alpha} + \frac{\partial u_\gamma}{\partial r_\alpha}\frac{\partial u_\gamma}{\partial r_\beta}\right) \tag{8}$$

and, if the material is incompressible, in the linear regime, the free energy is

$$F_{\text{el}} = \frac{1}{2} Y e_{\alpha\beta} e_{\beta\alpha}, \tag{9}$$

where Y is Young's modulus. Approximately, Young's modulus is given by

$$Y \approx kT\rho_c, \tag{10}$$

where ρ_c is the number density of crosslinks in the elastomer network. If an external stress $\sigma_{\alpha\beta}$ is applied, the elastic free energy becomes

$$F_{\text{el}} = \frac{1}{2} Y e_{\alpha\beta} e_{\beta\alpha} - e_{\alpha\beta}\sigma_{\alpha\beta} \tag{11}$$

When the system is in equilibrium, minimizing the elastic free energy gives the strain **e**.

1.3 Liquid Crystal Elastomers

LCEs are polymer networks incorporating mesogenic molecules as part of their architecture, either as parts of the polymer main chains, or as pendant side chains. As proposed by de Gennes, these materials show combined aspects of elasticity and liquid crystallinity. The polymer chains containing mesogenic units may be regarded as performing an anisotropic random walk between crosslinks; the anisotropy is due to orientational order. The step length tensor is of the form

$$l_{\alpha\beta} = l_{\perp}\delta_{\alpha\beta} + (l_{\parallel} - l_{\perp})n_{\alpha}n_{\beta}, \tag{12}$$

where n_{α} is a component of the nematic director.

The free energy can be approximated as the sum of liquid crystalline and elastomeric contributions, as well as a coupling term. For nematic LCEs, this takes the form

$$F_{\text{nlce}} = F_{\text{nem}} + F_{\text{el}} - \gamma Q_{\alpha\beta}e_{\beta\alpha}, \tag{13}$$

where the last term represents the simplest symmetry-allowed coupling between orientational order and strain. The coupling constant γ is proportional to the crosslink density and the step length anisotropy $l_{\parallel} - l_{\perp}$, and can be positive or negative.

This coupling indicates that changes in the order parameter will affect the strain, and conversely, that changes in shape will affect the orientational order. Specifically (13) and (11) show that the effect of the order parameter on strain is the same as that of an external stress $\sigma_{\alpha\beta}$, and (13) and (4) show that the effect of strain on the orientational order is the same as that of an applied external field $E_{\alpha}E_{\beta}$. This means that applying a uniaxial strain to a nematic LCE with $\gamma > 0$ will tend to increase orientational order and align the director along the strain direction, while changes in orientational order give rise to strain deformations. Young's modulus for typical LCEs is of the order of 10^5 Pa, which also gives a measure of the coupling constant γ. Finally, conventional liquid crystals and isotropic rubbers as well as LCEs conserve volume to a good approximation. Much of the behavior of LCEs to be discussed below can be understood on basis of this simple description.

2 The Effects of LCEs on Light

We now consider how the properties of LCEs affect light. Light propagation in typical uniaxial nematic liquid crystals is the same as in uniaxial solid crystals; two eigenmodes are allowed, the extraordinary mode with polarization parallel, and the ordinary mode, with polarization perpendicular to the plane defined by the wave vector $\mathbf{k}$ and the optic axis – the nematic director – $\hat{\mathbf{n}}$. Although they are soft and

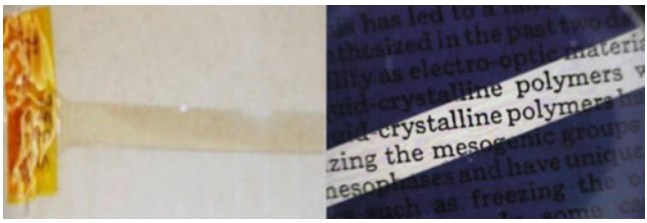

Fig. 1 Transparent LCE sample attached to yellow tape (*left*). Sample between crossed polarizers (*right*)

flexible materials, monodomain nematic LCEs therefore behave optically as birefringent crystals, and allow light transmission when placed between crossed polarizers, as shown in Fig. 1.

2.1 Refractive Indices

The refractive indices of the propagating eigenmodes in nematic LCEs depend on the principal values of the relative dielectric tensor as in ordinary nematics, that is, the index of the ordinary mode is given by

$$n_{\mathrm{o}}^2 = \varepsilon_\perp \tag{14}$$

and the index of the extraordinary mode is

$$n_{\mathrm{e}}^2 = \frac{\varepsilon_\perp \varepsilon_\parallel}{\varepsilon_\perp + (\varepsilon_\parallel - \varepsilon_\perp)(\hat{\mathbf{k}} \cdot \hat{\mathbf{n}})^2}, \tag{15}$$

where $\mathbf{k}$ is the wave vector. Since the dielectric permittivity is linear in the order parameter [cf. (3)], as in the case of ordinary nematics, any change in orientational order will result in a change of the refractive indices. In addition to temperature, fields of particular interest in the case of LCEs are mechanical strain and changes in composition. Measuring the individual refractive indices of LCEs is more challenging than for conventional liquid crystals, nonetheless this has been carried out using both Abbe refractometers [6] and Brewster angle measurements [7].

It is straightforward to measure the birefringence as function of temperature [8] as well as strain [9]. One experimental consideration to take into account is the change in sample thickness due to strain. The response can be readily understood in terms of the simple model described in the Introduction. LCEs have been swollen with both isotropic and anisotropic solvents [8, 10, 11]. Isotropic solvents reduce the number density of mesogens and, hence, the critical temperature $T_{\mathrm{c}} = \rho U/5k$. They also reduce the crosslink density and the influence of the network. Nematic solvents, on the other hand, up to first order do not reduce the mesogen density, but

primarily diminish the influence of the network. In unswollen nematic LCEs, the orienting effect of the network is comparable to that of electric fields of magnitude $E \sim \sqrt{Y/\varepsilon_o \Delta\varepsilon} \sim 10\,\mathrm{V}/\mu\mathrm{m}$, so the effect of practically achievable electric fields is small. Swelling diminishes the aligning effect of the network, and, in the case of nematic solvents, this allows applied electric fields to reorient the nematic director [12].

2.2 Polydomain LCEs, Gels, and LC Networks

The network structure of LCEs is determined by processing during sample production. Side-chain nematic LCEs with siloxane main chain [13] are typically partially polymerized in a centrifuge, from which they are removed in the solvent-swollen isotropic state. As the solvent evaporates, the mesogen number density increases, and the sample locally undergoes the isotropic–nematic transition. Polymerization continues as the sample is baked, until it is complete and the structure is locked in. If there is no symmetry breaking to establish a preferred direction, the director of the emerging nematic regions is random, and a polydomain sample with randomly oriented nematic domains results. The domain size is determined by competition between the Frank director distortion energy and the random aligning effects of the network [14]; the resulting domain size length scale l_d is of the order $l_\mathrm{d} \sim \sqrt{K/Y} \approx 10^{-7}\mathrm{m}$. Since the domain size is comparable to an optical wavelength, polydomain samples scatter light and appear opaque. Some structural information can be extracted by large angle light scattering [15, 16].

Monodomain samples produced by this method are stretched slightly while the solvent evaporates; this symmetry breaking is sufficient to align the emerging nematic domains all in the same direction. It is interesting to note that such transparent monodomain samples transform to scattering polydomain structures when swollen with solvents that weaken the aligning effect of the network, and, as the solvent concentration increases, become transparent again in the isotropic phase. Figure 2 such swollen networks are formally gels, dispersions of liquids in

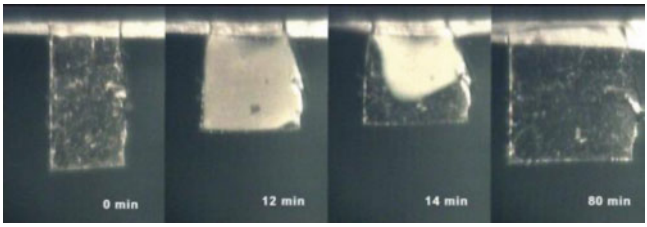

Fig. 2 Monodomain LCE swollen in chloroform vapor, which forms nematic monodomain (0 min), polydomain (12 min) and isotropic structures (14–80 min) as the solvent evaporates

Fig. 3 Nematic LC gel showing mono- to polydomain transition. Electrical field off (*left*), electrical field on (*right*). From [17]

a continuous solid phase. LC gels can be formed not only by swelling covalently crosslinked elastomeric networks, but also by forming physical crosslinks. Polymers can form physical networks in solvents in which the endgroups are not soluble. Such a nematic gel has been realized [17, 18], shown in Fig. 3 where the polystyrene endgroups of triblock copolymers form physical crosslinks in the nematic phase of the liquid crystal 5CB, in which they are insoluble in the nematic phase. Above the nematic–isotropic transition, this material becomes a liquid, and can be reconfigured before cooling into the nematic gel phase. Finally, it is worth noting that elastomers, by definition, are "rubber-like", and have a modest Young's modulus, typically below 10^6 Pa. Highly crosslinked liquid crystalline materials, showing similar behavior but with a greater modulus, are referred to as LC networks [19–21].

2.3 Lasing in Cholesteric LCEs

Materials whose dielectric properties vary periodically in space are capable of localizing photons. Such photonic band gap materials, whose structure can be regarded as a distributed laser cavity, can also lase. Cholesteric liquid crystals can act as such lasers. In addition, cholesteric elastomers can allow the distributed cavity, and hence the lasing wavelength, to be tuned by mechanical strain.

The conditions for lasing are as follows: A simple laser consists of two mirrors enclosing an optically pumped active medium, which provides gain. A plane wave, with complex electric field amplitude E_o propagating in an active medium, will gain phase, will be both absorbed and amplified, and will be reflected by the mirror. After completing the return path, in the steady state, the amplitude must again be E_o. That is

$$E_o = E_o e^{(ik-\alpha+\gamma)L} r e^{(ik-\alpha+\gamma)L} r, \tag{16}$$

where α is the absorption and γ is the gain coefficient, L is the cavity length and r is the reflection coefficient of the mirrors. This gives the conditions for the cavity modes

$$kL = m\pi \tag{17}$$

and for the threshold gain (γ_{th})

$$\gamma_{\text{th}} = \alpha - \frac{\ln r^2}{2L}. \tag{18}$$

The lasing threshold is therefore determined by the requirement that the gain must be sufficient to overcome absorption and cavity losses.

An alternate approach is to note that in quantum mechanics, according to Fermi's golden rule [22], the decay probability for an excited atom, that is, the photon emission rate Γ, is given by

$$\Gamma = \Gamma_{\text{o}} \rho(\omega), \tag{19}$$

where Γ_{o} is a bare transition rate, and $\rho(\omega) = \mathrm{d}k/\mathrm{d}\omega$ is the density of states (DOS) available for occupation and into which the excited atom can decay. For a given structure, the effective wave number k can be determined from the phase shift of transmitted light. For a Fabry–Perot cavity consisting of two facing plane mirrors, this gives for the DOS

$$\rho = \frac{\mathrm{d}k}{\mathrm{d}\omega} = \frac{n}{c} \frac{1 - r^4}{1 - 2r^2 \cos(2kL) + r^4}. \tag{20}$$

The maxima occur when $kL = m\pi$, with

$$\rho_{\text{MAX}} = \frac{n}{c} \frac{1 + r^2}{1 - r^2}. \tag{21}$$

Equation (18) for the threshold gain can be written in terms of ρ_{MAX}; for $r \approx 1$

$$\gamma_{\text{th}} \simeq \alpha + \frac{2n}{c\rho_{\text{MAX}} L}. \tag{22}$$

Since lasing first occurs at the wavelength where the threshold gain γ_{th} is a minimum, the DOS determines both the lasing wavelength and the lasing threshold.

2.4 Optical Properties of Cholesterics

The optical properties of cholesteric liquid crystals have been studied extensively [23, 24]. Light propagation in helical cholesterics is governed by the spatially periodic relative dielectric tensor, whose eigenvalues are $\varepsilon_{\parallel}$ and $\varepsilon_{\perp}$ for the electric field parallel and perpendicular to the director $\hat{\mathbf{n}}$. It can be written as

$$\varepsilon = \varepsilon_{\perp} \mathbf{I} + (\varepsilon_{\parallel} - \varepsilon_{\perp}) \hat{\mathbf{n}} \hat{\mathbf{n}}, \tag{23}$$

where nonlocal contributions to the polarization have been ignored. Useful quantities are the average dielectric constant

$$\bar{\varepsilon} = \frac{1}{2}(\varepsilon_{\parallel} + \varepsilon_{\perp}) \tag{24}$$

and the dielectric anisotropy

$$\delta = \frac{1}{2}(\varepsilon_{\parallel} - \varepsilon_{\perp}). \tag{25}$$

Solving Maxwell's equations in a helical cholesteric structure gives the secular equation for the eigenvalues

$$n^2 = \bar{\varepsilon} + \beta^2 \pm \sqrt{\delta^2 + 4\bar{\varepsilon}\beta^2}, \tag{26}$$

where $\beta = \lambda_o/p = q_o\lambda_o/2\pi$, and the optical eigenmodes

$$\mathbf{E} = E_o\{(\hat{\mathbf{x}} + i\hat{\mathbf{y}})e^{i((\frac{2\pi}{\lambda_o}n - \frac{2\pi}{p})z - \omega t)} + \frac{\delta}{(n+\beta)^2 - \bar{\varepsilon}}(\hat{\mathbf{x}} - i\hat{\mathbf{y}})e^{i((\frac{2\pi}{\lambda_o}n + \frac{2\pi}{p})z - \omega t)}\}, \tag{27}$$

where $\hat{\mathbf{x}}$ and $\hat{\mathbf{y}}$ are unit vectors in the x–y plane (plane of the director), and light propagates along the helix axis in the z-direction. The eigenvalue n^2 in (26) has two branches, the branch corresponding to the negative radical is negative for $\sqrt{\varepsilon_{\parallel}} < \beta < \sqrt{\varepsilon_{\perp}}$, where the index n is imaginary. In this regime, there is no light propagation; the modes are exponentially decaying evanescent waves. This region therefore corresponds to the photonic band gap, with the low energy band edges at $\lambda_o = pn_{\parallel} = p\sqrt{\varepsilon_{\parallel}}$ and the high-energy edge at $\lambda_o = pn_{\perp} = p\sqrt{\varepsilon_{\perp}}$. Outside the band, the eigenmodes are combinations of left-and right-circularly polarized waves, propagating with different velocities. Inside the band, the mode corresponding to imaginary n is evanescent, with counter-propagating circularly polarized waves. At the band edges, $n = 0, \bar{\varepsilon} - \beta^2 = \pm\delta$, and the modes are standing waves, with $\mathbf{E}$ parallel to the director at the low energy edge, and perpendicular at the high-energy edge.

Ignoring finite size effects, the DOS is

$$\rho = \frac{\mathrm{d}k}{\mathrm{d}\omega} = \frac{\mathrm{d}}{\mathrm{d}\omega}\frac{2\pi n}{\lambda_o} = \frac{n}{c} - \frac{\lambda_o}{2nc}\frac{\mathrm{d}n^2}{\mathrm{d}\lambda_o}. \tag{28}$$

Since n^2 is a smoothly varying function of λ_o, as shown in Fig. 4, the DOS diverges at the band edges as $1/n$, where $n \to 0$. Photon emission by excited atoms and molecules and distributed feedback lasing is therefore expected at the band edges. Alternately, for wavelengths at the band edges (where the refractive index is zero), the material simply acts as a Fabry–Perot cavity for circularly polarized waves. If excited dye or LC molecules are present, there is gain and the material, acting both as the cavity and the gain medium, can lase.

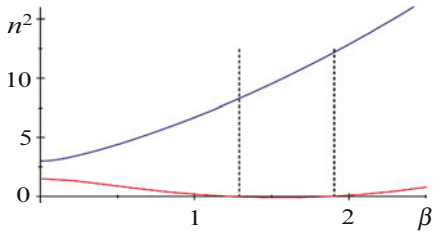

Fig. 4 Plot of both branches of n^2 versus $\beta = \lambda_o/p$ for $\varepsilon_{\parallel} = 3$ and $\varepsilon_{\perp} = 2$. The *dashed lines* show the band edge where the density of states diverges

2.5 *Distributed Feedback Lasing in Cholesteric LCEs*

In 1971, Kogelnik and Shank [25] proposed that an external cavity was not required for lasing, and that Bragg reflections in periodic structures could play a role similar to external mirrors. Such distributed feedback lasing was demonstrated, and it forms the basis of mirrorless lasing in liquid crystals today. Citing the work of Kogelnik and Shank, in 1973 Schnur and Goldberg proposed and obtained a US patent on a "tunable internal-feedback liquid crystal-dye laser" [26]; however, there is no corresponding demonstration or evidence of lasing in the literature. Their basic idea was to use a fluorescent dye dissolved in the liquid crystal to provide gain, and to use the periodic structure of helical cholesterics to provide distributed feedback. To demonstrate lasing, in addition to light emission, it is necessary to demonstrate line narrowing, directional emission, excited state lifetime reduction, threshold behavior and coherence. Ilchishin et al. [27] have demonstrated modification of fluorescent emission, but the first unequivocal demonstration of lasing in polymer-stabilized cholesteric liquid crystals was by the group of Genack [28]. Shortly thereafter, it was independently demonstrated in pure cholesterics by Taheri et al. [29]. Considerable work on lasing in cholesteric liquid crystals followed [30–55]. A recent review is available [56] (Fig. 5).

In 2001, Finkelmann synthesized, for the first time, a cholesteric LCE [57]. Monodomain samples were obtained using a novel anisotropic de-swelling method. The resulting network, investigated via optical microscopy and X-ray measurements, was shown to be a highly ordered cholesteric LCE with the helical axis perpendicular to the biaxial extension axes. The cholesteric pitch of the samples could be varied by a biaxial extension. A biaxial strain shortens the pitch, giving rise to a blue-shift of the reflected light. The effect of strain on the band structure has been analyzed in detail [58]. A dye can be readily incorporated into the sample by dissolving DCM in toluene, swelling the cholesteric LCE with the dye solution, and then removing the toluene. If samples with ~0.2 wt% DCM are optically pumped by pulses at 532 nm, they lase at the low energy cholesteric band edge. A biaxial strain applied to these samples changes the pitch and hence the location of the band edge, and thus the lasing wavelength. These cholesteric LCE samples are therefore mechanically tunable "rubber lasers," whose emission can be color tuned by simply stretching the samples [59]. The laser emission for different strain is shown in Fig. 6. The simple tunability of cholesteric LCE lasers has received considerable attention [60].

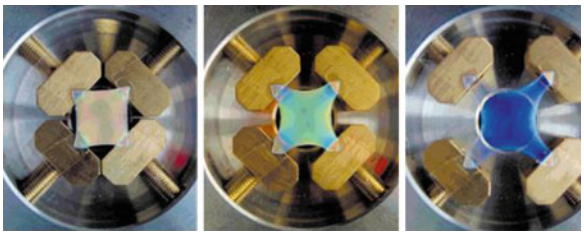

Fig. 5 Appearance of cholesteric elastomer under white light illumination as function of biaxial strain (increasing strain from *left* to *right*)

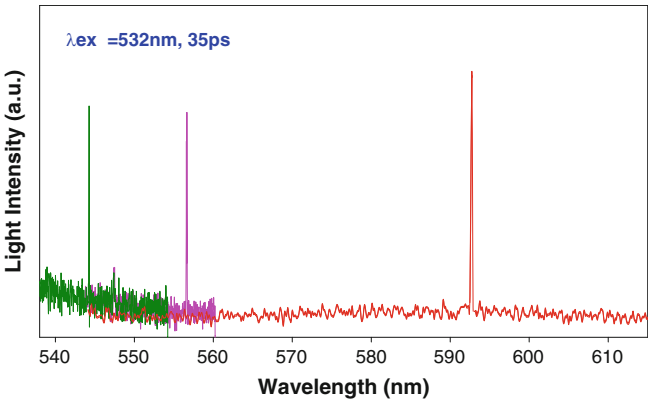

Fig. 6 Laser emission from the DCM-doped cholesteric LCE for different strains

Distributed feedback lasing [36] and the band structure of cholesteric LCEs has been subsequently studied [6, 31]. As a consequence of strain, additional gaps arise, and their width varies with strain. If two cholesteric networks are joined together, a discontinuous jump of the director usually takes place at the interface. Defect mode lasing, due to the phase jump of the cholesteric helix at such an interface, has also been demonstrated [61].

2.6 Non-lasing Applications

Due to elasticity and the strong coupling between orientational order and the polymer network, LCEs are mechanically tunable birefringent optical materials. This aspect holds considerable promise for display and electo-optic applications [62]. In spite of their considerable potential, LCEs have not yet found widespread use in technology. One promising feature is the tunable and compliant photonic bandgap structure of cholesteric LCEs; these show the potential for adaptive optics and mechanically tunable lasing. A beautiful and intriguing potential application

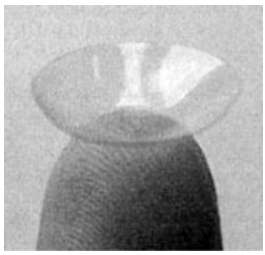

Fig. 7 Bifocal contact lens made from LC hydrogel. From [62]

involves the use of soft birefringent liquid crystal hydrogels for bifocal contact lenses [63] (Fig. 7). The constituents are polymer networks with non-ionic amphiphilic monomers, swollen with water, and having long-range orientational order. The binary monomer–water mixture exhibits lamellar and smectic phases. In the smectic phase, the director is aligned with a magnetic field in the plane of the circumference of the lens, and the material is photopolymerized. The resulting materials are nontoxic and hydrated, with good oxygen transport capability. They are strongly birefringent, and the two refractive indices give rise, simultaneously, to two focal lengths.

3 Effects of Light on LCEs

One of the remarkable properties of LCEs is their mechanical response to light. LCEs can be made photosensitive by the incorporation of light-absorbing materials. They can then exhibit striking responses to visible radiation, ranging from large and rapid changes in shape to light-driven rotary motion. Because of the versatility and ease of implementation of such schemes, perhaps the greatest potential of LCEs for technological applications lies in photoactuation.

3.1 Optomechanical Coupling Mechanisms

A variety of processes exist that produce mechanical stresses in LCEs as a result of illumination. Such stresses can subsequently cause shape changes, deformation and motion. Some possible processes are described in Sects. 3.1.1–3.1.3

3.1.1 Direct Optical Stresses and Torques

The radiation field exerts direct forces and torques on condensed matter via the Minkowski stress [64]. Radiation pressure Π_r is on the order of $\Pi_r \approx DE \approx I/c \approx P/Ac$ where D is the electric displacement, I is the irradiance, c is the speed of light, P is the incident power, and A is the area. If the direct optical force is to cause a deformation, the radiation pressure would have to overcome the aligning effect of

the network, that is, Π_r would have to be equal to or greater than Young's modulus Y. For a 1 W CW laser focused to a beam waist of 1 mm, $\Pi_r \approx 3 \times 10^{-3}$Pa, which is negligible compared to $Y \approx 10^5$Pa. The same scaling argument holds for the direct optical torque. In conventional LCs, a direct optical torque can reorient the director at the optical Freedericksz transition [65], but in LCEs, direct optical torques and forces due to practically realizable fields are altogether insufficient to overcome the aligning effects of the network and to produce a distortion.

3.1.2 Thermal Effects

Heating via linear absorption of light can result in very significant temperature increases, which in turn change the order parameter and result in stress. In the steady state, the temperature increase due to absorbed light can be estimated as $\Delta T \approx P/\kappa A$, where P is the absorbed power, κ is the thermal conductivity, and A is the area through which the heat current flows. Since $\kappa \approx 0.2\,\mathrm{W/m \cdot k}$, even 1 mW of absorbed power can lead to very significant temperature changes. Since the nematic isotropic transition temperature is close to room temperature, the nematic free energy/mesogenic unit is on the order of kT. Since the number density of mesogenic units in LCEs typically far exceeds that of network crosslinks, it follows that the effect of the network on the response of the order parameter to changes in temperature is negligible (except very near to the nematic–isotropic transition). Heating the sample then results in order parameter changes very similar to those in conventional nematics. Minimizing the free energy of (13) with respect to strain shows that strain $e_{\alpha\beta}$ is proportional to the order parameter $Q_{\alpha\beta}$, and that changes in strain due to heating follow the changes of the order parameter. Simple heating, optical or otherwise, therefore results in large strains and stresses in LCEs. Since LCEs are usually transparent, dyes or other absorbers are typically added to increase the absorption. Metallic nanoparticles show sharp plasmon resonances in the visible range, they are excellent absorbers (similar to dyes), and can be tailored to absorb particular wavelengths. Both dyes and plasmonic nanoparticles can be spatially localized to enable spatially resolved photoactuation.

3.1.3 Effect of Photoisomerizable Constituents

Azo dyes undergo photoisomerization when irradiated by light at optical frequencies. The extended mesogen-like *trans*-conformer undergoes isomerization on irradiation with light of short wavelengths (near UV), and changes to the bent, non-mesogen-like *cis*-conformation. The *cis*-conformer is metastable in a local shallow energy minimum; it spontaneously relaxes back into the *trans*-conformation; this relaxation can be speeded up by irradiation by light of longer (red) wavelengths. The effect of azo dyes and similar photoisomerizable constituents is similar to that of heating the sample. In effect, photoisomerization reduces the

number density of mesogens, and, since $T_c = \rho U/5k$, it reduces the transition temperature. As can be seen from (4), this is equivalent to increasing the temperature. This point is discussed in detail in [66]. The effects of photoisomerization alone are very similar to heating. In addition to photoisomerization, azo and similar compounds also absorb a considerable amount of light, and the temperature consequently rises. Both mechanisms – heating and conformational changes – are necessarily both present. Determining the relative importance of these two mechanisms is a challenging problem; measurements directed at addressing this question are under way [67].

3.1.4 Indirect Optical Torque

In 1990, Janossy showed that a small amount of dye added to a nematic liquid crystal dramatically reduces the threshold intensity of the optical Freedericksz transition [68]. Subsequently, it was demonstrated that the underlying process is an optically driven Brownian ratchet mechanism [69–71]. Here, energy, but not momentum, from the radiation field causes unidirectional continuous rotation of dye molecules in the nematic, exerting a torque on the director that exceeds the direct optical torque by orders of magnitude. Similar mechanisms could, in principle, be realized in LCEs. Whether such processes are viable in overcoming the orienting effect of the network is not clear; the viability of such Brownian motor processes in LCEs is an intriguing open problem.

Since direct optical forces and torques are too small to overcome the orienting effects of the network, viable photoactuation processes must all involve effective energy transfer from the radiation field to the material. Some illustrative examples are given in Sect. 3.2.

3.2 Photoactuation

In a seminal work exploring in LCEs, photoactuation, Finkelmann and coworkers incorporated azo-group containing crosslinkers into a siloxane-based side chain nematic LCE. They found that a monodomain sample will contract along the director on UV illumination [66], and will recover to its original shape in the dark. The response of the system is shown in Fig. 8; the characteristic response times are tens of minutes. One possible mechanism here, not discussed in [66], is the contraction of crosslinks formed by the azo compounds, which would induce anisotropy (contraction along the polarization direction) even in isotropic rubbers. Heating, which certainly takes place on illumination, reduces the orientational order. Since the order parameter tensor plays the role of stress, a reduction of order gives rise to contraction along the director. It is pointed out that the effects of *trans–cis* photoisomerization are not readily distinguishable from heating through absorption. This work introduced a new optomechanical effect in solids, and related

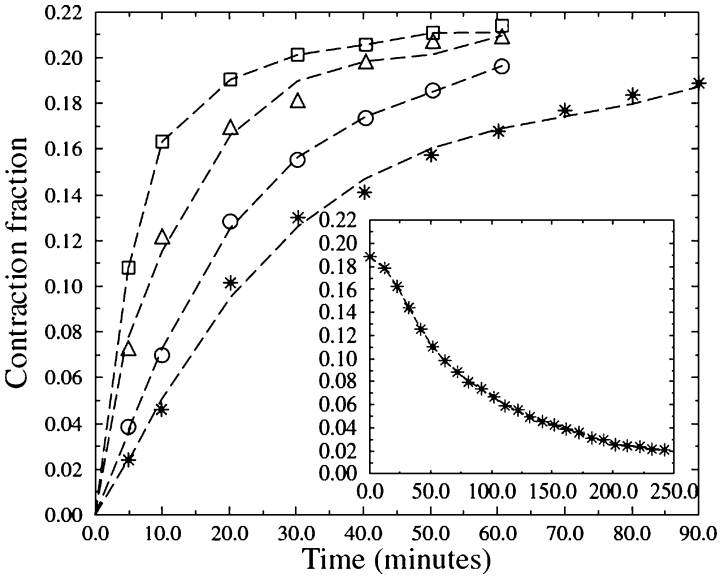

Fig. 8 Contraction of azo crosslinker containing a nematic side chain LCE. The *inset* shows relaxation on removal of excitation. Symbols indicate temperature; 298K (*), 303K (○), 308K (△), 313K (□) From [66]

the observations to theory. It laid the groundwork for much subseqent research on photoactuation of LCEs photosensitized by the incorporation of azo-compounds.

Working with thin films of polydomain LC networks with azo dyes, Ikeda and coworkers in 2003 demonstrated polarization-dependent curling of samples in response to UV radiation [72]. When flat polydomain samples, 7 μm thick, are irradiated by polarized UV light at 366 nm, the samples curl about an axis parallel to the plane of the film and perpendicular to the polarization direction (Fig. 9). This phenomenon can be understood by noting that the mesogen-like *trans*-isomers tend to align with the nematic director, and that the absorption moment of *trans*-isomers is along their long axis. Absorption therefore occurs predominantly in those domains where the nematic director is along the polarization direction. Absorption in these domains leads to reduction of the degree of order, and, as above, contraction along the director. Since the intensity of light decreases as it penetrates the film, there is less contraction at the bottom of the film than at the top, and the film curls up. The curl of the strain is the curvature. The response time, with the light intensities used, is on the order of 10 s. The effects of light attenuation on the photoresponse has been studied in detail [73, 74].

Camacho-Lopez and coworkers in 2004 showed that nematic LCEs with dissolved, rather than covalently bonded, azo dyes are capable of large and fast deformations under photoexcitation with visible light [75]. Using an Ar laser, they demonstrated the bending of 300-μm thick monodomain nematic cantilevers with 20 ms rise time and 75 ms relaxation time (Fig. 10). Siloxane-based side chain

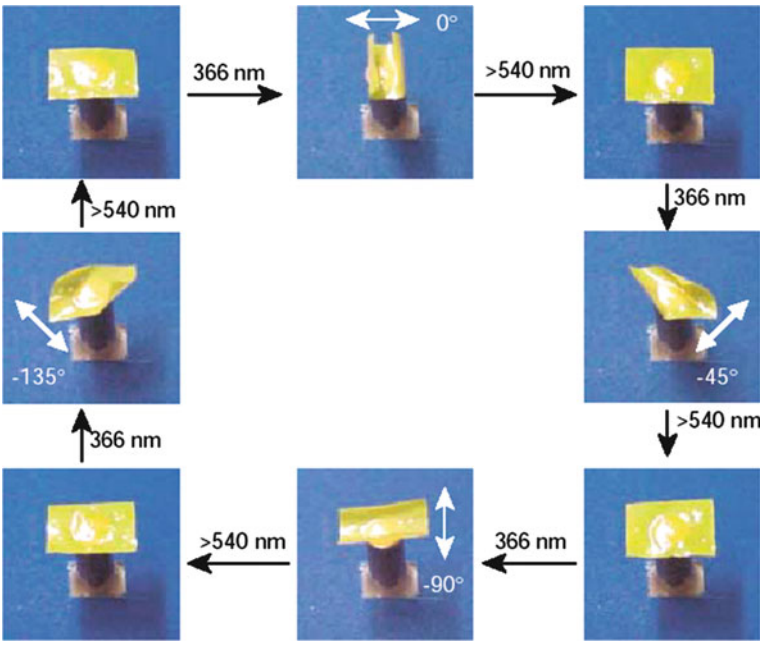

Fig. 9 Films of polydomain LC networks curl as the intensity of light increases From [72]

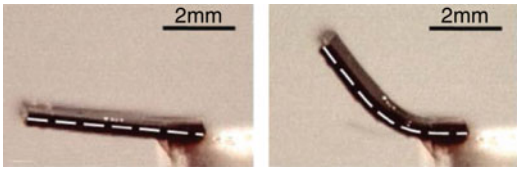

Fig. 10 Nematic cantilever bends when a 60 ms pulse of light from a 60 mWAr laser is incident from above. The scale bar is 2mm. From [75]

nematic LCEs were swollen with toluene in which the azo dye Disperse Orange I had been dissolved. After solvent evaporation, about 0.1 wt% of the dye remained in the sample. Another remarkable phenomena observed was that when LCE samples floating on water were irradiated by green light from above, the samples swam away from the light. This phenomenon might be due to an inherent instability associated with the characteristic saddle-shape of photoexcited LCE samples. When samples are illuminated, they contract along the director and, due to volume conservation, expand in the two orthogonal directions. Since light is attenuated as it propagates in the sample, the strains are greater on the top surface than on the bottom. Contraction along the director produces a deformation that is concave up, while expansion in the perpendicular direction produces a deformation that is concave down; the two curvatures are orthogonal. A typical saddle-shape produced by illumination from above is shown in Fig. 11. If the sample is displaced, the shoulders of the saddle move, exerting a force on the water, which in turn exerts a

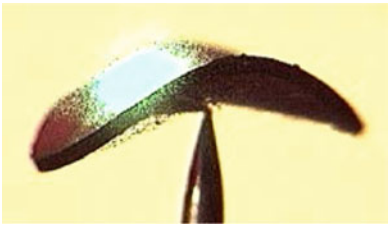

Fig. 11 Flat nematic LCE sample takes on a saddle shape when illuminated from above. From [75]

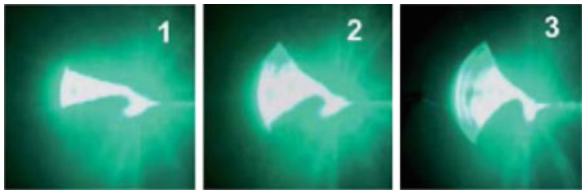

Fig. 12 Cantilever from azo-LC network oscillates under illumination from the right. Frequencies up to 270 Hz were observed. From [76]

force on the sample, pushing it in the direction of the original displacement. Via this process, remarkably, the samples of arbitrary shape swim away from light.

The response time of photoinduced bending can be shortened dramatically if, instead of using relatively thick LCE samples, thin films of LC networks with less inertia are used. Tabiryan and coworkers produced such acryloxy-based networks, Cantilevers cut from 50-μm thick films are not only fast, they also exhibit bidirectional bending, and oscillate [76] (Fig. 12). A vertical cantilever illuminated from the front will bend forward, towards the light. If the deformation is sufficiently large, the cantilever will expose its back surface to the light, resulting in a bend towards the original vertical position. As the cantilever straightens up, the front surface is again exposed, and the process begins again. Oscillations at frequencies ranging from 23 to 271 Hz have been observed; oscillations can be produced not only with laser excitation, but also by focused sunlight. The general problem of extracting mechanical work from photoisomerization and the efficiency of such a process have been considered [77]. The limits on the efficiency of energy conversion have not yet been clearly established.

Photoinduced bend deformations in LCEs and LC networks have traditionally relied on different levels of photoexcitation near the two sample surfaces due to the absorption of light in the sample. Broer's group introduced heterogeneous structures, with different director orientations at the surfaces [78, 79]. A practically useful configuration is the splay-bend configuration, where the director is in the plane of the front surface and perpendicular to the rear surface. Illuminating a film having such director structure would cause a contraction along the director of the front surface and an expansion at the rear, causing the film to bend towards the light even if the light intensity at the two surfaces was the same. Networks with such non-uniform director structures are particularly useful for practical photoactuation. Recently, van Oosten and coworkers devised a scheme to print photoactuated

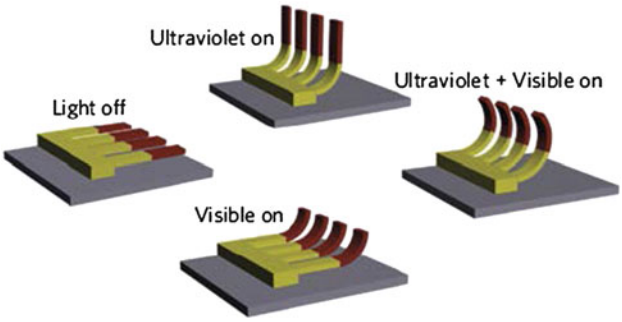

Fig. 13 Schematic of printed artificial cilia. The articulation enables pumping of fluids. From [80]

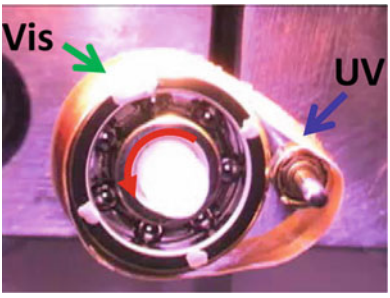

Fig. 14 Light-driven LCE motor. From [84]

cilia using inkjet printers [80] (Fig. 13). Two different dyes are used in the cilia at different locations to enable addressable actuation; the splay-bend architecture is also utilized. The addressability and articulation allows non-reciprocal motion, enabling the pumping of fluids [81].

Ikeda and coworkers have pioneered the development of many photoactuated devices, ranging from "walkers" and "robotic arms" [82] to polymer fibers [83]. Perhaps the most striking device is the light-driven LC network motor [84] shown in Fig. 14. It consists of two pulleys, joined by a laminated belt consisting of an azobenzene-containing nematic LCE on a layer of low density polyethylene for added strength. The nematic director and the azo-containing mesogens are aligned parallel to the edge of the belt. When UV light is shined on the small pulley on the right, and visible light on the large pulley on the left, the motor runs and the pulleys rotate continuously in the counterclockwise direction. The operating mechanism proposed here differs somewhat from that in [79]. UV irradiation produces a bend of the LCE towards the light, essentially increasing the length of the lever arm above the small pulley relative to that below. This results in a non-zero torque on the small pulley, and rotation. Visible light at the large pulley assists the relaxation of the *cis*-isomers and of the LCE to its undeformed state. This elegant light-driven motor serves as an icon indicating the broad range of responses and possible applications of LCEs.

An unusual application has been proposed recently by Warner and coworkers – using LCEs for solar-to-electric energy conversion [85]. Since the dielectric tensor of LCs and LCEs depend linearly on the order parameter, increasing the temperature reduces the dielectric constant for fields along the director. A charged capacitor with an appropriately aligned LC dielectric will increase its voltage and stored energy on heating. The heating can be done by sunlight, converting solar to electrical energy directly. The efficiency of the process increases with the voltage across the capacitor. Since the dielectric breakdown strength of LCEs greatly exceeds that of conventional LCs, LCEs offer a viable scheme for solar-to-electric energy conversion.

3.3 Modeling the Interaction of Light and LCEs

Although a great deal is now known about LCEs and about the optics of liquid crystals, modeling the interaction of light and LCEs is a challenging undertaking. The general dynamic response of LCEs involves the time evolution of the order parameter, together with momentum conservation in a dissipative system with free boundaries. Light-induced effects further involve the optical properties of a dynamic heterogeneous birefringent medium, which sensitively depends on the global radiation field. The radiation field, in turn, depends on the optical properties of the LCE host. Although key aspects of light propagation in LCEs and of the resulting mechanical response have been worked out [86, 87] and attempts have been made to model the response of LCEs to illumination [88, 89], the general problem remains unsolved. Emerging research topics, such as the combination of LCEs with plasmonic nanoparticles will probably bring new questions and problems. Yet, the development of efficient materials for practical applications, such as adaptive optics or soft robotics needs effective modeling. This will probably be achieved through sophisticated mathematical modeling tools together with efficient and accurate numerical simulations. This is a challenging but exciting area in which considerable growth can be expected.

4 Conclusions and Outlook

Due to the coupling of orientational order and mechanical strain, light–matter interactions in LCEs involve an exceptionally broad range of unusual phenomena. These raise a number of intriguing questions, and open the door to a variety of novel device applications. Particularly appealing aspects of LCEs from the applications point of view are the ease of changing optical properties by mechanical deformations, the possibility of readily deformable optical elements, and the ability to deliver energy to specific locations without electrodes. Before LCE devices can be made practically useful, considerable challenges must be overcome both in

understanding of the relevant physical processes and in materials design and development. The most appealing aspect of light–matter interactions in LCEs, however, is the promise of new physics waiting to be discovered.

Acknowledgements P. P.-M. acknowledges support from the NSF under DMR 0907508, the collaboration of P. Luchette, J. Neal and T. Toth-Katona, and discussions with D. Broer, H. Finkelmann, H. Godinho, T. Ikeda, M. Warner and Xiaoyu Zheng.

References

1. de Gennes PG (1975) Réflexions sur un type de polymères nématiques. C R Acad Sci Ser B 281:101–103
2. Finkelmann H, Kock H, Rehage G (1981) Investigations on LC polysiloxanes: 3. Liquid crystalline elastomers - a new type of liquid crystalline material. Makromol Chem Rapid Commun 2:317–322
3. Goldstone J, Salam A, Weinberg S (1962) Broken symmetries. Phys Rev 127:965
4. Frank FC (1958) I. Liquid crystals. On the theory of liquid crystals. Discuss Faraday Soc 25:19–28
5. Landau LD, Lifshitz EM (1986) Theory of elasticity. Elsevier, Oxford
6. Schmidtke J, Kniesel S, Finkelmann H (2005) Probing the photonic properties of a cholesteric elastomer under biaxial stress. Macromolecules 38:1357–1363
7. Lazo I, Palffy-Muhoray P (2008) Determination of the refractive indices of liquid crystal elastomers. In: APS March Meeting. New Orleans, LA: Bull Am Phys Soc
8. Yusuf Y, Minami N, Yamaguchi S, Cho DU, Cladis PE, Brand HR, Finkelmann H, Kai S (2007) Shape anisotropy and optical birefringence measurements of dry and swollen liquid single crystal elastomers. J Phys Soc Jpn 76:073602
9. Finkelmann H, Greve A, Warner M (2001) The elastic anisotropy of nematic elastomers. Eur Phys J E 5:281–293
10. Urayama K, Arai Y, Takigawa T (2006) Swelling and shrinking dynamics of nematic elastomers having global director orientation. Macromolecules 38:3469
11. Chambers M, Verduzco R, Gleeson JT, Sprunt S, Jákli A (2009) Calamitic liquid-crystalline elastomers swollen in bent-core liquid-crystal solvents. Adv Mater 21:1622–1626
12. Yusuf Y, Huh JH, Cladis PE, Brand HR, Finkelmann H, Kai S (2005) Low-voltage-driven electromechanical effects of swollen liquid-crystal elastomers. Phys Rev E 71:061702
13. Kupfer J, Finkelmann H (1991) Nematic liquid single-crystal elastomers. Makromol Chem Rapid Commun 12:717–726
14. Verduzco R, Meng GN, Kornfield JA, Meyer RB (2006) Buckling instability in liquid crystalline physical gels. Phys Rev Lett 96:147802
15. Clarke SM, Nishikawa E, Finkelmann H, Terentjev EM (1997) Light-scattering study of random disorder in liquid crystalline elastomers. Macromol Chem Phys 198:3485–3498
16. Clarke SM, Terentjev EM, Kundler I, Finkelmann H (1998) Texture evolution during the polydomain-monodomain transition in nematic elastomers. Macromolecules 31:4862–4872
17. Kempe MD, Scruggs NR, Verduzco R, Lal J, Kornfield JA (2004) Self-assembled liquid-crystalline gels designed from the bottom up. Nat Mater 3:177–182
18. Palffy-Muhoray P, Meyer RB (2004) Bridging the experiment-theory gap. Nat Mater 3:139–140
19. Harris KD, Cuypers R, Scheibe P, van Oosten CL, Bastiaansen CWM, Lub J, Broer DJ (2005) Large amplitude light-induced motion in high elastic modulus polymer actuators. J Mater Chem 15:5043–5048

20. Zhao Y, Ikeda T (2009) Smart light-responsive materials: azobenzene-containing polymers and liquid crystals. Wiley, Hoboken
21. van Oosten CL, Corbett D, Davies D, Warner M, Bastiaansen CWM, Broer DJ (2008) Bending dynamics and directionality reversal in liquid crystal network photoactuators. Macromolecules 41:8592–8596
22. Orear J, Fermi E (1950) Nuclear physics, a course given by Enrico Fermi at the University of Chicago, Revised edition. University of Chicago Press, Chicago
23. Belyakov VA (1992) Diffraction optics of complex-structured periodic media. Springer, Berlin, 380 p
24. de Vries H (1951) Rotatory power and other optical properties of certain liquids crystals. Acta Cryst 4:219
25. Kogelnik H, Shank CV (1971) Stimulated emission in a periodic structure. Appl Phys Lett 18:152–154
26. Goldberg LS, Schnur JM (1973) Tunable internal feedback liquid crystal laser. US Patent 3,771,065
27. Ilchishin IP, Tikhonov EA, Tischenko VG, Shpak MT (1981) Generation of tunable radiation by impurity cholesteric liquid crystals. JETP Lett (Translation of Pis'ma v Zhurnal Eksperimental'noi i Teoreticheskoi Fiziki) 32:27–30
28. Kopp VI, Fan B, Vithana HKM, Genack AZ (1998) Low-threshold lasing at the edge of a photonic stop band in cholesteric liquid crystals. Opt Lett 23:1707–1709
29. Taheri B, Palffy-Muhoray P, Kabir H (1999) Lasing in cholesteric band-gap materials. In: ALCOM symposium. Chiral materials and applications. 18–19 Feb 1999, Cuyahoga Falls, OH
30. Palffy-Muhoray P, Munoz A, Taheri B, Twieg R (2000) Lasing in cholesteric liquid crystals. Journal of the Society for Information Display Symposium Digest of Technical Papers, 31, pp 1170–1173
31. Schmidtke J, Stille W (2003) Fluorescence of a dye-doped cholesteric liquid crystal film in the region of the stop band: theory and experiment. Eur Phys J B Condensed Matter 31:179–194
32. Cao W (2005) Fluorescence and lasing in liquid crystalline photonic band gap materials. In: Chemical Physics Interdisciplinary Program, Kent State University
33. Alvarez E, He M, Munoz AF, Palffy-Muhoray P, Serak SV, Taheri B, Twieg R (2001) Mirrorless lasing and energy transfer in cholesteric liquid crystals doped with laser dyes. Mol Cryst Liq Cryst 57:369
34. Serak SV, Arikainen EO, Gleeson HF, Grozhik VA, Guillou J-P, Usova NA (2002) Laser-induced concentric colour domains in a cholesteric liquid crystal mixture containing a nematic azobenzene dopant. Liq Cryst Today 29:19–26
35. Munoz A, Palffy-Muhoray P, Taheri B (2001) Ultraviolet lasing in cholesteric liquid crystals. Opt Lett 26:804–806
36. Schmidtke J, Stille W, Finkelmann H, Kim S-T (2002) Laser emission in a dye doped cholesteric polymer network. Adv Mater 14:746
37. Shibaev PV, Tang K, Genack AZ, Kopp V, Green MM (2002) Lasing from a stiff chain polymeric lyotropic cholesteric liquid crystal. Macromolecules 35:3022–3025
38. Ozaki M, Kasano M, Ganzke D, Haase W, Yoshino K (2002) Mirrorless lasing in a dye-doped ferroelectric liquid crystal. Adv Mater 14:306–309
39. Ozaki M, Kasano M, Kitasho T, Ganzke D, Haase W, Yoshino K (2003) Electro-tunable liquid-crystal laser. Adv Mater 15:974–977
40. Kasano M, Ozaki M, Yoshino K, Ganzke D, Haase W (2003) Electrically tunable waveguide laser based on ferroelectric liquid crystal. Appl Phys Lett 82:4026–4028
41. Strangi G, Barna V, Caputo R, Luca AD, Versace C, Scaramuzza N, Umeton C, Bartolino R, Price GN (2005) Color-tunable organic microcavity laser array using distributed feedback. Phys Rev Lett 94:063903–1–063903–4
42. Chanishvili A, Chilaya G, Petriashvili G, Barberi R, Bartolino R, Cipparrone G, Mazzulla A (2004) Lasing lasing in dye-doped cholesteric liquid crystals: two new tuning strategies. Adv Mater 16:791–795
43. Funamoto K, Ozaki M, Yoshino K (2003) Discontinuous shift of lasing wavelength with temperature in cholesteric liquid crystal. Jpn J Appl Phys 42:L1523–L1525

44. Moreira MF, Carvalho ICS, Cao W, Bailey C, Taheri B, Palffy-Muhoray P (2004) Cholesteric liquid-crystal laser as an optic-fiber based temperature sensor. Appl Phys Lett 85:2691–2693
45. Chanishvili A, Chilaya G, Petriashvili G, Barberi R, Bartolino R, Cipparrone G, Mazzulla A, Oriol L (2003) Phototunable lasing in dye-doped cholesteric liquid crystals. Appl Phys Lett 83:5353–5355
46. Bobrovsky AY, Boiko NI, Shibaev VP, Wendorff JH (2003) Cholesteric mixtures with photochemically tunable, circularly polarized fluorescence. Adv Mater 15:282–287
47. Shibaev PV, Sanford RL, Chiappetta D, Milner V, Genack A, Bobrovsky A (2005) Light controllable tuning and switching of lasing in chiral liquid crystals. Opt Express 13:2358–2363
48. Ilchishin IP, Yaroshchuk OV, Gryshchenko SV, Shaydiuk EA (2004) Influence of the light-induced molecular transformations on the helix pitch and lasing spectra of cholesteric liquid crystals. Proc SPIE 5507:229–234
49. Shibaev PV, Madsen J, Genack AZ (2004) Lasing and narrowing of spontaneous emission from responsive cholesteric films. Chem Mater 16:1397–1399
50. He GS, Lin T-C, Hsiao VKS, Cartwright AN, Prasad PN, Natarajan LV, Tondiglia VP, Jakubiak R, Vaia RA, Bunning TJ (2003) Tunable two-photon pumped lasing using a holographic polymer-dispersed liquid-crystal grating as a distributed feedback element. Appl Phys Lett 83:2733–2735
51. Shirota K, Sun H-B, Kawata S (2004) Two-photon lasing of dye-doped photonic crystal lasers. Appl Phys Lett 84:1632–1634
52. Ozaki M, Ozaki R, Matsui T, Yoshino K (2003) Twist-defect-mode lasing in photopolymerized cholesteric liquid crystal. Jpn J Appl Phys 42:L472–L475
53. Schmidtke J, Stille W (2003) Photonic defect modes in cholesteric liquid crystal films. Eur Phys J E Soft Matter 12:553–564
54. Song MH, Park B, Shin K-C, Ohta T, Tsunoda Y, Hoshi H, Takanishi Y, Ishikawa K, Watanabe J, Nishimura S, Toyooka T, Zhu Z, Swager TM, Takezoe H (2004) Effect of phase retardation on defect-mode lasing in polymeric cholesteric liquid crystals. Adv Mater 16:779–783
55. Cao W, Palffy-Muhoray P, Taheri B, Marino A, Abbate G (2005) Lasing thresholds of cholesteric liquid crystals lasers. Mol Cryst Liq Cryst 429:101–110
56. Blinov LM, Bartolino R (2010) Liquid crystal microlasers. Transworld Research Network, Kerala
57. Kim ST, Finkelmann H (2001) Cholesteric liquid single-crystal elastomers (LSCE) obtained by the anisotropic deswelling method. Macromol Rapid Commun 22:429–433
58. Warner M, Terentjev EM, Meyer RB, Mao Y (2000) Untwisting of a cholesteric elastomer by a mechanical field. Phys Rev Lett 85:2320–2323
59. Finkelmann H, Kim ST, Muñoz A, Palffy-Muhoray P, Taheri B (2001) Tunable mirrorless lasing in cholesteric liquid crystalline elastomers. Adv Mater 13:1069–1072
60. Graham-Rowe D (2009) A new twist to tuning lasers. Nat Photonics 3:182–183
61. Schmidtke J, Stille W, Finkelmann H (2003) Defect mode emission of a dye doped cholesteric polymer network. Phys Rev Lett 90:083902
62. Kornfield J, Clark NA, Dalton L, Marder S, Ober C, Palffy-Muhoray P, Perry JW, Thomas N, Walba DM, Wu ST (2002) New liquid crystal materials enabling revolutionary display devices. P Soc Photo-Opt Ins 4712:336–349
63. Amigo-Melchior A, Finkelmann H (2002) A concept for bifocal contact- or intraocular lenses: liquid single crystal hydrogels. Polym Adv Technol 13:363–369
64. Eu BC (1986) Statistical foundation of the Minkowski tensor for ponderable media. Phys Rev A 33:4121–4131
65. Jánossy I (1991) Optical effects in liquid crystals, 1st edn. Perspectives in condensed matter physics. Kluwer Academic, Dordrecht, 232 p
66. Finkelmann H, Nishikawa E, Pereira GG, Warner M (2001) A new opto-mechanical effect in solids. Phys Rev Lett 87:015501

67. Dawson NJ, Kuzyk MG, Neal J, Luchette P, Palffy-Muhoray P (2011) Cascading of liquid crystal elastomer photomechanical optical devices. Opt Commun 284:991–993
68. Janossy I, Lloyd AD, Wherrett BS (1990) Anomalous optical Freedericksz transition in an absorbing liquid-crystal. Mol Cryst Liq Cryst 179:1–12
69. Kreuzer M, Marrucci L, Paparo D (2000) Light-induced modification of kinetic molecular properties: enhancement of optical Kerr effect in absorbing liquids, photoinduced torque and molecular motors in dye-doped nematics. J Nonlinear Opt Phys 9:157–182
70. Kosa T, Weinan E, Palffy-Muhoray P (2000) Brownian motors in the photoalignment of liquid crystals. Int J Eng Sci 38:1077–1084
71. Palffy-Muhoray P, Kosa T, Weinan E (2002) Brownian motors in the photoalignment of liquid crystals. Appl Phys A Mater Sci Process 75:293–300
72. Yu YL, Nakano M, Ikeda T (2003) Directed bending of a polymer film by light – miniaturizing a simple photomechanical system could expand its range of applications. Nature 425:145
73. Corbett D, van Oosten CL, Warner M (2008) Nonlinear dynamics of optical absorption of intense beams. Phys Rev A 78:013823
74. Corbett D, Warner M (2007) Linear and nonlinear photoinduced deformations of cantilevers. Phys Rev Lett 99:174302
75. Camacho-Lopez M, Finkelmann H, Palffy-Muhoray P, Shelley M (2004) Fast liquid-crystal elastomer swims into the dark. Nat Mater 3:307–310
76. Serak S, Tabiryan N, Vergara R, White TJ, Vaia RA, Bunning TJ (2010) Liquid crystalline polymer cantilever oscillators fueled by light. Soft Matter 6:779
77. Hugel T, Holland NB, Cattani A, Moroder L, Seitz M, Gaub HE (2002) Single-molecule optomechanical cycle. Science 296:1103–1106
78. Harris KD, Cuypers R, Scheibe P, Mol GN, Lub J, Bastiaansen CWM, Broer DJ (2005) Molecular orientation control for thermal and UV-driven polymer MEMS actuators. Smart Sensors, Actuators, and MEMS II 5836:493–503
79. Mol T, Harris KD, Bastiaansen C, Broer DJ (2005) Stimulated mechanical responses of liquid crystal networks with a splayed molecular organization. Emerging Liquid Crystal Technologies 5741:47–55
80. van Oosten CL, Bastiaansen CWM, Broer DJ (2009) Printed artificial cilia from liquid-crystal network actuators modularly driven by light. Nat Mater 8:677–682
81. Palffy-Muhoray P (2009) Printed actuators in a flap. Nat Mater 8:614–615
82. Yamada M, Kondo M, Miyasato R, Naka Y, Mamiya J, Kinoshita M, Shishido A, Yu YL, Barrett CJ, Ikeda T (2009) Photomobile polymer materials-various three-dimensional movements. J Mater Chem 19:60–62
83. Yoshino T, Mamiya J, Kinoshita M, Ikeda T, Yu YL (2007) Preparation and characterization of crosslinked azobenzene liquid-crystalline polymer fibers. Mol Cryst Liq Cryst 478:989–999
84. Yamada M, Kondo M, Mamiya JI, Yu YL, Kinoshita M, Barrett CJ, Ikeda T (2008) Photomobile polymer materials: towards light-driven plastic motors. Angew Chem Int Ed 47:4986–4988
85. Hiscock T, Warner M, Palffy-Muhoray P (2011) Solar to electrical conversion via liquid crystal elastomers. J Appl Phys 109:104506
86. Warner M, Blaikie RJ (2009) Two-color nonlinear absorption of light in dye layers. Phys Rev A 80:033833
87. Warner M, Mahadevan L (2004) Photoinduced deformations of beams, plates, and films. Phys Rev Lett 92:134302
88. Zhu W, Shelley M, Palffy-Muhoray P (2011) Modeling and simulation of liquid-crystal elastomers. Phys Rev E 83:051703
89. Selinger RLB, Mbanga BL, Selinger JV (2008) Modeling liquid crystal elastomers: actuators, pumps, and robots – art. no. 69110A. Emerging Liquid Crystal Technologies III. 6911, p. A9110

Adv Polym Sci (2012) 250: 119–146
DOI: 10.1007/12_2010_107

Published online: 8 April 2011

Electro-Opto-Mechanical Effects in Swollen Nematic Elastomers

Kenji Urayama

Abstract Nematic elastomers swollen by low molecular weight nematogens (nematic gels) exhibit fast response to electric fields with a large change in optical birefringence together with macroscopic deformation. This electro-opto-mechanical (EOM) effect is a direct consequence of the deformation coupled to electrically driven director rotation in nematic gels under a mechanically unconstrained geometry. This article describes the static and dynamic features of the EOM effects of nematic gels. We will discuss recent investigations into the influences of field strength, frequency, and external mechanical constraints on the EOM effects. The relation between director rotation and macroscopic deformation is elucidated on the basis of optical and mechanical data in a steady state. The dynamics of the EOM effects are also discussed, on the basis of optical and mechanical response times to field imposition and removal. We also introduce a simple model to capture the main features of the static and dynamic aspects of the EOM effects.

Keywords Electro-mechanical effect · Electro-optical effect · Liquid crystal elastomers · Nematic gels

Contents

K. Urayama
Department of Materials Chemistry, Kyoto University, Nishikyo-ku, Kyoto 615-8510, Japan
e-mail: urayama@rheogate.polym.kyoto-u.ac.jp

1 Introduction

Liquid crystal elastomers (LCEs) are, as the name implies, hybrid materials composed of liquid crystals (LCs) and elastomers. A marked characteristic of LCEs is a strong coupling between the macroscopic shape and the molecular orientation of the constituent mesogens. This strong coupling results in the unique stimulus-responsive properties of LCEs [1–4]. When an external field alters the degree or direction of mesogen orientation in LCEs, a corresponding change in the macroscopic shape occurs simultaneously. As a familiar example, a temperature variation causes finite uniaxial deformation of nematic elastomers as a result of a change in the orientational order of the mesogens, the details of which are described by Kramer et al. [5].

Electric field is also expected as an effective external field to drive finite and fast deformation in LCEs, because, as is well known for low molecular mass LCs (LMM-LCs), an electric field is capable of inducing fast rotation of the director toward the field direction [6]. This electrically driven director rotation results in a large and fast change in optical birefringence that is called the electro-optical (EO) effect. The EO effect is a key principle of LC displays. Electrically induced deformation of LCEs is also attractive when they are used for soft actuators: a fast actuation is expected, and electric field is an easily controlled external variable. However, in general, it is difficult for LCEs in the neat state to exhibit finite deformation in response to the modest electric fields accessible in laboratories. Some chiral smectic elastomers in the neat state show finite deformation stemming from electroclinic effects [7, 8], but that is beyond the scope of this article; we focus on deformation by director rotation.

Early work by Zentel [9] and several other researchers [10–14] observed the electro-mechanical (EM) effect, i.e., finite distortions under modest electric fields, for the LCEs that were swollen by LMM-LCs. Swelling by miscible LMM-LCs considerably softens LCEs without losing their liquid crystallinity. This softening significantly reduces the field strength required for actuation. However, the simultaneous mesogen reorientation (resulting in the EO effect) was too small to detect or not characterized in most of these studies.

Other groups [15, 16] studied the EO effect in monodomain nematic gels that were directly prepared in EO cells in the presence of a large amount of LMM-LC, but none of these studies clearly observed finite macroscopic deformation. The gel specimens

in these studies were effectively sandwiched between the two rigid electrodes, and this constrained geometry prevented strain in the field direction. A theoretical study [17] suggests that such a constraint significantly enhances the elastic barrier, and thus the field strength required for finite distortion becomes very high.

The strong coupling of director and macroscopic deformation in LCEs implies that the response to electric fields appears as EM effects accompanied by EO effects. This electro-opto-mechanical (EOM) effect was demonstrated using a monodomain nematic elastomer swollen by LMM-LC that was placed in an unconstrained geometry where the specimen had no mechanical constraints from electrodes [18, 19]. The combination of the monodomain sample with the unconstrained geometry facilitates director rotation and the resultant deformation under electric fields. In addition, the field-driven director configuration of unconstrained nematic elastomers is considerably different from that in the conventional Fredericks effects of nematic liquids. Figure 1 shows the schematics of the field-driven director configurations of nematic liquids and an unconstrained nematic elastomer slab floating in fluid between rigid electrodes. They both initially have a uniform planar configuration before the field imposition. In the case of nematic liquids (Fig. 1a), the directors at the surfaces are anchored, and the rotation angle of the director has a finite distribution, with the maximum at the middle layer of the cell. The recovery to the initial planar configuration in response to field-off originates from the Frank elasticity. In contrast, the director of unconstrained nematic elastomers (Fig. 1b) is capable of uniform rotation under electric fields. The Frank elasticity plays no role in the recovery to the initial configuration.

The EOM effect also provides an important basis for elucidating the correlation between the director rotation and macroscopic deformation. Experimentally, it has often been investigated by mechanically stretching the monodomain nematic elastomers in the direction normal to the initial director [20–25]. However, the mechanical constraint by clamping at the ends significantly affects the director rotation, and the resultant director reorientation often becomes inhomogeneous [26–28]. In contrast, the EOM effect in Fig. 1b enables us to observe unambiguously the characteristic

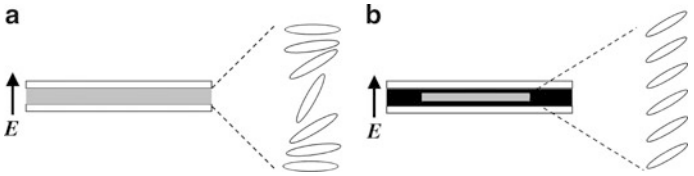

Fig. 1 Field-driven director configurations in (**a**) a nematic liquid (conventional Fredericks effect) and (**b**) a nematic elastomer slab floating in liquid between rigid electrodes. They initially have a uniform planar orientation before imposing field E in the direction shown by the *arrow*. In (**a**), the director at the surfaces are anchored, and the rotation angle of director has a finite distribution along the field axis, with the maximum at the middle layer of the cell. The recovery force for the director originates from the Frank elasticity. In (**b**), the director is capable of uniform rotation under electric fields, and the Frank elasticity plays no role in the recovery force

deformation mode driven by director rotation. Furthermore, the dynamic aspect of this phenomenon (i.e., the rate of response to the imposition and removal of electric fields) is an interesting issue, especially in view of the comparison with the dynamics of the EO effect in LMM-LCs. The dynamic properties are also important for exploring the possibility of this effect in novel soft actuators. A primary goal of this article is to review various aspects of the EOM effects that have been elucidated by recent studies.

In Sect. 2, we introduce the details of the materials and the experimental setup. Static features such as the voltage dependencies of optical birefringence and strain are described in Sect. 3. Polarized Fourier transform infrared spectroscopy (FTIR) studies to characterize the electrically driven mesogen realignment are also discussed in Sect. 3. Dynamic features of the optical and mechanical responses are described in Sect. 4. A simple model to capture the main characteristics of EOM effects is introduced in Sect. 5. Conclusions and directions for future research are given in Sect. 6.

2 Materials and Observation Geometry

2.1 Materials

Most of the investigations introduced in this article employed a side-chain-type nematic elastomer that has the polyacrylate backbone with cyanobiphenyl side group. This nematic elastomer was obtained by the photopolymerization of the monoacrylate mesogenic monomer (A-6OCB; Fig. 2) and the cross-linker 1,6 hexandiol diacrylate (HDDA; Fig. 2) using a miscible nonreactive LMM-LC as a solvent [29]. The mixing of the nonreactive nematic solvent with A-6OCB (1:1 by molar ratio) was required to broaden the temperature range of the nematic state, since the nematic phase of pure A-6OCB exists in a limited temperature range because of the high crystallizability.

To obtain monodomain nematic elastomers with a global orientation, the photopolymerization was performed in a glass cell whose surfaces were coated with uniaxially rubbed polyimide layers. In this glass cell, the nematic mixture in the low-temperature nematic state was allowed to align globally in the rubbing direction. The photopolymerization was conducted at a temperature in the nematic state by

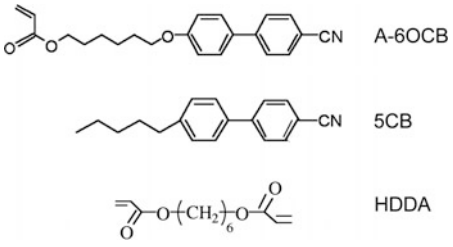

Fig. 2 Chemical structures of the mesogenic monoacrylate monomer (A-6OCB), cross-linker (HDDA), and the low molecular weight nematogen (5CB)

Table 1 Sample characteristics of monodomain nematic gels

Nematic gel	Crosslinker concentration (c_x) (mol%)	Gel thickness (d_g^0) (μm)	Spacer thickness (d_p) (μm)	Cell gap (d_t) (μm)	Solvent content (vol%)
SNE-3	3	26	20	40	82
SNE-7	7	34	25	40	74
SNE-7D	7	43	40	50	78
SNE-10D	10	40	40	50	73
SNE-14	14	23	25	40	50

irradiating the cell using a wavelength of 526 nm. The cell gap was controlled using a spacer with a thickness of d_p ranging from 20 to 40 μm (Table 1). The cross-linker concentration (c_x) was varied from 3 to 14 mol%. The resulting gel films were carefully separated from the cell and immersed in dichloromethane to wash out the unreacted materials and nematic solvent. The swollen films were gradually deswollen by increasing the methanol content in the swelling solvent. The fully deswollen films were dried and thereafter allowed to swell in a cyanobiphenyl type LMM-LC, 4-*n*-pentyl-4′-cyanobiphenyl (5CB; Fig. 2) at 25°C until the swelling was equilibrated. The 5CB content in the swollen films increases with a decrease in c_x and ranged from 82 to 50 vol% (Table 1). In the fully swollen films, the LCE and 5CB are completely miscible and form a single nematic phase, which is confirmed by a single nematic-isotropic transition temperature [30]. It should be noted that both of the constituent nematogens, A-6OCB and 5CB, in the swollen elastomers are dielectrically positive, i.e., the molecular long axis of each nematogen tends to align parallel to the direction of electric fields.

2.2 Observation Geometry

As demonstrated later, unconstrained geometry is crucial for the observation of pronounced EOM effects. The swollen elastomer films were placed between two glass plates with optically transparent indium tin oxide (ITO) electrodes so that the films could have no mechanical constraints from the rigid electrodes, i.e., the cell gap was larger than the film thickness, as shown in Fig. 3. The cell was filled with a silicone oil, which was optically transparent and immiscible with the swollen elastomers, in order to observe the EO effect purely originating from the gels. The gel thickness (d_g^0) and cell gap (d_t) for each sample are listed in Table 1.

A square AC electric field was imposed normally on the initial director of the swollen elastomers. The frequency was 1 kHz unless specified otherwise. In the measurement of optical birefringence, the specimen was placed such that the initial director was at an angle of 45° relative to the crossed polarizers. The intensity of the transmitted light (I) was measured by a photodiode detector as a function of voltage amplitude (V_0). The effective birefringence in the x–y plane (Δn_{eff}) was evaluated

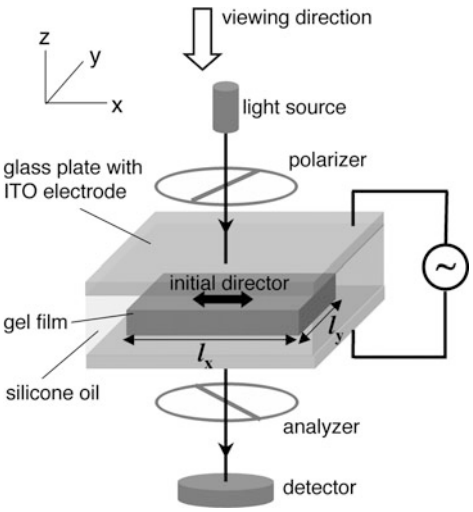

Fig. 3 Experimental setup for EOM effect and polarized FTIR measurements of nematic gels under electric fields. For the optical birefringence measurements, the initial director of the specimen has an angle of 45° relative to the crossed polarizers. For the polarized FTIR measurements, the optical axis of the polarizer is parallel or normal to the initial director for evaluating absorbances A_x or A_y, respectively, and no analyzer is used. l_x and l_y are the dimensions of the film in the x- and y-directions, respectively

from the familiar relation $I/I_{\max} = \sin^2(\pi d\Delta n_{\text{eff}}/\lambda)$ where λ is the wavelength of a He–Ne laser ($\lambda = 633$ nm). The change in film thickness (d) was less than 15% in the V_0 range examined, and thus the initial thickness was used for the sake of simplicity in the calculation of Δn_{eff} at each V_0.

The electrically induced strains in the x- and y-directions were measured using an optical microscope. The dimensional change in the z-direction (field axis) is not directly measurable, but can be straightforwardly estimated from the dimensional variations in the x- and y-directions because of the constant volume before and after deformation.

3 Static Aspects

3.1 Electro-Mechanical Effect

The most prominent feature of the electrical deformation of monodomain nematic gels in an unconstrained geometry is two-dimensional [18], as shown in Fig. 4a. The gel film contracts in the direction of the initial director (x-direction) and elongates in the field direction (z-direction) without an appreciable dimensional change in the y-direction normal to both the initial director and the field axis. The elongation in the z-direction is estimated from the dimensional changes in the x- and y-directions because the gel volume is constant during deformation. It should be noted that the y-direction without dimensional variation is identical to the axis of rotation of the director. An mpeg movie of this electrical deformation is available in the supporting information of [31].

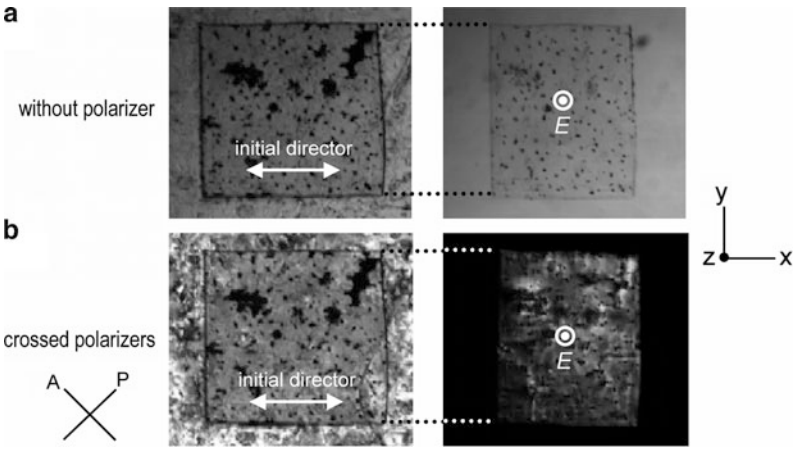

Fig. 4 Electro-opto-mechanical effect of a monodomain nematic gel observed (**a**) without polarizer and (**b**) with crossed polarizers. A 26-μm thick gel with $c_x = 4$ mol% is placed in a 40-μm thick EO cell filled with a nematic solvent (5CB). The 5CB content in the gel is 82 vol%. An AC field (E) with an amplitude of 750 V and a frequency of 1 kHz is imposed in the z-direction. The field induces a two-dimensional deformation, i.e., a shortening of ca. 20% in the x-direction, no dimensional change in the y-direction, and a lengthening of ca. 20% in the z-direction (due to volume conservation). The appearance of the gel (and surrounding 5CB) under cross-polarized conditions changes from bright to dark as a result of the almost full rotation of the director toward the field direction. A and P stand for the optical axes of analyzer and polarizer, respectively. An mpeg movie is available in the supporting information of [31]

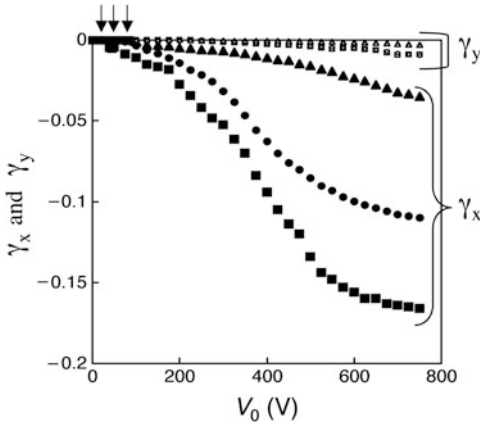

Fig. 5 Strains γ_x (*closed symbols*) and γ_y (*open symbols*) as a function of voltage amplitude (V_0): SNE-3 (*squares*), SNE-7 (*circles*), SNE-14 (*triangles*). The *arrows* indicate the threshold voltage (V_{0c}) for the onset of deformation, and V_{0c} increases with c_x. The surrounding fluid in the EO cell (Fig. 3) is a silicone oil. From [19]

Figure 5 shows the strain in the x- and y-direction (γ_x and γ_y, respectively) as a function of voltage amplitude (V_0) for specimens with various cross-linker concentrations (c_x) [19]. The strain is defined by:

$$\gamma_i = \frac{l_i - l_{i0}}{l_{i0}} \tag{1}$$

where l_i ($i = x,y,z$) is the dimension in the i-direction and the subscript 0 denotes the undeformed state. As can be seen in Fig. 5, the contractive strain in the x-direction increases with V_0 above a threshold voltage amplitude (V_{0c}), and levels off at sufficiently high V_0. In contrast, γ_y remains almost zero even at high V_0. The two-dimensional deformation mode is independent of V_0 and c_x. A reduction in c_x increases the magnitude of the strain, and the maximum $|\gamma_x|$ reaches ca. 15% for $c_x = 3$ mol%. A decrease in c_x also reduces V_{0c}. A detailed discussion of V_{0c} will be given in Sect. 3.5.

Nematic gels with random polydomain textures under electric fields exhibit simple (three-dimensional) uniaxial deformation [13]. Figure 6 shows the electrical deformation of a cylindrical-shaped polydomain nematic gel in an unconstrained geometry. The chemical structures of the mesogen, the cross-linker, and the swelling solvent are identical to those of the monodomain samples in Figs. 4 and 5. The cross-linking reaction without taking mesogen alignment into account results in a nematic elastomer with a polydomain texture that possesses randomly oriented local directors without a global director. As shown in Fig. 6, the field-induced deformation is uniaxial elongation along the field axis: The dimension in the electric field increases, whereas the dimensions in the other two directions decrease equivalently. The directors have a random configuration in the initial state, and the electric field induces a rotation of the local directors toward the field direction.

The results shown in Figs. 4–6 were obtained for nematic gels with dielectrically positive mesogens whose molecular long axes are parallel to the dipole moment. The director of dielectrically positive nematogens aligns in the field direction. The electrical stretching of dielectrically positive nematic gels is parallel to the field direction, independently of the type of initial director configuration (monodomain or polydomain). Figure 7 shows the electrical deformation of a cylindrical-shaped polydomain nematic gel with negative dielectric anisotropy [13]. Both the mesogen and the swelling solvent in this gel, whose chemical structures are shown in Fig. 7a, are dielectrically negative (i.e., the long axes are normal to the dipole moment).

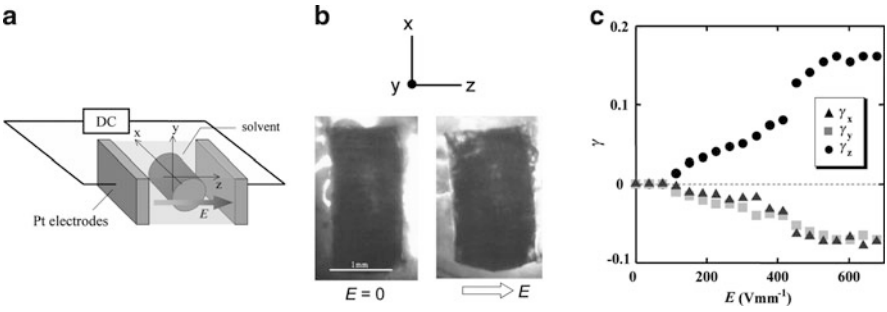

Fig. 6 Electro-mechanical effect of a cylindrical-shaped polydomain nematic gel with positive dielectric anisotropy. (**a**) Observation geometry. (**b**) Electrical deformation under a DC field of $E = 0.6$ MV/m. The specimen is elongated in the field direction and contracted in the other two directions. Observation under natural light. (**c**) Strains as a function of field strength. From [13]

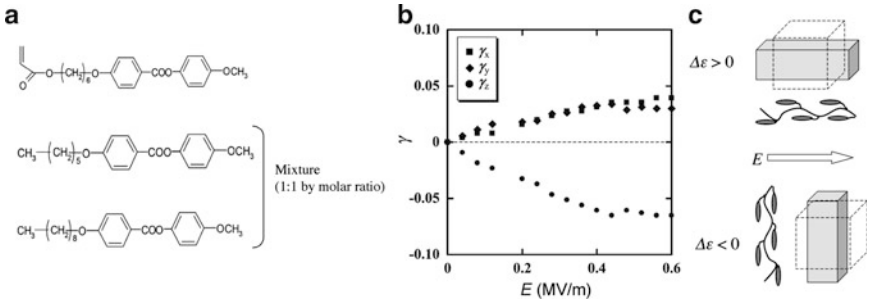

Fig. 7 Electro-mechanical effect of a cylindrical-shaped polydomain nematic gel with negative dielectric anisotropy. (**a**) Molecular structures of the constituent mesogen and swelling solvent in the gel. (**b**) Strains as a function of field strength. From [13]. (**c**) Schematics of electrical deformation of dielectrically positive ($\Delta\varepsilon > 0$) or negative ($\Delta\varepsilon < 0$) polydomain nematic gels. In the nematic gels in the present study (Fig. 2), the stretching direction of network backbone is parallel to the mesogen alignment [33, 34]

The dielectrically negative nematic gels are elongated in the direction normal to the field axis in accordance with the realignment direction of the local directors. These results indicate that the stretching direction in the electrical deformation of nematic gels is governed by the sign of the dielectric anisotropy, which is schematically shown in Fig. 7c. In general, the stretching direction of polymer backbone becomes either parallel or normal to the alignment direction of dangling mesogens, depending on the spacer length and the chemical structures of side-chain type LCEs [32]. The LCEs in this study correspond to the former case (i.e., parallel), which was confirmed by FTIR spectroscopy [33, 34].

3.2 *Electro-Optical Effect*

The characteristic two-dimensional deformation of monodomain nematic gels under electric fields originates from the rotation of the director. The electrically driven director rotation is evident from the large change in optical birefringence as shown in Fig. 4b. The appearance of the gel under cross-polarized conditions changes from bright to dark, which corresponds to a change in the director orientation from the x-direction to the z-direction.

Figure 8a shows the effective birefringence (Δn_{eff}: $\Delta n_{\text{eff}} = n_x - n_y$ where n_x and n_y are refractive indices in the x- and y-directions, respectively) in the x–y plane as a function of V_0 [19]. Note that the birefringence data in Fig. 8 was obtained using a cell filled with optically transparent silicone oil in order to observe the optical effect purely originating from the gel, although 5CB was employed as the surrounding fluid in Fig. 4. The gels exhibit a finite Δn_{eff} at $V_0 = 0$ ($\Delta n_{\text{eff}}{}^0$) due to the original global uniaxial orientation in the x-direction (i.e., $n_{x0} > n_{y0} = n_{z0}$

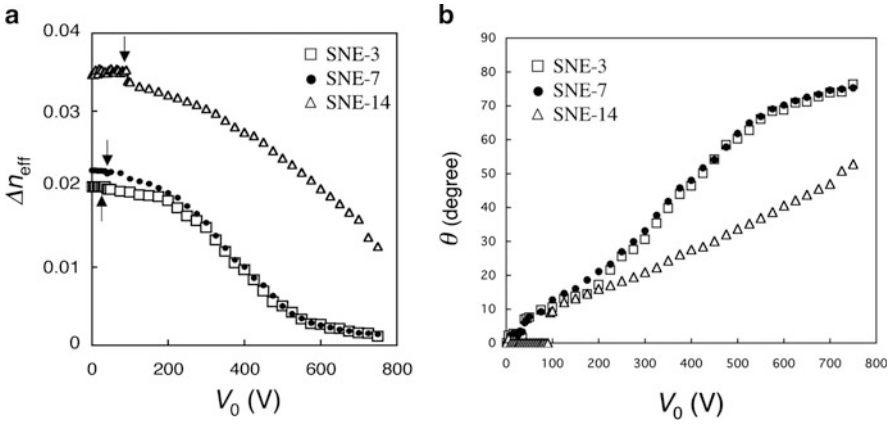

Fig. 8 Electro-optical effect of nematic gels. (**a**) Effective birefringence (Δn_{eff}) as a function of voltage amplitude (V_0). The *arrows* indicate the threshold voltage (V_{0c}) for the onset of deformation, and V_{0c} increases with c_x. (**b**) The V_0 dependence of the rotation angle θ of the director estimated from the birefringence data. The surrounding fluid in the EO cell (Fig. 3) is a silicone oil. From [19]

where n_{i0} is the refractive index in the i-direction in the initial state). The birefringence Δn_{eff} decreases with an increase in V_0 above a threshold V_{0c} and it reduces to ca. 5% of the initial value at high V_0 for the specimens with $c_x = 3$ and 7 mol%. This large reduction in Δn_{eff} indicates that sufficiently high V_0 achieves almost full (90°) rotation of the director toward the field direction around the y-axis (i.e., $n_x \approx n_{y0} = n_{z0}$). The birefringence is not completely lost, even at high V_0. This is probably because the surface layer firmly anchored in plane does not respond to the field. An increase in c_x suppresses the reduction in Δn_{eff} and increases V_{0c}.

The variations in optical birefringence provide a basis for evaluating the degree of the director rotation. When uniform rotation of the director around the y-axis is assumed, the rotation angle (θ) of the director is correlated with Δn_{eff} using the following general relation for systems with uniaxial optical anisotropy ($n_x \geq n_y = n_z$):

$$\sin^2\theta = \frac{{n_{y0}}^2}{{n_{x0}}^2 - {n_{y0}}^2}\left\{\frac{{n_{x0}}^2}{{n_x(\theta)}^2} - 1\right\} \tag{2}$$

where n_{i0} and $n_i(\theta)$ ($i = x,y$) are the refractive indices along the i-axis at $\theta = 0$ and $\theta = \theta$, respectively, and $\theta = 0°$ corresponds to the initial state at $V_0 = 0$ whereas $\theta = 90°$ corresponds to full rotation toward the field direction. If the birefringence is sufficiently small relative to the principal refractive indices, i.e., $n_{y0} \gg \Delta n_{\text{eff}}$ and $n_{y0} \gg {\Delta n_{\text{eff}}}^0$, (2) can be simplified to:

$$\sin^2\theta \approx 1 - \frac{\Delta n_{\text{eff}}(\theta)}{{\Delta n_{\text{eff}}}^0} \tag{3}$$

where $\Delta n_{\text{eff}}{}^{0} = n_{x0} - n_{y0}$. The samples satisfy the condition for this simplification: $\Delta n_{\text{eff}}{}^{0}$ is of the order of 10^{-2} whereas the refractive index normal to the long axis ($n_{\perp}$) for 5CB is ca. 1.5 at 25°C [35]. Figure 8b shows the V_0 dependence of θ obtained using (3) with the data in Fig. 8a. The results demonstrate the rotation process of the director from 0° toward 90°.

3.3 Director Rotation Characterized by Polarized FTIR

The director-rotation behavior under electric fields was also characterized by polarized FTIR [33]. Polarized FTIR has been used to characterize mesogen reorientation and mobility in monodomain LCEs in response to external mechanical fields [25, 36]. The dependence of the absorbance A of a characteristic band on the polarizer angle reflects the average orientation of the bond: A is proportional to $\langle(\boldsymbol{\mu} \cdot \mathbf{E})^2\rangle$ where vector $\boldsymbol{\mu}$ denotes the molecular transition dipole moment, vector $\mathbf{E}$ denotes the electric field of the IR beam, and the bracket represents averaging over all molecules in the measured region. In usual optical birefringence measurements, the information obtained is only the difference of the contributions in two directions such as ($n_x - n_y$). Polarized FTIR provides further information about the mesogen reorientation, because this technique gives information about the contribution in each direction separately.

Almost the same observation geometry used in the optical birefringence measurement (Fig. 3) was employed for the polarized FTIR measurements. CaF_2 plates with ITO electrodes that are transparent to infrared beams were used. The absorption band of the stretching vibration of the terminal cyano group parallel to the long axes of the mesogens (A-6OCB) and solvent (5CB) at around 2,225 cm^{-1} was used to characterize the director rotation. The absorbances of the incident polarized light parallel and normal to the initial director axis (denoted by A_x' and A_y', respectively) were evaluated from the area of the corresponding peak as a function of V_0. The absorbance of the silicone oil at around the wavelength of interest (2,225 cm^{-1}) was negligible. The absorbances A_x' and A_y' reflect the total contributions from the mesogens of the LCE and the solvent, and they are used to analyze the director-rotation behavior.

Figure 9a shows the V_0 dependencies of the reduced absorbances A_x [$=A_x'/(\lambda_z A_{y0}')$] and A_y [$=A_y'/(\lambda_z A_{y0}')$], where A_x' and A_y' are reduced by λ_z to consider the variation in effective thickness due to deformation, and A_{y0}' is the value of A_y' at $V_0 = 0$. The absorbance A reflects the average orientation of the C≡N bond parallel to the long axis of the mesogens. A finite difference in A_x and A_y at $V_0 = 0$ (denoted A_{x0} and A_{y0}, respectively) reflects the initial uniaxial orientation (original director) in the x-direction. As V_0 increases, the difference in A_x and A_y becomes smaller while A_y remains almost unchanged. Furthermore, A_x becomes nearly equal to A_y at high V_0. When a uniform reorientation of mesogens in the specimen is assumed, A_x and A_y correspond to the long and short axes of the intersection in the x–y plane at

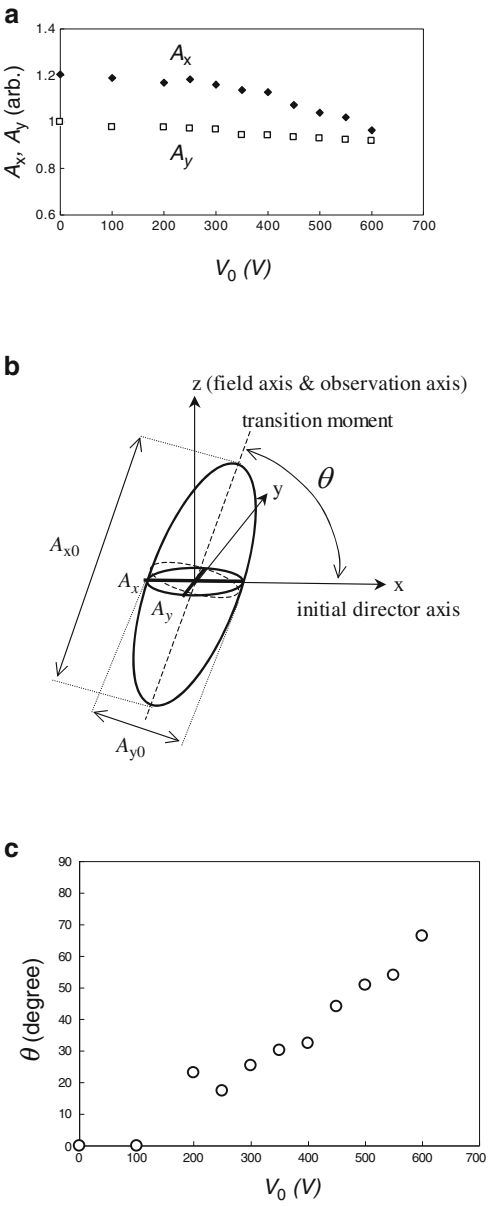

Fig. 9 (**a**) Reduced absorbances (A_x and A_y) as a function of voltage amplitude (V_0) for SNE-7D. (**b**) Absorbance ellipsoid and geometry in polarized FTIR measurements. The coordinate system is the same as in Fig. 3. (**c**) The V_0 dependence of the rotation angle θ of the director estimated from the absorbance data. From [33]

$z = 0$ for the absorption ellipsoid of the director that rotates about the y-axis at an angle of θ (Fig. 9b). The absorbances A_{x0} and A_{y0} at $\theta = 0$ give the long and short axes of the ellipsoid, respectively. The shape of the intersection varies from an ellipse ($A_{x0} > A_{y0}$) to nearly a circle ($A_x \approx A_y$), with almost no change in the short axis ($A_y \approx A_{y0}$). The relation $A_x \approx A_y$ at high V_0 shows a nearly 90° rotation of the

director. In addition, $A_y(V_0) \approx A_{y0}$ indicates that the director rotates around the y-axis with no appreciable change in the orientational order in the plane where the director is confined during the rotation. No macroscopic distortion in the y-direction under electric fields (Fig. 5) results from this type of director rotation.

The absorbance data provide information for estimating the rotation angle θ of the director. In this geometry, $A_x(\theta)$ can be expressed [37] by:

$$A_x(\theta) = a\left[\frac{1-S}{3} + S\cos^2\theta\right] \tag{4}$$

where a is a constant of proportionality and S is the orientational order parameter of the mesogens. The parameter S is defined by:

$$S = \frac{1}{2}\left[3\langle\cos^2\phi\rangle - 1\right] \tag{5}$$

where the bracket denotes the spatial average and ϕ is the angle between the mesogen and the director. In the present case, S is assumed to be independent of θ because the director rotates uniformly around the y-axis. The value of S is obtained from A_{x0} and A_{y0} using the following relation for uniaxial orientation [37]:

$$S = \frac{A_{x0} - A_{y0}}{A_{x0} + 2A_{y0}} \tag{6}$$

From (4) and (6), $\sin^2\theta$ is expressed as a function of A_x:

$$\sin^2\theta = \frac{A_{x0} - A_x}{A_{x0} - A_{y0}} \tag{7}$$

Figure 9c shows the V_0 dependence of θ evaluated from (7) using the data in Fig. 9a. The same trend as in Fig. 8b based on the birefringence data is observed.

3.4 *Correlation Between Director Rotation and Macroscopic Deformation*

In addition to the two-dimensional deformation, the correlation between the rotation angle (θ) of the director and the strain (γ_x) gives an important basis for understanding the deformation coupled to director rotation in an unconstrained geometry. Figure 10 shows γ_x and γ_y as a function of $\sin^2\theta$ estimated from the optical birefringence using (3) for the three specimens. In the range examined, γ_x is linearly proportional to $\sin^2\theta$ whereas γ_y is independent of θ. Figure 10 also shows a similar plot using $\sin^2\theta$ evaluated from the polarized FTIR via (7), for SNE-7D.

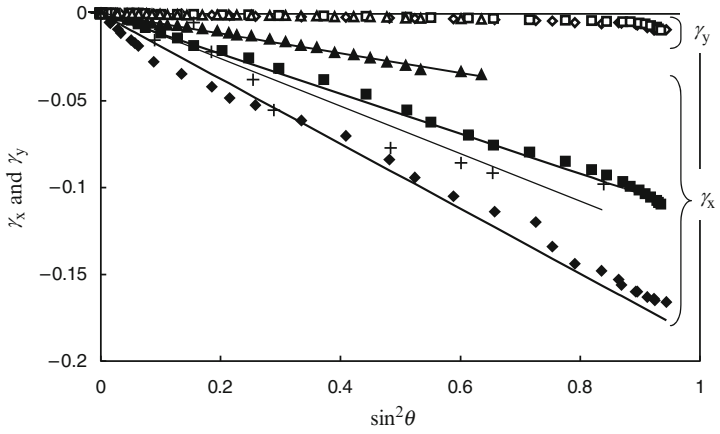

Fig. 10 Strains γ_x (*closed symbols*) and γ_y (*open symbols*) as a function of $\sin^2\theta$ for SNE-3 (*diamonds*), SNE-7 (*squares*), and SNE-14 (*triangles*), where θ is the rotation angle of the director estimated from the birefringence data. The *crosses* represent the data for SNE-7D obtained by polarized FTIR measurements. From [19, 33]

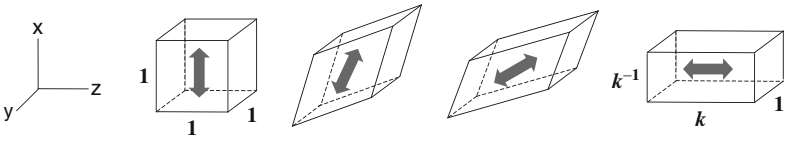

Fig. 11 Deformation of small volume element represented by (8). The *arrow* indicates the director. The rotation angle of director is 0°, 30°, 45°, 60° and 90° from left to right. k elongation, k^{-1} contraction

A linear correlation is observed, and the slope (−0.13) is almost identical with that (−0.12) of the plot using the birefringence data for the similar specimen (SNE-7). This good agreement indicates that the results obtained by the two different methods are consistent. The linear relation $\gamma_x \sim \sin^2\theta$ and the two-dimensional deformation are the two key features of the deformation induced by director rotation for unconstrained nematic elastomers.

Several researchers theoretically considered the deformation mode induced by director rotation in nematic elastomers without external mechanical constraints [1, 38, 39]. The theory is based on the soft elasticity characteristic of ideal nematic elastomers [40]. The expected deformation is a pure shear combined with body rotation, which is illustrated in Fig. 11. When the director rotates by 90°, the cube elongates by k along the realigned director (z) and contracts by k^{-1} along the initial director (x) with no dimensional change along the rotation axis of the director (y). The corresponding deformation gradient tensor is expressed [39] as:

$$\lambda = \begin{pmatrix} 1-(1-k^{-1})\sin^2\theta & 0 & (k-1)\sin\theta\cos\theta \\ 0 & 1 & 0 \\ (1-k^{-1})\sin\theta\cos\theta & 0 & 1+(k-1)\sin^2\theta \end{pmatrix} \tag{8}$$

where k is a measure of the anisotropy of the dimensions of the constituent polymer chains and is equivalent to the dimensional ratio $l_x(0°)/l_x(90°)$ or $l_z(90°)/l_z(0°)$. The anisotropic Gaussian network model relates k to the orientational order parameter of network backbone (S_B) [1]:

$$k^2 = \frac{1+2S_B}{1-S_B} \tag{9}$$

The dimension l_i ($i = x,y,z$) along the i-axis at $\theta = \theta$ is obtained as:

$$l_x = l_x^0\left(\lambda_{xx} + \frac{l_z^0}{l_x^0}\lambda_{xz}\right) \approx l_x^0\lambda_{xx} \tag{10a}$$

$$l_y = l_y{}^0 \tag{10b}$$

$$l_z = l_z^0\left(\lambda_{zz} + \frac{l_x^0}{l_z^0}\lambda_{zx}\right) \tag{10c}$$

where λ_{ij} ($i,j=x,y,z$) is the ij component of λ. For sufficiently thin films with $l_z{}^0/l_x{}^0 \ll 1$ ($l_z{}^0/l_x{}^0 \approx 10^{-2}$ in the present case), the contribution of the shear λ_{xz} to l_x in (10a) is negligible. The expression for γ_i using (1) is given by [19]:

$$\gamma_x = -\left(1-\frac{1}{k}\right)\sin^2\theta \tag{11a}$$

$$\gamma_y = 0 \tag{11b}$$

$$\gamma_z = (k-1)\sin^2\theta + \frac{l_x^0}{l_z^0}\left(1-\frac{1}{k}\right)\sin\theta\,\cos\theta \tag{11c}$$

Most characteristically, the theory predicts γ_x proportional to $\sin^2\theta$ and $\gamma_y = 0$ independent of θ, which accords with the experimental observation.

The value of k estimated from the slope in Fig. 10 for the specimen with $c_x = 7$ mol% is 1.15, which corresponds to $S_B \approx 0.1$. This value of S_B is comparable to the orientational order parameter for the dangling mesogen ($S \approx 0.1$) that was estimated from the absorbance data without an electric field in Fig. 9a. The modest values of S_B and S originate from the swelling effect because S in the dry state is 0.3–0.4.

In a recent paper [41], Corbett and Warner provided a more detailed theoretical explanation for the EOM effects observed by taking into account the deviation from ideal soft elasticity and possible misalignment of the initial director. They also

showed that the deformation is dominated by that driven by director rotation while the contribution of the Maxwell effect to strain is minor, until the director rotation is completed [41].

3.5 Threshold for the Onset of EOM Effect

A finite threshold for the onset of EOM effects is observed in Figs. 5 and 8. In the case of nematic liquids, the determinant of the threshold for the director rotation is voltage, which is a main feature of the Fredericks transition [6, 42]. Does electric field or voltage determine the threshold for LCEs? This issue was first discussed in studies of the EO response of nematic gels in the constrained geometry of $\gamma_z = 0$ [15, 16]. Figure 12 shows Δn_{eff} in the low V_0 region for the two unconstrained samples with the same c_x (14 mol%) but different film thicknesses ($d_g{}^0 = 23$ and 47 μm) and cell gaps ($d_t = 40$ and 60 μm) [19]. In cells composed of two layers (film and silicone oil) differing in thickness and dielectric constant, the voltage ($V_{c,g}$) and field strength ($E_{c,g}$) acting on the film are given by:

$$V_{c,g} = \frac{\varepsilon_s d_g^0 V_c}{\varepsilon_s d_g^0 + \varepsilon_g \left(d_t - d_g^0 \right)} \tag{12a}$$

$$E_{c,g} = \frac{V_{c,g}}{d_g^0} \tag{12b}$$

where ε_g and ε_s are the dielectric constants for the gels along the field axis and silicone oil, respectively. For simplicity, we assume no pre-tilting of nematogens in the initial state, and approximate ε_g by the dielectric constant normal to the long

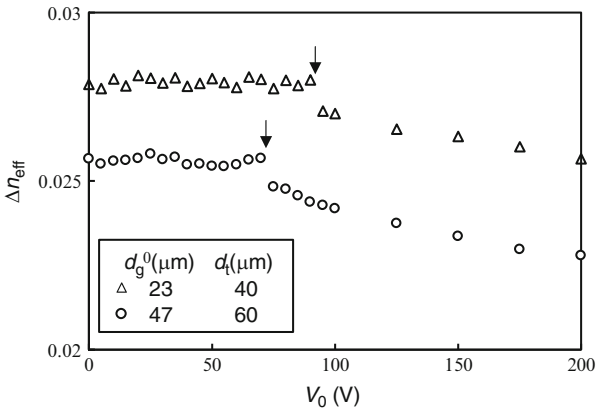

Fig. 12 Effective birefringence (Δn_{eff}) at low-voltage amplitudes for nematic gels with $c_x = 14$ mol% and different values of $d_g{}^0$ and d_t. The *arrows* indicate the threshold voltage amplitudes (V_{0c}) for the onset of electro-optical effects. From [19]

axis of 5CB. The calculated values of $V_{c,g}$ and $E_{c,g}$ are $V_{c,g} = 2.1 \times 10^1$ V and $E_{c,g} = 8.2 \times 10^{-1}$ MV/m for $d_g{}^0 = 23$ μm, and $V_{c,g} = 4.7 \times 10^1$ V and $E_{c,g} = 9.5 \times 10^{-1}$ MV/m for $d_g{}^0 = 47$ μm. The two samples are largely different in $V_{c,g}$ but similar in $E_{c,g}$. This indicates that the threshold is determined by field rather than voltage, which is similar to the earlier result in the constrained geometry [15, 16]. This results from the different anchoring origins in usual nematic liquids (including uncross-linked nematic polymers) and nematic elastomers (Fig. 1). The anchoring effect in usual nematic liquids stems only from the surface of the electrodes (substrates), whereas the anchoring effect in elastomer solids originates from the bulk elastomer matrix. The initial director is memorized in the whole elastomer matrix at the cross-linking stage. The threshold field $E_{c,g}$ corresponds to the field required to overcome the memory effect of the initial director. A more quantitative discussion of $E_{c,g}$ will be given in Sect. 5.

3.6 *Effect of Field Frequency*

Figure 13 shows the dependencies of the change in Δn_{eff} and γ_x on frequency (f) of the imposed field for SNE-7 [18]. The two effects have a similar dependence on f. Neither EO nor EM effects are observed at frequencies above 10^5 Hz. When f is too high, it does not induce a dipolar reorientation of the mesogens, as in the case of LMM-LCs. At frequencies less than 10^4 Hz, the EO and EM effects become pronounced. At low frequencies, the deformation and the change in Δn_{eff} increases with f. This may be because of a reduction in the effective voltage amplitude caused by an ionic current of impurities that becomes appreciable at low frequencies.

The dielectric relaxation frequency (f_c) of 5CB at room temperature is in the order of 10^6 Hz [43], whereas f_c of the neat LCE (without solvent) corresponding to SNE-7 (unpublished results from this laboratory) and f_c of an uncross-linked side-chain LC polymer with the similar mesogen [44] are in the order of 10 Hz at 70°C (above the glass transition temperatures of ca. 50°C). The significantly lower values of f_c for the neat LCE and the side-chain LC polymers are due to the constraint effect of the network and polymer backbone on the motion of the dangling

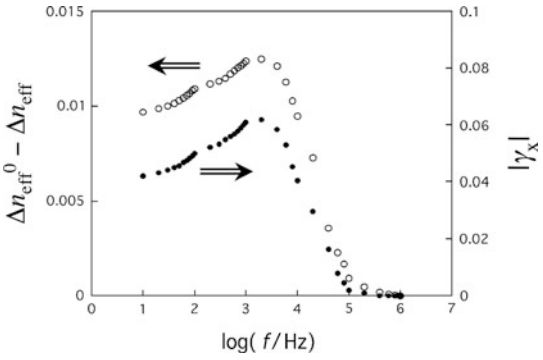

Fig. 13 Effects of field frequency (f) on the strain (γ_x) and the change in optical birefringence (Δn_{eff}) for SNE-7 at $V_0 = 400$ V. From [18]

mesogens. The onset frequency of the EOM effect for SNE-7, which is a mixture of the neat LCE and 5CB, is in the order of 10^4 Hz and lies between the values of f_c of these two components. This result indicates that 5CB inside the gel moves together with the gel matrix, which will also be shown in the dynamics of the EO effects described in Sect. 4.2.

3.7 *Effect of Constrained Geometry*

The mechanically unconstrained condition is crucial for observing pronounced EOM effects. The imposition of a mechanical constraint considerably suppresses director rotation under electric fields. Figure 14 compares the EO effects of SNE-7 in the constrained and unconstrained states [19]. In the constrained state, the gel is firmly sandwiched by rigid electrodes so that strain in the field direction can be strictly prohibited ($\gamma_z = 0$). In the constrained geometry, the reduction in Δn_{eff} saturates at high fields, and the total drop from the initial value is only 40%. This is considerably smaller than a total drop of ca. 95% in Δn_{eff} in the unconstrained state. In addition, the threshold field strength in the constrained state ($E_{c,g} = 6.3$ MV/m) is an order of magnitude higher than $E_{c,g} = 0.62$ MV/m in the unconstrained state. These results clearly indicate that the geometry prohibiting the deformation strongly suppresses director rotation. This is also a direct consequence of the strong correlation in LCEs between the director and the macroscopic shape.

In the constrained geometry, both deformation and director configuration become considerably nonuniform, and the effect of the Frank elasticity of LCs becomes significant. In contrast, the Frank elasticity has essentially no role in the unconstrained case where the director rotates uniformly. Some theoretical studies [16, 45, 46] suggest that several characteristic patterns of director configuration and macroscopic distortion appear, depending on the nematicity, film thickness, and field strength. The corresponding experimental studies [16] are quite limited because of

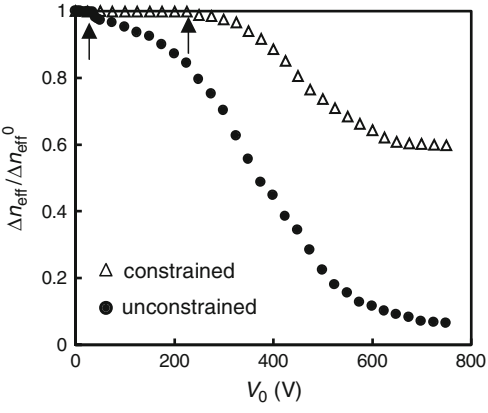

Fig. 14 Effect of mechanical constraints on electro-optical effects for SNE-7. The *arrows* indicate the threshold voltage amplitudes (V_{0c}) for the onset of electro-optical effects. From [19]

the difficulty of direct observation of the deformation and director rotation in the x–z plane. A rich variety of expected patterns of director configuration and deformation in a constrained geometry are an interesting characteristic of LCEs that possess the two types of elasticity, i.e., rubber elasticity and Frank elasticity.

4 Dynamic Aspects

4.1 Rise and Decay Times

In this section, we describe the dynamic features of EOM effects. In particular, we focus on the response times to field-on and field-off; these are the rise and decay times, respectively. In the case of the EO effects of nematic liquids, the rise and decay times exhibit the characteristic dependencies on voltage, and these characteristic times reflect the elastic, viscous, and dielectric properties of the materials. They have fully characterized the dynamics of the electric-field responses of LMM-LCs in experiments and established the theoretical background [6]. The dynamic features of the EOM effects in nematic gels are expected to differ from those of the EO effects in LMM-LCs, because the gels possess rubber elasticity and also have a different origin of the memory of the initial director. In addition, the dynamic properties give important information about the applicability of EOM effects in practical applications.

Figure 15 shows examples of the time courses of EO and EM effects in response to the imposition and removal of electric fields. These effects require a finite time to reach steady states after the field imposition, and to recover the initial states after the field removal. The rise and decay times were defined to be the times required for 70% of the total change. Figure 16 displays the optical and mechanical rise times (designated as ${\tau_{\mathrm{on}}}^{\Delta n}$ and ${\tau_{\mathrm{on}}}^{\gamma}$, respectively) as a function of the field strength acting on the specimen (E_{g}). The optical rise times are of the order of milliseconds and almost proportional to ${E_{\mathrm{g}}}^{-2}$, which is similar to that for pure LMM-LCs. The E_{g} dependence of ${\tau_{\mathrm{on}}}^{\gamma}$ is also approximated by ${\tau_{\mathrm{on}}}^{\gamma} \sim {E_{\mathrm{g}}}^{-2}$, but ${\tau_{\mathrm{on}}}^{\gamma}$ is about an order of magnitude larger than ${\tau_{\mathrm{on}}}^{\Delta n}$. An increase in the cross-linker concentration results in an increase in ${\tau_{\mathrm{on}}}^{\Delta n}$ and a slight increase in ${\tau_{\mathrm{on}}}^{\gamma}$.

Figure 17 shows the optical and mechanical decay times (${\tau_{\mathrm{off}}}^{\Delta n}$ and ${\tau_{\mathrm{off}}}^{\gamma}$, respectively) as a function of E_{g}. Both ${\tau_{\mathrm{off}}}^{\Delta n}$ and ${\tau_{\mathrm{off}}}^{\gamma}$ are substantially independent of E_{g}, similarly to ${\tau_{\mathrm{off}}}^{\Delta n}$ for LMM-LCs. As in the case of the rise times for the mechanical and optical responses, ${\tau_{\mathrm{off}}}^{\gamma}$ is about ten times larger than ${\tau_{\mathrm{off}}}^{\Delta n}$.

The trigger of the EM effects in nematic elastomers is the rotation or recovery of the director, each of which is observed as an EO effect. The deformation follows the motion of the director. The finite retardation of EM effects is probably due to viscoelastic effects, or a time lag between the orientation of dangling mesogens and the induced deformation of network backbone. The dynamics of EOM effects for main-chain type nematic gels will give important information about this issue.

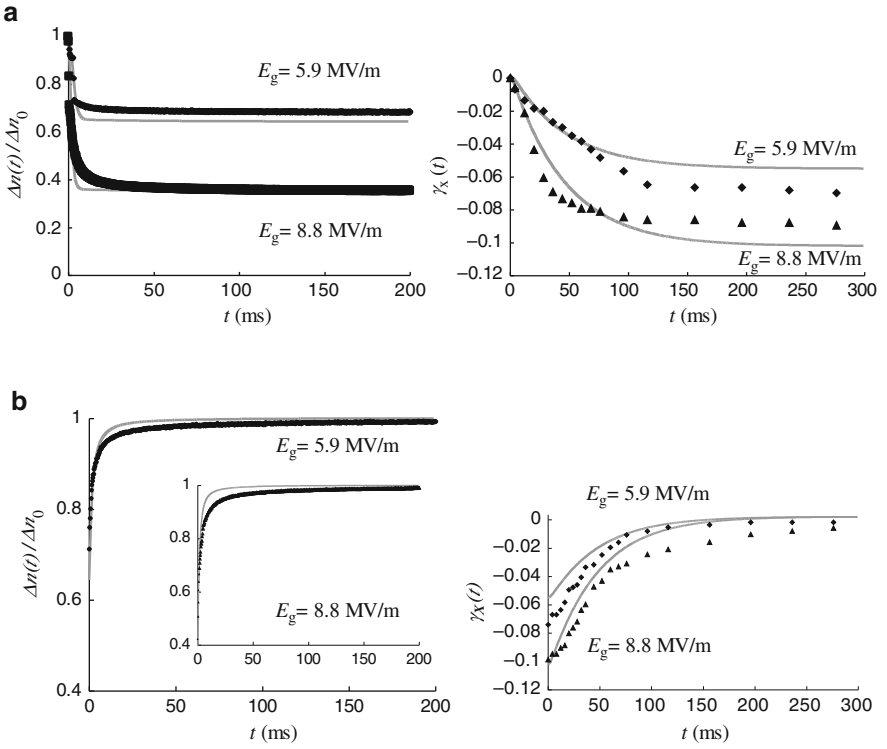

Fig. 15 Time courses of optical birefringence (Δn) and strain (γ_x) after (**a**) applying and (**b**) removing fields of 5.9 and 8.8 MV/m for SNE-7D. The *gray solid lines* indicate the numerical results obtained from the model. From [31]

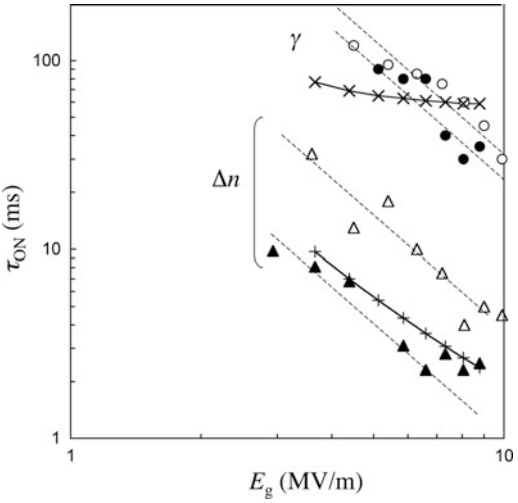

Fig. 16 Optical (Δn) and mechanical (γ) rise times (τ_{ON}) as a function of field strength E_g for SNE-7D (*closed symbols*) and SNE-10D (*open symbols*). The slope of the *dashed lines* is 2. The *crosses* indicate the theoretical results fitted to the data for SNE-7D. From [31]

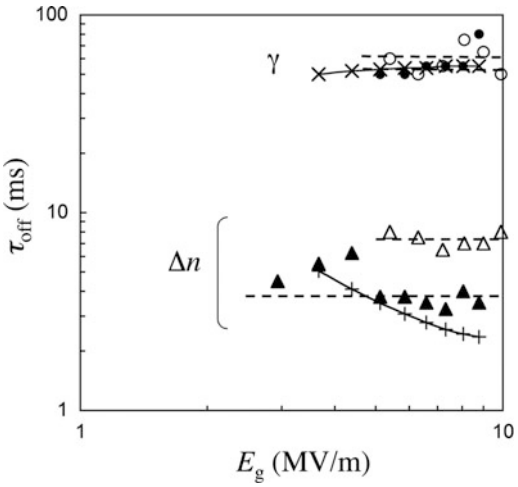

Fig. 17 Optical (Δn) and mechanical (γ) decay times (τ_{off}) as a function of field strength E_g for SNE-7D (*closed symbols*) and SNE-10D (*open symbols*). The *crosses* indicate the theoretical results fitted to the data of SNE-7D. From [31]

4.2 Comparison of Dynamics for Swollen Nematic Elastomers and Nematic Liquids

The optical decay times directly reflect the recovery force of the director inherent in the materials, as is physically evident from the independence of field strength. In the case of nematic liquids, the recovery force originates from Frank elasticity. As a result, ${\tau_{off}}^{\Delta n}$ strongly depends on cell thickness (d_{cell}) and becomes smaller with a decrease in d_{cell} as ${\tau_{off}}^{\Delta n} \sim {d_{cell}}^{-2}$. It is interesting to compare ${\tau_{off}}^{\Delta n}$ for SNE-7D and the pure LMM-LC (5CB; swelling solvent) confined in a cell with a gap of 25 μm that is comparable to the gel thickness: ${\tau_{off}}^{\Delta n}$ for the nematic gel (ca. 3 ms) is about three orders of magnitude smaller than that (ca. 2 s) for the pure 5CB, despite the high content of 5CB (78 vol%). The recovery force of the director in nematic gels originates from the memory effect of the initial director that is imprinted in the cross-linking stage. Since this memory is a bulk matrix effect, the decay time is independent of gel thickness, in contrast to that for nematic liquids strongly depending on d_{cell}. The recovery force in nematic gels is considerably stronger than that (Frank elasticity) in nematic liquids. The results also indicate that the solvent inside the gels moves together with the gel matrix.

5 Simple Model Capturing Main Features

A minimal model for interpreting the main features of the static and dynamic aspects of EOM effects [31] is introduced in this section. To reduce complexity, this model does not explicitly consider the anisotropic effect on elastic and viscous properties. More realistic expressions considering the anisotropy [47–50] are available, but the limited experimental data makes it difficult to unambiguously determine a larger set of material parameters.

The free energy of nematic gels under electric fields may be written as the sum of the Frank energy (F_F), the electrostatic energy (F_{el}), and the gel elasticity energy (F_g):

$$F = F_F + F_{el} + F_g \tag{13}$$

It should be noted that $F_F \approx 0$ in the present case where the director rotates uniformly around the y-axis, i.e., the director is always confined to the x–z plane.

The electrostatic energy is:

$$F_{el} = -\frac{\varepsilon_0}{2}\int_A (\varepsilon_a(\nabla\varphi(x)\cdot\mathbf{n}(x))^2 + \varepsilon_\perp|\nabla\varphi(x)|^2)\mathrm{d}x - \frac{\varepsilon_0}{2}\int_B (\varepsilon_s|\nabla\varphi(x)|^2)\mathrm{d}x \tag{14}$$

where φ is the electric potential, $\mathbf{n} = (\cos\theta, 0, \sin\theta)$ is the nematic director, and A and B are the spaces occupied by gel and silicone oil, respectively. The dielectric constant ε_s is for silicone oil, whereas $\varepsilon_{\|}$ and $\varepsilon_\perp$ are those parallel and normal to $\mathbf{n}$ for the gel, respectively, and $\varepsilon_a = \varepsilon_{\|} - \varepsilon_\perp$.

The elastic energy of the gel is:

$$F_g = \int\left[\frac{G}{2}|e_u(x) - e_0(\mathbf{n}(x))|^2 + f_{an}(\mathbf{n}(x))\right]\mathrm{d}x \tag{15}$$

where G is the shear modulus and e_u is the linear strain with components $(e_u)_{ij} = (\partial u_i/\partial x_j + \partial u_j/\partial x_i)/2$. The quantity $u_i(x)$ is the ith component of the displacement at point x of the gel with respect to its reference configuration (chosen as the configuration the specimen would take in a high-temperature isotropic state), and x_j is the jth coordinate of x. The strain $e_0(\mathbf{n})$ corresponds to that in the stress-free state associated with $\mathbf{n}$, which we assume to be a uniaxial stretching along n. This is expressed by the following matrix as a function of the angle θ:

$$[e_0(\mathbf{n})] = \begin{bmatrix} \frac{3}{2}g(\cos^2\theta - \frac{1}{3}) & 0 & \frac{3}{2}g\sin\theta\cos\theta \\ 0 & -\frac{g}{2} & 0 \\ \frac{3}{2}g\sin\theta\cos\theta & 0 & \frac{3}{2}g(\sin^2\theta - \frac{1}{3}) \end{bmatrix} = [e_0(\theta)] \tag{16}$$

where g is a measure of the chain anisotropy in the gel and related to k as $g = 2(k-1)/(k+2)$. The dimensional variation in the x direction driven by the rotation (θ) of the director in the x–z plane is given by $(e_u)_{11} = [e_0(\theta)]_{11}$. The corresponding strain γ_x is given by:

$$\gamma_x(\theta) = \frac{l_x(\theta) - l_x{}^0}{l_x{}^0} = \frac{[e_0(\theta)]_{11} - [e_0(0)]_{11}}{1 + [e_0(0)]_{11}} = -\frac{3g}{2(1+g)}\sin^2\theta \tag{17}$$

This relation is substantially equivalent to (11a) since the parameter k is given by $k = l_x(0)/l_x(90°)$.

In (15), f_{an} is the anisotropic energy density for the memory effect of the director, driving the director $\mathbf{n}$ towards the initial director $\mathbf{n_0} = (1,0,0)$ at cross-linking.

The phenomenological expression of f_{an} may be given by the elastic energy of a nonlinear spring with the two independent constants k_1 and k_2:

$$f_{\mathrm{an}}(\mathbf{n}) = \frac{k_1}{2}\sin^2\theta + \frac{k_2}{4}\sin^4\theta \tag{18}$$

A similar expression is found in [50] and in (8.30) of [1].

The dynamics of a nematic gel are assumed to be governed by the viscoelasticity of the gel, the rotational viscoelasticity of the director, and electrostatics. The governing equations for the dynamics are derived from the balance between the rates of free-energy release and viscous dissipation. In the present case, strain rates and stresses are spatially uniform because of the unconstrained geometry. Therefore, the governing equations for the dynamics of the strain and the director are obtained from the free energy as [31]:

$$\eta_{\mathrm{g}}\frac{\mathrm{d}}{\mathrm{d}t}e_{\mathrm{u}} = -G[e_{\mathrm{u}} - e_0(n)] \tag{19}$$

and

$$\eta_{\mathrm{n}}\frac{\mathrm{d}}{\mathrm{d}t}\theta = T_{\mathrm{G}} + T_{\mathrm{an}} + T_{\varphi} \tag{20}$$

where η_{g} and η_{n} are the frictional coefficients of the deformation and the director motion, respectively. In (20), the elastic torque T_{G}, the restoring torque T_{an}, and the electrostatic torque T_{φ} are given by:

$$T_{\mathrm{G}} = 3Gg\left\{(e_{\mathrm{u}})_{13}(\cos^2\theta - \sin^2\theta) + \left[(e_{\mathrm{u}})_{33} - (e_{\mathrm{u}})_{11}\right]\sin\theta\,\cos\,\theta\right\} \tag{21a}$$

$$T_{\mathrm{an}} = -(k_1 + k_2\sin^2\theta)\sin\theta\,\cos\,\theta \tag{21b}$$

$$T_{\varphi} = \varepsilon_0\varepsilon_{\mathrm{a}}\left(\frac{V_0}{d(\theta)}\right)^2\sin\theta\,\cos\,\theta \tag{21c}$$

Note that only the 11, the 33, and the 13 strain components are nontrivial because the director rotates in the x–z plane.

In the steady state ($\mathrm{d}e_{\mathrm{u}}/\mathrm{d}t = 0$), the relation $e_{\mathrm{u}} \equiv e_0(n)$ is obtained from (19). Equation (21a) with this relation leads to $T_{\mathrm{G}} = 0$ in the steady state. Therefore, the torque balance equation for the director in the steady state is given from (20) as:

$$0 = T_{\mathrm{an}} + T_{\varphi} \tag{22}$$

The equilibrium values of θ and γ (θ^{s} and γ^{s}, respectively) at each V_0 are calculated from (17) and (22). Figure 18 shows a comparison of the steady-state

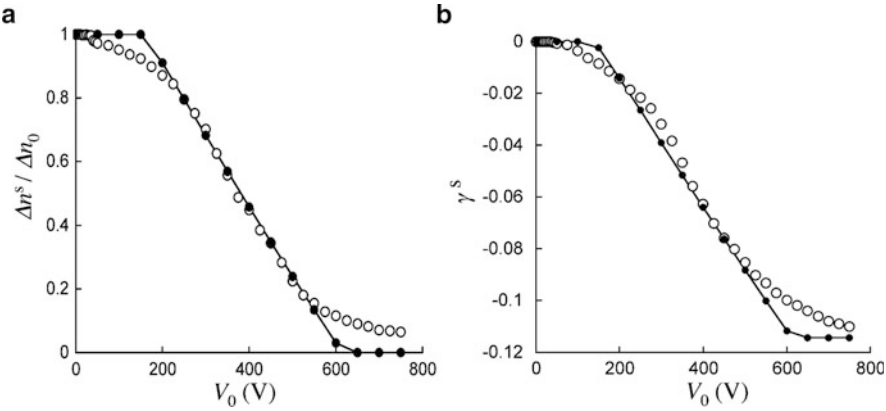

Fig. 18 Numerical (*closed symbols*) versus experimental (*open symbols*) results for (**a**) optical birefringence (Δn) and (**b**) strain in the steady state (γ^S) as a function of voltage amplitude (V_0). From [31]

data for SNE-7 with the theoretical results using the fitted parameter values of $g = 0.0825$, $k_1 = 650$ J/m^3 and $k_2 = 4{,}100$ J/m^3. The theoretical value of reduced birefringence $\Delta n^s/\Delta n_0$ in the figure is given by $\cos^2\theta^s$ [see (3)]. The theoretical results describe the main features in the experimental data such as the presence of the threshold for the onset of director rotation and the maximum value of strain at high voltages. The theoretical strain reaches a maximum at $\theta = 90°$, where the birefringence becomes zero, and $|\gamma^s|_{max}$ is given by $3g/[2(1 + g)]$ ($\equiv 1 - k^{-1}$). The theoretical expression for the threshold field strength $E_{g,c}$ for the gel is obtained from (22) as:

$$E_{g,c} = \sqrt{\frac{k_1}{\varepsilon_0 \varepsilon_a}} \tag{23}$$

This equation gives a physical explanation for the threshold for director rotation. The threshold is determined by field strength rather than voltage, and the director starts to rotate when the dielectric force overcomes the strength of the memory of the initial director at cross-linking.

The time courses of Δn_{eff} and γ in response to field-on and field-off are computed from (19) and (20). The gray solid lines in Fig. 15 indicate the numerical results for $E_g = 5.9$ and 8.8 MV/m. It should be noted that when selecting the material parameter values, we first tune the parameters g, k_1, and k_2 to fit the steady-state data (see Fig. 7 in [31] for specimen SNE-7D in Fig. 15). Then, using these values ($g = 0.12$, $k_1 = 300$ J/m^3 and $k_2 = 6{,}000$ J/m^3), we tune the parameters η_g, η_n, and G to fit the dynamic data: $\eta_g = 50$ Js/m^3, $\eta_n = 12$ Js/m^3 and $G = 2{,}000$ J/m^3. The theoretical values of the rise times for the optical and mechanical responses are compared with the experimental data in Fig. 16. The model successfully describes the $\tau_{on}^{\Delta n} \sim E_g^{-2}$ behavior in the experiments. In contrast, the model exhibits a much weaker E_g dependence of τ_{on}^{γ} than the experiments suggest. In Fig. 17, the

theoretical values of the optical and mechanical decay times are compared with the experimental values. The theory captures well the lack of E_g dependence of ${\tau_{off}}^{\gamma}$ observed in the experiments. However, the theoretical ${\tau_{off}}^{\Delta n}$ values are slightly E_g-dependent in contrast to the experimental values that are substantially independent of E_g. These discrepancies originate from the fact that the real response times for director and deformation are not as widely separated as assumed in the model.

It is worth comparing the viscous coefficients for swollen nematic elastomers obtained here with those in neat elastomers as estimated from dynamic light scattering [51]. The relaxation times ${\tau_{off}}^{\Delta n}$ for the director in Fig. 17 are not very different from those in Fig. 5 in [51] in view of the finite difference in elastic modulus between the neat and swollen states. The swollen nematic elastomers are considerably softer than the neat ones: k_1 is two orders of magnitude smaller than D_1 in [51]. Correspondingly, the viscous coefficient η_n for the director in the gels, estimated from ${\tau_{off}}^{\Delta n} \approx \eta_n/k_1$, is significantly smaller than the η_{loss} in neat elastomers, evaluated from $\tau \approx \eta_{loss}/D_1$.

6 Conclusion and Outlook

Nematic elastomers swollen by LMM-LCs (nematic gels) exhibit pronounced EM effects combined with EO effects. This EOM effect is a direct consequence of the macroscopic deformation driven by electrically induced director rotation. Swelling by LMM-LCs considerably reduces the field strength for actuation, because of a significant softening of the nematic elastomers without loss of the liquid crystallinity. The electrical strain in nematic gels primarily originates from the strain caused by director realignment. The stretching direction is governed by the direction of the molecular long axis of mesogens under electric fields: the dielectrically positive and negative nematic gels are elongated in the directions parallel and normal to the field axis, respectively. External mechanical constraints to prohibit the strain in one direction considerably suppress the director reorientation and resultant deformation under electric fields.

The director rotation is considerably facilitated under unconstrained conditions where the gel floats in fluid between rigid electrodes whose gap is larger than the gel thickness. The monodomain nematic gels under electric fields exhibit a two-dimensional deformation where the dimension along the initial director decreases, and the dimension along the field axis increases, without an appreciable dimensional change along the rotation axis of the director. The director of unconstrained monodomain nematic gels rotates purely around the axis normal to both the field and initial director axes, leading to the two-dimensional distortion. Characteristically, the strain is almost linearly proportional to $\sin^2\theta$ (where θ is the rotation angle of the director). This behavior is in good agreement with the predictions of soft elasticity theory for thin nematic elastomer films in which the shear contribution is negligible.

The rise and decay times of the EOM effects are similar in their dependencies on field strength to those of the EO effect of LMM-LCs, although the mechanical

response times are about an order of magnitude larger than the optical times. Importantly, the recovery rate of the director (estimated from the optical decay time) in nematic gels is about three orders of magnitude higher than that in LMM-LCs confined in the cell with the same gap as the gel thickness. This indicates that the memory effect of the initial director, which is imprinted at cross-linking, is much stronger than the Frank elasticity. The memory effect of the initial director in nematic gels is a bulk matrix effect. This is also recognized by the fact that the threshold for the onset of EOM effects is determined by the field strength, in contrast to the Fredericks transition of LMM-LCs whose threshold is determined by voltage.

So far, EOM effects have been reported for only a limited number of nematic gels. There is great potential for enhancing the performance of the electric-field response. The molecular characteristics of nematic elastomers and solvents have not yet been optimized for high performance. Possible options might include: (1) employment of main-chain-type nematic elastomers; (2) optimization of the cross-linker geometry; and (3) an increase in the dielectric anisotropy of mesogens. The first and second options are aimed at increasing the electrical strain, i.e., enhancing the coupling between mesogen orientation and macroscopic deformation. Many investigations of thermally induced deformation have indicated that these options are effective for this purpose. The third option contributes to reducing the actuation voltage [see (23)] and to shortening the field-on response time. This is based on an analogy with the effect of dielectric anisotropy on EO effects in LMM-LCs.

The EM effects of nematic elastomers have great potential for practical applications such as soft actuators. For practical purposes, actuation must be fast and low-voltage with a large strain (generating a large stress). Establishing the fundamentals of the molecular design of nematic elastomers with high EM performance will also meet these industrial demands.

Acknowledgments The author thanks Y. O. Arai, H. Kondo, S. Honda, A. Fukunaga, S. Kohjiya, and T. Takigawa for their great contributions to the experiments. The author appreciates P. Koelsch for his crucial comment in polarized FT-IR. The author also thanks A. DeSimone and L. Teresi for their principal contribution to the modeling. The author is grateful for a Grant-in-Aid in the Priority Area "Soft Matter Physics" (No. 21015014) and a Grant-in-Aid for Scientific Research (B) (No. 21350123). Valuable support was also received from the Global COE Program "International Center for Integrated Research and Advanced Education in Materials Science" (No. B-09) from the Ministry of Education, Culture, Sports, Science and Technology of Japan.

References

1. Warner M, Terentjev EM (2007) Liquid crystals elastomers (revised edition). Clarendon, London
2. Xie P, Zhang RJ (2005) J Mater Chem 15:2529
3. Brand HR, Pleiner H, Martinoty P (2006) Soft Matter 2:182
4. Urayama K (2007) Macromolecules 40:2277

5. Kramer D, Brömmel F, Finkelmann H (2011) In: De Jeu WH (ed) Liquid crystal elastomers: materials and applications. Adv Polym Sci. Springer, Heidelberg, Berlin, doi: 10.1007/12_2012_168
6. Oswald P, Pieranski P (2005) Nematic and cholesteric liquid crystals. CRC, Boca Raton
7. Lehmann W, Skupin H, Tolksdorf C, Gebhard E, Zentel R, Kruger P, Lösche M, Kremer F (2001) Nature 410:447
8. Spillmann CM, Ratna BR, Naciri (2007) J Appl Phys Lett 90
9. Zentel R (1986) Liq Cryst 1:589
10. Barnes NR, Davis FJ, Mitchell GR (1989) Mol Cryst Liq Cryst 168:13
11. Kishi R, Suzuki Y, Ichijo H, Hirasa O (1994) Chem Lett:2257
12. Huang C, Zhang QM, Jakli A (2003) Adv Funct Mater 13:525
13. Urayama K, Kondo H, Arai YO, Takigawa T (2005) Phys Rev E 71:051713
14. Yusuf Y, Huh JH, Cladis PE, Brand HR, Finkelmann H, Kai S (2005) Phys Rev E 71:061702
15. Chang CC, Chien LC, Meyer RB (1997) Phys Rev E 56:595
16. Terentjev EM, Warner M, Meyer RB, Yamamoto J (1999) Phys Rev E 60:1872
17. Terentjev EM, Warner M, Bladon P (1994) J Phys (Paris) II 4:667
18. Urayama K, Honda S, Takigawa T (2005) Macromolecules 38:3574
19. Urayama K, Honda S, Takigawa T (2006) Macromolecules 39:1943
20. Zubarev ER, Talroze RV, Yuranova TI, Plate NA, Finkelmann H (1998) Macromolecules 31:3566
21. Mitchell GR, Davis FJ, Guo W (1993) Phys Rev Lett 71:2947
22. Roberts PMS, Mitchell GR, Davis FJ (1997) J Phys (Paris) II 7:1337
23. Kundler I, Finkelmann H (1995) Macromol Rapid Commun 16:679
24. Tammer M, Li JJ, Komp A, Finkelmann H, Kremer F (2005) Macromol Chem Phys 206:709
25. Li J, Tammer M, Kremer F, Komp A, Finkelmann H (2005) Eur Phys J E 17:423
26. Verwey GC, Warner M, Terentjev EM (1996) J Phys (Paris) II 6:1273
27. Conti S, DeSimone A, Dolzmann G (2002) J Mech Phys Solids 50:1431
28. Fried E, Sellers S (2006) J Appl Phys 100:043521
29. Urayama K, Arai YO, Takigawa T (2005) Macromolecules 38:3469
30. Urayama K, Arai YO, Takigawa T (2005) Macromolecules 38:5721
31. Fukunaga A, Urayama K, Takigawa T, DeSimone A, Teresi L (2008) Macromolecules 41:9389
32. Finkelmann H, Kock HJ, Gleim W, Rehage G (1984) Makromol Chem Rapid Commun 5:287
33. Fukunaga A, Urayama K, Koelsch P, Takigawa T (2009) Phys Rev E 79:051702
34. Urayama K, Mashita R, Kobayashi I, Takigawa T (2007) Macromolecules 40:7665
35. Simon R, Nicholas DM (1985) J Phys D Appl Phys 18:1423
36. Aksenov V, Stannarius R, Tammer M, Kolsch P, Kremer F, Rossle M, Zentel R (2007) Liq Cryst 34:87
37. Zbinden R (1964) Infrared spectroscopy of high polymers. Academic, New York
38. Olmsted PD (1994) J Phys (Paris) II 4:2215
39. Verwey GC, Warner M (1995) Macromolecules 28:4303
40. Warner M, Bladon P, Terentjev EM (1994) J Phys (Paris) II 4:93
41. Corbett D, Warner M (2009) Soft Matter 5:1433
42. de Gennes PG, Prost J (1993) The physics of liquid crystals, 2nd edn. Oxford University Press, New York
43. Kreul H-G, Urban S, Wurflinger A (1992) Phys Rev A 45:8624
44. Garcia-Bernabe A, Diaz-Calleja R (2001) Polym Int 50:165
45. Skacej G, Zannoni C (2006) Eur Phys J E 20:289
46. Muller O, Brand HR (2005) Eur Phys J E 17:53
47. Terentjev EM, Warner M (2001) Eur Phys J E 4:343
48. Fradkin LJ, Kamotski IV, Terentjev EM, Zakharov DD (2003) Proc R Soc Lond Ser A Math Phys Eng Sci 459:2627
49. Martinoty P, Stein P, Finkelmann H, Pleiner H, Brand HR (2004) Eur Phys J E 14:311
50. Teixeira PIC, Warner M (1999) Phys Rev E 60:603
51. Schonstein M, Stille W, Strobl G (2001) Eur Phys J E 5:511

Adv Polym Sci (2012) 250: 147–186
DOI: 10.1007/12_2010_103

Published online: 12 November 2010

The Isotropic-to-Nematic Conversion in Liquid Crystalline Elastomers

Andrija Lebar, George Cordoyiannis, Zdravko Kutnjak, and Boštjan Zalar

Abstract This chapter reviews the experimental findings that help determine the critical properties of the isotropic-to-nematic transition in side-chain and main-chain liquid single-crystal elastomers. Special focus is given to heat-capacity and deuteron nuclear magnetic resonance (^{2}H-NMR) experiments, which can reliably provide information about the local and macroscopic nature of the isotropic-to-nematic conversion. In particular, it is shown that a critical point exists in the generalized temperature–mechanical-stress phase diagram for both side- and main-chain liquid single-crystal elastomers. Here, the internal frozen mechanical stress field was varied by changing a single chemical parameter, i.e. the density of the crosslinkers. A detailed analysis shows that, due to the local heterogeneities, the critical point is actually smeared in both the temperature and the stress axes. It is also shown that by varying some particular chemical and physical parameters (such as crosslinking temperature, the externally applied stress field during crosslinking and the density of crosslinkers), the system can be prepared in a subcritical or supercritical regime, which correspond to the fast (on–off) or to the continuous (slow) thermomechanical response, respectively. This implies that the thermomechanical response can be influenced by controlling the critical properties of the isotropic-to-nematic transition.

Keywords Calorimetry · Deuteron nuclear magnetic resonance orientational order · Isotropic-to-nematic transition · Liquid-crystalline elastomers · Order parameter · Phase transition criticality

A. Lebar (✉), G. Cordoyiannis, Z. Kutnjak, and B. Zalar
Condensed Matter Physics Department, Jožef Stefan Institute, Jamova 39, 1000 Ljubljana, Slovenia
e-mail: andrija.lebar@ijs.si

Contents

Abbreviations

^{2}H-NMR	Deuteron nuclear magnetic resonance
I	Isotropic
LC	Liquid crystal
LCE	Liquid-crystalline elastomer
LdG	Landau-de Gennes
N	Nematic
OP	Order parameter
PN	Paranematic
TM	Thermomechanical

1 The Isotropic-to-Nematic Transition

A recently revived topic in the field of liquid-crystalline elastomers (LCEs) is the nature of the isotropic-to-nematic (I–N) transition in connection with the type of elasticity in these materials, being either soft, semisoft or nonsoft [1–5]. The type

of elasticity is directly linked to the giant thermomechanical (TM) response that has been observed in monodomain LCEs (henceforth LCEs stands for monodomain liquid-crystalline elastomers, unless otherwise stated). The giant TM response and its control is of particular interest for applications. The TM response approximately follows the temperature evolution of the nematic order parameter in LCEs [6, 7], as illustrated in Fig. 1, and most of it occurs in the vicinity of the I–N phase transition, i.e. where most of the enthalpy change is observed. As a consequence, the sharpness of the I–N transition is simply related to the temperature range in which most of the elongation or contraction occurs. Hence, by controlling the nature of the I–N transition it is, for example, possible to change the response from on to off (sharp, narrow temperature range) to a continuous (gradual, broad temperature range) response. In order to achieve this, it is important to understand the underlying mechanisms of the I–N transition and to define all the essential physical and chemical parameters that allow us to change its nature.

In this chapter we will give a review of recent advances in understanding the nature of the nematic phase transition in LCEs [3–5]. In addition, this chapter explores the possibilities of controlling the critical behaviour of the nematic transition and, thus, the type of thermomechanical response. In Sect. 1, the nature of the nematic transition will be briefly discussed for pure liquid crystals (LCs) and LCEs. Sections 2 and 3 focus on the application of two essential experimental techniques, high-resolution ac calorimetry and deuteron nuclear magnetic resonance (^{2}H-NMR) spectroscopy, to these systems. Section 4 explains the nature of the nematic transition in LCEs as revealed by the two techniques. Section 5 is devoted to experimental studies that systematically explored the possibilities of tailoring the TM response of LCEs by a variation of the chemical composition and other parameters during the synthesis.

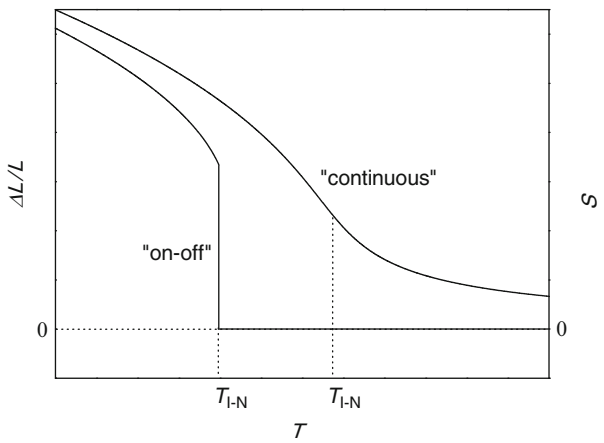

Fig. 1 Evolution of the thermal expansion ($\Delta l/l$) and the order parameter (S) for a discontinuous phase transition (*left*) and for a supercritical conversion (*right*), corresponding to an "on–off" and a "continuous" response, respectively

1.1 The Isotropic-to-Nematic Transition in LCs

The nematic phase is the mesophase with the highest symmetry or, alternatively, with the lowest order. For thermotropic LCs, the nematic phase forms as the temperature is decreased from that of the liquid isotropic phase. The I–N transition can be described with a simple mean-field Landau-de Gennes (LdG) approach for nematics [8, 9], in which the free energy (F) for nematic LCs includes a cubic term that induces the first-order character:

$$F = \frac{1}{2}AS^2 + \frac{1}{3}BS^3 + \frac{1}{4}CS^4 \tag{1}$$

where A, B, and C are the Landau expansion coefficients and S is the order parameter. The coefficients $B < 0$ and $C > 0$ are considered as temperature independent, whereas for A a linear temperature dependence $\alpha(T–T^*)$ is assumed. The quantity T^* is the (mean-field) absolute stability limit of the isotropic phase. The minimization of the free energy provides a solution for the order parameter S. For the above free energy, the temperature dependence of the order parameter exhibits a discontinuity (see Fig. 2a and the curve denoted by $G = 0$ in Fig. 3) at the I–N phase transition temperature $T_{IN} = T^* + (2B^2/9\alpha C)$.

The nematic phase can be viewed as a liquid characterized by orientational order, i.e. the long axes of the molecules are aligned on average along one direction, defined by the director **n**. The nematic order parameter S is defined as:

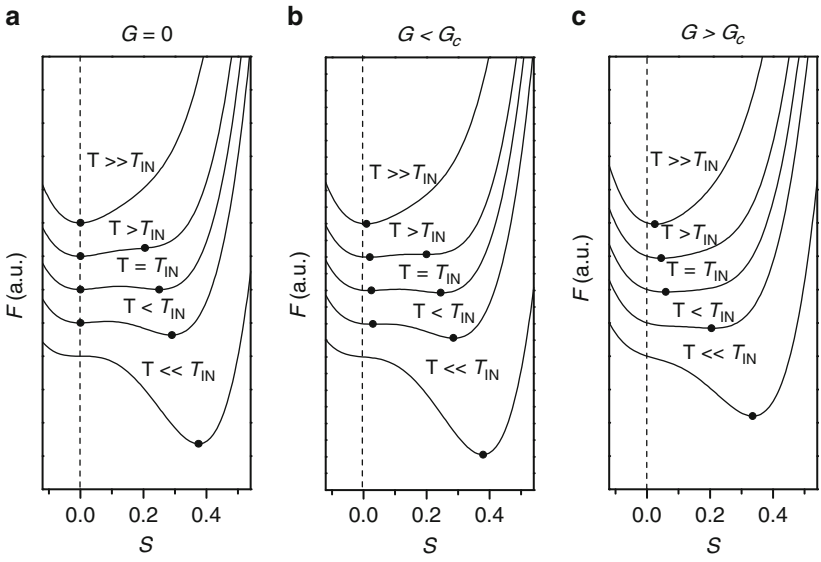

Fig. 2 Free-energy curves at various temperatures versus the order parameter, for various field values: $G = 0$ (**a**), $G < G_C$ (**b**) and $G > G_C$ (**c**)

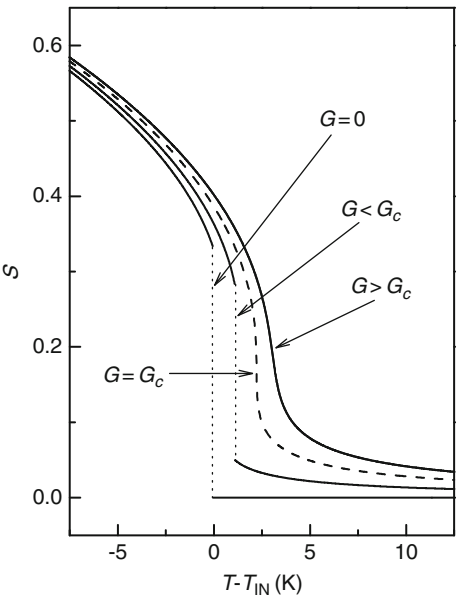

Fig. 3 Evolution of the order parameter for various fields ranging from no field ($G = 0$) to below-critical ($G < G_C$), and supercritical ($G > G_C$). The *dotted lines* denote the discontinuity for the cases $G = 0$ and $G < G_C$, the *dashed line* stands for the continuous evolution of the order parameter at the critical point ($G = G_C$) and T_{IN} denotes the transition temperature of the case without a field ($G = 0$)

$$S = \frac{1}{2}\left(3\langle\cos^2\theta\rangle - 1\right), \tag{2}$$

where θ denotes the angle between the molecular axis and the director **n**. In the isotropic phase, the molecular orientations are random and $\langle\cos^2\theta\rangle = 1/3$, which yields $S = 0$, while in the nematic phase S $\neq 0$.

Externally applied fields that conjugate to the nematic order parameter can induce some orientational order in the isotropic phase (which is called the paranematic order, in analogy with, e.g. paramagnetism) and suppress or even eliminate the I–N discontinuity for strong field values. An additional linear term $-GS$ must be added to the free-energy expansion to account for the coupling between the applied field G and the order parameter S:

$$F = \frac{1}{2}\alpha(T - T^*)S^2 + \frac{1}{3}BS^3 + \frac{1}{4}CS^4 - GS. \tag{3}$$

Providing the field is smaller than its critical value:

$$G_C = -B^3/27C^2, \tag{4}$$

the discontinuity decreases but the phase transition remains first order (see Figs. 2 and 3). The discontinuity vanishes at $G = G_C$ and the transition becomes continuous (second order) at a single critical point. When $G > G_C$, the transition is driven beyond the critical point to the supercritical regime. The term "supercritical"

implies that there is no real phase transition but only a smooth evolution of the properties of the system between the paranematic and the nematic states. In the presence of the field G, the paranematic-to-nematic (PN–N) phase transition occurs at a slightly shifted temperature $T_{\mathrm{PN–N}}$:

$$T_{\mathrm{PN–N}} = T^* + \frac{2B^2}{9\alpha C} + \frac{3CG}{\alpha B}. \tag{5}$$

1.2 The Paranematic-to-Nematic Transition in Liquid-Crystalline Elastomers

In accordance with the described mean-field model, for pure LCs a sharp, weakly first-order I–N transition is typically observed, exhibiting a narrow (only a few mK) two-phase region. Large, externally applied electric or magnetic fields are needed to impose a continuous conversion because the electric or magnetic susceptibility of LCs is low [9–13]. Nevertheless, transition smearing can be observed when strong random fields are introduced to the system, such as the mechanical stresses imposed on LCs confined in random porous media [14].

In contrast to LCs, for LCEs the situation remained elusive for several years. For the nematic LCEs, the early experimental studies reported a continuous or supercritical-like evolution of the order parameter [15–18]. Most of the characterizing techniques employed in these studies, such as the thermoelastic response, birefringence and X-ray scattering [17–20], are sensitive to macroscopic or collective rather than local or microscopic quantities. These techniques detect a smooth temperature dependence of the averaged order parameter without any discontinuity at the phase transition. It was, therefore, generally accepted that the phase transition in LCEs is supercritical [15, 21, 22], which was supported by some theoretical predictions about the possible existence of a critical point [22–24]. Nevertheless, there were also ideas that the continuous phase transition is a manifestation of the heterogeneous nature of LCEs [2] and the effects of quenched disorder [25].

The above experiments suggesting a supercritical response also imply the existence of the field term $-GS$ in the free energy F. Here G represents a mechanical field. Such a mechanical field most probably arises from the aligning process during the synthesis of a monodomain LCE. Moreover, the polymer-backbone-induced structural disorder might lead to a distribution of the mechanical fields $w_G(G)$, resulting in a random field picture [25]. On the other hand, the structural disorder could introduce heterogeneity in the system, reflected in the distribution of other Landau parameters, which is typically expressed in the distribution of the transition temperatures $w_T(T_{\mathrm{PN–N}})$ [2]. Both pictures, the existence of mechanical fields and the heterogeneity, would lead to continuous

temperature profiles for the average physical quantities. Therefore, the question remains as to whether the critical point exists for these systems, and if so, are the LCEs confined to only one part of the temperature–field (T–G) phase diagram or can they explore all possible states within it by changing some controlling physical or chemical parameters? In order to answer this question one should employ a method that is able to precisely determine the small quantities of latent heat that are expected to be observed in the vicinity of the critical point. In addition, it is essential to probe the local order parameter rather than the average one. High-resolution calorimetry and ^{2}H-NMR spectroscopy, which are introduced in the following two sections, represent a natural choice for such methods.

2 Energy Fluctuations Near the Paranematic-to-Nematic Conversion

2.1 High-Resolution Calorimetry

In this section, the basic principles of high-resolution calorimetry and its modes of operation are presented. Moreover, the use of the method in order to study phase diagrams is explained. The theoretical background of various high-resolution calorimetric techniques was developed in the 1960s by independent groups [26–28]. In the years that followed these techniques were used in numerous studies of soft and solid materials, revealing many subtle features of phase transitions and critical phenomena [29, 30].

Here, we will focus on a specific high-resolution calorimetric technique, i.e. nonadiabatic scanning calorimetry. This technique implies a calorimeter apparatus capable of operating in the ac as well as in the relaxation mode. The combination of these modes makes it possible to distinguish between the continuous and discontinuous transitions.

2.2 The ac Mode and the Relaxation Mode of Operation

In the principal ac mode of operation, an oscillating power is applied to the investigated sample. The frequency is appropriately chosen to eliminate any temperature gradients within the sample as well as to achieve good thermal equilibrium between the sample and the bath. The heat capacity C_p is derived as a function of the applied power, the oscillating frequency and the temperature oscillations around its mean value. The ac mode of operation is in fact sensitive only to the continuous

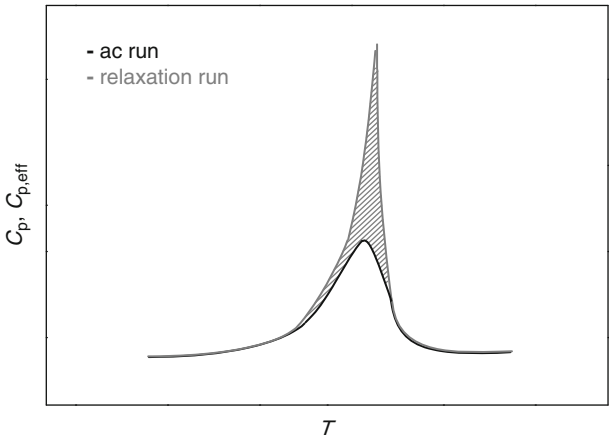

Fig. 4 Heat-capacity profiles of the ac mode (C_p) and the relaxation mode ($C_{p,eff}$) in the case of a broad first-order phase transition, similar to the ones observed in LCEs. The difference of the integrals (*gray-shaded area*) yields the latent heat involved in the transition

changes of the enthalpy and it cannot yield the absolute value of latent heat when the latter is involved in a first-order transition. Hence, this mode is impractical in distinguishing between the discontinuous, continuous and supercritical evolution near the critical point, i.e. in the case of discontinuous order transitions with a small amount of latent heat.

In order to determine precisely the latent-heat values, the calorimeter has to be operated in the relaxation mode. In the most recent version of this mode, the bath is accurately stabilized and then a linearly ramped power is applied to the sample [31]. This mode of operation is sensitive not only to the continuous but also to the discontinuous part of the enthalpy change, i.e. the latent heat L. Hence, L can be quantitatively determined by subtracting the integrals of the resulting C_p and $C_{p,eff}$ anomalies of the ac and relaxation modes, respectively:

$$L = \Delta H^{(\text{relaxation})} - \Delta H^{(\text{ac})} = \int C_{p,\text{eff}} \mathrm{d}T - \int C_p \mathrm{d}T. \tag{6}$$

A simple schematic explanation of the above can be seen in Fig. 4, where the heat-capacity profiles of the two modes of operation are shown in the case of a first-order transition. The integral of the gray-shaded part corresponds to the amount of latent heat released. Note that in the case of a second-order transition ($L = 0$) one obtains identical C_p and $C_{p,eff}$ profiles. In Figs. 5 and 6, the resolution of the relaxation runs is somewhat smaller than that of the ac runs. Nevertheless, they are very important when a precise determination of the latent heat is an issue. The following section shows some examples of the heat-capacity response near the critical point for LCs and LCEs.

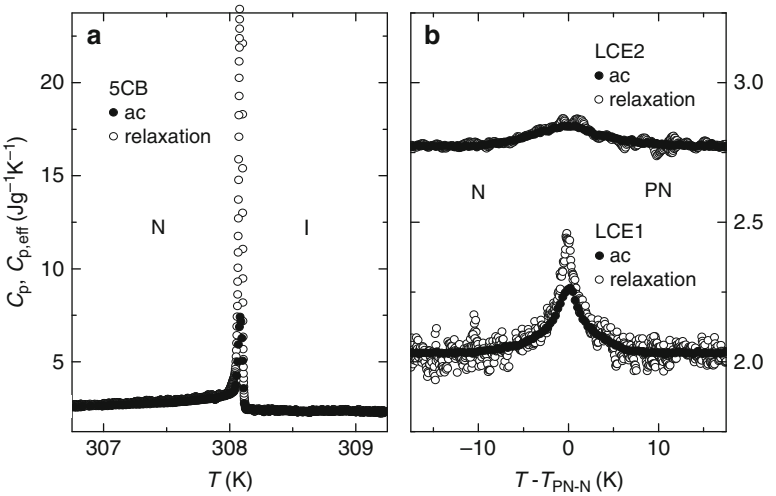

Fig. 5 $C_p(T)$ and $C_{p,eff}(T)$ profiles for the I–N transition of a pure 5CB liquid crystal (**a**) and corresponding profiles for the PN–N transition of two liquid-crystalline elastomers, one with below-critical (LCE1) and one with supercritical (LCE2) behaviour (**b**). Note that the data sets in (**b**) have been shifted along the *y*-axis for clarity. The data are plotted versus $T–T_{PN–N}$ for a direct comparison. $T_{PN–N}$ denotes the phase-transition temperature obtained from the C_p data

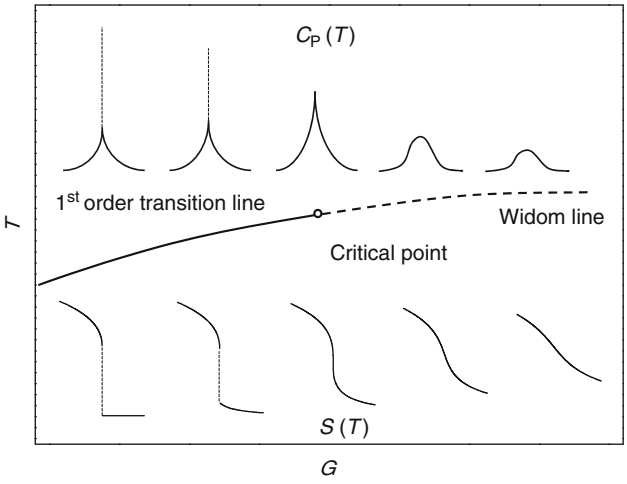

Fig. 6 *T–G* (temperature-field) phase diagram for a system that exhibits first-order transitions (*solid line*) that are terminated at a single critical point of the water-vapour type. The supercritical evolution emanates further from the critical point along a Widom line (*dashed line*). The heat-capacity C_p and order-parameter *S* temperature profiles corresponding to different *G* values are shown in the graph. The *dotted lines* represent the discontinuity in the $C_p(T)$ and $S(T)$ profiles, corresponding to the phase-coexistence region in which the latent heat is released

2.3 Heat-Capacity Response Near the Nematic Transition in LCs and LCEs

For pure LCs, the nematic transition is weakly first order with a narrow coexistence region having a width of between 10 mK and 100 mK. This is shown in Fig. 5a for pentylcyanobiphenyl (5CB).

In the case of LCEs, the PN–N transition is greatly broadened. This is also reflected in the broadening of the temperature coexistence range. In Fig. 5b, the heat-capacity profiles are shown for two different types of LCEs: one with latent heat (LCE1) and the other without latent heat (LCE2). For LCE1 we can see a mismatch between the ac and the relaxation mode C_p data, indicating a first-order transition. On the other hand, the match between the ac and relaxation mode C_p data for LCE2 indicates either a continuous (second-order) transition or a gradual supercritical evolution.

2.4 Temperature–Mechanical Field Phase Diagram

Due to its ability to distinguish between (strongly or weakly) first-order and second-order transitions, high-resolution calorimetry is a powerful technique for studies of phase diagrams near critical points. It probes the evolution of the latent heat in the regime of first-order transitions via the mismatch between the ac and relaxation runs. In the case of a continuous or gradual evolution, the two modes of operation yield identical anomalies.

A typical heat-capacity response is illustrated in Fig. 6 for the case of the *T*–*G* phase diagram for various fields, where a line of first-order transitions is terminated at a critical point. For the fields exceeding the critical value, a supercritical evolution is observed along the Widom line [32]. The resulting heat-capacity anomalies are shown for various parts of this diagram together with the corresponding curves of the order parameter, as described by (3) in Sect. 1.1.

3 Distribution of the Local Order Parameter and the Domain Director Alignment in LCEs

3.1 NMR of Deuterium-Labelled Mesogens in Liquid-Crystalline Materials

Nuclear magnetic resonance (NMR) detects the irradiation–absorption frequencies of the observed type of nuclei in matter that is put into a strong, uniform magnetic field. The central resonant frequency is determined by the Zeeman interaction of the nuclear magnetic moment with the external magnetic field, and it depends on the

type of the observed nuclei as well as on the magnitude of the magnetic field. Additionally, other types of interaction of the observed nuclei with their local neighbourhood give rise to corrections in the central resonant frequency. Accordingly, these interactions are reflected in a NMR spectrum in the form of frequency shifts, multiplets, line broadenings and other spectral features. The experimental determination of these spectral variations enables an identification of particular interactions, thus revealing the structure, the ordering and the dynamics of atoms or molecules in the matter.

The NMR spectroscopy of deuterium-labelled mesogens is a very powerful experimental method for the study of the local ordering in LCs and other liquid-crystalline materials, such as LC polymers, polymer-dispersed LCs, LC emulsions and LCEs [3–5, 15, 33–39]. Selective deuteration, i.e. the replacement of only particular hydrogen atoms by deuterium, is of great advantage as it enables observing only a selected part of the mesogenic molecule (e.g. a rigid core or a soft tail), which is not accessible with the widely spread ^{1}H or ^{13}C NMR. However, the main advantage of selective deuteration is the relatively simple spectral shape, rich in information and straightforward to interpret, particularly in the case of LCEs. On the other hand, the need for selectively deuterated compounds may represent a serious drawback if the investigated compound is a complex one so that its isotopologue is difficult to obtain. Nevertheless, this obstacle can be overcome by using a strongly diluted mixture of the investigated substance and some standard deuterium-labelled probe molecules [3–5, 33–38]. In the case that such a liquid-crystalline mixture exhibits "ideal mixing", we would expect that the original mesogens and the probe mesogens attain the same order and alignment. In such a case, the NMR response of the deuterated probe will be a good approximation of a spectrum that would otherwise be obtained from the investigated compound if it was deuterated.

Some very popular deuterated probes are the *n*-cyanobiphenyls, where *n* stands for the length of their carbon chain [3–5, 34, 40]. The ^{2}H-NMR studies of side-chain LCEs presented in this chapter have, in most cases, been conducted with alpha-deuterated octyl-cyanobiphenyl (αD_2-8CB) as a NMR probe (Fig. 7). The alpha

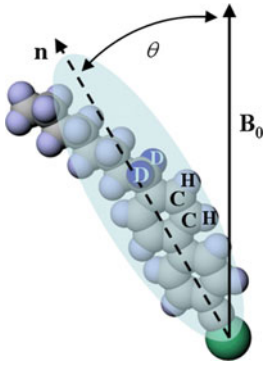

Fig. 7 α-deuterated 8CB molecule aligned along director **n** and at an angle θ with respect to the external magnetic field $\mathbf{B_0}$

position corresponds to the first alkyl-chain atom adjacent to the aromatic core. This position is, in most cases, optimal for deuteration as it best reflects the ordering of the rigid part of the liquid crystalline molecule and at the same time it provides a large spectral resolution, i.e. the separation of individual resonance lines in the NMR spectrum is the largest for this particular position. 8CB has been found to mix well with most of the studied side-chain LCEs [3, 41]. Most often, the probe mesogens are introduced by swelling the LCEs in a solvent, such as toluene, in which probe mesogens are also dissolved. After the LCE is taken out of the swelling mixture, the solvent is evaporated, so that one is left with a LCE that is weakly swollen by the ^{2}H-labelled probe mesogens. The concentration of these guest molecules is typically kept below 10% by weight.

For deuterium nuclei in LCs, the Zeeman and the quadrupolar interactions are by far the most dominant interactions of the nuclei with their surroundings. In such a case, a ^{2}H-NMR spectrum is always symmetrical. A spectrum of a single selectively deuterated liquid crystal molecule is a pair of lines (doublet) that are positioned at the frequencies (ν):

$$\nu^{\pm} = \pm\frac{3}{8}\nu_{\mathrm{Q}} S P_2(\cos\theta) \tag{7}$$

relative to the central resonant frequency, which from now on we take to be zero [42, 43]. Here, ν_{Q} is the average constant of the quadrupolar interaction that depends on the position of the deuteration. Its value for the deuteration at the alpha-position is about 60 kHz. S is the local order parameter and $P_2(\cos\theta)$ stands for the second Legendre polynomial, i.e. $(3\cos^2\theta - 1)/2$. θ is the average tilt of the liquid crystal molecule with respect to the external magnetic field of the NMR spectrometer. Both S and θ are expected to be constant over the whole particular liquid-crystalline domain. Thus, the above equation reflects the ability of the ^{2}H-NMR to simultaneously measure both the molecular order parameter S and the domain-director relative alignment θ.

3.2 ^{2}H-NMR Spectra of Nematic LCs and LCEs

A "single-molecular" spectrum, such as the one described by (7), can in practise only be recorded on a true liquid-crystalline monodomain with a perfectly homogeneous order parameter and average molecular tilt. A textbook example of such a spectrum is the ^{2}H-NMR of a deuterated bulk liquid crystal in the nematic phase shown in Fig. 8a. The narrow spectral lines in this spectrum provide evidence of perfect homogeneity for both the order parameter and the director alignment throughout the sample. A homogeneous order parameter is a common property of bulk LCs. The uniform director orientation, on the other hand, is a consequence of the strong magnetic field of the NMR spectrometer that perfectly aligns all the LC molecules with their long axes along its direction, so that $\theta = 0$ throughout the sample.

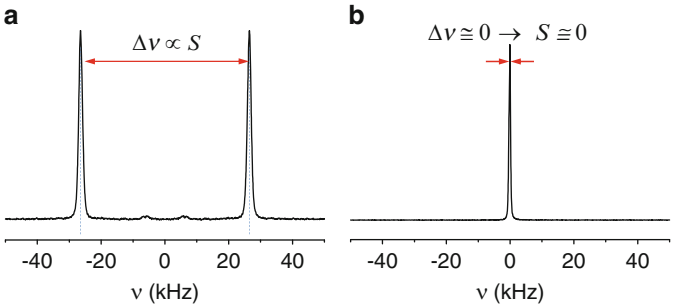

Fig. 8 ^{2}H-NMR spectrum of an αD_2-8CB liquid crystal in (**a**) the nematic phase and (**b**) the isotropic phase

The spectrum in Fig. 8b corresponds to the same bulk liquid crystal in the isotropic phase. Here, since $S = 0$, the splitting of the doublet is also zero, so that the doublet lines overlap and give rise to a single spectral line at zero frequency.

The LCEs are significantly more inhomogeneous systems than the bulk LCs. Also, the mesogens in LCEs are bonded so, unlike in LCs, they cannot be realigned by the external magnetic field. This is why the ^{2}H-NMR spectra of the LCEs in comparison to bulk LC spectra reveal a moderate level of inhomogeneity, reflected as a broadening of the spectral lines. This inhomogeneity is of two types:

1. Inhomogeneity of the domain-director alignment
2. Inhomogeneity of the local order parameter

The former reflects the slightly imperfect alignment of the domain directors, whereas the latter is a consequence of a smeared phase transition in the LCEs. Figure 9a,b serves as an example of how the ^{2}H-NMR spectra are altered by the inhomogeneity of the domain-director alignment and of the local order parameter in side-chain LCEs. Both spectra were recorded on LCEs doped with deuterated probes and oriented with their principal aligning direction parallel to the magnetic field.

3.3 Inhomogeneity of the Director Alignment

The spectrum in Fig. 9a has been recorded deep in the nematic phase. It features the usual pair of spectral lines, which are pronouncedly inwardly broadened (compared to the narrow lines of the spectrum in Fig. 8a). This characteristic broadening results almost exclusively from the misalignment of the directors of individual domains. The outermost part of the spectral lines corresponds to the molecules aligned parallel to the magnetic field [the largest value of $P_2(\cos\theta)$], whereas the inner part represents the most misaligned molecules. Therefore, the value of the order parameter is given by the maximum frequency shift $\nu_{\max}$. The width of the spectral line is a measure of the average misalignment angle $\delta\theta$, which for most LCE monodomains typically lies between 10° and 15°.

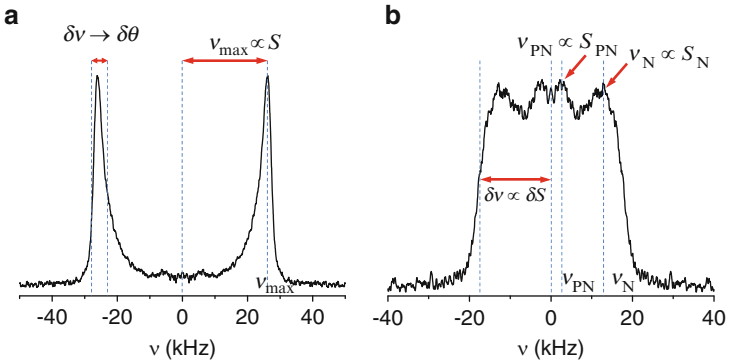

Fig. 9 ^{2}H-NMR spectrum of a conventional side-chain LCE doped with an αD_2-8CB liquid crystal recorded deep in the nematic phase (**a**) and in the vicinity of the PN–N phase transition (**b**). The spectrum (**a**) reflects the distribution of the domain–director alignment, and (**b**) reflects the distribution of the local order parameter

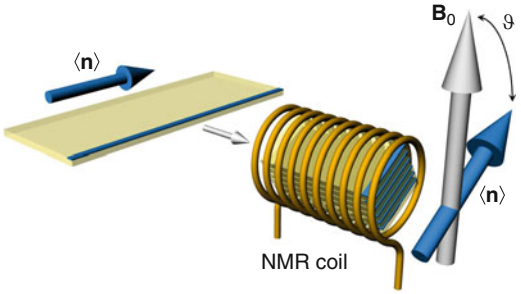

Fig. 10 Typical LCE sample geometry and the preparation of the sandwich sample for angular-dependent ^{2}H-NMR measurements

An analysis of the domain-director misalignment in LCEs is most easily conducted with spectra that are recorded deep in the nematic phase at various relative orientations of the LCE's principal aligning direction with respect to the external magnetic field. Figure 10 shows a typical setup for the ^{2}H-NMR of LCEs allowing this. An LCE strip with the average director orientation (denoted by $<\mathbf{n}>$) along the strip's long dimension is carefully cut into smaller, identically sized rectangular pieces. These are stacked together into a block, while great care is taken to ensure that the principal aligning orientation of the LCE perfectly matches for all the stacked pieces. Such a specimen is fitted into the coil of the NMR probehead equipped with a goniometer that makes it possible to set up an arbitrary orientation of the sample with respect to the external magnetic field $\mathbf{B_0}$. The orientation is specified by the tilt angle $\vartheta \angle(<\mathbf{n}>, \mathbf{B_0})$.

Examples of ^{2}H-NMR spectra recorded at different angles ϑ are plotted in Fig. 11 together with the fitted theoretical spectra. The latter were calculated by assuming that the domain-director directions are distributed uniaxially according to the probability distribution $w_{\mathbf{n},0}(\theta)$, which is given by:

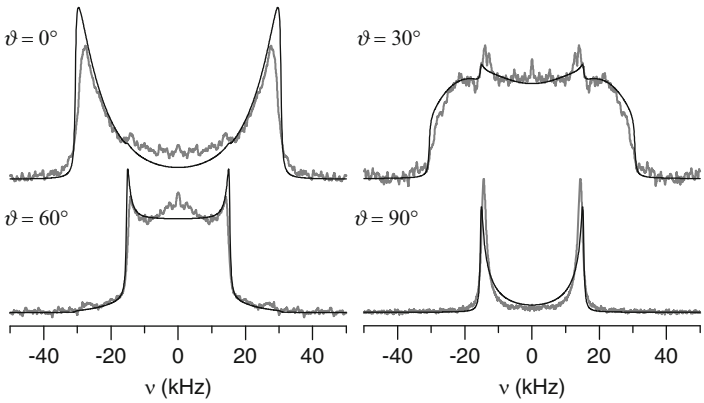

Fig. 11 Selection of ^{2}H-NMR spectra of a conventional side-chain LCE in a nematic phase recorded at various alignments ϑ of the LCE's principal aligning direction with respect to the magnetic field. A simultaneous fit of these spectra with the distribution $w_{\mathbf{n},0}(\theta)$ from (8) yields $\sigma_\theta = 17^o$

$$w_{\mathbf{n},0}(\theta) \propto \exp\left[-\sin^2\theta/2\ \sin^2\sigma_\theta\right]. \tag{8}$$

This distribution, sometimes referred to in the literature as the "spherical Gaussian", has been employed to describe the molecular orientations in various materials [44, 45]. It describes the probability of finding the domain director **n** aligned at an angle θ relative to the LCEs' principal aligning axis $<\mathbf{n}>$. The angle θ in (8) is the same as the angle θ in (7) for the case $\vartheta = 0$ or $<\mathbf{n}> \| \mathbf{B_0}$, which is indicated by 0 in the index of $w_{\mathbf{n},0}$. The distribution $w_{\mathbf{n},0}$ has only one parameter, σ_θ, which represents the width of the distribution.

3.4 Inhomogeneity of the Local Order Parameter

Apart from the nonuniform director alignment, the inhomogeneity of the local order parameter is also encountered in LCEs. This is best observed in a ^{2}H-NMR spectrum (Fig. 9b) recorded in the vicinity of the phase transition. The spread $\delta\nu$ of the spectral intensity between 0 and 20 kHz in this spectrum corresponds to a spread of the local order parameter δS in the range between approximately 0 and 0.45. Two pronounced peaks can be noted in each half-spectrum, corresponding to the coexisting paranematic (lower S, inner peak at ν_{PN}) and nematic components (higher S, outer peak at ν_N).

It appears that the understanding of the local order parameter's inhomogeneity is closely connected with the understanding of the phase transition in LCEs. However, in comparison with the inhomogeneity of the domain-director alignment, the characterization of the heterogeneity of the local order parameter appears much less accessible. This is due to the lack of any general model that predicts the distribution of the local order parameter $w_S(S)$ in LCEs.

Since the frequency shift of a NMR line is proportional to the local order parameter, in principle $w_S(S)$ could be directly deduced from the ^{2}H-NMR spectra. However, here one needs to take great care of the possible dynamically induced averaging effects. A substantial alteration to the ^{2}H-NMR spectrum may occur if dynamical processes, such as fluctuations of the nematic order parameter or molecular diffusion, are present in the investigated system. This problem is particularly acute with guest deuterated LC molecules, which are free to diffuse over the whole LCE network, i.e. among the nematic and the paranematic domains. Significant alterations to the ^{2}H-NMR spectra occur if these domains are small enough, so that this exchange process occurs on a timescale that is comparable to the timescale of the NMR experiment [35, 42, 46]. For typical bulk values of the 8CB self-diffusion coefficient, one can estimate that this occurs if the (unknown) size of the nematic and the paranematic domains in the LCEs is smaller than ~100 nm.

In order to exclude dynamically induced effects the analysis of the ^{2}H-NMR lineshape has to rely on other spectral parameters, which are invariant to the motionally induced averaging processes, such as the spectral moments [47]. Specifically, the first and second moments, $M_{\nu,1}$ and $M_{\nu,2}$, which can be calculated from a ^{2}H-NMR lineshape $\tilde{F}(\nu)$, according to:

$$M_{\nu,1} \equiv \int \nu \tilde{F}(\nu)\, \mathrm{d}\nu \equiv \langle \nu \rangle \tag{9a}$$

and:

$$M_{\nu,2} \equiv \int \left(\nu - M_{\nu,1}\right)^2 \tilde{F}(\nu)\, \mathrm{d}\nu \equiv \langle \nu^2 \rangle - \langle \nu \rangle^2, \tag{9b}$$

represent a robust measure for the average value and the width of the ^{2}H-NMR spectral line. By comparing the measured values of $M_{\nu,1}$ and $M_{\nu,2}$ with the theoretical values, given as (the derivation can be found in the Appendix):

$$M_{\nu,1}(\cos\vartheta) \equiv \frac{3}{4} \nu_Q M_{S,1} S_2 P_2(\cos\vartheta), \tag{10a}$$

and:

$$M_{\nu,2}(\cos\vartheta) \equiv \frac{9}{16} {\nu_Q}^2 \Big\{ \left(M_{S,2} + {M_{S,1}}^2\right) \Big[\frac{18}{35} S_4 P_4(\cos\vartheta) + \frac{2}{7} S_2 P_2(\cos\vartheta) + \frac{1}{5}\Big] - {M_{S,1}}^2 S_2 P_2(\cos\vartheta) \Big\}, \tag{10b}$$

one can extract information about the average nematic order parameter and its dispersion:

$$M_{S,1} \equiv \int S\, w_S(S)\, dS, \tag{11a}$$

and:

$$M_{S,2} \equiv \int \left(S - M_{S,1}\right)^2 w_S\,(S)\, dS. \tag{11b}$$

The degree of the domain misalignment in (10) is hidden in the coefficients S_2 and S_4 (see Appendix for details).

4 Smeared Paranematic-to-Nematic Phase Transition in LCEs

In this section, the nature of the PN–N phase transition in LCEs will be presented, as revealed by ^{2}H-NMR and supported by ac calorimetry. It will be demonstrated that the smooth phase transition in LCEs is a manifestation of both the field conjugate to the local order parameter (which in LCEs takes up close-to critical values) and the pronounced heterogeneity of LCEs, in the sense of distributed random fields. Particular attention will be paid to the description of a simple model based on the LdG approach, which considers these two features of LCEs. This model predicts the temperature profiles of the first and the second moment of the ^{2}H-NMR spectral lines. The accordance of this model with the experimental results will be discussed. Finally, the idea of a "smeared criticality" in LCEs will be presented.

4.1 LCEs: Heterogeneous, Supercritical or Both?

Figure 12 shows three ^{2}H-NMR spectra of a typical nematic LCE that were recorded at temperatures close to the PN–N transition. Three observations about these spectra should be noted:

1. The temperature evolution of the average resonant frequency of a particular spectral line is continuous, which implies a continuous temperature dependence of the local order parameter
2. Even at high temperatures there is a nonzero splitting of the spectral doublet, which indicates a residual nonzero paranematic order
3. Spectral lines are pronouncedly broadened at temperatures close to the phase transition

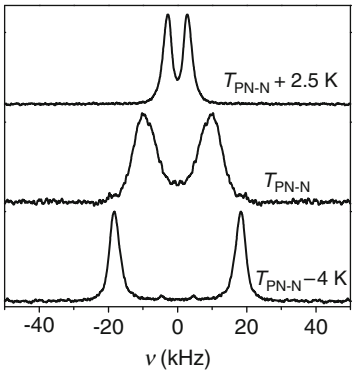

Fig. 12 Temperature-dependent ^{2}H-NMR spectra of a typical side-chain LCE. Data taken from [3]

From these observations, the calorimetric measurements (Fig. 5b) and the observations from other studies in the search for an appropriate description of the PN–N phase transition in LCEs, it seems that we start from two radically different, but not mutually exclusive, assumptions:

1. *LCEs are close-to critical or even supercritical*. The behaviour of $S(T)$ in LCEs can be attributed to the supercritical character of the PN–N transition [48]. It was shown in Sect. 1 (3) that a linear coupling of the nematic order parameter with a conjugate internal or external field G (accounted for by the free-energy term $-GS$) can drive the transition into the supercritical regime, characterized by zero latent heat and a smooth, continuous $S(T)$ profile (Fig. 13a). This occurs whenever G exceeds the critical value G_C. The effect of this field may be regarded as similar to, e.g. the effects of a high magnetic field, which recently has been successfully used to suppress the first-order character of the I–N transition in polymer LCs [11]. Microscopically, this field may be regarded as the sum of the local direct and indirect interactions between a mesogen and its neighbouring mesogens, the polymer-backbone segments and the crosslinkers. Such an assumption is supported by the fact that in many conventional LCE networks with a broad transition region, nonzero values of S have been experimentally determined at temperatures that are more than 20 or 30 K above the nominal $T_{PN–N}$. On the other hand, this scenario is questioned by the fact that in most of the investigated LCEs, the latent heat has been detected at the phase transition (see Fig. 5b and also Sect. 5).
2. *LCEs are heterogeneous*. LCEs are inherently heterogeneous materials due to the composite nature of their structure at the nanoscopic level. Any local variations in the concentrations of their constituents, the polymer backbone, the crosslinkers and the mesogen, can result in a distribution of the intermolecular coupling coefficients. This introduces a certain degree of glass-like behaviour to the thermodynamics of the system [25].
   The description of this heterogeneity may be very complicated when starting from a microscopic model. A much more accessible picture for introducing the

heterogeneity on a phenomenological level comes from dividing the system into microdomains, each of them with a well-defined set of LdG free-energy expansion coefficients. The average order-parameter temperature profile of the system $\langle S(T)\rangle$ then results in a superposition of $S(T)$ profiles arising from the individual domains [2]. In this case, the experimentally observed, smooth $S(T)$ profile in the transition region can be reproduced with a proper selection of the distribution functions, even if the phase transition in individual domains is discontinuous. Macroscopically, such a heterogeneous system eventually exhibits a smeared PN–N transition, with a broad coexistence region of the two phases and a spatially inhomogeneous S (Fig. 13b).
Firm evidence for such a picture is the pronounced NMR line broadening observed at the PN–N transition, indicating a broad spread of the order parameter values (Figs. 11b and 12). Moreover, the phase transition region is also distinguished by a nonzero latent heat, released over a broad temperature interval (Fig. 5b).

Both the above-described assumptions seem to provide a qualitatively satisfactory description of the order parameter's continuous temperature profile in LCEs. It is likely that, in real systems, the two mechanisms go hand in hand. However, the remaining questions are: which one prevails and can the properties of LCEs be tailored so that either the heterogeneous or the supercritical nature is promoted? Only recently, has this ambiguity been satisfactorily resolved by combining nuclear magnetic resonance and high-resolution calorimetry [3, 4]. It is the purpose of this chapter to discuss the approach used in these studies, with particular emphasis on an analysis of the experimental NMR data.

4.2 Distribution of Landau-de Gennes Expansion Parameters

The LdG expansion of free energy (Sect. 1) has been used in the form as in (3) for an approximate (qualitative) description of the phase transitions in LCEs in a number of studies. In these studies, the homogeneous order parameter S was always assumed in order to describe the temperature profiles of the LCE's stress and strain or birefringence [2, 17, 22, 24]. Here, it is assumed that the order parameter in LCEs is inhomogeneous. The "heterogeneity" of the LCEs may be, in principle, implicated by distributing any of the LdG parameters (α,B,C,G or T^*). We will proceed by introducing the Gaussian distributions $w_{T^*}(T^*)$ and $w_G(G)$ of the two parameters in the LdG expansion with the most obvious physical meaning, i.e. the spinodal temperature T^* [corresponding to a distribution of the transition temperatures $T_{\mathrm{PN–N}}$ via (5)], and the internal mechanical field G:

$$w_{T^*} = \frac{1}{\sqrt{2\pi}\sigma_{T^*}} \exp\left[-\frac{(T^* - \langle T^*\rangle)^2}{2{\sigma_{T^*}}^2}\right], \quad w_G = \frac{1}{\sqrt{2\pi}\sigma_G} \exp\left[-\frac{(G - \langle G\rangle)^2}{2\,{\sigma_G}^2}\right]. \quad (12)$$

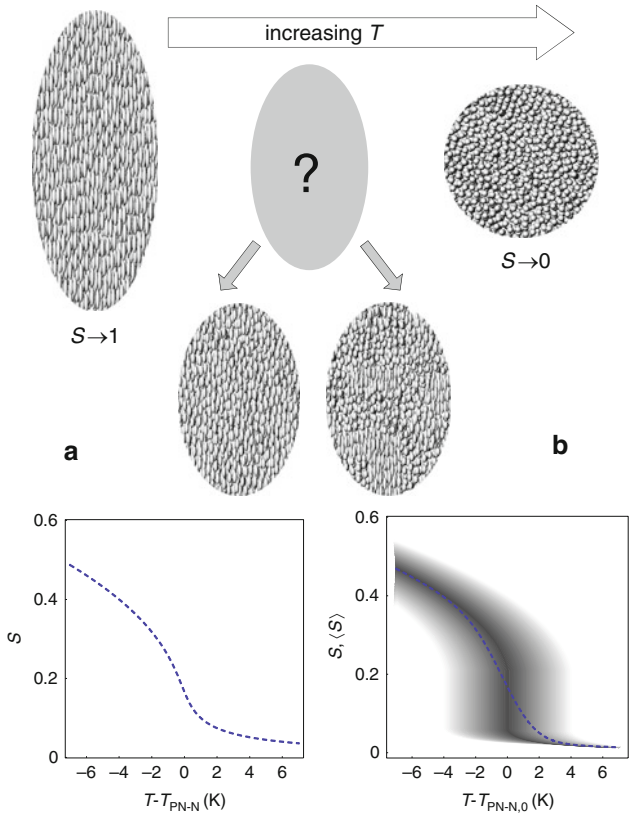

Fig. 13 Schematic representation of an effective, i.e. time averaged, molecular shape and the continuous temperature evolution of the order parameter S of mesogenic molecules in LCEs according to two possible scenarios: (**a**) the "supercritical" scenario in which the order parameter S is homogeneous and $S(T)$ is continuous because of the supercritical value of the internal field G, and (**b**) the "heterogeneous" scenario in which the domain structure exists in the LCE. In each domain, the PN–N phase transition occurs at a different temperature $T_{\mathrm{PN–N}}$, distributed symmetrically around the mean value $T_{\mathrm{PN–N,0}}$. This results in a smeared transition and the continuous temperature dependence of the average order parameter $\langle S \rangle$, even if the phase transition in individual domains is discontinuous

This results in an order parameter being distributed according to w_S [2]:

$$w_S = \int w_{T^*}\, w_G\, \delta[S - S_{\mathrm{LdG}}]\, \mathrm{d}T^* \mathrm{d}G, \tag{13}$$

where $S_{\mathrm{LdG}} = S_{\mathrm{LdG}}\,(T,T^*,\alpha,B,C,G)$, the solution to the nematic order parameter, is obtained from the minimization of the LdG free energy (3).

Section 3.4 shows that the mean value and the dispersion of the local order parameter can be expressed by the first and the second moment of the order

parameters $M_{S,1}$ and $M_{S,2}$, which in turn are accessible from the first and the second moment of the ^{2}H-NMR spectral line shapes, $M_{v,1}$ and $M_{v,2}$ (10). Thus, the NMR observables $M_{v,1}$ and $M_{v,2}$ are expressed as functions of the mean values and the dispersions of the Landau parameters (α,B,C, T; $\langle T^* \rangle$,σ_{T^*},$\langle G \rangle$,σ_G). In addition, the effect of the domain-director misalignment can be included by taking, e.g. the spherical Gaussian (8) as our $w_{\mathbf{n},0}(\theta)$. Calculated this way, the ^{2}H-NMR spectral line moments $M_{v,1}$ and $M_{v,2}$ encompass and probe the three basic structural characteristics of LCEs:

1. Average internal mechanical field $\langle G \rangle$
2. Heterogeneity, quantified by σ_{T^*} and σ_G
3. Misalignment of the domains, quantified by σ_θ

The values of these parameters can be estimated from the simultaneous fits (with a single set of parameters for both $M_{v,1}$ and $M_{v,2}$) of the experimentally determined $M_{v,1}(T)$ and $M_{v,2}(T)$ profiles with the theoretical expressions. In addition, σ_θ can be independently determined in advance from the ^{2}H-NMR spectroscopic measurements of a sample at different orientations with respect to the magnetic field (see Sect. 3.3).

4.3 Smeared Criticality

The application of the above-described model to the experimental ^{2}H-NMR data demonstrates that the only plausible scenario for the PN–N transition in LCEs is the one that considers both the field G taking up values that are comparable to the critical value G_C, as well as the heterogeneity, which is manifested as a distribution of LdG parameters. This is best illustrated in Fig. 14, where two diagrams show the experimentally determined $M_{v,1}$ and $M_{v,2}$ temperature dependencies of a typical above-critical side-chain LCE together with three sets of theoretical $M_{v,1}(T)$ and $M_{v,2}(T)$ curves. The parameters for the theoretical curves were selected in such a way that all three theoretical $M_{v,1}(T)$ profiles give a very good fit to the $M_{v,1}(T)$ experimental data and, at the same time, correspond to the three very different scenarios, none of which considers a distribution of the mechanical field ($\sigma_G = 0$):

1. Pure "supercritical scenario" ($\sigma_{T^*} = 0$, $G \gg G_C$)
2. Below-critical "heterogeneous scenario" (large σ_{T^*}, $G \lesssim G_C$)
3. Mixed scenario: heterogeneity of the LCE is manifested via a nonzero σ_{T^*}, at the same time as the field in the LCE takes up supercritical values ($\sigma_{T^*} \neq 0$, $G \gtrsim G_C$)

From the comparison, it is obvious that it is the second moment of the ^{2}H-NMR spectrum ($M_{v,2}$) and not the first moment ($M_{v,1}$) that distinguishes between the three scenarios. While all the $M_{v,1}(T)$ curves are practically indistinguishable, the $M_{v,2}(T)$ profiles are very different. It is also clearly evident that the mixed scenario

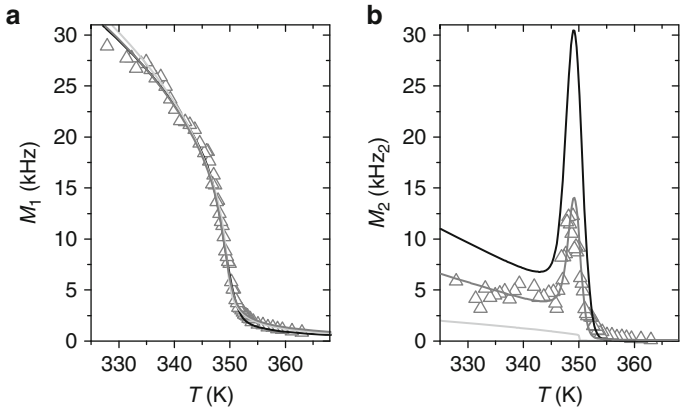

Fig. 14 The best simultaneous $M_{v,1}(T)$ (**a**) and $M_{v,2}(T)$ (**b**) fits of the theoretical model from Sect. 4.2 (*dark gray line*) to the experimental data (*triangles*) for the LCE shown in Fig. 12. Also shown are the forced $\sigma_{T^*} = 0$ fit (*light-gray solid line*) and the forced $G \lesssim G_C$ fit (*black line*). For the displayed LCE, the best fit is obtained for $G/G_C = 1.5$ and $\sigma_T = 1.0$ K. Data taken from [3]

(i.e. $\sigma_{T^*} \neq 0$, $G \gtrsim G_C$) gives by far the best possible match between the theoretical prediction and the experiment.

Unlike the first two scenarios , where the parameters were set by fitting only the experimental $M_{v,1}(T)$ data, for the mixed scenario the fit was made simultaneously for both the $M_{v,1}(T)$ and $M_{v,2}(T)$ datasets. In this way, the relative values of the parameters were determined with relatively high precision (the typical maximum error for any parameter among α, B, C, or G for the displayed fit is about 15%). Actually, since these parameters are not independent, only the relative values (ratios) of these parameters can be determined from the ^{2}H-NMR data, e.g. G/G_C. Their absolute values are accessed from an additional calorimetric measurement, e.g. a measurement of the latent heat released at the phase transition.

Obviously, the involvement of the heterogeneity of the transition temperatures makes a sensible description of the phase transition in LCEs. However, one finds an even better match with the experimental data when considering only the heterogeneity of the mechanical field G instead ($\sigma_{T^*} = 0$, $\langle G \rangle \neq 0$, $\sigma_G \neq 0$). The $w_S(T)$ profiles corresponding to the disorder in T^* are different from the profiles corresponding to the disorder of G. This is so since the changes in T^* merely result in a shift of $T_{PN-N,}$ while the shape of $S_{LdG}(T)$ is preserved, whereas the changes in G also alter the temperature profile of $S_{LdG}(T)$. Exploiting this fact, it is found that the high-temperature tails of $M_{v,2}(T)$ can be reproduced more accurately by distributing the internal fields G rather than the transition temperatures T^* (Fig. 15). On the basis of such a comparison one can conclude that the disorder in S mainly arises from the disorder in the local mechanical fields G. Although a model in which all the LdG parameters undergo some distribution is probably closest to the real picture, due to a large number of independent free parameters

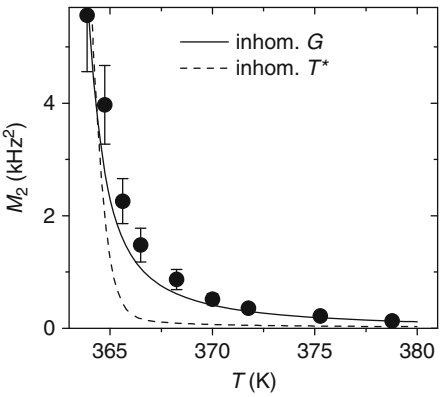

Fig. 15 High-temperature tails of the $M_{v,2}(T)$ in a typical LCE (*circles*), together with the results of the best simultaneous fits of the $M_{v,1}(T)$ and $M_{v,2}(T)$, considering either only the distribution of G (*solid line*) or only the distribution of T^* (*dashed line*). Data taken from [4]

(5), it does not appear reasonable to consider the distribution of more than a single LdG parameter.

Using the above-described ^{2}H-NMR data-analysis approach, the typical experimentally determined values of σ_{T^*} in LCEs lie between 1 and 3 K, if G is considered homogeneous. For homogeneous T^*, on the other hand, σ_G is estimated to typically lie between $0.5G_C$ and $0.8G_C$ [4], while the typical values of the mean field $\langle G \rangle$ are $0.5G_C$–$2.0G_C$ (see Sect. 5). This means that in LCEs, the tails of the G-distribution function $w_G(G)$ extend below the critical value G_C, even if $\langle G \rangle > G_C$, and vice versa, in systems with $\langle G \rangle < G_C$, they extend above the critical value G_C. Even though the average response of the system is supercritical, the local response in some domains can be critical or below critical. The opposite also applies: in an effectively below-critical system, there are domains that respond in a critical or supercritical manner.

One should thus not regard LCEs as entirely below-critical or above-critical systems, but rather as systems in which both types of phase-transition behaviours may be found, the extent of which is determined by the values of $\langle G \rangle$ and σ_G. We shall introduce the term "smeared criticality" for such behaviour. In Fig. 16a, the graphical representation illustrates the extent of each type of phase transition behaviour in two LCEs, one prevalently below critical and the other prevalently above critical. A straightforward manifestation of the smeared criticality is the presence of latent heat in many LCE systems that exhibit a supercritical, effective thermodynamic response (see Sect. 5). This latent heat is released by the below-critical component of the LCE whose extent is given by the surface of the shaded area in Fig. 16.

We shall see in Sect. 5 that LCEs can be tailored to exhibit a thermodynamic response spanning from subcritical to supercritical. However, the classification in terms of subcritical, critical or supercritical is, in the presented picture of smeared criticality, applicable only for describing the average (effective) response of LCEs.

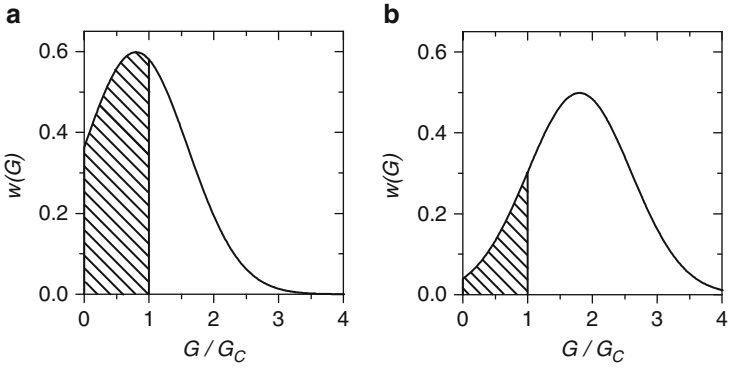

Fig. 16 Smeared criticality in LCEs from the point of view of the distribution function $w_G(G)$ of the internal mechanical field G. The depicted distributions are calculated for $\langle G \rangle = 0.8\ G_C$ and $\sigma_G = 0.8\ G_C$ corresponding to an effectively subcritical LCE (**a**) and for $\langle G \rangle = 2.0\ G_C$ and $\sigma_G = 0.8\ G_C$ corresponding to an effectively supercritical LCE (**b**). The extent of the below-critical component ($G < G_C$) of each LCE is given by the surface of the *shaded area*

5 Tailoring the Thermomechanical Response of LCEs by Influencing the Critical Behaviour

In the previous sections, the basic principles of the PN–N transition in LCEs and the experimental techniques were introduced to the reader. The issue of a "smeared criticality" observed in LCEs was introduced in Sect. 4. In this section, the experimental results providing an insight for the understanding of the PN–N transition are presented. These data were obtained by deuteron NMR and ac calorimetry on side-chain and main-chain LCEs. The distinct role of each parameter that affects the critical behaviour of the PN–N phase transition of LCEs will be demonstrated in different subsections. These parameters influence the relative strength of the locked-in mechanical field G and, as demonstrated in the previous sections, they may alter the order of the PN–N transition.

5.1 Impact of Chemical Composition: Crosslinking Density

The idea that the critical behaviour of LCEs may be influenced by varying the geometry and density of the crosslinkers was introduced in an early theoretical work [23]. Indications that an increased crosslinking density leads to a more gradual (more supercritical-like) thermoelastic response and birefringence temperature dependence may be found in various publications [7, 18]. Recently, the first systematic and dedicated experimental investigation, by means of ^{2}H-NMR and high-resolution calorimetry [4, 5], demonstrated that the increase in the crosslinkers

density drives the transition towards the supercritical regime in various types of LCEs (both side- and main-chain).

In that study, conventional polysiloxane-based side-chain LCEs were used; the chemical formulae of their components (mesogen, polymer backbone, crosslinkers) are shown in Fig. 17a. First, the effect of the concentration of the rod-like bifunctional crosslinker denoted as V6 was studied. LCE samples with crosslinking densities x_{SC} equal to 0.075, 0.105, 0.125, 0.150 and 0.160 were prepared and investigated. Here, x_{SC} denotes the coverage of the active groups of the siloxane-based polymer chain and is (in the case of full coverage) equal to the mol% of crosslinker $\times$ crosslinker functionality. Additionally, LCEs of the same composition but with a trifunctional crosslinker, denoted as V3, were also prepared. The investigated crosslinking densities in this case were equal to 0.075, 0.105 and 0.125.

In order to further investigate the role of the crosslinking topology, a similar study was performed for main-chain LCEs (the components' chemical formulas are shown in Fig. 17b). The crosslinking of the main-chain LCEs was realized by a pentafunctional cyclic siloxane crosslinker (denoted as HD5) [7]. LCEs with crosslinker-mesogen molar ratios x_{MC} of 0.025, 0.04, 0.06, 0.08 and 0.12 were prepared and investigated. In contrast to the side-chain LCEs, in main-chain LCEs the crosslinking density is characterized by $x_{MC,}$ which is the ratio of the number of crosslinkers to the number of mesogens. Obviously, due to the different crosslinker

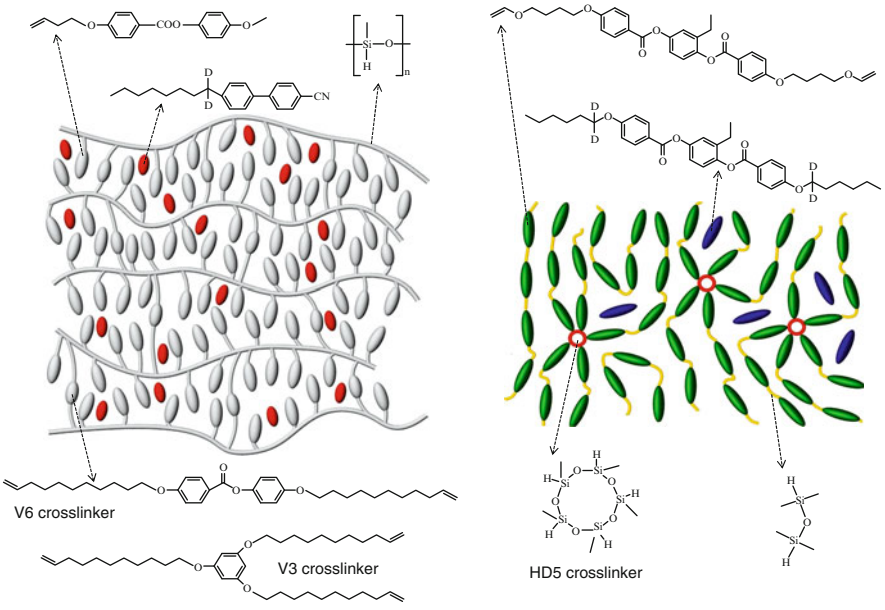

Fig. 17 Schematic drawing (only illustrative) of the (**a**) side-chain and (**b**) main-chain LCEs used in this study together with the chemical formulas of the LCE components and deuterated probe molecules. The various crosslinkers are denoted as V6, V3 and HD5

functionalities and the different network topology, the absolute values of x_{SC} and x_{MC} should not be directly compared.

All the LCE samples were prepared by the two-step crosslinking procedure [49]. Each of the samples was cut into two parts. One part was used for the calorimetric investigations, while the other part was doped with an amount (~8–10%) of deuterated probe mesogens that was high enough to render the LCEs ^{2}H-NMR-sensitive, and at the same time low enough so that it did not alter the intrinsic PN–N transition behaviour. αD_2-8CB has been used for side-chain LCEs, and a deuterated variation of the original main-chain mesogen has been used for main-chain LCEs. After being prepared in the same way as described in Sect. 3.1, these samples were used for ^{2}H-NMR investigations.

The heat-capacity temperature profiles obtained via the ac and relaxation runs for low-, mid- and high-crosslinking densities of side-chain (V6-crosslinked) and main-chain LCEs are shown in Fig. 18. A considerable mismatch is observed between the ac and relaxation runs for lower crosslinking densities, which is evidence of the presence of latent heat along a few-Kelvin-wide coexistence region of the paranematic and nematic phases. The mismatch of the data obtained by the two modes gradually decreases for higher concentrations and finally vanishes within the experimental error for the $x_{SC} = 0.15$ and $x_{MC} = 0.12$ samples. At these high crosslinking densities, a very broad and suppressed C_p anomaly and

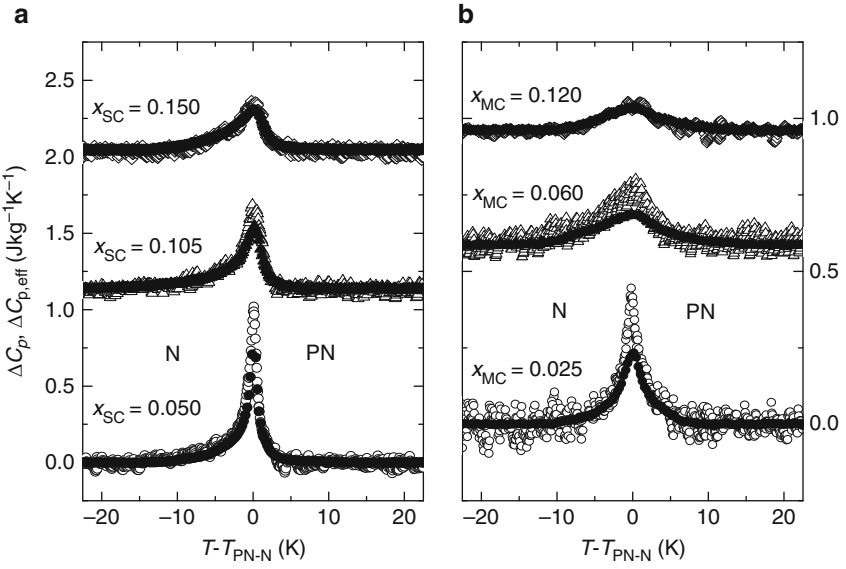

Fig. 18 Selected heat-capacity temperature profiles obtained by ac and relaxation runs for (**a**) side-chain LCEs (V6-crosslinked) and (**b**) main-chain LCEs (HD5-crosslinked) with various concentrations of V6 crosslinkers. The *solid symbols* stand for the ac and the *open symbols* for the relaxation runs. The different datasets have been shifted along the *y*-axis (C_p) for clarity. Data taken from [4, 7]

Table 1 Values of the reduced parameters $\langle G \rangle$ and σ_G of the distribution w_G, obtained from the best simultaneous fit of the $M_{1,\nu}(T)$ and $M_{2,\nu}(T)$ data of side-chain LCEs with various crosslinker concentrations x_{SC}. Alongside are values of the latent heat L determined from calorimetric and ^{2}H-NMR experiments. Data taken from [4]

x_{SC}	$\langle G \rangle / G_C$	σ_G / G_C	$L_{(calorimetry)}$ (J g^{-1})	$L_{(NMR)}$ (J g^{-1})
0.075	0.4 ± 0.1	0.6 ± 0.3	0.45 ± 0.10	0.51 ± 0.16
0.105	1.15 ± 0.15	0.7 ± 0.2	0.30 ± 0.10	0.16 ± 0.06
0.125	1.45 ± 0.3	0.6 ± 0.2	0.10 ± 0.10	0.11 ± 0.04
0.15	2.0 ± 0.2	0.8 ± 0.2	0.05 ± 0.05	<0.01
0.16	N/A	N/A	0 ± 0.05	<0.01

N/A not applicable

practically zero latent heat indicate that these systems are beyond the critical point in the supercritical regime. This can be read from the experimentally determined latent heat L values that are collected in Table 1 [4]. The presented results clearly demonstrate that the increase in the crosslinking density drives the transition towards and beyond the critical point, into the supercritical regime, where more broad and suppressed anomalies are typically observed.

Results similar to the ones described above are also obtained for the V3-crosslinked side-chain LCEs, i.e. LCEs with different crosslinker geometry and functionality. The measurements of these LCEs showed that the critical point is shifted to essentially lower crosslinking densities in the case of flexible trifunctional crosslinkers, as significantly smaller latent-heat values have been observed already at lower V3 densities [4] (See Fig. 21).

In addition to the above calorimetric results, ^{2}H-NMR measurements were performed for LCEs of the same crosslinking concentrations, doped with deuterated probe mesogens. A selection of the ^{2}H-NMR spectra recorded at temperatures close to the phase transition for various x_{SC} and x_{MC} are shown in Fig. 19. Particularly when comparing the spectra of the side-chain LCEs corresponding to samples with different crosslinker concentrations (Fig. 19a), three obvious features can be observed:

1. The shift of the individual spectral line away from the zero frequency is clearly more gradual in LCEs with higher crosslinker concentrations, indicating a more gradual temperature profile of the order parameter.
2. The broadening of the spectral line is very moderate for the $x_{SC} = 0.15$ sample and much more pronounced for the LCEs with lower crosslinker concentrations. This pronounced broadening arises primarily from the distribution of the local order parameter S, which indicates either a higher heterogeneity or phase-transition behaviour closer to below-critical in less crosslinked LCEs, or both. This is particularly obvious for the $x_{SC} = 0.075$, for which one can observe a coexisting nematic and paranematic component (inner and outer peak) at $T_{PN–N}$.
3. At high temperatures (several degrees above $T_{PN–N}$), the splitting of the doublet in the ^{2}H-NMR spectra increases for the samples with the higher crosslinking

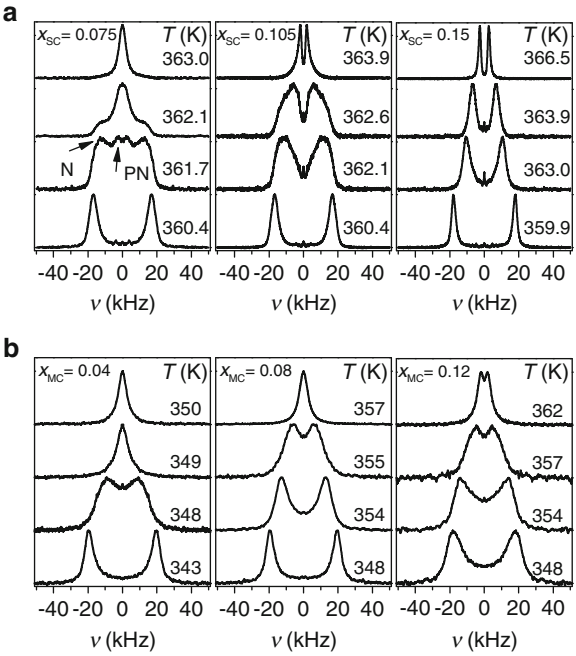

Fig. 19 Selection of ^{2}H-NMR spectra recorded at temperatures close to the phase transition for various x_{SC} in side-chain LCEs (**a**) and various x_{MC} in main-chain LCEs. *Arrows* denote the spectral features attributed to the paranematic (PN) and nematic (N) phases. Data taken from [4, 7]

densities. Obviously, in the more crosslinked LCEs the residual local order parameter in the paranematic phase is higher than in the less crosslinked LCEs.

The interpretation of the ^{2}H-NMR spectra of doped main-chain LCEs is not as straightforward as for the side-chain systems, because the spectral lines in the former are significantly broader than the spectral lines in the spectra of side-chain LCEs. Possible reasons for this are the larger network heterogeneity, the lower degree of nematic domain alignment and, most probably, the slow dynamics of the mesogens in the main-chain LCEs, which (unlike the side-chain LCEs) are attached at both their ends. Nevertheless, by comparing the spectra of the main-chain LCEs with different crosslinking densities (Fig. 19b), one may draw similar conclusions as in the case of side-chain LCEs (but with somewhat more uncertainty, due to much broader spectral lines). It is worth noting that only the most densely crosslinked main-chain LCE ($x_{MC} = 0.12$) clearly exhibits a spectral doublet at high temperatures. The doublet is without much doubt also present in the spectra of the low-crosslinked main-chain LCEs; however, due to the pronounced width and the overlapping of the individual NMR lines it appears as a single spectral line.

While representing valuable qualitative support, due to the intense overlapping of the spectral lines, the ^{2}H-NMR spectra of the main-chain LCEs do not allow for a precise calculation of the values of the spectral line moments ($M_{1,v}$ and $M_{2,v}$) and an

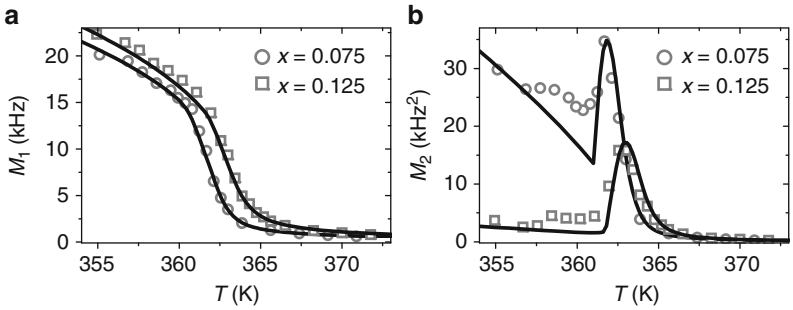

Fig. 20 Experimental $M_{1,v}(T)$ (**a**) and $M_{2,v}(T)$ (**b**) values for side-chain LCEs with $x_{SC} = 0.075$ (*circles*) and $x_{SC} = 0.125$ (*squares*). The fit with the model from Sect. 4.2 is displayed as a *solid line*

analysis of the $M_{1,v}(T)$ and $M_{2,v}(T)$ profiles. On the other hand, for side-chain LCEs with $x_{SC} = 0.075$, 0.105, 0.125 and 0.15, the values of $M_{v,1}$ and $M_{v,2}$ were extracted from their ^{2}H-NMR spectra and the $M_{v,1}(T)$ and $M_{v,2}(T)$ temperature profiles were fitted with the approach described in Sect. 4.2. The distribution of the conjugate field G rather than the distribution of T^* was considered as a manifestation of the heterogeneity. The diagrams in Fig. 20 show some examples of fitted $M_{1,v}(T)$ and $M_{2,v}(T)$ data for a below-critical ($x_{SC} = 0.075$) and for an above-critical ($x_{SC} = 0.125$) LCE. These diagrams clearly demonstrate that the main impact on phase-transition smearing comes from the heterogeneity, as there is only a small difference between the $M_{1,v}(T)$ curves of the two LCEs. On the other hand, the huge difference between the corresponding $M_{2,v}(T)$ curves demonstrates that $M_{2,v}(T)$ is the relevant quantity for probing the heterogeneity and the criticality of a LCE.

The values of the dimensionless quantities $\langle G\rangle/G_C$ and σ_G/G_C obtained from the optimal $M_{1,v}(T)$ and $M_{2,v}(T)$ fitting parameters are collected in Table 1. The increasing values of the reduced mean field G/G_C, upon increasing the cross-linking density, represent a quantitative confirmation that a denser crosslinking leads to a more supercritical behaviour of LCEs. The fact that the values of σ_G/G_C increase slightly with an increasing G/G_C may be regarded as a consequence of disregarding a possible distribution of T^* or some other LdG parameter. Consequently, it is realistic to expect that the width of the G-distributions is smaller than that obtained from the model, i.e. the obtained values of $\langle G\rangle$ and σ_G represent the limiting values of the internal mechanical field G that is expected in LCEs.

For a more direct comparison with the calorimetric measurements, the latent-heat L values have also been calculated (see Table 1) from the obtained parameters via the equation:

$$L_{NMR} = \frac{\alpha}{2\rho}\int w_G(G)T_{PN-N}(G)\left[S_N^2(G) - S_{PN}^2(G)\right]dG, \tag{14}$$

which is a generalization of the standard I–N latent-heat expression [50] for inhomogeneous systems. Here, S_N and S_{PN} are the order parameters of the

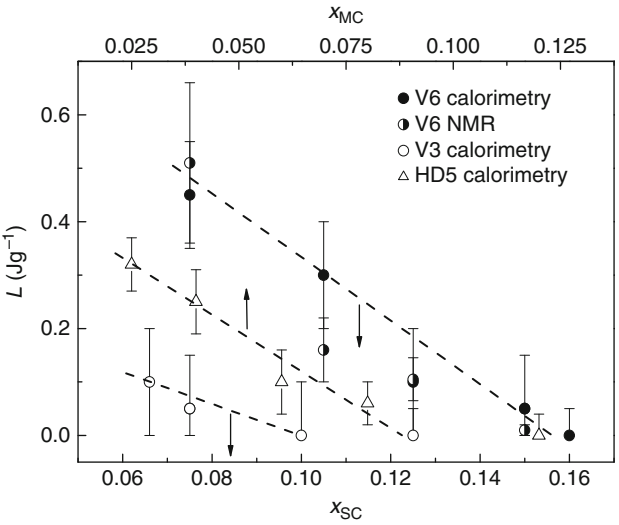

Fig. 21 Values of latent heat (L) for side-chain LCEs (with V6 and V3 crosslinkers) and main-chain LCEs (HD5 crosslinker) for various values of crosslinking density x_{SC} (*bottom axis*, applies to side-chains) and crosslinker concentration x_{MC} (*top axis*, applies to main-chains). The latent-heat values determined for the V6 crosslinkers by (14) are also displayed. Data taken from [4, 7]

coexisting nematic and paranematic phases at the transition temperature $T_{PN–N}$, whereas ρ is the density of the LCE network ($\rho \approx 1$ mg/mm^3). The absolute value of the LdG parameter α here represents a scaling parameter whose optimal value is adjusted by comparing the measured (calorimetry) and the calculated (NMR) values of L. As can be seen in Fig. 21, the dependences of the measured and calculated values of L on the crosslinking density of LCE exhibit a very good agreement.

Taking into account the obtained values of the $w_G(G)$ parameters, the recorded NMR spectra (Fig. 19) and the measured values of latent heat L, one can state that LCEs with lower crosslinker concentrations ($x_{SC} \lesssim 0.075$, $x_{MC} \lesssim 0.04$) exhibit a prevalently subcritical behaviour, whereas the LCEs with higher crosslinker concentrations ($x_{SC} \gtrsim 0.15$, $x_{MC} \gtrsim 0.12$) exhibit a prevalently supercritical behaviour. In LCEs with intermediate concentrations the smeared criticality is most evident. Although being on average supercritical (judging from the value of $\langle G \rangle / G_C$), the features of below-criticality such as a nonzero L and a pronounced broadening of the ^{2}H-NMR spectral line at the phase transition are still present.

Thus, the increase of the crosslinking density in the LCEs results in a shift of their phase-transition behaviour towards and beyond supercritical. As this trend is now confirmed for both the side- and main-chain nematic LCEs, i.e. two LCE families with drastically different crosslinking topologies, it can be anticipated that the link between the crosslinking concentration and the phase-transition criticality holds universally for most types of LCEs.

5.2 Impact of Synthesis Parameters

The well-established synthetic procedure for producing monodomain LCEs [49] relies on two steps: a fast initial step (of several hours) in which about half of the crosslinking chemical groups react in the presence of a solvent, and a slow (of several days) second crosslinking step in the absence of solvent, during which the mesogens in the LCE are aligned by stretching the LCE. The conditions in the second step crucially determine the resulting quality of the domain alignment. This is so, because during this step the remaining nonreacted crosslinkers tend to fix the state in which the LCE network is found [23, 24]. Thus, for the best possible domain alignment the LCE has to be stretched with a sufficiently high tension, and the synthesis should be done at temperatures below the $T_{PN–N}$ phase transition [6, 23]. A recent calorimetric study has revealed that the variation of these two synthetic conditions (aligning stress and temperature at which the second crosslinking step is performed) has an important influence on the phase-transition behaviour of the resulting main-chain LCEs.

5.2.1 Stretching During Second Crosslinking Step

A comparison has been made for two main-chain LCE samples with their compositions identical to that of the main-chain LCE with $x_{MC} = 0.04$ mentioned in Sect. 5.1. During the second crosslinking step of the otherwise identical synthesis procedure, these two samples were stretched with different tensions (24 kPa and 91 kPa). Both tensions were high enough for the realization of a monodomain LCE. Both samples were synthesized at temperatures below the $T_{PN–N}$ transition.

The heat-capacity temperature profiles for the two samples are shown in Fig. 22. The heat-capacity anomalies exhibit differences in the steepness as well as in the mismatch between the ac and relaxation runs. The sample crosslinked under the lower mechanical load exhibits a clear first-order character with the latent heat $L = 0.49 \pm 0.05$ J g^{-1}. On the other hand, an experimentally negligible latent heat is detected for the sample crosslinked under the higher load.

Obviously, for main-chain LCEs the value of the applied load during the second crosslinking step has a very important impact on the phase-transition behaviour of the resulting LCE. It is expected that such modifications of the LCE's critical behaviour are accordingly reflected in its thermomechanical response. Several studies have revealed a more gradual TM response and temperature dependence of the average order parameter when the LCE was stretched with a higher stress along its principal aligning direction [7, 17]. Thus, it appears that in terms of the modification of the phase-transition behaviour, the application of a high load during the second crosslinking step produces a similar effect to applying tension to fully synthesized LCEs.

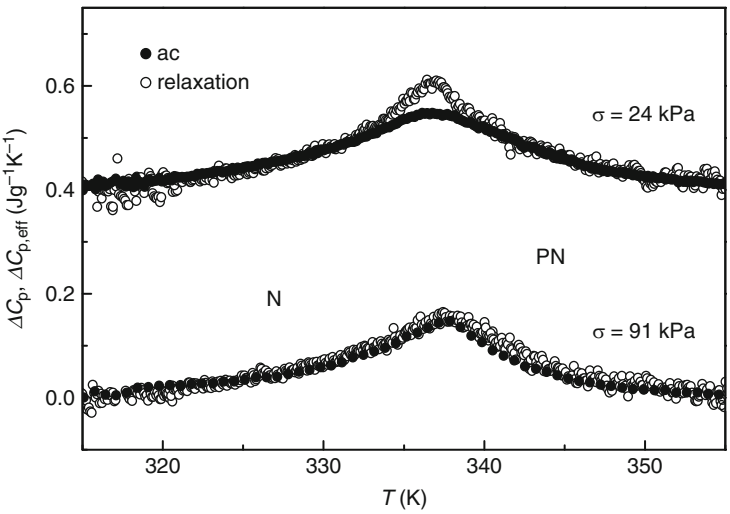

Fig. 22 The ac (*solid symbols*) and relaxation (*open symbols*) run heat-capacity temperature profiles ΔC_p and $\Delta C_{p,eff}$ for the nematic main-chain LCEs stretched with different mechanical loads (24 kPa and 91 kPa) during the second crosslinking step. Data taken from [7]

5.2.2 Temperature in the Second Crosslinking Step

In order to investigate the impact of the temperature at which the second crosslinking step takes place, again two main-chain LCE monodomain samples were compared [51]. Both of the samples had identical compositions and both were prepared in the same manner as in Sect. 5.2.1. During the second crosslinking step an identical aligning stress, exceeding the threshold aligning value, was imposed on both samples. The only difference between the two synthetic procedures was the temperature at which the second crosslinking step was made. This temperature was 373 K (i.e. well above the $T_{PN–N}$ of about 335 K) for one sample and 323 K (i.e. corresponding to the nematic phase) for the other sample.

The heat-capacity anomalies obtained for the two samples by ac and relaxation runs are shown in Fig. 23. The results show a striking effect on the phase-transition behaviour. The LCE crosslinked in the PN phase exhibits a smeared and suppressed C_p anomaly, with only a slight mismatch between the ac and relaxation data, yielding a latent heat of the order of the estimated experimental error (0.05 J g^{-1}). In contrast, the LCE crosslinked in the nematic phase shows a much narrower and steeper anomaly, reminiscent of the I–N transition in LCs, with a significant amount of latent heat ($L = 0.78 \pm 0.05$ J g^{-1}). The temperature range in which half of the enthalpy change occurs is three times broader for the LCE crosslinked in the isotropic phase. This indicates that LCEs of the same composition crosslinked in the nematic phase will exhibit a TM response that is a rather on–off type of response, in contrast to the LCEs crosslinked in the paranematic phase, which would have a more gradual thermomechanical response. When compared to

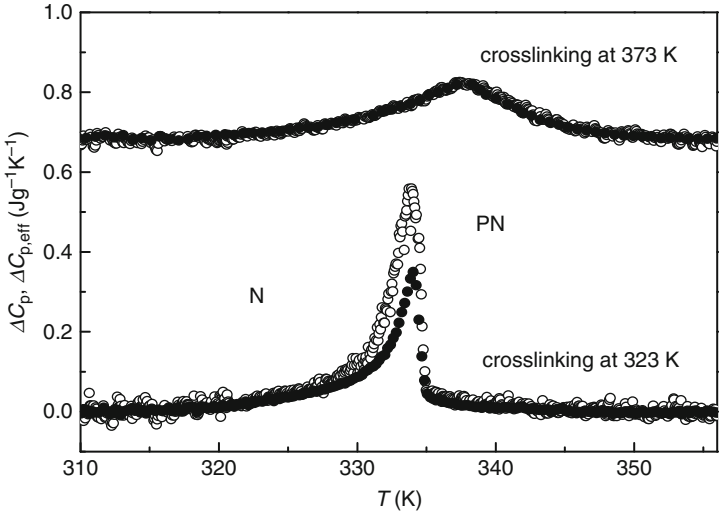

Fig. 23 The ac (*solid symbols*) and relaxation (*open symbols*) run heat-capacity temperature profiles ΔC_p and $\Delta C_{p,eff}$ for the nematic main-chain LCEs crosslinked in the isotropic phase (*above*) and in the nematic phase (*below*). Data taken from [51]

other ways of influencing the critical behaviour in LCEs (crosslinking density and applied mechanical load), it appears that the variation of the crosslinking temperature represents the largest effect.

5.3 *Impact of Processing: Swelling with Low-Molar-Mass Nematogen*

In the previous subsections it has been demonstrated that a more supercritical behaviour in LCEs is promoted by LCE modifications that result in a harder network, e.g. increasing the crosslinking density, fully stretched polymer chains during the final crosslinking stage. Here, we show that an opposite effect can be obtained by softening the LCE network, e.g. by swelling the LCE with smaller mesogenic molecules, which play the role of plasticizers. This finding relies on a combined ^{2}H-NMR/calorimetry study, in which the effect of varying the amount of dopant deuterated mesogen (8CB) on the LCE's I–N phase transition has been investigated [3].

In this study, the investigated side-chain LCE was composed of the same mesogen and polymer as the LCEs in Sect. 5.1, with an effective 20% crosslinking concentration achieved with a mixture of two bifunctional crosslinkers, which in the literature are denoted as V1 and V2 [49]. Three samples were prepared from a single LCE strip. They were swollen according to the procedure explained in

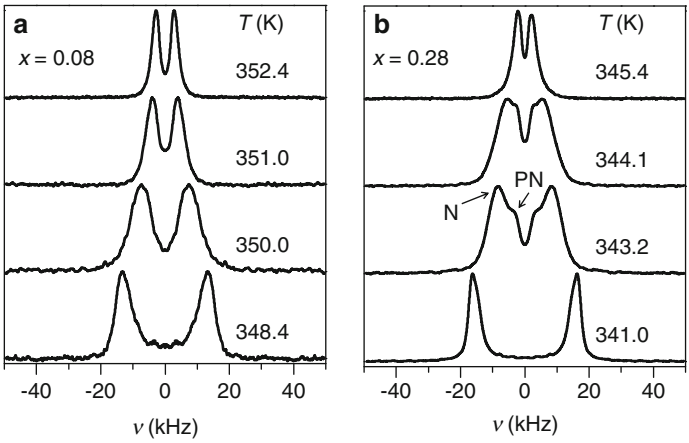

Fig. 24 Selection of ^{2}H-NMR spectra of side-chain LCEs doped with (**a**) 8 and (**b**) 28 wt% of αD_2-8CB. *Arrows* denote spectral features attributed to paranematic (PN) and nematic (N) phases. Data taken from [3]

Sect. 3.1 with various weight concentrations of αD_2-8CB, i.e. $x_{LC} = 0.28$, 0.08 and 0.006. The last of the listed samples represented a control sample. Although it contained practically no 8CB molecules it underwent the swelling with solvents, which resulted in the extraction of the nonreacted mesogens, the crosslinkers and the short polymer segments, and was thus free of all the additives that might have induced the plasticizing effect.

In Fig. 24, we compare ^{2}H-NMR spectra of the above-mentioned LCEs with $x_{LC} = 0.08$ and $x_{LC} = 0.28$ in the vicinity of their phase transition. It is obvious from the comparison that the behaviour of a highly doped sample appears much closer to below-critical than the behaviour of the LCE with a smaller amount of dopant molecules, i.e. the spectra of the former exhibit significantly broader spectral lines as well as feature coexisting paranematic and nematic peaks at $T_{PN–N}$. Also, the high-temperature splitting (corresponding to the paranematic order parameter) is much smaller for the $x_{LC} = 0.28$ sample than for the $x_{LC} = 0.08$ sample. These observations are in accordance with the outcomes of the quantitative $M_{1,\nu}(T)$ and $M_{2,\nu}(T)$ data analysis, which results in a below-critical $\langle G \rangle / G_C = 0.95 \pm 0.2$ for $x_{LC} = 0.28$ and a supercritical value $\langle G \rangle / G_C = 1.5 \pm 0.2$ for $x_{LC} = 0.08$.

A confirmation of the above finding also follows from the calorimetric measurements. Figure 25 compares the $C_p(T)$ responses of the highly doped $x_{LC} = 0.28$ LCE and the "extracted" control sample $x_{LC} = 0.006$. While the latter is clearly supercritical, as zero latent heat is released at its phase transition, a mismatch between the ac and relaxation runs is detected for $x_{LC} = 0.28$ LCE. The measured latent heat 0.24 ± 0.05 J g^{-1} is in good agreement with the value 0.30 ± 0.05 J g^{-1} calculated by (14) from the parameters obtained in the fit of the $M_{1,\nu}(T)$ and $M_{2,\nu}(T)$ experimental data.

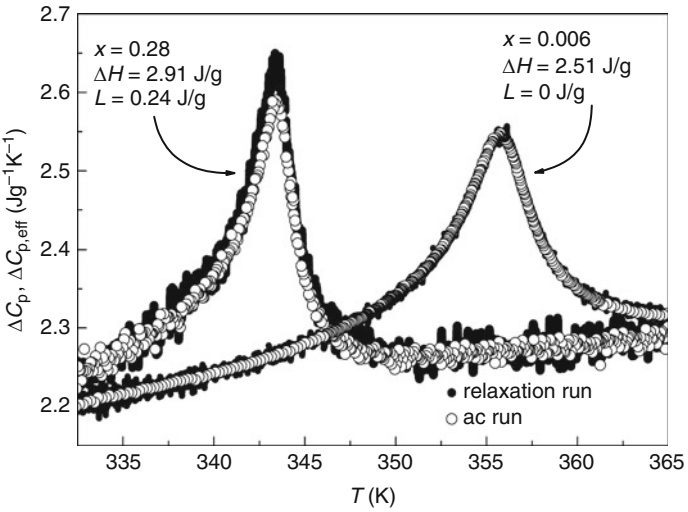

Fig. 25 The ac (*solid symbols*) and relaxation (*open symbols*) run heat-capacity temperature profiles ΔC_p and $\Delta C_{p,eff}$ for nematic side-chain LCEs doped with 0.6 and 28 wt% of αD_2-8CB. The large phase-transition temperature shift of the highly doped sample occurs because the transition temperature of the 8CB (315 K) is significantly lower than that of the undoped LCE (355 K). Data taken from [3]

As demonstrated above, the phase-transition behaviour of the LCEs can be modified even after their synthetic finalization. This is simply achieved by the addition of small molecules, preferably mesogens that mix well with the original mesogens in LCEs so that the liquid-crystalline ordering is preserved. Obviously, if the added mesogens are compatible with a particular LCE network, very large amounts (several tens of weight percent) of liquid crystal can be admixed. Such high concentrations of added mesogen are sufficient to render the originally supercritical transition in the LCEs into a below-critical one.

6 Conclusion

As shown in this review, the critical properties of the PN–N phase transition in LCEs can be controlled by adjusting various chemical and physical parameters during and after their synthesis, e.g. the density of crosslinkers, the externally applied stress during crosslinking, the temperature of the second crosslinking stage and the content of the dopant liquid-crystalline molecules.

Specifically, the variation of these parameters can shift the PN–N transition in the temperature–stress phase diagram along a line of discontinuous transitions, across the single continuous critical point terminating this line, into the so-called supercritical region. Strictly speaking, in the supercritical region no phase transition

is taking place, rather it is a continuous evolution from a high-temperature state to a low-temperature state possessing the same local symmetry.

The heat-capacity and ^{2}H-NMR experiments show that in the case of LCEs this critical point is smeared in both the temperature and mechanical stress directions for both side-chain and main-chain LCEs. The smearing of the critical point is a direct consequence of the heterogeneity of the locked-in mechanical fields and the phase-transition temperatures.

In the subcritical (discontinuous) region of the temperature–stress phase diagram, an on–off or rather a fast TM response is obtained, while in the supercritical region the TM response exhibits a continuous or sluggish response. Thus, LCEs represent highly customizable systems for possible applications as soft organic actuators. The desired type of TM response is directly attainable with a proper adjustment of the basic parameters of their synthesis.

Appendix: Derivation of ^{2}H-NMR Spectral Moments

In accordance with (7) the ^{2}H-NMR spectrum of a perfect LC monodomain is a doublet of sharp resonance peaks that can be written in terms of two shifted Dirac δ-functions,

$$f(\nu; S, \theta) = \frac{1}{2}\left\{\delta\left[\nu + \frac{3}{4}\nu_Q S P_2 \cos\theta)\right] + \delta\left[\nu - \frac{3}{4}\nu_Q S P_2 \cos\theta)\right]\right\}. \tag{15}$$

In LCEs the domains are never ideally aligned, and moreover, they may exhibit a different orientational order S. Thus, a distribution function $w(S,\cos\theta,\varphi;\cos\vartheta)$ is introduced. θ and φ are the spherical coordinates of the domain director $\mathbf{n}$ in the laboratory frame $\mathbf{XYZ}$ with $\mathbf{Z}\|\mathbf{B_0}$ while $\vartheta\angle(<\mathbf{n}>,\mathbf{B_0})$, where $<\mathbf{n}>$ is the LCE uniaxiality axis. Assuming that the distributions of S and $\mathbf{n}$ are uncorrelated, the cumulative ^{2}H-NMR spectrum is given by:

$$F(\nu; \cos\vartheta) = \int\int\int w_S(S)\, w_{\mathbf{n}}(\cos\theta, \phi; \cos\vartheta) f(\nu; S, \theta)\, \mathrm{d}S\, \mathrm{d}\cos\theta\, \mathrm{d}\phi. \tag{16}$$

$w_{\mathbf{n}}$ must possess cylindrical symmetry about <n>. Consequently, at the orientation $\vartheta = 0$ where $\mathbf{c}$ matches $\mathbf{B_0}$, $w_{\mathbf{n},0} = w_{\mathbf{n}}(\vartheta = 0)$ can be expanded in terms of Legendre polynomials $P_l(\cos\theta)$ as:

$$w_{\mathbf{n},0}(\cos\theta) = \frac{1}{4\pi}\sum_{l=0}^{\infty}(2l+1) S_l P_l(\cos\theta). \tag{17}$$

Here $S_l \equiv \langle P_l(\cos\theta)\rangle = 2\pi\int w_{\mathbf{n},0}(\cos\theta) P_l(\cos\theta)\, d\cos\theta$ are the nematic director order parameters [52]. The spectrum is then calculated as a superposition of the two mirrored components, $F(\nu) = 1/2\left[\tilde{F}(\nu) + \tilde{F}(-\nu)\right]$, with:

$$\tilde{F}(\nu;\cos\vartheta) = \frac{2}{9\nu_Q}\sum_{l=0}^{\infty}(2l+1)S_l P_l(\cos\vartheta)\, S_l \int \frac{w_S(S)\, P_l[\chi(\nu,S)]}{S\chi(\nu,S)}\mathrm{d}S, \qquad (18)$$

where $\chi(\nu,S) = \sqrt{1/3(1+8\,\nu/3\,\nu_Q S)}$.

The lineshape analysis can be greatly simplified by considering the moments of the ^{2}H-NMR spectrum $F(\nu)$. By integrating $\tilde{F}(\nu;\cos\vartheta)$ one obtains (10a) and (10b) for the first moment ($M_{\nu,1} \equiv \int \nu\tilde{F}(\nu)\,d\nu$) and for the second moment ($M_{\nu,2} \equiv \int \left(\nu - M_{\nu,1}\right)^2 \tilde{F}(\nu)\,d\nu$).

References

1. Warner M, Terentjev EM (2003) Liquid crystal elastomers. Clarendon, Oxford
2. Selinger JV, Jeon HG, Ratna BR (2002) Isotropic-nematic transition in liquid-crystalline elastomers. Phys Rev Lett 89:225701
3. Lebar A, Kutnjak Z, Žumer S, Finkelmann H, Sánchez-Ferrer A, Zalar B (2005) Evidence of supercritical behavior in liquid single crystal elastomers. Phys Rev Lett 94:197801
4. Cordoyiannis G, Lebar A, Zalar B, Žumer S, Finkelmann H, Kutnjak Z (2007) Criticality controlled by cross-linking density in liquid single-crystal elastomers. Phys Rev Lett 99:197801
5. Cordoyiannis G, Lebar A, Rožič B, Zalar B, Kutnjak Z, Žumer S, Brömmel F, Krause S, Finkelmann H (2009) Controlling the critical behavior of paranematic to nematic transition in main-chain liquid single-crystal elastomers. Macromolecules 42:2069–2073
6. Küpfer J, Finkelmann H (1994) Liquid-crystal elastomers – influence of the orientational distribution of the cross-links on the phase-behavior and reorientation processes. Macromol Chem Phys 195:1353–1367
7. Krause S, Zander F, Bergmann G, Brandt H, Wertmer H, Finkelmann H (2009) Nematic main-chain elastomers: coupling and orientational behavior. C R Chim 12:85–104
8. de Gennes PG, Prost J (1993) The physics of liquid crystals. Oxford Science, Oxford
9. Gramsbergen EF, Longa L, de Jeu WH (1986) Landau theory of the nematic isotropic-phase transition. Phys Rep Rev Sect Phys Lett 135:195–257
10. Rosenblatt C (1981) Magnetic-field dependence of the nematic-isotropic transition-temperature. Phys Rev A 24:2236–2238
11. Boamfă MI, Viertler K, Wewerka A, Stelzer F, Christianen PCM, Maan JC (2003) Magnetic-field-induced changes of the isotropic-nematic phase transition in side-chain polymer liquid crystals. Phys Rev E 67:050701(R)
12. Helfrich W (1970) Effect of electric fields on temperature of phase transitions of liquid crystals. Phys Rev Lett 24:201–203
13. Ostapenko T, Wiant DB, Sprunt SN, Jákli A, Gleeson JT (2008) Magnetic-field induced isotropic to nematic liquid crystal phase transition. Phys Rev Lett 101:247801
14. Iannacchione GS (2004) Review of liquid-crystal phase transitions with quenched random disorder. Fluid Phase Equilibria 222:177–187
15. Disch S, Schmidt C, Finkelmann H (1994) Nematic elastomers beyond the critical-point. Macromol Rapid Commun 15:303–310
16. Clarke SM, Hotta A, Tajbakhsh AR, Terentjev EM (2001) Effect of cross-linker geometry on equilibrium thermal and mechanical properties of nematic elastomers. Phys Rev E 64:061702
17. Schatzle J, Kaufhold W, Finkelmann H (1989) Nematic elastomers – the influence of external mechanical-stress on the liquid-crystalline phase-behavior. Makromol Chem 190:3269–3284

18. Greve A, Finkelmann H (2001) Nematic elastomers: the dependence of phase transformation and orientation processes on crosslinking topology. Macromol Chem Phys 202:2926–2946
19. Assfalg N, Greve A, Finkelmann H (1999) Influence of a mechanical field on the liquid crystalline to isotropic phase transformation. Mol Cryst Liq Cryst Sci Technol Sect A 330:1675–1683
20. Mitchell GR, Davis FJ, Guo W (1993) Strain-induced transitions in liquid-crystal elastomers. Phys Rev Lett 71:2947–2950
21. Finkelmann H, Greve A, Warner M (2001) The elastic anisotropy of nematic elastomers. Eur Phys J E 5:281–293
22. Kaufhold W, Finkelmann H, Brand HR (1991) Nematic elastomers. 1. Effect of the spacer length on the mechanical coupling between network anisotropy and nematic order. Makromol Chem 192:2555–2579
23. Verwey GC, Warner M (1997) Nematic elastomers cross-linked by rigid rod linkers. Macromolecules 30:4196–4204
24. Brand HR, Kawasaki K (1994) On the macroscopic consequences of frozen order in liquid single-crystal elastomers. Macromol Rapid Commun 15:251–257
25. Petridis L, Terentjev EM (2006) Nematic-isotropic transition with quenched disorder. Phys Rev E 74:051707
26. Kraftmaker YA (1962) Zh Prikl Mekh Tekh Fiz 5:176
27. Handler P, Mapother DE, Rayl M (1967) AC measurement of the heat capacity of nickel near its critical point. Phys Rev Lett 19:356–358
28. Sullivan PF, Seidel G (1968) Steady-state, ac-temperature calorimetry. Phys Rev 173:679–685
29. Garland CW, Nounesis G (1994) Critical-behavior at nematic smectic – a phase-transitions. Phys Rev E 49:2964–2971
30. Kutnjak Z, Petzelt J, Blinc R (2006) The giant electromechanical response in ferroelectric relaxors as a critical phenomenon. Nature 441:956–959
31. Yao H, Ema K, Garland CW (1998) Nonadiabatic scanning calorimeter. Rev Sci Instrum 69:172–178
32. Widom B, Rowlinson JS (1970) New model for study of liquid-vapor phase transitions. J Chem Phys 52:1670–1684
33. Vaz NA, Vaz MJ, Doane JW (1984) Molecular ordering and motion within the smectic-E phase – ^{2}H NMR-study. Phys Rev A 30:1008–1016
34. Golemme A, Žumer S, Doane JW, Neubert ME (1988) Deuterium NMR of polymer dispersed liquid-crystals. Phys Rev A 37:559–569
35. Lebar A, Kutnjak Z, Tanaka H, Zalar B, Žumer S (2008) Phase separation in nematic microemulsions probed by one-dimensional spectroscopic deuteron magnetic resonance microimaging. Phys Rev E 78:031707
36. Domenici V, Ambrožič G, Čopič M, Lebar A, Drevenšek-Olenik I, Umek P, Zalar B, Zupančič B, Žigon M (2009) Interplay between nematic ordering and thermomechanical response in a side-chain liquid single crystal elastomer containing pendant azomesogen units. Polymer 50:4837–4844
37. Feio G, Figueirinhas JL, Tajbakhsh AR, Terentjev EM (2008) Critical fluctuations and random-anisotropy glass transition in nematic elastomers. Phys Rev B 78:020201(R)
38. Figueirinhas JL, Cruz C, Filip D, Feio G, Ribeiro AC, Frere Y, Meyer T, Mehl GH (2005) Deuterium NMR investigation of the biaxial nematic phase in an organosiloxane tetrapode. Phys Rev Lett 94:107802
39. Zalar B, Gregorovič A, Blinc R (2000) Interlayer molecular exchange in an anticlinically ordered chiral liquid crystal. Phys Rev E 62:R37–R40
40. Feio G, Figueirinhas JL, Tajbakhsh AR, Terentjev EM (2008) Critical fluctuations and random-anisotropy glass transition in nematic elastomers. Phys Rev B 78:020201
41. Yusuf Y, Ono Y, Sumisaki Y, Cladis PE, Brand HR, Finkelmann H, Kai S (2004) Swelling dynamics of liquid crystal elastomers swollen with low molecular weight liquid crystals. Phys Rev E 69:021710

42. Abragam A (1961) Principles of nuclear magnetism. Oxford University Press, New York
43. Zalar B, Lavrentovich OD, Zeng H, Finotello D (2000) Deuteron NMR investigation of a photomechanical effect in a smectic-A liquid crystal. Phys Rev E 62:2252–2262
44. Pschorn U, Spiess HW, Hisgen B, Ringsdorf H (1986) Deuteron NMR-study of molecular order and motion of the mesogenic side groups in liquid-crystalline polymers. Makromol Chem 187:2711–2723
45. Zalar B, Blinc R, Albert W, Petersson J (1997) Discrete nature of the orientational glass ordering in Na1-xKxCN. Phys Rev B 56:R5709–R5712
46. Vilfan M, Apih T, Gregorovič A, Zalar B, Lahajnar G, Zumer S, Hinze G, Bohmer R, Althoff G (2001) Surface-induced order and diffusion in 5CB liquid crystal confined to porous glass. Magn Reson Imag 19:433–438
47. Cowan B (1997) Nuclear magnetic resonance and relaxation. Cambridge University Press, Cambridge
48. de Gennes PG (1975) One type of nematic polymers. C R Acad Sci Ser B 281:101–103
49. Küpfer J, Finkelmann H (1991) Nematic liquid single-crystal elastomers. Makromol Chem Rapid Commun 12:717–726
50. Jamée P, Pitsi G, Thoen J (2002) Systematic calorimetric investigation of the effect of silica aerosils on the nematic to isotropic transition in heptylcyanobiphenyl. Phys Rev E 66:021707
51. Rožič B, Krause S, Finkelmann H, Cordoyiannis G, Kutnjak Z (2010) Controlling the thermomechanical response of liquid-crystalline elastomers by influencing their critical behavior. Appl Phys Lett 96:111901
52. Boeffel C, Spiess HW (1988) Highly ordered main chain in a liquid-crystalline side-group polymer. Macromolecules 21:1626–1629

Adv Polym Sci (2012) 250: 187–234
DOI: 10.1007/12_2010_105

Published online: 3 December 2010

Order and Disorder in Liquid-Crystalline Elastomers

Wim H. de Jeu and Boris I. Ostrovskii

Abstract Order and frustration play an important role in liquid-crystalline polymer networks (elastomers). The first part of this review is concerned with elastomers in the nematic state and starts with a discussion of nematic polymers, the properties of which are strongly determined by the anisotropy of the polymer backbone. Neutron scattering and X-ray measurements provide the basis for a description of their conformation and chain anisotropy. In nematic elastomers, the macroscopic shape is determined by the anisotropy of the polymer backbone in combination with the elastic response of elastomer network. The second part of the review concentrates on smectic liquid-crystalline systems that show quasi-long-range order of the smectic layers (positional correlations that decay algebraically). In smectic elastomers, the smectic layers cannot move easily across the crosslinking points where the polymer backbone is attached. Consequently, layer displacement fluctuations are suppressed, which effectively stabilizes the one-dimensional periodic layer structure and under certain circumstances can reinstate true long-range order. On the other hand, the crosslinks provide a random network of defects that could destroy the smectic order. Thus, in smectic elastomers there exist two opposing tendencies: the suppression of layer displacement fluctuations that enhances translational order, and the effect of random disorder that leads to a highly frustrated equilibrium state. These effects can be investigated with high-resolution X-ray diffraction and are discussed in some detail for smectic elastomers of different topology.

W.H. de Jeu (✉)
Polymer Science and Engineering, University of Massachusetts, Amherst, MA 01003, USA
e-mail: dejeu.science@gmail.com

B.I. Ostrovskii
Institute of Crystallography, Academy of Sciences of Russia, Leninsky prospect 59, Moscow 117333, Russia
e-mail: ostrenator@gmail.com

Keywords Disorder · Liquid crystal elastomer · Orientational order · Positional order · Random field · X-ray scattering

Contents

Abbreviations

FWHM	Full-width-at-half-maximum
I	Isotropic
LC	Liquid crystal(line)
LSCE	Liquid single crystal elastomer
N	Nematic
NMR	Nuclear magnetic resonance
SANS	Small angle neutron scattering
Sm	Smectic

1 Introduction

Conventional low-molecular-mass liquid crystals (LC) are anisotropic fluids composed of relatively stiff rod-like molecules. The nematic phase is characterized by long-range orientational order in a preferred direction, given by the director **n**.

Nematic LC are well known for their remarkable electro-optical properties, and are now featured in numerous applications as, for example, flat panel color displays. LC order and polymer properties can be combined by linking mesogenic fragments with polymer chains, thus forming LC polymers. The backbone polymer, in turn, can be weakly crosslinked to form a LC elastomer. For the chemical aspects of this process we refer to Kramer et al. [1]. The macroscopic rubber elasticity introduced via such a percolating network interacts with the LC ordering field. This provides a strong shape response when electric, optical, or mechanical fields are applied. An important feature of nematic LC elastomers is that the overall molecular shape varies parallel to the degree and direction of the orientational order.

At the beginning of the nematic polymer age, De Gennes [2] considered nematic elastomer networks as the most promising way to couple the orientational order to overall molecular shape. Nowadays this promise seems to be fulfilled, both experimentally and theoretically. Over the last two decades, a wealth of LC elastomers have been synthesized and characterized, including nematic, diverse smectic, and discotic phases. We refer to Brand and Finkelmann [3] for a review of work up to about 1997 and to the revised edition of the monograph of Warner and Terentjev [4] for more recent information. The potential applications of nematic elastomers include low frequency, large amplitude actuators and transducers driven by weak electric and optical fields, and components of artificial muscles (biomimetic sensors). A recent overview of LC elastomers as actuators and sensors has been published by Ohm et al. [5]. It is clear that the most attractive applications would involve a strong response to a low electric field. This has led to intense investigations of LC elastomers swollen with low-molecular-mass nematic materials. In the course of these studies, large volume changes and volume transitions have been found, as well as quite significant electromechanical effects in moderate electric fields. These aspects are discussed by Urayama [6].

Prior to discussing LC elastomers, we will consider in Sect. 2 in some detail the conformations and chain anisotropy of their polymer counterparts because the polymer backbone generates the shape anisotropy and elastic response of the elastomer network. In this context, note that two different classes of thermotropic LC polymers exist: main-chain and side-chain (comb-like), as depicted in Fig. 1). In side-chain LC polymers, the pendant mesogenic groups are linked to a linear polymer backbone

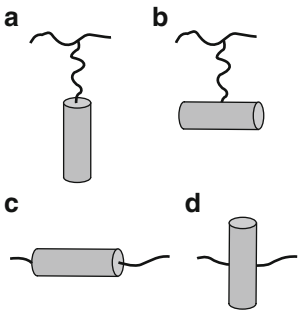

Fig. 1 Various possibilities for connecting a mesogenic side group to a polymer chain: main-chain (**a**, **b**) and side-chain (**c**, **d**)

by an (often flexible) spacer. Main-chain LC polymers are built up by combining rod-like mesogenic fragments and flexible moieties in alternating succession. In a somewhat more modern terminology, one can divide each case into "end-on" and "side-on" LC polymers, which differ in the way the rod-like mesogenic fragment is attached to the spacer. The properties of the nematic phase formed by these two types of polymer appear to be very different. In Sect. 3, these results are extended to the properties and anisotropic shapes of nematic elastomers.

Monomer and polymer smectic LC phases are discussed in Sects. 4 and 5. Smectic systems consist of stacks of liquid layers in which thermally excited fluctuations cause the mean-squared layer displacements to diverge logarithmically with the system size (Landau–Peierls instability). As a result, the positional correlations decay algebraically as $r^{-\eta}$ (η being small and positive) and the discrete Bragg peaks change into singular diffuse scattering with an asymptotic power-law form (see Sect. 4.1). In Sect. 4.2, some background information is summarized about random fields, the presence of which can lead to disorder. For smectic elastomers, the layers cannot move easily across the crosslinking points where the polymer backbone is attached. Consequently, layer displacement fluctuations are suppressed, which under certain assumptions has been predicted to effectively stabilize the one-dimensional (1D) periodic layer structure. On the other hand, crosslinks provide a random network of defects that could destroy the smectic order. Thus, in smectic elastomers two opposing tendencies exist: suppression of layer displacement fluctuations that enhances the translational order, and random quenched disorder that leads to a highly frustrated equilibrium state. These two aspects are discussed in Sect. 4.3. The signature of (dis)order is found in the lineshape of the X-ray peaks corresponding to the smectic layer structure. For experimental aspects of the high-resolution X-ray methods involved we refer to Obraztsov et al. [7]. The experimental situation regarding order/disorder due to crosslinking smectic elastomers is reviewed in Sect. 5.1 for end-on side-chain smectic polymers and includes a discussion of the nematic–smectic transition. In Sect. 5.2, the discussion is extended to main-chain smectic elastomers and to a particular side-on side-chain system in Sect. 5.4. Finally, in Sect. 6 some conclusions and an outlook are given.

2 Liquid-Crystalline Polymers

2.1 Conformation and Structure

When LC fragments are covalently linked to a polymer chain, the material acquires the properties of a mesogenic polymer. Such polymeric liquid crystals have an intrinsic conflict between the drive of the backbone to adopt a random coil conformation and the tendency to LC order associated with the mesogenic units. Flexibility of the backbone chain as well as of the connecting spacer is essential to give the

mesogenic cores enough freedom to self-assemble into LC phases [8–10]. Ordinary polymers as well as LC polymers in the isotropic phase adopt an overall spherical shape, i.e., their gyration volume is a sphere. By contrast, small angle neutron scattering (SANS) measurements of LC polymers in their mesomorphic state indicate that the backbone conformation deviates from a three-dimensional (3D) Gaussian random coil into a prolate or oblate shape [11–13]. The anisometric shape formed by the backbone can be expressed by the main components $R_{g//}$ and $R_{g\perp}$ of the radii of gyration tensor with respect to the nematic director **n** (see Fig. 2).

Nematic polymers are qualitatively identical to their simple low-molar-mass counterparts. At elevated temperatures, highly fractioned LC polymers display a first-order transition from the nematic to the isotropic phase. In both types of system there is a jump in the scalar orientational order parameter. The orientational order of the rod-like mesogenic fragments of the polymers is rather similar as for classical nematics. It can be directly measured using nuclear magnetic resonance (NMR) spectroscopy, infrared dichroism of selective absorption bands, optical birefringence and some others methods [14]. At lower temperatures a nematic–smectic-A phase transition may take place. The smectic-A order parameter is a 1D density wave that is parallel to layer normal (director **n**). The features of smectic ordering can be revealed by high resolution X-ray diffraction, as discussed in Sect. 5.

The main tool for determining the actual conformation of the polymer backbone is SANS of selectively deuterated samples [15, 16]. Upon decreasing the temperature it is possible to align the nematic phase by an external magnetic field or by mechanical stretching. Subsequently, the shape of the polymer chain and its anisotropy can be determined from the two-dimensional (2D) SANS patterns. The contrast of SANS is determined by proper deuterization of the sample, while the intensity decay with the scattering vector **q** reflects the coil anisotropy and the effective rigidity of the constituting fragments. Generally, for long enough chains described by Gaussian statistics, the mean square end-to-end vector can be written as:

$$\langle R_i R_j \rangle = \frac{1}{3} l_{ij} L, \tag{1}$$

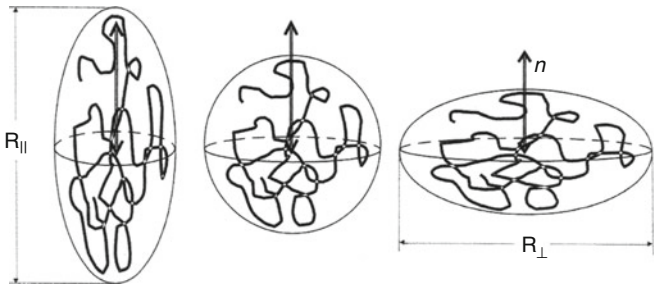

Fig. 2 Various shapes of the gyration tensor spheroid with main components $R_{g//}$ and $R_{g\perp}$. The nematic director is indicated by **n**. Side groups are omitted for clarity (after [4])

where l_{ij} is the effective step lengths tensor and L the contour length of the chain. For conventional nematic or smectic LC polymers of uniaxial symmetry this expression reduces to the main components of the radii of gyration and step lengths tensor with respect to **n**: $R_{g//}$, $R_{g\perp}$ and $l_{//}$, $l_{\perp}$, respectively. The average value of the contour length of the chain is given by $L = Na$, in which N is the average number of monomers in the chain and a the monomer size. Knowing these values, the main components of the step length tensor $l_{//}$ and $l_{\perp}$ can be determined. In main-chain polymers, the measured anisotropy $l_{//}/l_{\perp} = (R_{g//}/R_{g\perp})^2$ is generally very large. The anisotropy induced in the backbones of side-chain polymers is much smaller and often is oblate, $l_{//}/l_{\perp} < 1$. Many macroscopic properties, for example the optical and dielectric anisotropy, follow the order of the mesogenic rods. However, for polymer networks the backbone anisotropy is of primary importance because it causes the dramatic elastic response. In the next section, we give a brief overview of the essential results obtained so far for chain anisotropies of the various classes of LC polymers.

2.2 *Chain Conformation of "End-On" Side-Chain Polymers*

For "end-on" side-chain LC polymers, the coupling of the backbones with the ordering field of the mesogenic rod-like fragments varies over a wide range depending on the flexibility of the backbone, the spacer, and the rod–rod interactions. Possibly this explains why these mesogenic polymers exhibit practically the same wealth of LC polymorphism as their low-molar-mass counterparts, including smectic, hexatic, and crystalline phases [10, 17–19].

SANS results on several nematic polyacrylates indicate that the backbone preferably adopts a weakly prolate shape with $R_{g//}/R_{g\perp}$ approximately equal to 1.2–1.5, i.e., the average direction of the backbone is parallel to **n** [10, 20] and is imposed by the alignment of the mesogenic side groups (Fig. 3a). These observations have been confirmed by NMR studies of LC polyacrylates [23]. This type of prolate conformation of the backbone is also typical for nematic polysiloxane-based end-on polymers, especially when the spacer is relatively short. However, less flexible LC polymethacrylates with the same side-chain and spacer length tend to coil up in the nematic phase in a subtle oblate configuration (side-chains preferably perpendicular to the backbone) [11, 12]. In the smectic phase, both acrylates and methacrylates have an oblate configuration and the anisotropy becomes even more pronounced: $R_{g//}/R_{g\perp}$ is approximately 0.3–0.5 [12, 24] (Fig. 3b). The backbones are to some extent confined in 2D between the smectic sublayers of the mesogenic cores [22]. Furthermore, the backbone statistics differ in the directions parallel and perpendicular to the director. In the perpendicular direction, the mean square of the radius of gyration $\left\langle R_{g\perp}^2 \right\rangle$ is proportional to the degree of polymerization, indicating a trend towards a Gaussian walk in the plane of layers. Parallel to the director, the chains show a rod-like behavior, which corresponds to crossing defects, i.e., backbones hopping from one layer to another [24] (Fig. 3b). Such a behavior has already

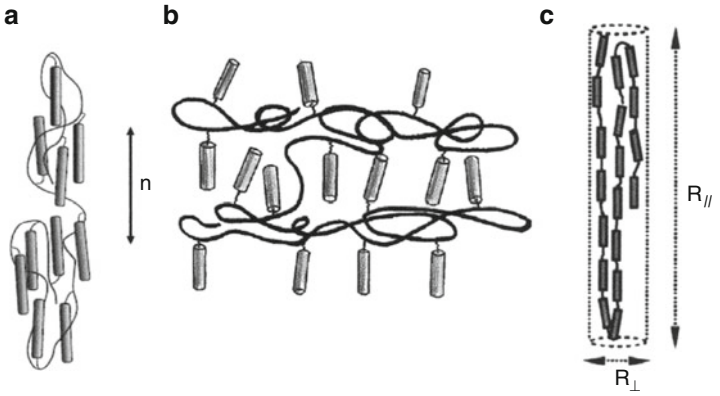

Fig. 3 Side-chain LC polymer with (**a**) prolate nematic conformation and (**b**) oblate smectic conformation. (**c**) Representation of two hairpin defects confined to a long, thin cylinder (after [21, 22])

been examined theoretically [25–27]. According to these models, a confined backbone can cross a mesogenic sublayer, creating a local distortion of the smectic layers. A typical distance between two adjacent side groups along a backbone (say 0.5 nm) is factor of six smaller than a typical layer spacing. This implies that for an oblate configuration about six side-chains do not fit into the smectic lamellae at each crossing event. Hence, a sufficiently large density of crossing defects would induce a stressed state of the smectic layers.

A special case of inversion of the backbone anisotropy was reported for LC polyacrylate with cyano-terminated side groups possessing a low-temperature re-entrant nematic phase [13]. The phase sequence with decreasing the temperature is: nematic–smectic-A_d–re-entrant nematic. In the smectic-A_d phase with partial overlap of antiparallel mesogenic cores, the packing in the area of the terminal chains will be less dense than in a conventional monolayer smectic-A phase. SANS results indicate an oblate backbone conformation in both the nematic and the smectic-A_d phase, which transforms to prolate in the re-entrant nematic phase. X-ray measurements indicate that the change in backbone conformation takes place in a small pretransitional smectic-A_d region in the re-entrant nematic phase [28]. Similar behavior has been observed for highly fractioned polyacrylates with phenyl benzoate side groups possessing a low-temperature re-entrant nematic phase [29]. Though distinct from the above-mentioned cyano-terminated polyacrylates, whose phase behavior is determined by dipolar frustrations [30–32], the same type of the changeover of the backbone conformation occurs. Thus, an end-on LC polymer can possess in the nematic phase opposite types of backbone anisotropy (oblate and prolate) with varying temperature or phase sequence. Evidently, for a specific LC polymer the backbone conformations are very sensitive to the steric confinement introduced by the mesogenic rod–rod interactions.

2.3 Chain Conformation of Main-Chain Polymers

During the last two decades, main-chain LC polymers have been intensively studied by means of SANS, in particular materials based on polyesters and polyethers [21] with relatively long flexible spacers (8–11 carbon atoms). SANS measurements in the isotropic phase of a series of polyesters of different molecular mass [33] indicate $\langle R_g^2 \rangle$ to be proportional to the degree of polymerization. This provides proof of the Gaussian character of the main chain in the isotropic phase, with a persistence length, l, of 1.6 nm, which is close to that of well-known flexible polymers (0.8–1 nm). In spite of the large fraction of rod-like mesogenic fragments, the main chain remains rather flexible.

In the nematic phase, SANS patterns of oriented samples show extremely anisotropic chain conformations, the chain size parallel to **n** being about an order of magnitude larger than in the perpendicular direction [34–36]. For example, D'Allest et al. [34] report a ratio of gyration radii as large as $R_{g//}/R_{g\perp} \approx 8$, giving for the ratio of step lengths, $l_{//}/l_{\perp} \approx 60$. Under these conditions, whole chains are forced into an elongated shape: short chains unfold and become nearly rod-like while longer chains can show rapid reversals of chain direction – so-called hairpin defects (Fig. 3c). The formation of hairpins recovers part of the entropy initially lost during the chains straightening, due to their random placements along the chain contour length. Upon decreasing the temperature, hairpin defects become exponentially unlikely and their increasing separation causes the effective step length $l_{//}$ to grow with the nematic order [35, 37, 38].

The number of hairpins in a nematic main-chain polymer is given by $L/2H$, where L is the average contour length of the chain and $2H$ its dimension parallel to **n**. SANS of both polyesters [35] and polyethers [21] gives similar results: the polymer chains are confined in very long ($2H \approx 20$–35 nm), thin ($R \approx 0.8$–1.8 nm) and well-oriented (order parameter $P_2 \approx 0.8$–0.9) cylinders (see Fig. 3c). The number of hairpins for such a cylinder varies from one to two. We conclude that, in contrast to the situation in the isotropic phase, in the nematic phase the chain organization of main-chain polymers is very different from that of conventional flexible polymers. The chain conformation appears to be effectively fully extended.

Apart from hairpins, other types of defect can be present in main-chain polymers (see Fig. 4). First, we note that chain ends represent a source of the local distortion of the director field [39]. Furthermore, a certain number of hairpins could become entangled. In contrast to standard hairpins, these kinds of defect cannot be removed by applying mechanical stress. Such entangled hairpins can easily suppress chain reptation and thus represent a source of (physical) crosslinking in the polymer matrix. Although not being quenched, as crosslinks in elastomer networks they introduce local sources of random orientational disorder in the director field.

Main-chain polymers seem to have little tendency to smectic phases. Only relative recently has the synthesis been reported of some main-chain systems with a direct transition from the isotropic to either a smectic-A [40, 41] or a smectic-C

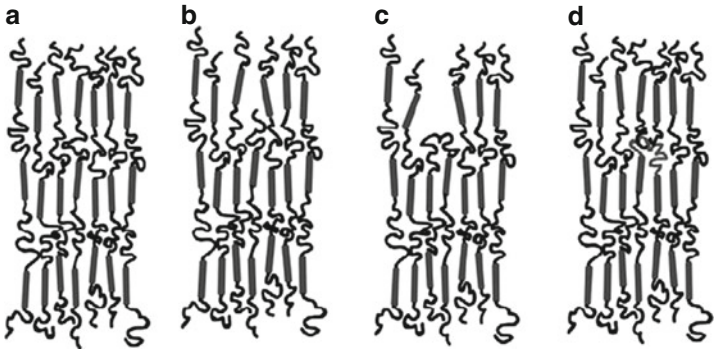

Fig. 4 Cartoons of a main-chain smectic polymer: (**a**) standard picture, (**b**) end defect, (**c**) hairpin, and (**d**) entangled hairpin

phase [42, 43]. X-ray study of these polymers and elastomers will be discussed in Sect. 5.2. In smectic main-chain polymer systems the chains connect neighboring smectic layers. As a result, any defects of the polymer chain directly translate into layer distortions, in contrast to the situation described in Fig. 3b for side-chain polymers.

2.4 Chain Conformation of "Side-On" Side-Chain Polymers

Linking mesogenic rods "side-on" via a spacer to side-chain polymers clearly promotes extension of the backbone along **n**. The symmetry is similar to main-chain systems [44]. However, quantitatively this effect is influenced by the nature of the spacer (see Fig. 1b). For side-on nematic polymers, a short spacer group (four to six carbon atoms in the alkyl chain) leads to considerable stretching of the polymer backbone to give a "jacketed nematic structure" [45] with a strongly prolate backbone conformation [16, 46]. The ratio of gyration radii can reach values $R_{g//}/R_{g\perp} \approx 4$–5, i.e., close to that of main-chain LC polymers. Increasing the spacer length up to about 12 carbon atoms practically uncouples the mesogens from the backbone [47], and the orienting effect of the side groups on the polymer backbone is much weaker. Another way to modify the interaction between the flexible polymer chain and mesogenic rods is to decrease the relative number of mesogenic groups attached to the backbone. For such a "diluted" polymer, SANS measurements demonstrate a dramatic diminishing of the prolate anisotropy with decreasing density of mesogenic groups. The anisotropy of backbone conformation can be reduced from $R_{g//}/R_{g\perp} \approx 2.7$ for mesogenic groups fixed to 55% of the available backbone positions to $R_{g//}/R_{g\perp} \approx 1.1$ for 30%.

Side-on LC polymers with longer spacers in principle allow for smectic phases, but very few examples have been reported so far [48–50]. For the above-mentioned siloxane polymer with 55% mesogenic groups and a spacer length of ten carbon

atoms, SANS indicated a reversible inversion of the backbone anisotropy at the phase transition from nematic to smectic-C. In the high temperature nematic phase, a weak prolate anisotropy, $R_{g//}/R_{g\perp} \approx 1.2$, was measured. At the phase transition from nematic to smectic-C, the backbone anisotropy continuously changes from weakly prolate to spherical (isotropic) and then to strongly oblate: $R_{g//}/R_{g\perp} \approx 0.5$. Intuitively for a side-on type of linking it seems difficult to impose smectic layering and to confine the backbone in between these layers. In fact, neutron diffraction measurements of these polymers show the polymer backbone to be partly distributed in the middle of the mesogenic layers [51]. The observed inversion of the backbone anisotropy in the side-on smectic system can be related to the high flexibility of the polysiloxane chain and the long spacer. The intrinsically conflicting preferred orientations of mesogenic cores, backbones, and aliphatic spacers in these polymer molecules leads to strongly disordered smectic layering.

3 Shape Anisotropy and Orientational Order in Nematic Elastomers

3.1 Structure and Diversity

LC polymers can be covalently crosslinked to form a 3D network leading to a LC elastomer (Fig. 5). Since the synthesis of the first LC elastomer based on a polysiloxane backbone by Finkelmann et al. [52], a number of different types of elastomers

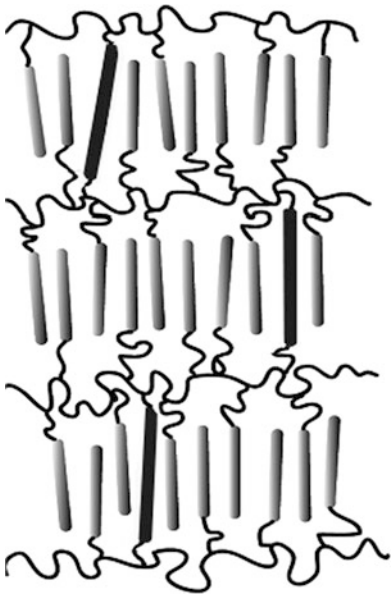

Fig. 5 Representation of an end-on side-chain smectic LC elastomer

have been reported. These include elastomers containing polyacrylates and polymethacrylates with a number of mesogenic pendant groups [53–55]. The concept has been extended to crosslinked main-chain as well as combined main-chain and side-chain materials [53, 54]. The early development of the field is described in various review articles [56–58]; for more recent developments we refer to Kramer et al. [1]. The macroscopic rubber elasticity introduced via the percolating rubbery network interacts with the LC ordering field, which is the basis for the specific properties of LC elastomers. For a low crosslink density, the conformation of the chain segments is not affected and the mesogenic moieties have enough freedom to orient along **n**. Crosslinking between chains prevents their translational motion (flow) and the polymer melt becomes an elastic solid – a rubber or polymer gel. As a consequence, LC elastomers exhibit resistance to the shape changes under external mechanical stress.

Network formation can be induced chemically by copolymerization of polymer chains with a given proportion of reaction positions and bi-, tri-, or multifunctional crosslinking units added to the system. Alternatively, polymerization can be accomplished by addition of a photoinitiator to the system and subsequent exposure to UV light. The size of the crosslinking moieties might be comparable or larger than the constitute mesogenic groups, whereas the linkage can be either stiff (rod-like) or flexible (lengthy terminal alkyl chains). The flexibility of the crosslinker was reported to affect the layer stability in certain side-chain smectic elastomers [7]. Polyacrylate elastomers have low backbone anisotropy and a high glass transition temperature. Methacrylate chains are less flexible, and thus not so sensitive to network formation. The most flexible polysiloxanes form networks with a high elastic response due to the large chain anisotropy, whereas they remain liquid crystalline at room temperature. This explains why the majority of side-chain elastomers synthesized to date utilize siloxane backbones. For main-chain networks, siloxane ring molecules with multifunctional crosslinking positions have been used systematically (see Kramer et al. [1]). However, it is not evident that for such a type of crosslinker all reactive positions are activated. Weak crosslinking of mesogenic polymers appears to have little effect on the range of stability of nematic and smectic phases. However, the elastic properties of the network and the character of long-wavelength excitations of the ordering field depend crucially on whether the LC order was established before or after crosslinking. For example, monodomain nematic elastomers crosslinked in the nematic phase are transparent, indicating suppressed director fluctuations, in contrast to the milky appearance of conventional nematics.

A fundamental question is how many crosslinks are required to transform a polymer melt into a full polymer network (gel) that behaves under external action as a uniform structure. Gelation is a type of connectivity transition that can be described by bond percolation models [59, 60]. Slightly below the transition (gel point c_0), the system consists of a mixture of polydisperse branched polymers. Slightly beyond the gel point, the situation is still approximately the same, but at least one chain percolates through the entire system. Simultaneously, the system, as a whole, acquires a nonzero static shear modulus (response) [61]. The fully developed

network exists far above the percolation threshold c_0. For a system of long linear precursor chains with a degree of polymerization $N \gg 1$ (so-called vulcanization universality class), the mean-field gelation theory predicts $c_0 = 1/(f-1)$, where f denotes the functionality of the constituting monomers. The effective functionality of a long chain with N crosslinkable monomers is very large, $f \cong N$. Hence, at the threshold value $c_0 = 1/(f-1) \cong 1/N \ll 1$ we have on average one crosslink per chain. The end of the gelation regime corresponds to an average of two crosslinks per chain [59, 62]. Moreover, for long precursor chains the number of other chains within their pervaded volume varies, $\sim N^{1/2}$, thus guaranteeing sufficient overlap for most of the crosslinking reaction. For LC elastomers, polymer chains with N of 10^2–10^3 are quite usual, leading to a small threshold density of crosslinks $c_0 \ll 1$. This result is hardly surprising, as, for example, a simple cubic lattice of bonds is known to have a percolation threshold $c_0 \cong$ 1–4. For long chains filling space, the majority of bonds are already linked in polymer chains, reducing the crosslinking bonds to minimal numbers. Experimentally, a volume (molar) fraction of mesogenic-like crosslinks of about 4–5% is sufficient to make a mechanically stable LC elastomer sample (see Finkelmann and Kramer [1]).

3.2 Nematic Rubber Elasticity

Let us consider in more detail the elasticity of nematic rubbers, which is at the heart of understanding their specific properties. Consider a weakly crosslinked network with junction points sufficiently well spaced to ensure that the conformational freedom of each chain section is not restricted. We recall that for a conventional isotropic network the stress–strain relation for simple stretching (compression) of a unit cube of material can be derived as [62, 63]:

$$\sigma = n_s k_B T\left(\lambda - \frac{1}{\lambda^2}\right) = \mu\left(\lambda - \frac{1}{\lambda^2}\right), \tag{2}$$

where σ is the mechanical stress, n_s is the average number of individual chain segments (strands) between successive crosslinks per unit volume, k_B is the Boltzmann constant, $k_B T$ is the thermal energy, μ is the rubber modulus, and λ is the extension ratio. Furthermore, $\mu = n_s k_B T$, which is approximately 10^5–10^6 N/m^2. Equation (2) is derived under the assumption that the chain segments obey Gaussian statistics, i.e., the deformations have an affine character and the material is essentially incompressible. The latter condition is satisfied because the energy scale of rubber elastic energies is determined by the characteristic rubber modulus μ, which is about 10^{-4} times the bulk compressional modulus (10^9–10^{10} N/m^2 for polymeric melts). Thus, the entropic effects of rubber elasticity are insignificant compared with the energies required for a volume change, and rubber deformations occur at constant volume. The average density of crosslinks, c, is proportional to the number

of chain segments, n_s, and inversely proportional to the functionality of the cross-link f (the number of chains emanating from a junction point) such that $c \cong n_s/f$.

An important consequence of (2) is that for $\sigma = \text{constant} > 0$, as the temperature increases, the magnitude of λ diminishes, i.e., the rubber is compressed upon heating and expands upon cooling (opposite to gas behavior). This is a direct consequence of the entropic origin of the elasticity of the polymer networks. The effects of changing external conditions (in the above example, temperature) have been systematically studied for classical isotropic elastomers. As we shall see, even more dramatic effects from a heating–cooling cycle or photo-actuation are emerging for nematic elastomers.

The difference between nematic and isotropic elastomers is simply the molecular shape anisotropy induced by the LC order, as discussed in Sect. 2. The simplest approach to nematic rubber elasticity is an extension of classical molecular rubber elasticity using the so-called neo-classical Gaussian chain model [64]; see also Warner and Terentjev [4] for a detailed presentation. Imagine an elastomer formed in the isotropic phase and characterized by a scalar step length l_0. After cooling down to a monodomain nematic state, the chains obtain an anisotropic shape described by the step lengths tensor l_{ij}. For this case the stress–strain relation can be written as:

$$\sigma = \mu\left(\lambda\frac{l_0}{l_{/\!/}} - \frac{1}{\lambda^2}\frac{l_0}{l_\perp}\right). \tag{3}$$

Equation (3) is close to the expression for a classical elastomer undergoing uniaxial extension. However, instead of an overall pre-factor accounting for the change in chain size, separate factors $l_0/l_{/\!/}$ and $l_0/l_\perp$ occur for the parallel and perpendicular directions, respectively. Now in the absence of external stress, $\sigma = 0$, the system will show spontaneous extension [4, 65]:

$$\lambda_m = (l_{/\!/}/l_\perp)^{1/3}. \tag{4}$$

We conclude that upon cooling from the isotropic to the nematic phase, there must be a spontaneous uniaxial elongation λ_m providing possibilities for temperature-controlled actuation. The overall distortion must be volume preserving. In this example we assumed the chain conformation to be prolate. If, by contrast, the chain backbone was flattened in the nematic phase to an oblate shape, $l_{/\!/}/l_\perp < 1$, then upon entering the nematic phase a contraction would be observed, $\lambda_m < 1$. The spontaneous distortion $\lambda_m = (l_{/\!/}/l_\perp)^{1/3}$ at the isotropic to nematic transition is the most essential result of neo-classical rubber elasticity. For Gaussian chains it provides a direct measure of backbone anisotropy at the given conditions. The step length ratio can be deduced from thermal expansion experiments, $l_{/\!/}/l_\perp = \lambda_m^3$, and compared with data from SANS measurements of selectively deuterated chains.

As an example, we consider oriented samples of side-chain polysiloxane nematic elastomers [66] that show spontaneous elongations up to $\lambda_m = 1.6$ upon cooling through the clearing point (Fig. 6). This corresponds to a rather large step

length anisotropy $l_{//}/l_{\perp} = (R_{g//}/R_{g\perp})^2 = \lambda_m{}^3$ of about 4. The shape change occurs not just at transition but continues to lower temperatures as the orientational order parameter $S(T)$ gets larger and the backbone anisotropy increases. One can simultaneously measure the thermal distortion along the nematic director **n** and the variation of the orientational order parameter, which show a close correspondence [66, 67]. The step length anisotropy is in general a function of $S(T)$, satisfying the linear limit $(l_{//}/l_{\perp}) - 1 \cong \alpha S$ at small S [4]. In main-chain elastomers, the orientational order corresponds directly to the backbone; $\alpha \cong 3$ for a model of freely joint chains. However, for the side-chain elastomers of the end-on type, the values of α are much smaller ($\alpha \leq 0.5$) and can even take small negative values.

Not surprisingly, oriented samples of nematic elastomers composed fully or partly of main-chain polymers show the strongest shape anisotropy [68] of up to 400%. From $\lambda_m = 4 = (l_{//}/l_{\perp})^{1/3}$, we arrive at a ratio of the radii of gyration $R_{g//}/R_{g\perp} = (l_{//}/l_{\perp})^{1/2} = \lambda_m{}^{3/2}$ of about 8. This number is consistent with the characteristic values quoted above for main-chain polymers (Sect. 2.3). Such materials are a prime candidate for use as artificial muscles or mechanical actuators. These examples correspond to a prolate backbone anisotropy, which translates into a spontaneous elongation along **n**. The case of an oblate structure is much less common but has been observed in some side-chain nematic elastomers [53, 54, 69, 70].

To summarize this section, we note that the orientational order in nematic elastomers induces a chain anisotropy, which in turn determines the macroscopic shape of the sample. The manipulation of these shape spheroids by temperature and by electrical, mechanical, and optical fields is at the origin of many of the effects

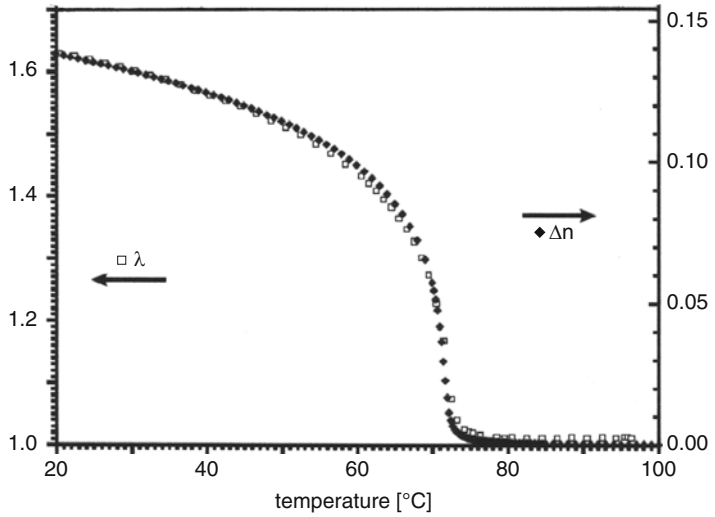

Fig. 6 Spontaneous distortion, λ, and optical anisotropy, Δn, of an elastomer as a function of temperature at a fixed external stress of 4 mN/mm^2 [66]

observed in these materials. Obviously this requires oriented monodomain samples, which will now be discussed in some detail.

3.3 Monodomain "Single Crystal" Nematic Elastomers

Without special precautions, nematic elastomers form nonuniform polydomain textures during fabrication. As a result, such a sample is opaque due to strong light scattering by disoriented domains. Over the years many attempts, stimulated by the analogy with the conventional liquid crystals, have been made to align polydomain nematic elastomers with magnetic or electric fields. These attempts proved to be unsuccessful, leading to the conclusion that the fields are too weak to cause any significant re-alignment. Under these conditions, mechanical stretching is the only remaining appropriate external field. Alignment of a polydomain elastomer by stretching is readily observed with the naked eye: after a certain degree of extension the initially opaque sample becomes clear and fully transparent [52]. The threshold stress, σ_c, is small, of the order of 10^4 N/m^2. The optical transparency of monodomain elastomer samples is rather perfect, in contrast to aligned samples of low-molecular-mass nematics that are still turbid due to thermal director fluctuations. However, for elastomers, **n** is anchored to the rubbery matrix and the director fluctuations are suppressed. This observation gives a hint as to why application of electric or magnetic fields is insufficient to orient nematic elastomers. The field acts on the highly polarizable mesogenic cores and its influence is amplified by the cooperative nature of the long-range orientational order. However, in elastomers the nematic cooperative factor is limited by the net size (4–5 nm) and, compared to low-molecular-mass nematics, much larger electric (magnetic) fields are needed to align the director. In a typical rubber, the average distance between crosslinks is small. Using the characteristic value of the rubber modulus $\mu = n_s k_B T \cong 10^5$ N/m^2 at room temperature ($k_B T \cong 4 \times 10^{-21}$ J), the average separation is $n_s^{-1/3} \cong 4$ nm. Mechanical fields act directly on the polymer network as a whole, and thus the reorientation of the mesogenic cores linked to the backbones is much easier than by electric or magnetic fields.

A small mechanical strain, $\varepsilon = \lambda - 1 \cong 10\%$, acting directly on the polymer backbones, is enough to align the mesogenic cores. These then can be crosslinked to create a highly ordered elastomer monodomain. A very successful procedure along these lines is the two-step crosslinking process by Kupfer and Finkelmann [71, 72], who developed an important yet simple technique for making so-called liquid single crystal elastomers (LSCE). Chains are first lightly crosslinked in the isotropic swollen state. These are then stretched in a uniaxial fashion and the solvent is slowly removed while a second crosslinking proceeds in the aligned nematic state. After this reaction is complete, the stress is removed and the system becomes a clear monodomain. Its stability is remarkable, even after heating to the isotropic phase and cooling back down to the nematic state. Hence, the overall director orientation is "imprinted" by the second crosslinking step, which provides the

required memory. Depending on whether the final crosslinking is done in the isotropic or the nematic phase, the material emerging has different properties. In particular, when the crosslinking is done in the nematic phase, this information is fixed in the vicinity of the crosslinking points leading to "frozen-in" orientational order. Some variants of preparing monodomain nematic elastomers combining crosslinking with the mechanical stretching have also been reported [73].

An alternative strategy for producing well-oriented nematic elastomer samples makes use of polymeric liquid crystals containing a photo-initiator. First, a uniform nematic orientation is obtained using standard means like an aligned polyimide substrate or a magnetic field, which is subsequently fixed by photocrosslinking using UV radiation. An overview of these methods is given by Ohm et al. [5]. Recent measurements of the complex shear modulus of aligned samples prepared by photocrosslinking indicate that the polymer strands possess Gaussian statistics [74]. By contrast, elastomer samples prepared by the two-step crosslinking process are more stretched. In the latter case, the chain segments show deviations from a Gaussian distribution. Though these results need further confirmation, they do question the applicability of linear nematic rubber elasticity (based on Gaussian statistics) to elastomer samples prepared by stretching in the nematic phase.

The equilibrium elastic properties of monodomain nematic rubbers have been well studied, both theoretically and experimentally [4, 75, 76]. Of fundamental interest is the relative rotation of the two subsystems, the mesogenic parts and the network [77], which plays a crucial role in understanding the response of nematic elastomers to external fields. In low-molecular-mass nematics, the internal orientational degrees of freedom are determined by the director field $\mathbf{n}(\mathbf{r})$. Any distortion of the director field is energetically unfavorable and is penalized by the Frank elastic energy density, $K(\nabla \boldsymbol{n})^2$. In nematic networks, the antisymmetric part of the strain is also present, expressed by the local rotation vector of the network $\Omega(\mathbf{r})$. It contributes to the total elastic energy F when Ω deviates from the director rotation vector $\omega = [\mathbf{n} \times \delta\mathbf{n}]$, leading to $\Delta F \sim D_1[\mathbf{n} \times (\Omega - \omega)]^2$. Model expressions for elastomer elastic constants show, apart from the rubber elastic energy $\mu = n_s k_B T$, a dependence on the backbone step lengths anisotropy $D_1 \sim \mu(l_{//}/l_{\perp} - 1)^2$. Quite naturally, the effects of the relative network rotations become insignificant if the elastomer anisotropy diminishes. Thus, a deviation of Ω from ω costs energy, and this relative rotation is at the origin of a number of unique orientational effects in nematic elastomers.

Director reorientation in monodomain nematic elastomers by an external stress perpendicular to $\mathbf{n}$ leads to an extraordinary phenomenon [71, 72, 78]. For intermediate strain values, a shape change costs very little energy. In the stress–strain diagram a plateau region is observed with a very small slope close to zero. Qualitatively the system behaves as if the deformation energy is compensated by the anisotropic reshaping of the backbone coil. This phenomenon has been interpreted as "soft" or "semi-soft" elasticity [79–81]. Consider a nematic network with its director initially oriented along the z-axis. The sample is first subjected to large stretching in the perpendicular x-direction, and then to a slight xz-shear. Using symmetry arguments, coupling of director rotation to the strain leads to zeros in the

shear modulus when the large initial stretching takes the elastomer to the onset or end of director rotation. Recent dynamic light-scattering experiments indeed demonstrate that the onset of the semi-soft plateau is associated with a dynamic soft mode [82]. With increasing strain perpendicular to the director, the relaxation rate of the nematic director fluctuations decreases to a very small value at the onset of the soft elastic response. At this point the director becomes unstable and starts to rotate. An alternative explanation of the above phenomenon has been given on the basis of the macroscopic dynamics of nematic elastomers in the nonlinear regime [76, 83].

3.4 Nematic–Isotropic Transition

Phase transitions in liquid crystals have long been attractive for the general physics community because of the wealth of symmetry-breaking scenarios enabling tests of modern theories of phase transition (see [84] and references therein). The presence of a polymer network in nematic elastomers brings truly new aspects to this seemingly well-known area. First, there is a large spontaneous shape change associated with the nematic–isotropic (N–I) transition in monodomain LC elastomers. Second, the N–I transition no longer exists in the LSCEs prepared according to the two-step crosslinking process (Sect. 3.3) once the concentration of crosslinks exceeds a certain number. According to the experiments of Cordoyiannis et al. [85], this number corresponds to a fraction of about 12% of active groups of the polymer backbone. In analogy to the usual gas–liquid critical point, the N–I transition in such a LSCE is "beyond the critical point", i.e., in the supercritical region where no difference between nematic and isotropic phases exists. In low-molecular-mass liquid crystals and in LC polymers, this transition is first order with a jump of the orientational order parameter $S(T)$ and the entropy $\Sigma(T)$ at the clearing temperature T_{NI}. During the last two decades, experiments on various types of LC elastomers showed that both $S(T)$ and the spontaneous strain change smoothly at N–I transition, with no visible first-order discontinuity [86, 87]. Such a behavior could be due either to a strong degree of spatial heterogeneity in the system [88] or to a supercritical character of the N–I transition [89]. Only recently have precise NMR and specific heat measurements revealed a small latent heat and a subtle discontinuity at N–I transition in side-chain LSCEs with a small crosslink density [85]. On increasing the crosslink density, the predominantly first-order N–I transition transforms into a supercritical transition. These data suggest that the critical properties of the N–I transition in LSCEs can be modified by varying the concentration of the crosslinks (Fig. 7). Recently, deuteron NMR and AC calorimetry have been used to also characterize both the orientational dynamics and the N–I transition in main-chain nematic elastomers [90]. Similarly to side-chain LC networks, the N–I transition in main-chain monodomain nematic elastomers shifts from first order to the critical and even to the supercritical regime on increasing the crosslinking density.

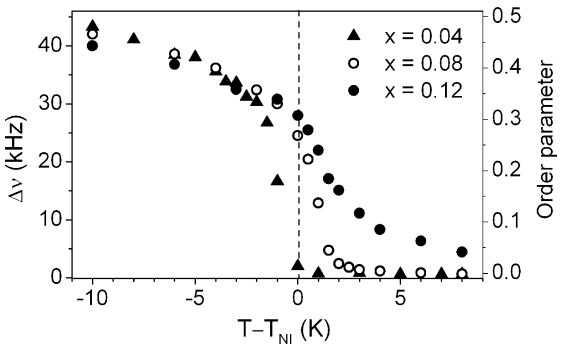

Fig. 7 Orientational order parameter of a nematic main-chain elastomer from D-NMR around the N–I transition for different crosslink concentrations x [90]

The origin of the observed behavior is quite clear: internal stress (independently of its origin) shifts the first-order N–I transition towards the critical point and further into the supercritical regime, characterized by zero latent heat and a continuous $S(T)$ profile. The necessary condition is a linear coupling of the nematic order parameter S with a conjugate field σ that adds a term $\sim -\sigma S$ to the free-energy expansion in the vicinity of the phase transition point [91]. The transition to a supercritical domain occurs whenever σ exceeds the critical value σ_c. In nematic elastomers, σ is the mechanical stress that may be associated with the monodomain state, imprinted internally in the system through the pattern of crosslinks. It could also come from an external field applied to the sample. Another important source of the nonuniform stress in the sample is due to random quenched disorder. In practice, crosslinking agents are always anisotropic and frequently made of fragments that are mesogenic themselves. Thus, one can always identify the direction of anisotropy, which is quenched because the crosslinks are not totally free to rotate under thermal motion [92, 93]. As a result, there is a local preferred direction of orientational and spatial order that acts as a random orienting (and pinning) field. For a more quantitative discussion of the N–I transition we refer to Lebar et al. [94].

From the discussion so far, the natural question arises whether it is possible to create an ideal nematic network without internal stress, in which the orientational order relaxes to zero at high temperatures in the isotropic phase. The actual answer is no, because in any case the random quenched disorder, introduced by crosslinks, is expected to affect the transition. Although the crosslinks are on average randomly functionalized into the polymer backbone, local variations in their density and orientation lead to quenched randomness. This will manifest itself macroscopically as a mechanical random field that induces smearing of the phase transition. Theory predicts different regimes of the N–I transition affected by quenched disorder [93]. The scalar order parameter S is predicted to be homogeneous in space, whereas the director **n** follows equilibrium randomly quenched texture with a characteristic size typical for elastomer domains. Depending on the strength of the disorder, one may

still see the first-order transition or a continuous-like transition with no phase coexistence. In this situation the thermomechanical history of the samples will be of crucial importance. The same is true for smectic elastomers, in which the phase of the density wave can be locked-in by the random field of crosslinks. These latter effects of a random field on phase transitions are considered in more detail in Secs. 4.2 and 5.

4 Order and Disorder in Smectic Systems

4.1 Landau–Peierls Instability

In a 3D crystal, the molecules vibrate around well-defined lattice positions with an amplitude that is small compared to the lattice spacing. As the dimensionality is decreased, fluctuations become increasingly important. Landau and Peierls [95, 96] were the first to show that translational order is destroyed in 1D and 2D systems by thermal fluctuations (see also, for example, [84]). In 3D space, similar arguments can be applied to systems of stacked fluid monolayers such as smectic-A monomeric or polymeric liquid crystals, surfactant membranes, and lamellar block copolymers. In such structures translation of a layer along the z-axis represents a 1D periodicity in a 3D medium with a typical period of 2–3 nm for thermotropic smectics. Elastic deformations in smectics are governed by the Landau–De Gennes free energy that involves two elastic modes: undulation and compression of the layers (see, for example, [97]). The first mode is characterized by the splay elastic modulus K (typically 10^{-11} N). The second constant B (typically 10^7 N/m^2) involves compression/dilatation of the layers. Fluctuations of the layers are described by the displacement field $u(\mathbf{r}) = u_z(r_\perp, z)$, which characterizes the layer displacements along the layer normal in dependence of the in-plane position $r_\perp$. It is noteworthy that a conventional smectic with liquid layers has no resistance to shear, and a term $[\nabla_\perp u(\mathbf{r})]^2$ is not allowed in the deformation energy. In the full spectrum of the layer displacement modes, from long wavelengths to molecular sizes, the long-wavelength fluctuations dominate. This can be understood from the observation that a uniform rotation of the layers (corresponding to infinite wavelength) does not require any energy. In the harmonic approximation, the equipartition theorem gives for each mode of the layer displacement $u(\mathbf{q})$ the mean square value:

$$\left\langle u^2(\mathbf{q})\right\rangle = \frac{k_\mathrm{B}T}{Bq_z^2 + Kq_\perp^4}. \tag{5}$$

Integrating over the full spectrum of displacement modes leads to a mean square layer displacement $\left\langle u^2(r)\right\rangle$ given by (see, for example, [14]):

$$\langle u^2(r)\rangle = \frac{k_B T}{8\pi\sqrt{KB}} \ln\left(\frac{L}{d}\right). \tag{6}$$

The weak logarithmic divergence with the sample size L is known as the Landau–Peierls instability. As a result, for sufficiently large L the fluctuations become of the order of the layer spacing, which means that the layer structure would be wiped out. However, for samples in the millimolar range and typical values of the elastic moduli $K \approx 10^{-11}$ N and $B \approx 10^7$ N/m^2, the layer displacement amplitude $\sigma = \sqrt{\langle u^2\rangle}$ does not exceed 0.5–0.7 nm. For a typical smectic period $d \approx 3$ nm this gives relative displacements $\sigma/d \approx 0.2$; the smectic layers are still well defined. Nevertheless, the displacements are large compared to those of a typical 3D crystal for which:

$$\langle u^2(r)\rangle = \frac{k_B T}{\pi a C}. \tag{7}$$

For a typical value of the elastic modulus $C = 10^{10}$ N/m^2 and a lattice size $a = 0.5$ nm, this leads to $\sigma \approx 0.02$ nm and $\sigma/d \approx 0.04$.

The pair density correlation function – the quantity essentially measured in an X-ray experiment – is defined as:

$$G(\mathbf{r}) = \langle \rho(\mathbf{r})\rho(0)\rangle - \langle \rho(\mathbf{r})\rangle\langle \rho(0)\rangle, \tag{8}$$

where the brackets indicate an average. As a result of the Landau–Peierls instability the correlation function shows a slow algebraic decay $G(r) \sim r^{-\eta}$. Writing $q_0 = 2\pi/d$, the exponent η is given by:

$$\eta = \frac{q_0^2 k_B T}{8\pi\sqrt{KB}}. \tag{9}$$

The resulting order is referred to as quasi-long-range order. It provides a marginal case between true long-range positional order and short-range order. These various types of order are illustrated in Fig. 8.

The scattered intensity $I(q)$ is proportional to the structure factor $S(q)$, the Fourier transform of the correlation function $G(r)$, and thus reflects the nature of the correlations in the system. In the case of long-range order, the correlation function $G(r)$ remains constant as $r \to \infty$. As a result, the Bragg reflections are nominally delta functions, $S(q) \sim \delta(q - q_n)$ at each reciprocal lattice vector q_n, accompanied by weak tails of thermal diffuse scattering $\sim(q - q_n)^{-2}$ (Fig. 8, upper graphs). In practice, the central part of the X-ray peak takes the form of a Gaussian due to the finite size of the ordered domains (grains) and/or the resolution of the setup. Short-range order is represented by an exponentially decaying function $G(r) \sim \exp(-r/\xi)$, in which ξ is the correlation length. The resulting lineshape is a Lorentzian (Fig. 8, lower graphs).

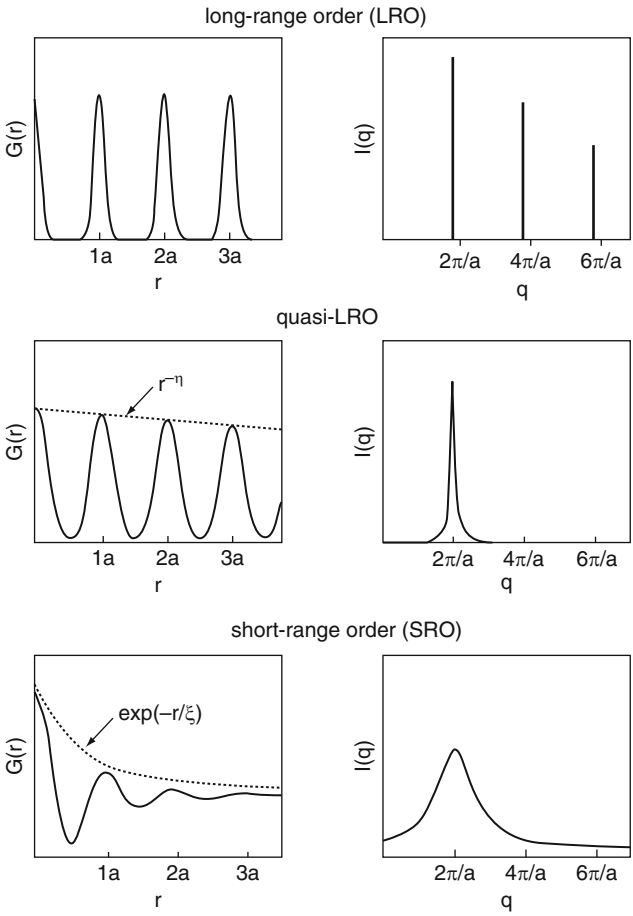

Fig. 8 Representation of correlation function, $G(r)$, and X-ray intensity, $I(q)$, for long-range order, algebraically decaying quasi-long-range order, and short-range order

Algebraically decaying order in smectics can be revealed by X-ray diffraction (Fig. 8, middle graphs). The scattering from the smectic density modulation produces X-ray peaks in reciprocal space along the layer normal at a scattering vector $q_n = nq_0$, n being an integer. As shown by Caillé [98, 99], the algebraic decay of the positional correlations transforms the discrete set of Bragg peaks into the power-law singularities of the form:

$$S(q_\perp = 0, q_z) \propto (q_z - q_n)^{-2+\eta_n}, \tag{10a}$$

$$S(q_\perp, q_z = q_n) \propto q_\perp^{-4+2\eta_n}, \tag{10b}$$

in which;

$$\eta_n = n^2\eta, \tag{11}$$

with η given by (11). This type of lineshape was first reported for low-molecular-mass smectics by Als-Nielsen et al. [100] and then confirmed for various thermotropic [101, 102] and lyotropic lamellar phases [103–105], smectic polymers [106], and lamellar block copolymers [107]. There are a finite number of power-law peaks of the type of (10a): when $\eta_n > 2$ the exponent changes sign and the singularities are replaced by cusp-like peaks. For thermotropic low-molecular-mass smectics, η is small and positive, typically 0.05–0.1 deep in the smectic-A phase. Equation (9) indicates that for less-compressible materials (B large), such as lyotropic smectics and some polymers, η can be even smaller. On the other hand, close to a smectic–nematic transition B can decrease strongly and η might be an order of magnitude larger. When several higher harmonics are present, the quasi-long-range order can be established unambiguously from the scaling relation $\eta_n = n^2\eta$.

Algebraic decaying order is demonstrated in Fig. 9 for a typical smectic elastomer. In a double-logarithmic plot with $q_z - q_n$ still on the x-axis, the characteristic features are a central plateau-like region at small deviations from q_n due to the finite size of the smectic domains, and a power-law behavior in the tails. The latter regions fulfill the scaling law $\eta_n/n^2 = \eta = 0.16 \pm 0.02$, providing a rigorous proof of algebraic decay.

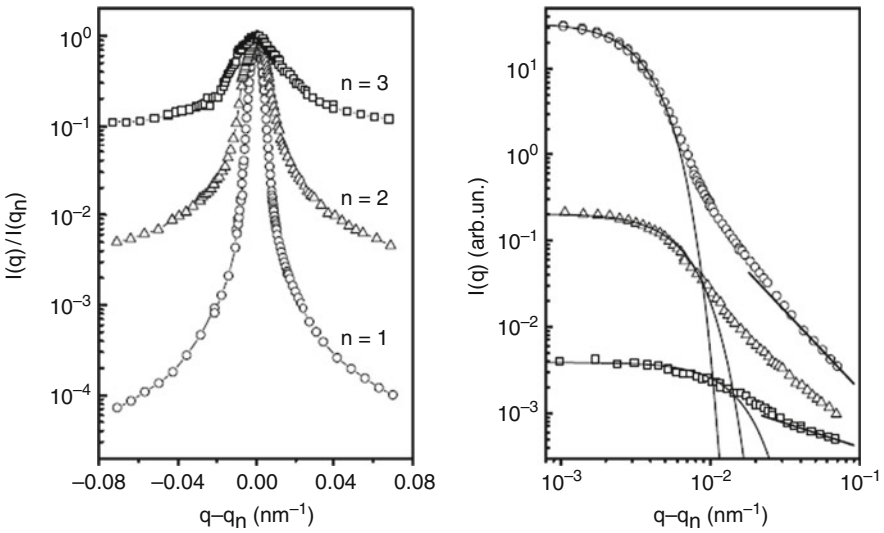

Fig. 9 Three orders of lineshape for the elastomer depicted in Fig. 11 with 10% crosslinks. The wings of the peaks (shown logarithmically for emphasis on the *right*) indicate algebraic decay following $(q - q_n)^{-(2-\eta_n)}$ (*straight lines*) [7]

The various contributions to the X-ray intensity distribution in the vicinity of the Bragg position in smectics have been outlined by Kaganer et al. [102]. Additionally to the finite size of the system, the effects of the mosaic distribution (distribution of the layer normals within the illuminated area) have to be taken into account. At large deviations from q_n we can find the power-law due to the algebraic decay of positional correlations leading to $(q_z - q_n)^{-2+\eta_n}$. At smaller distances from q_n the effect of the mosaic distribution gradually takes over, approximating finally to behavior like $(q_z - q_n)^{-1+\eta_n}$. The central part, including the full-width-at-half-maximum (FWHM), is determined by the residual Bragg peak due to finite-size domains of the sample [99, 108]. The intensity measured in the X-ray experiment can be represented by the convolution of the various factors mentioned [102]:

$$I(\mathbf{q}) = S(\mathbf{q}) \otimes F(\mathbf{q}) \otimes H(\mathbf{q}) \otimes R(\mathbf{q}). \tag{12}$$

$F(\mathbf{q})$ and $H(\mathbf{q})$ stand for the broadening due to the mosaic distribution and due the finite size, respectively, while $R(\mathbf{q})$ describes the resolution function of the setup. Deconvolution of the experimental data provides the required determination of the structure factor $S(\mathbf{q})$.

4.2 Random Disorder

In condensed matter physics, the effects of disorder, defects, and impurities are relevant for many materials properties; hence their understanding is of utmost importance. The effects of randomness and disorder can be dramatic and have been investigated for a variety of systems covering a wide field of complex phenomena [109]. Examples include the pinning of an Abrikosov flux vortex lattice by impurities in superconductors [110], disorder in Ising magnets [111], superfluid transitions of He^3 in a porous medium [112], and phase transitions in randomly confined smectic liquid crystals [113, 114].

Liquid crystals provide beautiful possibilities to study the structural and dynamic effects of quenched disorder. Their algebraic decay of positional correlations gives an interesting starting point, they are experimentally easily accessible, and can be confined within appropriate random porous media. Liquid crystals have been incorporated into the connected void space of an aerogel, which is a highly porous (up to 98% void) fractal-like network of multiply connected filaments of aggregated 3–5-nm diameter silica spheres. Alternatively, quenched disorder can be introduced in a liquid crystal by dispersing a hydrophilic aerosil (nanosize silica particles forming a hydrogen-bonded thiotropic gel). Both methods allow the study of the effects of weak random point forces and torques on the LC order, an idealized disordering mechanism that affects molecular location and orientation in random ways but occupies little physical space. Even at very low density of aerogel or aerosil (about 1–3%), the 1D smectic order is destroyed, in agreement with general theoretical predictions that generic quenched disorder should do so, no

matter how weak [115, 116]. More precisely, if the nematic–smectic phase transition is approached from above, the smectic correlation length does not diverge any more as observed normally, but instead reaches a finite value. Upon cooling through the smectic phase this value saturates at a length scale of the order of 100 nm providing "extended short-range order" [113, 114, 117–119] (see Fig. 10). Note that the correlation length is not limited by some sort of effective "pore size" as if the system has simply been broken up in small pieces. It is rather a result of competition between the randomizing effect of the confinement and the smectic elasticity.

Ordering effects and phase transitions in imperfect crystals are strongly influenced by the types of defects and their mobility (see, for example, [121]). If point defects have a high enough mobility to adjust (rearrange) to changing long-range order, their presence has no qualitative effect on the large-scale properties of the medium. Such weak "annealed disorder" causes only a finite renormalization of the effective parameters of the ordered state, and the phase transition to a less-ordered state remains sharp. In the case of "quenched disorder" the positions of the impurities are fixed in space and time and they produce a much stronger effect. Their effective field is linearly related to the order parameter and violates the symmetry of the ordered state. Under these conditions, defects can destroy the long-range-order in a 3D crystal, leading to a disordered state. Even weak quenched disorder destroys translational order below four dimensions, resulting in exponentially decaying positional correlations [122]. Under certain conditions a continuous transition can occur to a state with the peculiar property of being a glass with many metastable states and at the same time showing Bragg peaks as in conventional crystals – a so-called Bragg glass [123].

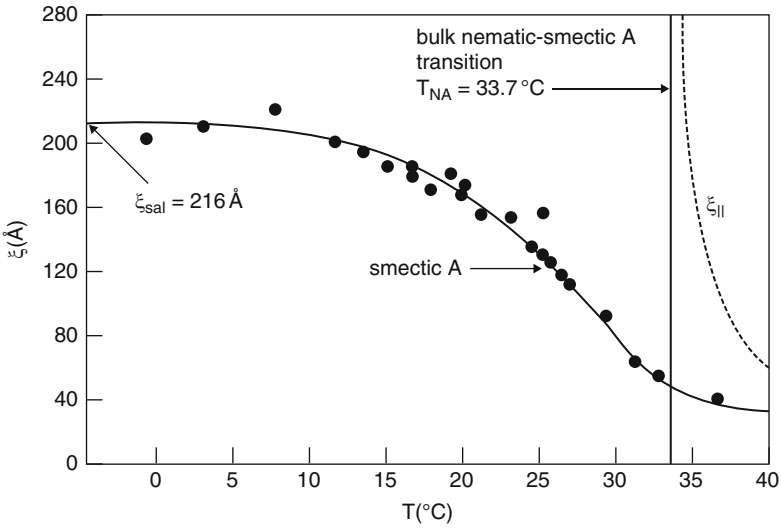

Fig. 10 X-ray correlation length, ξ, for the smectic layer order around the nematic–smectic-A transition (*solid vertical line*) for liquid crystal 8CB confined in 10% aerogels (after [120])

Radzihovsky and Toner [115, 116] studied smectic LC in a random environment, e.g., aerogels, in the framework of the classical Landau–De Gennes model. They introduced additional terms describing a linear coupling of random potentials g(**r**) and V(**r**), with the nematic director **n**(**r**) and smectic order parameter $\psi(\mathbf{r})$, respectively. Analysis of this model identifies two sources of disorder: layer displacement disorder, which represents the tendency of the aerogel to force the smectic layers to particular positions, and orientational (or tilt) disorder, reflecting the inclination of the aerogel to promote particular orientations of the director (and thus of smectic layers). The disorder leads to short-range smectic correlations that fall off exponentially in the direction of the layer normal: $\langle\psi(0)\psi(r)\rangle \propto \exp(r/\xi)$. This should happen even for arbitrarily weak quenched disorder (i.e., arbitrarily low aerogel or aerosil density), in agreement with the diffuse character of the X-ray scattering from the smectic layers in these dispersions [113, 114, 117, 118, 124] (see also Fig. 10). Another theoretical prediction is that a disordered smectic should possess an anomalous length-scale dependence of the elastic moduli. Furthermore, for weak disorder and a certain range of renormalized elastic constants, a sharp phase transition can occur to an orientationally ordered (but elastically distorted) smectic Bragg glass phase. Experimentally, for smectics confined in aerogels the glass-like dynamics and anomalous elasticity observed upon decreasing temperature suggest the presence of such a smectic Bragg glass [113]. However, somewhat surprisingly, such a behavior was not found in aerosils [114], which impose a more gentle distortion of the smectic than aerogels.

In the framework presented so far, the structure factor for X-ray scattering in a randomly disordered system can be written as:

$$S(q) \propto \frac{B_{\text{thermal}}}{1 + \xi_{//}^2(q_z - q_0) + \xi_{\perp}^2 q_{\perp}^2} + \frac{C_{\text{disorder}}}{\left[1 + \xi_{//}^2(q_z - q_0) + \xi_{\perp}^2 q_{\perp}^2\right]^2}. \tag{13}$$

Here, the Lorentzian term represents the (dynamic) thermal layer fluctuations, and the square Lorentzian the (static) variations in the smectic order due to quenched random field. The correlation lengths $\xi_{\Downarrow}$ and $\xi_{\perp}$ describe the extent of local smectic order parallel and perpendicular to **n**, respectively. Equation (13) arrives naturally from the theory of Radzihovsky and Toner [116] but also describes the short-range correlations induced by the quenched disorder in random field Ising magnets [111]. For smectics confined to aerogels, the smectic quasi-long-range order is clearly suppressed by the presence of the last term, which becomes dominant at lower temperatures. However, the situation is less clear for the aerosil networks that are gentler in introducing disorder due to their weaker hydrogen bonding. The latter property could lead to some compliance of an aerosil gel to the smectic elasticity, resulting in partial annealing of the disorder [125, 126]. In the disordered smectic phase, recent studies of smectics confined in an aligned colloidal aerosil gel reveal finite-size domains and power-law tails of diffuse scattering at low temperatures [119]. This situation bridges the gap between smectics confined in aerosils and smectic elastomer networks in which the quasi-long-range translational order survives up to certain concentration of crosslinks [7, 127].

4.3 Fluctuations and Disorder in Smectic Elastomers

In Fig. 1 we summarized the various ways in which LC order and polymer properties can be combined by attaching mesogenic molecules to, or incorporating in, a polymer backbone. Once the backbone polymer is weakly crosslinked to form an elastomer, the resulting macroscopic rubber elasticity interacts with the LC ordering field [4]. In smectic LC elastomers the layers cannot move easily across the crosslinking points where the polymer backbone is attached. Consequently, layer displacement fluctuations are suppressed, which effectively stabilizes the 1D periodic layer structure and could under certain assumptions reinstate true long-range order [128, 129]. On the other hand, the crosslinks provide a random network of defects that could destroy the smectic order [130–132]. Thus, in smectic-A elastomers two opposing tendencies exist: the suppression of layer displacement fluctuations that enhances translational order, and the effect of random disorder that leads to a highly frustrated equilibrium state.

Let us look at the physical origin of the predicted behavior in some more detail. On the continuum level, the coupling between the layer fluctuations and the elastic matrix can be considered as layer pinning by crosslinks, which constitutes a penalty for local relative displacements. This coupling is additive to the ordinary smectic elastic energy of deformations and to the elastic energy of anisotropic rubber network as a whole. The latter contains essentially the five terms expected for a uniaxial solid on the basis of its symmetry. This includes the deformation energy related to the shear elastic moduli perpendicular and parallel to $\mathbf{n}$, C_4 and C_5 respectively, that do not come into play for the liquid smectic layers. This is essentially the physical reason for a possible solid-like elastic response in weakly crosslinked smectic elastomers. The rubber elastic constants are renormalized by the smectic fluctuations and acquire effective values for two bulk (compression) and three shear moduli. The renormalization is determined solely by the rubber elastic parameters: shear modulus and coupling constants. This leads to a combination of four small and one large elastic constant ($C_i/C_3 \ll 1$, $i = 1, 2, 4, 5$), which is very different from conventional solids in which all elastic moduli have about the same large magnitude. A similar situation occurs in the crystal-B phase of liquid crystals (highly anisotropic molecular crystal) in which the Landau–Peierls instability is eliminated due to the presence of a term $C_4 q_\perp^2$ in the elastic energy. Nevertheless, large layer fluctuations are still found because of the small value of this elastic modulus compared to the other modulii [133, 134].

The expression for the free energy of a smectic elastomer as a function of layer displacements is rather complicated. However, it is relatively easy to study its implications for the two limiting cases, $q_z \to 0$ and $q_\perp \to 0$, leading to the following dispersion law for the elastomer phonon modes [129]:

$$\left\langle u^2(\mathbf{q}) \right\rangle_\perp = \frac{k_B T}{B^* q_z^2 + 2C_5^* q_\perp^2 + 2C_5^{\mathrm{eff}} (q_z^4 / q_\perp^2)}, \tag{14}$$

in which B^* and C_5^* are renormalized bulk compression and shear moduli, respectively. The elastic modes now feature a solid-like elastic energy proportional to an overall squared power of q. Consequently, in smectic-A elastomers, long-range positional order in the direction along layer normal could be reestablished due to the coupling of the smectic order to the rubbery network. This should result in Bragg-type diffraction peaks. Though layer displacement fluctuations are suppressed, they are strong enough to contribute to the thermal diffuse scattering in the vicinity of the Bragg peaks, $\sim(q - q_n)^{-2}$. The difference from algebraic decay is that the Caillé exponent η now attains the limit $\eta \to 0$. Because η is typically quite small, this makes the discrimination between Caillé lineshapes and thermal diffuse scattering of a true crystal difficult. The best way to discriminate between these two cases is to look at whether the scaling relation of (11) holds for various harmonics of the smectic layer diffraction, like in Fig. 9.

So far, we have assumed that the crosslinks pin the smectic layers at a number of points but do not disturb the smectic density wave. However, a sufficient large density of crosslinks might lead to layer distortions that could destroy the quasi-long-range order of 1D lamellar lattices [130, 131]. The crosslinks are randomly functionalized into the polymer backbone, and local density variations lead to quenched random disorder. This manifests itself as a mechanical random field that disturbs local layer positions and orientations. The effect of crosslinks on the smectic layer structure can be introduced via a corrugated potential that penalizes deviations of crosslinks from the local layer positions [4, 132]:

$$F_{\text{random field}} = \gamma \int c(\mathbf{r})\psi(\mathbf{r}) \cos\{q_0[z - u(\mathbf{r}) + v_z(\mathbf{r})]\}\mathrm{d}\mathbf{r}. \tag{15}$$

In this equation, γ is the interaction strength, $c(\mathbf{r})$ the crosslink concentration, $\psi(\mathbf{r})$ the smectic order parameter, and $v_z(\mathbf{r})$ the relative displacement of the rubber matrix. Witkowski and Terentjev [132] evaluated (15) for $|\psi(\mathbf{r})| = 1$, which is valid deep in the smectic phase, i.e., far below the smectic–nematic transition. Using the so-called replica trick, they integrated out the rubbery matrix fluctuations and obtained an effective free-energy density that depends only on the layer displacements $u(\mathbf{r})$. Under the restriction that wave vector components along the layer normal dominate over in-layer components, $q_\perp \ll q_z$, and considering only long-wavelength fluctuations, the authors obtained an expression for the mean-square amplitude of the displacement modes that contains a Lorentzian term and a square Lorentzian term like in (13). Though different coefficients come into play, again the first term corresponds to ordinary thermal fluctuations, modified by the coupling of smectic layering to the rubbery matrix, whereas the second term represents the effect of the random field of crosslinks. However, now the induced short-range order is characterized by a correlation length $\xi = (B/2\Lambda)^{1/2}$, where Λ is a coupling constant determined by the strength of interaction between smectic ordering and rubbery matrix. As Λ depends linearly on the volume density of crosslinks c, the relation between correlation length and crosslink density becomes: $\xi \sim c^{-1/2}$. However, in order to use this proportionality, we have to take the percolation

limit of an elastomer into account, i.e., the minimum density of crosslinks, c_0, needed to form a continuous rubbery network (see also Sect. 3.1). The elastic properties of the material should depend on the excess of crosslinks over this minimum, leading to the proportionality $\xi \sim (c - c_0)^{-1/2}$.

In conclusion, in analogy to the general theory for quenched disordered systems we can expect a transition to disorder in smectic-A elastomers for high-enough crosslink concentrations. However, this analogy might fail because in smectic elastomers the crosslinks are not rigidly "frozen" defects, but consist of flexible chains embedded in the slowly fluctuating elastomer gel. This could make the situation different from, for example, smectics confined to aerogel (or aerosil) networks, though the "softer" aerosil analogy might still be appropriate. Evidently, predictions from general theories of quenched disorder, when applied to LC elastomers, have to be treated with severe care. In the absence of theory for random crosslinks embedded in a fluctuating layered system, no definite predictions for the nature of these disordering effects in an elastomer network can be made.

5 Smectic Elastomers

5.1 "Single Crystal" Smectic Elastomers

In this section we will review high-resolution X-ray studies of well-aligned smectic elastomer samples. Recently, siloxane samples [7, 127, 135] were studied, prepared by a two-stage process similar to that described in Sect. 3.3 for nematic LSCEs [136, 137]. In the first step, the sample is slightly crosslinked in the isotropic phase while solvent still abundantly present. Subsequently, the solvent is slowly removed with the sample being kept under a uniaxial load. During this process the isotropic sample is thought to pass through a nematic phase and subsequently becomes smectic. In the transient nematic phase, the director is oriented in the direction of the uniaxial stress, which determines the long direction of the sample (smectic layer normal). This orientation is fixed by the second crosslinking step in the smectic phase.

Thermoelastic measurements on such samples reveal a spontaneous elongation along **n** at the transition to the smectic phase, indicating a prolate polymer backbone conformation in the smectic elastomer [137]. On another hand, SANS results for end-on side-chain polymers in the smectic phase indicate an oblate chain conformation, with the backbone preferentially confined in the plane of the layers (Sect. 2.2). Thus, the chain distribution and macroscopic shape of the smectic elastomer change their sign if crosslinking is made under uniaxial mechanical stress in the isotropic and/or nematic phase. This result is remarkable and indicates that the oblate chain conformation of a smectic end-on polymer can be easily turned into prolate by a low uniaxial extension during solvent evaporation.

When analyzing experimental results, it is important to consider how the smectic elastomer sample was prepared. If the smectic layers are aligned by a surface or an

external field and then crosslinked, we can expect the crosslinks to be in registry with the smectic layers and to stabilize the lamellar structure against layer displacement fluctuations. This situation will facilitate the theoretical prediction [128, 129] that translational order can be enhanced and even become a truly long-range order. If the crosslinking is first made in nematic or isotropic phase, then uniaxially alignment is accomplished to form a monodomain nematic elastomer, and only after that cooled down to the smectic phase, the result will be opposite. Though the sample will preserve uniaxial alignment, the layer positions will be frustrated due to random crosslink positioning. In this case, crosslinks provide a random network of defects that could destroy the smectic order [130–132]. The final thermodynamic state of the sample will depend on the relative impact of crosslinking at the first stage and at the final stage when the network is fixed.

Earlier experiments by Wong et al. [138] used a polyacrylate-based side-chain smectic elastomer samples with about 5 mol% crosslinks. In this case, the elastomer sample was prepared via reaction with a crosslinking agent in toluene. Alignment was achieved in situ by stretching by 25% the freely suspended sample in the nematic phase and subsequently cooling into an aligned smectic phase. This situation differs strongly from the method described in the previous paragraph.

There are several other possible ways to prepare well-aligned smectic elastomer samples crosslinked directly in the smectic phase. Low-molecular-weight mesogens are easily aligned by surface forces. Driven by the tendency to minimize the surface energy, smectic membranes (freely suspended smectic films) with a perfect homeotropic alignment are easily formed [134]. Smectic polymer materials are much more viscous than their low-molecular-weight counterparts. Still uniform smectic membranes can be made close to the clearing temperature to the isotropic phase or even above it. After cooling down into the smectic phase, the films can be crosslinked by UV irradiation. Such methods have been used to produce planar films [139–144] and even curved elastomer films in the shape of inflated balloons [145, 146]. However, no high-resolution X-ray work has been performed with these types of sample.

The elastic properties of monodomain smectic elastomers are different from those of nematic elastomers [147]. The stress–strain diagram shows a considerable anisotropy of the elastic moduli. Stretching along the layer normal is associated with a large modulus of $\sim 10^7$ N/m^2, comparable to the smectic compressional modulus B in low-molecular-mass and polymer smectics. This value is about two orders larger than the modulus in the plane of the layers, which is comparable to the shear modulus $\mu \sim 10^5$ N/m^2 characteristic of the isotropic state. These observations indicate that the crosslinks are strongly pinned by smectic layers. As a result, when stretching along the layer normal the crosslinks cannot glide through the layers. The associated modulus is therefore associated with deformation energy of the smectic layers and is not rubbery. The physical reason for the large anisotropy in smectic networks is clear: stretching along the layer normal attempts to change the layer spacing, which is resisted by the smectic ordering. The mechanical field acts on the mesogenic in the smectic layers rather than on the crosslinks responsible for rubber elasticity. Such high elastic anisotropy is unprecedented even in strongly

ordered nematic networks. In the latter case, both elastic moduli (parallel and perpendicular to the director) are of the same magnitude [4].

Upon stretching along the layer normal, at relatively small strain on a rubbery scale of about 5–7%, smectic elastomers may break up into stripes leading macroscopically to a cloudy appearance [148]. The striped texture corresponds to a local layer inclination (rotation) relative the average direction of the layer normal. The system prefers the layers to rotate in order to relieve any layer extension deformation in favor of lower-cost rubber distortions at constant layer spacing. This reaction is the rubbery equivalent of the classical instability to avoid layer dilation in low-molecular-mass smectics, described in [149]. However, this type of behavior is not universal because other samples show isotropic rubber behavior [142, 144, 145].

5.2 *"End-On" Side-Chain Elastomers*

5.2.1 Order at Small Crosslink Concentration

The structure of a series of end-on side-chain polysiloxanes is given in Fig. 11a. This is the only series known at present for which an extensive variation of crosslink concentration c has been realized (c = 5–20%). In addition, the nature of the crosslink has been varied using the flexible crosslink unit V1 and the stiffer V8 (for structures see Fig. 11a). Oriented elastomer samples were obtained through the two-step crosslinking process (Sect. 5.1). The elastomers and polymers were studied in the smectic-A phase at room temperature, well below their smectic–isotropic transition at around 65–75°C (depending on c). The smectic-A phase was identified through a set of sharp (00n) quasi-Bragg peaks along the layer normal at a wave vector q_n and a broad liquid-like peak from the in-plane short-range order (Fig. 11b). The X-ray scattering profiles of the first-order peak are displayed in

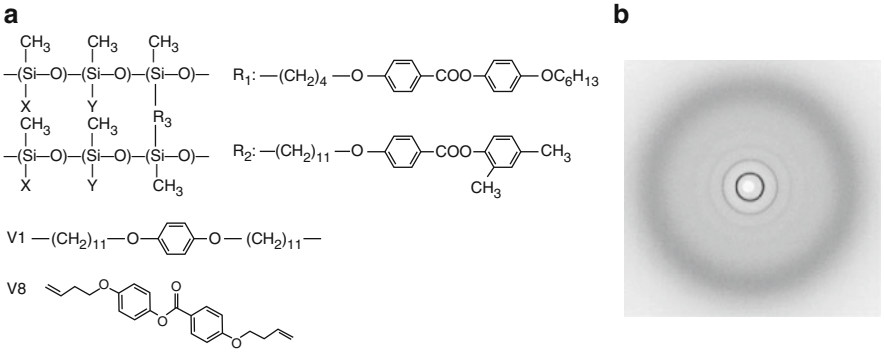

Fig. 11 (**a**) Structure of the side-chain polymer with two different mesogenic groups (X, Y)=(R1, R2). The corresponding elastomer is obtained by crosslinking with R3, which can be either V1 (flexible) or V8 (rigid). (**b**) 2D X-ray picture of the non-oriented elastomer

Fig. 12a for the homopolymer and the elastomer at low c, and in Fig. 12b for higher crosslink concentrations. The FWHM of the quasi-Bragg peaks is not resolution limited, and the central part can be well described by a Gaussian. For the first-order peak of the homopolymer this indicates smectic domains with a finite size along the layer normal, $L \approx 0.6$–0.7 μm. Away from the center of the peak, algebraic decay is observed with an exponent $\eta_n/n^2 = \eta = 0.15 \pm 0.02$, similar to that reported for other smectic polymers [106]. For the elastomer with $c = 10\%$, three harmonics are displayed in Fig. 9. Interestingly, the peak width Δq_z increases approximately linearly with the harmonic number n. In the tails of the peak, algebraic decay is nicely preserved and no evidence of true long-range order is found.

At small crosslink concentration, the peak width Δq_z of these systems (Fig. 12a) shows a remarkable trend. For $c = 5\%$, the finite size $L = 2\pi/\Delta q_z$ of the smectic domains is about five times larger than that of the corresponding homopolymer. At $c = 10\%$, the domain size has decreased somewhat, but is still two times larger than for the homopolymer. Only at 15% is the domain size back at about the homopolymer value. Evidently, the elastomer network initially enhances the stability of the smectic layer structure in the sense that the smectic order extends over larger domains than for the homopolymer. However, no evidence of true long-range order is found, as might follow from theory (Sect. 4.3). There are limited other data with which these results for small or moderate crosslink concentrations can be compared. We investigated a rather different siloxane with fluorinated end groups at the end-on mesogens and 9% crosslink V1. Scaling of η_n over five harmonics provided a rigorous proof of algebraic decay. Variation of the crosslink density led to a trend in the domain size that was qualitatively similar to that described above:

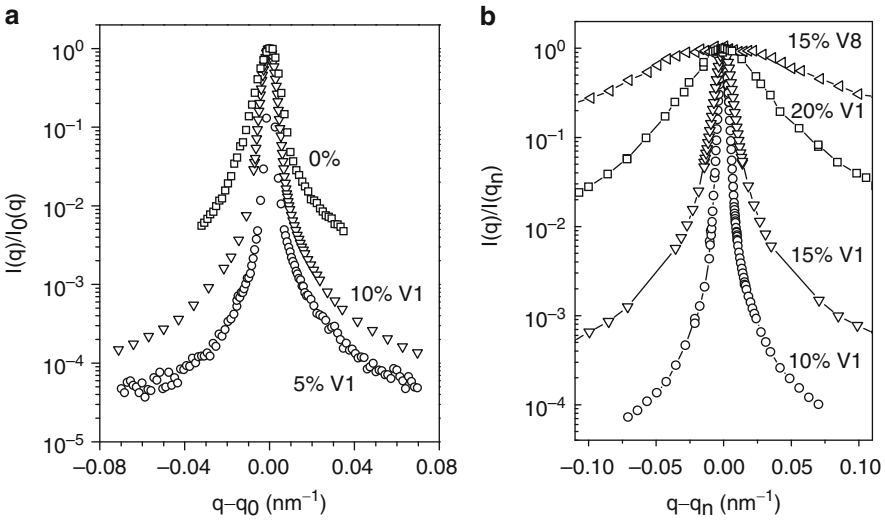

Fig. 12 Comparison of the first-order X-ray peaks of the elastomer of Fig. 11 for (**a**) low crosslink concentrations and (**b**) higher crosslink concentrations (after [7, 127])

the FWHM of the first-order peak changed from about 15 (homopolymer) via 11 (for $c = 9\%$) to 26 millidegrees (for $c = 12.5\%$). The situation in main-chain elastomers will be described in the next section.

Finally, an earlier report by Wong et al. [138] concerned a polyacrylate-based side-chain liquid-crystalline polymer that was about 2–5 mol% crosslinked. Alignment was achieved as described above in Sect. 5.2. They found at the tails of the smectic peaks convincingly had different slopes for the homopolymer (1.85 ± 0.10) and the elastomer (2.40 ± 0.10), as shown in Fig. 13. As algebraic decay leads necessarily to a slope <2, the larger slope for the elastomer was taken as evidence that long-range order was restored. Unfortunately, no higher orders could be measured. Several possibilities can be considered to explain why this behavior is rather different to that just discussed. One could assume that the Caillé limit and the correct exponent had not been reached yet and would turn up at larger offsets in $q - q_0$. However, the range of normalized intensity and offset from the center of the peak was very similar to those in Fig. 9, for which algebraic decay was confirmed by the appropriate scaling relation. Nevertheless, we note that for the first-order peak of Fig. 9 the necessary dynamic range was only just reached: for slightly smaller values of $q - q_0$, still comparable to those in [138], no correct value of η would have been obtained. Alternatively, one could imagine that the processing of the elastomer influences the resulting order. The uniform siloxane samples discussed above were made via the two-stage crosslink process, the present acrylate system that behaves differently through in situ stretching in the nematic phase. According to the discussion in Sect. 5.1, this should not make a major difference. Finally we mention the possibility that in this case the situation of a topologically ordered *XY* Bragg glass has been reached (compare [119]). In this

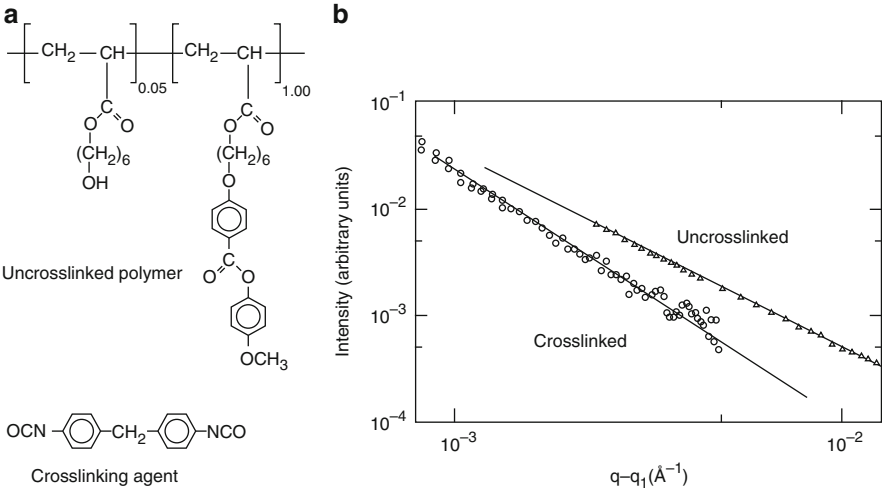

Fig. 13 (**a**) Structure of the polyacrylate-based side-chain LC compound. (**b**) Comparison of the asymptotic diffraction intensity tails from the crosslinked elastomer (*circles*; slope –2.40) and the corresponding uncrosslinked homopolymer (*triangles*; slope –1.85) [138]

case an exponent of 2.45, independent of temperature, has been predicted theoretically and is in good agreement with the present experiment. However, no further details are available to confirm this hypothesis.

5.2.2 Road to Disorder

We return to the siloxane elastomer of Fig. 11 and consider the situation for higher crosslink concentrations (Fig. 12b). For $c = 15\%$ crosslink, the domain size is already considerable smaller than for the homopolymer, indicating the end of the range of increased domain sizes due to crosslinking. With increasing c, the transparency of the samples decreases, which is also expressed by a larger mosaic distribution and fewer higher harmonics. Whereas for $c = 10\%$ three harmonics are observed (Fig. 9b), for $c = 15\%$ only two orders of diffraction occur. Algebraic decay of the positional correlations is still preserved with $\eta \simeq 0.15 \pm 0.01$ but is partly masked by a substantial broadening of the peak along q_z and by the increased mosaic spread. In Fig. 12b, the remaining first harmonic for $c = 20\%$ is compared with those at other crosslink densities. It is strongly broadened both along q_z (domain size about 100 nm) and along q_x (mosaic distribution of the smectic layer normal). In this figure, an additional result is included for 15% of the stiff crosslink V8, which behaves as anticipated for a concentration of the flexible crosslink V1 appreciably larger than 20%. The results for various concentrations of both types of crosslink are summarized in Fig. 14. With increasing concentration of crosslinks above 10%, the disorder gradually takes over, as indicated by (i) broadening of the X-ray peak along the layer normal (Δq_z) and (ii) a crossover of the lineshape from Gaussian to Lorentzian. Though this behavior is consistent with the general predictions for random quenched disorder, it is remarkable that the algebraic decay survives up to rather large crosslink densities of 15%.

To become more quantitative, we note that various factors contribute to the structure factor in smectics. These include in particular the finite size of the sample and the effects of the mosaic distribution [see (12) in Sect. 4.1]. For the present discussion we shall simplify things somewhat and emphasize (a) the broadening of the central part of the X-ray peak due to the finite size, $H(\mathbf{q})$, and (b) the possible power-law behavior in the tails of the peak. Let us start with the finite-size term. As discussed in some detail by Obraztsov et al. [7], a suitable distribution function to describe the central part of the X-ray peaks is given by:

$$H(z) = \exp\left[-\frac{(\sigma_\beta z)^{2\beta}}{2\beta}\right]. \tag{16}$$

This expression gives a Gaussian function for $\beta = 1$ and a simple exponential for $\beta = 0.5$, leading to a Gaussian and a Lorentzian lineshape, respectively. Equation (16) allows a smooth transition between these cases. The situation $0.5 < \beta < 1$ can be described as a stretched Gaussian or equivalently as a compressed

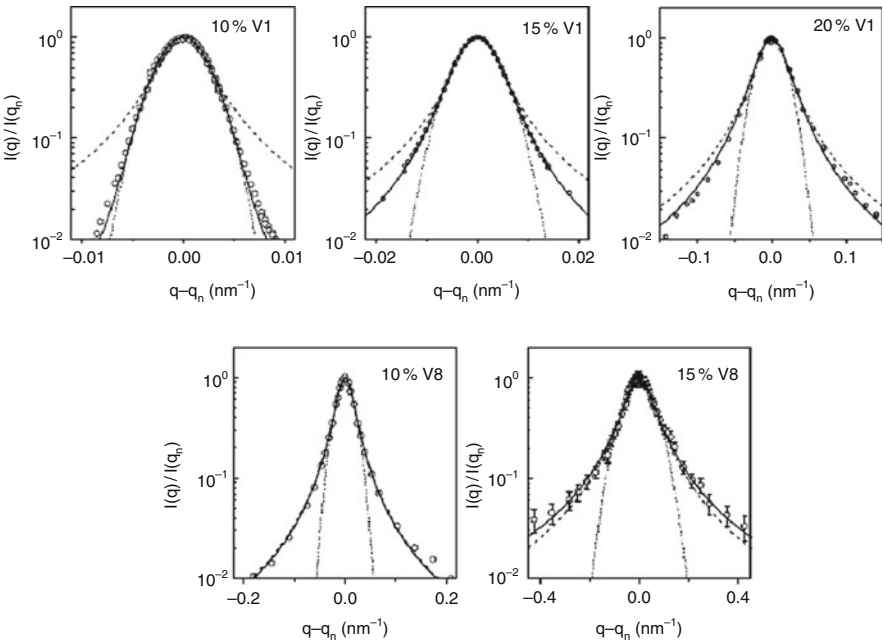

Fig. 14 Central part of the first-order diffraction of the elastomer of Fig. 11 for different crosslink concentrations. *Dashed line* Lorentzian fit ($\beta = 0.5$); *dotted line* Gaussian fit ($\beta = 1$); *solid line* best fit to (16) with β-values of 0.96, 0.66, 0.59, 0.51, 0.44 (from *left* to *right*). Note the different horizontal scales [7]

exponential; $\beta < 0.5$ corresponds to a stretched exponential. The variation of the central part of the observed lineshapes is illustrated in Fig. 14. In fitting these data, the various lineshapes are constrained to reproduce the correct FWHM. Going from $c = 10\%$ via 15% to 20% of crosslink V1, the lineshape changes from approximately Gaussian to close to Lorentzian. This is nicely expressed by the value of the exponent of (13) that varies from $\beta = 0.96 \approx 1$ (pure Gaussian) for $c = 10\%$ to close to 0.5 for $c = 20\%$. Most importantly, this trend is continued by the results for the stiff crosslink V8 (Fig. 14). The result for $c = 10\%$ of the stiff crosslink V8 is close to the situation for $c = 20\%$ of the flexible crosslink V1: a fit with variable β can hardly be distinguished from a pure Lorentzian ($\beta = 0.5$). Upon increasing the concentration of V8, the exponent β decreases further down to $\beta = 0.44$ for $c = 15\%$, corresponding to a stretched exponential correlation function. At this stage we cannot give a precise interpretation, but we note that a stretched exponential can be related to an average over dimensions varying over a broad range. A compressed exponential (or equivalently a stretched Gaussian) is often in a loose way associated with cooperative behavior (see, for example, [150, 151]). Summarizing, we encounter a gradual transition from well-distinguishable finite-size domains (flexible crosslinks; Gaussian) to an average over a broad range of sizes that leads first to a Lorentzian (large density of flexible crosslinks; medium

density of rigid crosslinks) and subsequently to a stretched Lorentzian (large density of rigid crosslinks).

The signature of disorder is, according to the theories of random disorder discussed in Sect. 4.3, a shape of the diffraction profile corresponding to a stretched Gaussian with $\beta \cong 0.7$. This value corresponds approximately to a square Lorentzian [last term of (13)]. For the flexible crosslinker V1, this point is reached for a crosslink concentration of about 15%, which is definitely much larger than predicted theoretically. The stiff crosslinker V8 shows a crossover to disorder at smaller concentrations than V1, providing a better connectivity with theory. Taking the onset of disorder for V8 at 7–8% and a percolation threshold $c_0 \cong 4\%$, we arrive at $c - c_0$ being approximately equal to 3–4%, in reasonable correspondence with theories of random disorder. Thus, the properties of smectic elastomers with a rigid crosslinker and low-molecular-mass smectics confined within aerosils are rather close to each other. Nevertheless, the quantitative interpretation of the behavior of smectic networks constitutes a major theoretical challenge.

The description of crosslinking in smectic elastomers involves effects arising from internal nonuniform strain. In smectic elastomers prepared according to the two-step crosslinking process, mechanical strain is imprinted in the system during the uniaxial alignment. In smectic networks, crosslinks can generate various types of defect with the associated elastic fields leading to additional stress. Strain-induced broadening of X-ray peaks is well known in various fields, for example, in metals subjected to cold work and in certain semiconductors [121, 152, 153]. Generally, two effects contribute to X-ray peak broadening: the finite size of the crystalline or smectic domains (as discussed above) and nonuniform strain. The strain broadening of a diffraction peak leads approximately to a linear increase of Δq_z with harmonic number n, whereas the size effect does not depend on it. Hence, the measured FWHM can be written as in [154], dropping for convenience the index z:

$$\Delta q_{\text{exp}}^2 = \Delta q_{\text{size}}^2 + n^2 \Delta q_{\varepsilon}^2, \tag{17}$$

in which Δq_{ε} is the strain-induced contribution and the instrumental resolution has been disregarded for convenience. Experimentally, the width of the quasi-Bragg peaks along q_z increases about linearly with n in agreement with (17). In a simple harmonic description, the width of the smectic peaks would be the same for all different orders of diffraction. We can in principle separate the two contributions using (17) and obtain an average domain size. However, to obtain a good accuracy several harmonics are needed that are not available for the present elastomers. For that reason, we have attributed the full width of the first-order peaks to finite-size effects, which is only approximately correct.

5.2.3 Smectic-A–Nematic Transition

An interesting extension of the above results is obtained if, in the siloxane system of Fig. 11, the side group R1 is replaced by a nematogenic side group M3.

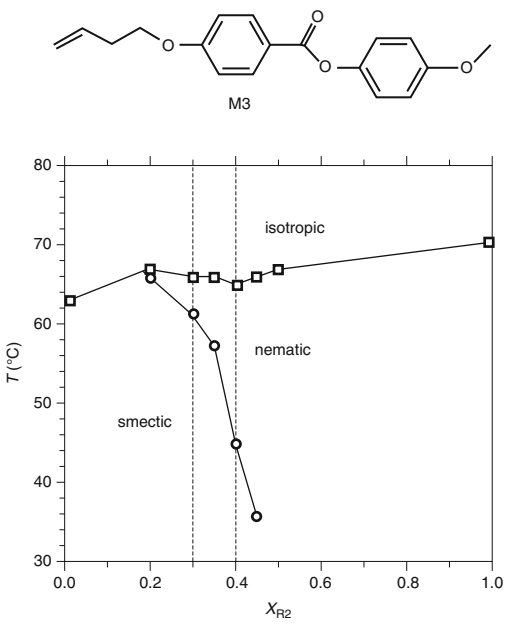

Fig. 15 Schematic phase diagram for mixing the nematogenic side group M3 into the system of Fig. 11 with X=Y=R2. The two compositions investigated are indicated by *vertical lines* and designated as E70/30 and E60/40, respectively, where the numbers give the percentage R2/M3. In the same terminology E100/0 stands for the fully smectic elastomer

The resulting phase diagram, sketched in Fig. 15, indicates that this provides access to a smectic-A–nematic (SmA–N) phase transition. We have studied the elastomers E70/30 and E60/40 with 30% and 40% of the nematogenic group M3, respectively, and two crosslink concentrations, 5% and 10%. Note that the fully smectic compounds discussed in the previous section would be indicated in this terminology as E100/0. The elastomer E70/30 5% has a stronger smectic tendency than E60/40 5%, as follows from the smaller nematic range, and twice as large a compression modulus B. Both samples with 5% crosslink show a clear SmA–N transition that can be determined precisely from a lineshape analysis as illustrated in Fig. 16a, b for E60/40 5%. In the nematic phase the lineshape is nicely Lorentzian, indicating short-range order characterized by correlation length $\xi = 2/\Delta q_z$ of the order of 10–100 nm (Fig. 16c). In agreement with the paranematic nature of the stretched monodomain sample (Sect. 3.4), no indication of the phase transition to the isotropic phase is found. In the smectic phase, deviations from a Lorentzian lineshape occur similar to the situation described above for E100/0 at low crosslink concentration. Approximating the central part of the peak by a Gaussian, an average domain size $L \cong 2\pi/\Delta q_z$ of about 500–800 nm is found. Second-order peaks have been observed at room temperature in the smectic phase of both elastomers with 5% crosslinks. These peaks are broadened by a factor of two relative to the first-order peaks, indicating strain-induced broadening as discussed in Sect. 5.2.2. The intensity profile shows power-law behavior at large $q - q_n$ while scaling is nicely obeyed, with a value $\eta = 0.22 \pm 0.02$ for E60/40 5%.

X-ray results for polymer networks containing 10% crosslinks are shown in Fig. 17. In a wide temperature range around the former SmA–N transition, all lineshapes

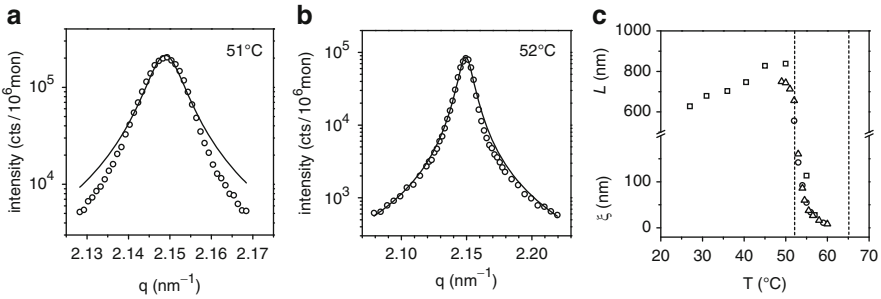

Fig. 16 Smectic–nematic transition in E60/40 5% as studied with high-resolution X-ray diffraction. Lineshape (**a**) just below and (**b**) just above the transition temperature, T_{NA}, of 52°C. The *solid lines* are fits to a Lorentzian. (**c**) Domain size L below T_{NA} and correlation length ξ from a Lorentzian fit above T_{NA}. *Vertical lines* indicate T_{NA} and T_{IN}

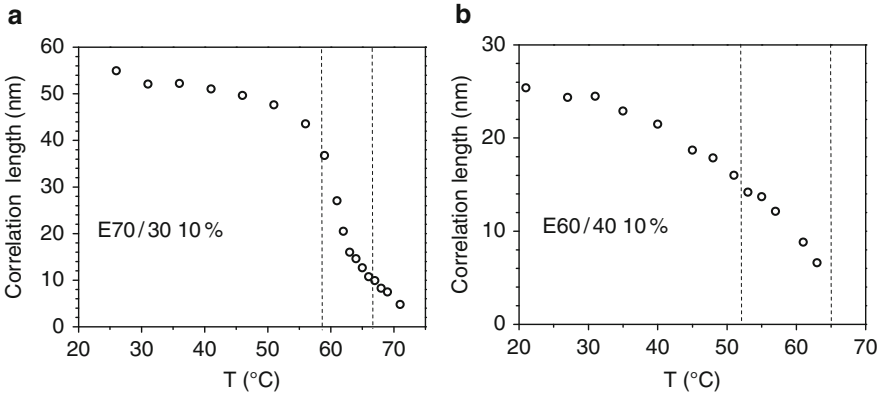

Fig. 17 Correlation length vs. temperature from Lorentzian fits to the lineshape of the smectic peak at various temperatures for the samples E70/30 and E60/40 for 10% crosslinks. *Vertical lines* indicate the original SmA–N and N–I transition temperatures of the corresponding 5% samples

can be well described by a simple Lorentzian corresponding to a disordered state. For E70/30, the correlation length ξ increases with decreasing temperature continuously from 5 nm to about 50 nm, and then saturates. The latter value corresponds to correlation over about 18 smectic layers. The temperature dependence of ξ as displayed in Fig. 17a shows an inflection point at 61°C. At this point we observed the subtle asymmetry in the X-ray profile, which is related to a small shift of the maximum of the mosaic spread in the sample. We assume that below the singular point E70/30 forms a randomly disordered smectic-like state, with some memory of the distribution of layer normals, that transforms to a nematic state with thermal layer fluctuations only.

For the more nematogenic compound E60/40 with 10% crosslinks, no inflection point is observed in the curve of $\xi(T)$ (Fig. 17b). Moreover, the saturated value of ξ

at low temperatures is about half that for E70/30. $\xi(T)$ behaves as if we are in a "para-smectic" regime of a first-order smectic–isotropic transition and reflects mainly changes associated in $S(T)$ and $\psi(T)$, the orientational and translational order parameters, respectively. Note that in the purely smectic elastomer E100/0, disordering effects of similar strength occurred only at a crosslink concentration of about 20% (Sect. 5.2.2). The smaller value observed in E60/40 can be attributed to its rather soft layer system, due to the wide nematic range and the reduced value of the elastic modulus B. Obviously E70/30, with a larger smectogenic component, represents an intermediate case between E60/40 and the purely smectic elastomer E100/0.

Interpretation of the above results is not straightforward. The overall results of Fig. 17 are reminiscent of the extended short-range layer correlations found in low-molecular-mass smectics confined in random silica aerogels or aerosils (see Sect 4.2 and Fig. 10). In the latter case, the lineshape has been fitted to a combination of a Lorentzian (describing the thermal layer fluctuations) and a squared Lorentzian (describing the effect of random fields), the latter becoming dominant at lower temperatures. It is clear from Fig. 16a that the present smectic elastomer lineshapes could be represented by such a combination of terms. As discussed in Sect. 4.3, short-range order induced by the random crosslinks can be characterized by the correlation length $\xi = (B/2\Lambda)^{1/2} \sim [B/2(c - c_0)]^{1/2}$. Using the data from Fig. 16 and B-values derived from stretching experiments, we can make some estimates. First, at the same crosslink density of 10%, the compression modulus B of E60/40 is about a third of that for E70/30. If the value $\xi \cong 50$ nm, characteristic of the low temperature state of E70/30, is divided by 3 we arrive at $\xi \cong 29$ nm, which is close to the saturated correlation length $\xi \cong 27$ nm of E60/40. Second, a reasonable value of the percolation limit of the present elastomers is $c_0 \cong 0.04$. Then, neglecting a possible temperature dependence of the modulus B, the ratio $\xi_{5\%}/\xi_{10\%}$ should be $(6)^{1/2} \cong 2.4$. Considering first E70/30, taking $\xi_{5\%} \cong 150$ nm (at the transition point to nematic phase) and $\xi_{10\%} \cong 50$ nm at low temperatures, we arrive at a ratio $\xi_{5\%}/\xi_{10\%} = 3$, close to our estimate. However, for E60/40 we find a ratio $\xi_{5\%}/\xi_{10\%} \cong 6$, which is too large. This discrepancy could indicate that for E70/30 10% the distortion of the smectic layers at low temperatures is due to random fields, whereas for the more nematogenic E60/40 10% the contribution from thermal disorder is still appreciable.

From the discussion so far we conclude that the available theories of random disorder can describe some important details of the disorder in fully smectic elastomers. The results around the SmA–N transition in elastomers indicate the complex interplay of thermal and random disorder mechanisms. Currently, there is no consistent theory to describe disorder in the SmA–N phase transition region, which constitutes a major theoretical challenge. Upon increasing the crosslink density, the fully smectic compound E100/0 showed a wide lineshape variation from Gaussian via stretched Gaussian to Lorentzian. A stretched Gaussian with $\beta \cong 0.7$ corresponds approximately to a square Lorentzian and thus could indicate the onset of disorder, in agreement with theory. The further evolution might be attributed to increasing dominance of the thermal disorder component.

5.3 *"End-On" Main-Chain Elastomers*

As mentioned earlier, for end-on main-chain smectic polymers the polymer chains connect the smectic layers. As a result, polymer defects are expected to be directly translated into layer distortions (Fig. 4b–d). This probably offsets any possible influence of damping of the layer fluctuations (potentially leading to increased order) because of the connectivity of the layer structure via the chains. As mentioned already in Sect. 2.3, main-chain polymers and elastomers have little tendency to form a smectic phase. They have been less thoroughly investigated than their side-chain counterparts. X-ray structural information of several main-chain elastomers with about 10% of approximately the same cyclic multifunctional crosslink have been compared with their homopolymer counterparts by De Jeu et al. [155]. As no results are available for other crosslink concentrations, little can be said about the specific contribution of the crosslinks to disorder.

As a typical example, we shall discuss the polymer and elastomer MeHQ, depicted in Fig. 18a. In this system, the rigid mesogenic groups are not only connected by an alkyl chain but also with a short siloxane fragment (chain extender). An overall X-ray view of the elastomer is shown in Fig. 18b and indicates a smectic-C structure with tilted layers. Let us first consider the polymer (MeHQ-pol) in some detail. The high-resolution data shown in Fig. 19a, b for its two harmonics indicate rather broad peaks. In fact, Δq_z varies little for the first and second harmonics. For both harmonics, fitting the wings in the double-logarithmic plot leads to a straight line compatible with $\eta_n/n^2 = \eta = 0.06 \pm 0.01$. In combination with other examples, we can conclude that for end-on main-chain smectic polymers algebraic decay is maintained within the smectic domains [155]. However, rather unusually for smectic polymers, the overall lineshape can be reasonably well fitted by a Lorentzian with a correlation length ξ that is of the same order for both harmonics. A straightforward interpretation of this Lorentzian as indicating short-range order can be excluded for two reasons. First, the correlation lengths and/or domain sizes are large, of the order of hundreds of nm. More importantly, for short-range order higher harmonics are hardly expected because the width Δq

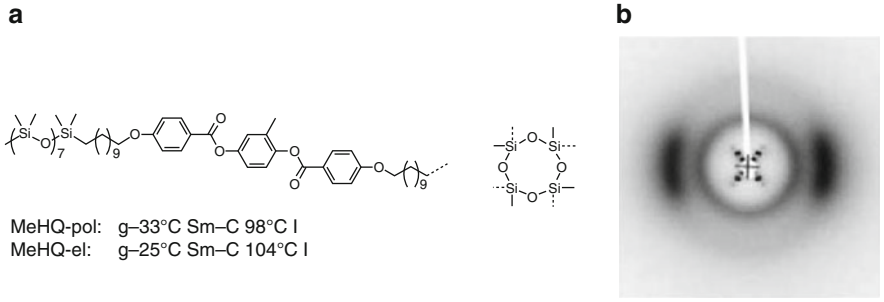

Fig. 18 (**a**) Molecular structure of the main-chain smectic polymer MeHQ and the cyclic crosslinker used. (**b**) X-ray picture of the elastomers MeHQ indicating a smectic-C phase

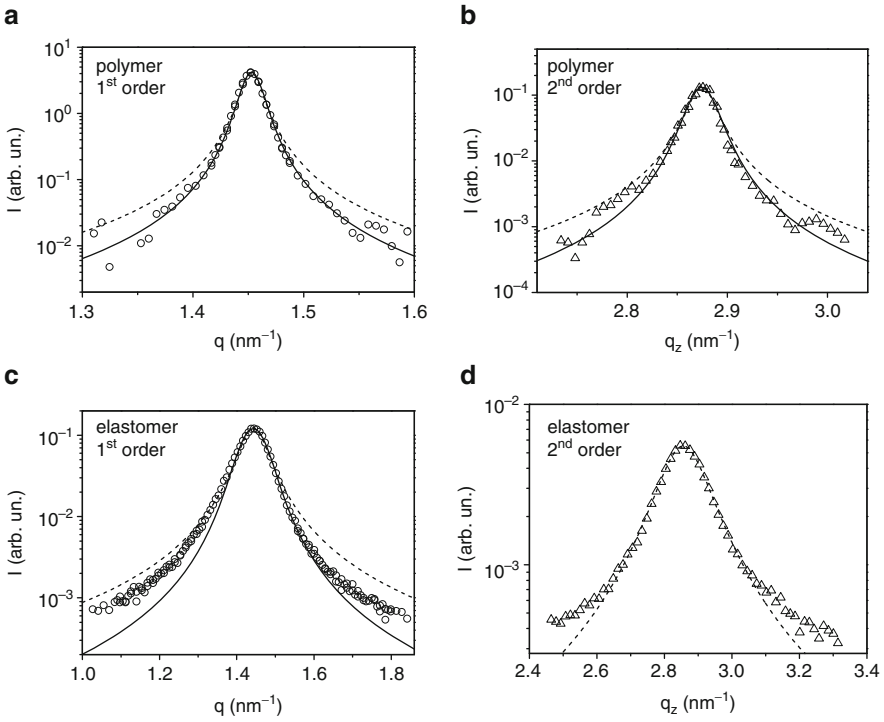

Fig. 19 First- and second-order peaks of MeHQ-pol (**a**, **b**) and MeHQ-el (**c**, **d**). *Dashed lines* Lorentzian fit, *solid lines* best fit to (15) giving $\beta = 0.61, 0.65, 071$ (for **a**, **b**, **c**, respectively) [155]

of the successive harmonics increases as n^2. This leaves as the most plausible explanation that the Lorentzian lineshape is due to a broad exponential-like distribution of domain sizes in the sample. Such situations have been well documented in powder diffraction (see, for example, [156]). The specific nature of the distribution (as compared to other smectic systems) could arise from the direct coupling between polymer defects and smectic layer correlations typical for main-chain systems only. The first candidates for such defects are hairpins (Fig. 4c) [37, 157, 158]. However, stress–strain experiments on nematic main-chain networks indicate that during the formation of a monodomain sample simple hairpins are probably removed by the mechanical strain and might play only a minor role [68]. On the other hand, this argument does not hold for entangled hairpins as depicted in Fig. 4d. The presence of such defects would be compatible with a plateau in the stress–strain curve. Additionally, chain ends may play a role. Analogous to the situation described for the nematic phase [39], these could also lead to local distortion of the smectic layers (Fig. 4b). In main-chain systems, the polymer chains themselves contribute to the building of the smectic layers. Due to dispersion of the polymer chain length, the layered structure in the direction along layer normal cannot be terminated at any arbitrary place, thus leading to finite-size

dispersion. Inside the domains/grains leading to the Lorentzian average, algebraic decaying smectic order still appears to be present.

Next, we come to the corresponding elastomer sample MeHQ-el (Fig. 19c, d). In this case, the domain sizes as measured (tens of nanometers) are appreciably smaller than for the corresponding polymer. The broadening of the smectic peaks with increasing harmonic number n is very similar to that observed for the end-on side-chain elastomer systems discussed in Sect. 3.3. In the latter situation, the broadening was attributed to the internal stress due to the aligning memory of the samples, random disordering effects, and other types of defects generated by the presence of crosslinks. Applying (17) to the present data one finds $\Delta q_{\text{size}} \approx 0.024\ \text{nm}^{-1}$, leading to intrinsic average domain size $L = 2\pi/\Delta q_{\text{size}} \cong 260$ nm, close to the value for the corresponding polymer. Similar results were obtained for the related compound, MC11-el, with an average domain size $L \cong 150$ nm. We conclude that main-chain elastomers at a crosslink concentration of about 10% differ from the corresponding polymers, mainly by an excess amount of strain.

Regarding the wings of the elastomer peaks, the situation is somewhat complicated. For MeHQ-el reasonable scaling was found with $\eta = 0.17$ from the first harmonic (Fig. 19c) and $\eta = 0.20$ from the second-order peak. However, for MC11-el no scaling relation could be established [155]. This does not allow strong conclusions because practical experimental considerations are probably involved at the limit of what could be measured. The intrinsic domain sizes being as small as 200 nm, the question arises whether algebraic decay can survive over such small distances. We speculate that in these small-size domains the internal strain is strong enough to modify the Caillé correlation function. Then, the latter will be multiplied by another correlation function describing correlations of displacements induced by the above-mentioned factors. The resulting power-law asymptotes could very well be different from that predicted by the Caillé function only, and rather ambiguous results could be anticipated from analysis of the wings of the elastomer peaks.

Summarizing, we note that in these main-chain elastomers we did not reach a disordered state as for the siloxane end-on side-chain (Sect. 5.2.2). Although we considered chemically very different mesogenic polymers, all systems involved a rather similar cyclic multifunctional crosslinker at a single concentration of about 10%. We expect from the topology that a point-like multifunctional cyclic crosslinker connecting main-chains would induce less disorder in the smectic polymer matrix than the stiff anisotropic mesogenic-like bifunctional crosslinks used for side-chain elastomers. Evidently there is a need for further study of the role of the crosslink topology, stiffness, and variation of crosslink density to improve our understanding of the disordering processes in main-chain polymer networks.

5.4 "Side-On" Elastomers

Finally, we come to side-on systems (see Fig. 1b, d) in which the preferred direction of the mesogenic groups changes orientation compared to the end-on systems of

Fig. 1a, c. Information on these systems is so far very limited. Let us first consider side-on side-chain smectic polymers (Fig. 1b) in which the polymer chains are on average oriented parallel to the smectic layer normal, thus connecting the layers similarly as in main-chain systems. We shall consider the material depicted in Fig. 20a, which has partly fluorinated end groups attached to the mesogenic central core. Figure 20b gives an X-ray overview of the oriented elastomer. Axially, we see two orders of diffraction from smectic layering and equatorially, at wide angles, we see diffuse crescents corresponding to the smectic-A liquid in-plane structure. At angles somewhat smaller than those corresponding to the smectic layers, a full diffuse ring is observed with weak maxima along the equator. This diffuse scattering is also observed for the homopolymer and survives in the isotropic phase. It has been attributed to poorly correlated short-range structures from local concentrations of the fluorinated end groups of the mesogens that "nanosegregate" from the hydrocarbon surroundings. As a result, "pre-existing" disorder is present in this system, which might make it not very typical for the class of side-on side-chain systems. The first-order smectic layer peak can be well described by a Lorentzian with a large correlation length, indicating order of about 20 smectic layers [135]. The width of the second-order peak is between two and three times larger than the first-order peak width, violating the quadratic increase with harmonic number that is expected for simple short-range order. This behavior is very similar to that described above for main-chain systems and is again attributed to a broad exponential-like distribution of domain sizes.

The described fluorinated compound shows interesting elastic properties [159]. The sample remains fully transparent when stretched either parallel or perpendicular to the director (Sect. 5.1). These results have been correlated with high-resolution X-ray scattering [135]. An increase in the FWHM of the smectic peak found during stretching corresponds to a decrease of the average domain size from the original 180 nm down to about 45 nm at the threshold to plastic deformation. At this level, at

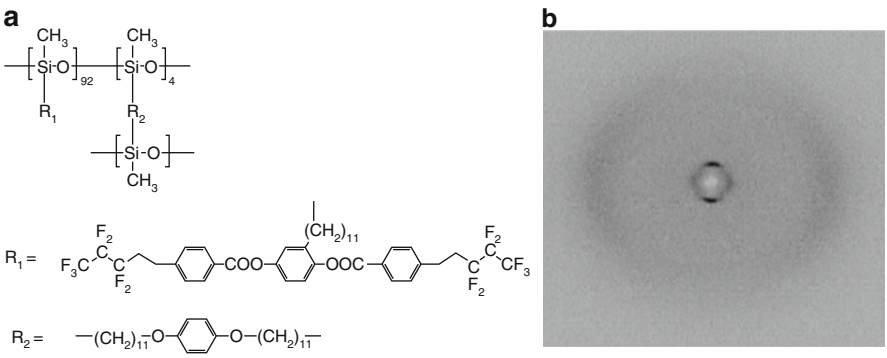

Fig. 20 (**a**) Molecular structure of the smectic side-chain elastomer with 96% side-on group R1 and 4% crosslinker R2. (**b**) 2D X-ray picture of the elastomer with the smectic layer peaks visible axially [135]

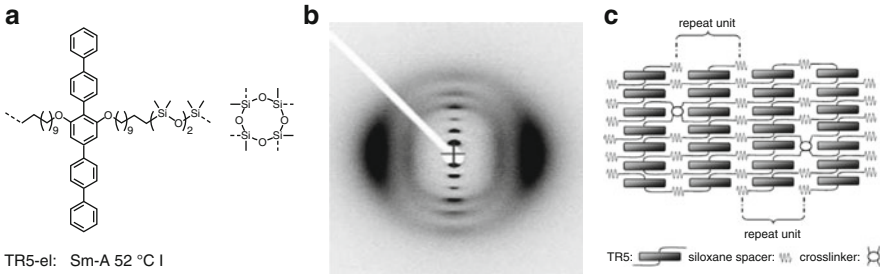

Fig. 21 (**a**) Molecular structure of the main-chain smectic system TR5 with pentaphenyl transverse rods. (**b**) X-ray picture of the smectic-A structure of the elastomer stretched at room temperature. (**c**) Structural model of the elastomer [160]

which the sample still remains transparent, a transition to a highly disordered nematic-like state occurs. At the highest strain, the X-ray peak reveals a correlation length $\xi \approx 10$ nm corresponding to only four smectic layers.

Finally, we come to an example corresponding to the symmetry of Fig. 1d: the side-on main-chain system. Again only one case has been studied in some detail [155, 160]. The structure of this compound (abbreviated as TR5-el) is shown in Fig. 21a. No X-ray data are available for the homopolymer. The X-ray picture of a stretched elastomer sample shows a smectic-A phase with an appreciable number of harmonics (Fig. 21b). However, the combination of the rigid pentaphenyl rod and the flexible siloxane main-chain leads to packing constraints that make the siloxane chains align parallel to the rods (see Fig. 21c). As a result, the appropriate scheme corresponding Fig. 1d (polymer chain perpendicular to smectic layer normal) does not apply. In agreement with the model of Fig. 21c, the high-resolution X-ray lineshape data fit into the general trends described earlier in this section for end-on main-chain elastomer systems.

6 Conclusions and Outlook

In this review we have discussed ordering and frustration in LC polymer networks. In the first part, we treated the dominant role of the polymer backbone anisotropy in shaping the specific properties of nematic polymers and elastomers. Using results of neutron and X-ray measurements and applying some theoretical models, we have demonstrated how orientational order induces chain anisotropy in nematic polymers, which, in turn, determines their macroscopic shape. In spite of these results there is still need for more extensive information on the anisotropic shape of LC polymers. Such results could provide clues for the application of a greater variety of polymers for crosslinking. Up to now, most elastomer systems use flexible siloxanes as the polymer backbone.

In the second part, we discussed smectic liquid-crystalline systems that show quasi-long-range order of the smectic layers (positional correlations decaying algebraically). In smectic elastomers, the smectic layers cannot move easily across the crosslinking points where the polymer backbone is attached. Consequently, layer displacement fluctuations are suppressed, which can stabilize the periodic layer structure. On the other hand, the crosslinks manifest themselves as a mechanical random field that disturbs local layer positions and orientations. The presence of crosslinks radically alters the positional and orientational order in smectics at large distances. Analysis of the X-ray lineshape of the quasi-Bragg peaks associated with the smectic layering indicates a transition from algebraic decaying order to disorder upon increasing the crosslink density. The broadening of higher harmonics of the X-ray peak points to strong nonuniform strain within the elastomer samples. Also in the case of a smectic–nematic phase transition, the smectic layer order disappears with increasing crosslink density and the transition can no longer be distinguished.

Theoretical studies of a smectic LC in a random environment identify, on short length scales, layer displacement disorder, i.e., the tendency of the random field to force the smectic layers to particular positions. This should provoke disorder of the smectic state even for arbitrarily weak quenched disorder, which has been confirmed in several classical systems. In smectic LC elastomers, the road to disorder seems to be rather universal: algebraically decaying order survives up to high crosslink density, in dependence of the nature of the crosslinks (somewhat stiff or more flexible). This leaves little space for classical quenched random disorder theories. Evidently, crosslinks are not rigidly "frozen" defects, but consist of flexible chains embedded in the slowly fluctuating elastomer gel. The challenge for further theoretical study would be to include flexibility of crosslinks and general conformational freedom of the network.

Most experiments on LC elastomers have so far used "single crystal" elastomers made via the two-step crosslinking process, which involves stretching in the LC state. There is increasing evidence that this situation represents a special thermodynamic state – smectic elastomers made in such a way are well aligned but their layer positions are frustrated due to the random crosslink distribution. Evidently, there is room for experiments on nematic and smectic elastomer samples oriented in different ways, for example by photo-crosslinking. In such a way, any memory of the aligning procedure imprinted in the samples will be avoided (at least partially) and new features of phases and phase transitions could be revealed.

Acknowledgments Our work on LC elastomers has evolved over a considerable time span. We are grateful to the following PhD students and post-docs for their contributions: Gerard Wong, Denitza Lambreva, Adrian Muresan, Evgeny Obraztsov (Amsterdam), Antoni Sánchez-Ferrer, Ansgar Komp, Dominic Kramer (Freiburg). Wolfgang Caliebe (Hasylab, DESY, Hamburg) and Steve Bennett (NSLS, Brookhaven) provided expert assistance at their respective beamlines. We thank Vladimir Kaganer (Berlin), Rudolf Zentel (Mainz), Eugene Terentjev (Cambridge) and Heino Finkelmann (Freiburg) for valuable interactions. BIO acknowledges partial support from the Russian Fund for Basic Research (under grant N 09-08-00362).

References

1. Kramer D, Brömmel F, Finkelmann H (2011) In: De Jeu WH (ed) Liquid crystal elastomers: materials and applications. Adv Polym Sci. Springer, Heidelberg, Berlin, doi: 10.1007/12_2012_168
2. De Gennes PG (1975) C R Acad Sci B 281:101
3. Brand HR, Finkelmann H (1998) Physical properties of liquid crystalline elastomer. In: Demus D, Goodby J, Gray GW, Spiess H-W, Vill V (eds) Handbook of liquid crystals. Wiley VCH, Weinheim, part IV p 277
4. Warner M, Terentjev EM (2007) Liquid crystal elastomers, revised edn. Clarendon, Oxford
5. Ohm C, Brehmer M, Zentel R (2010) Adv Mater 22:3366
6. Urayama (2011) In: De Jeu WH (ed) Liquid crystal elastomers: materials and applications. Adv Polym Sci. Springer, Heidelberg, Berlin, doi: 10.1007/12_2010_107
7. Obraztsov EP, Muresan AS, Ostrovskii BI, de Jeu WH (2008) Phys Rev E 77:021706
8. Finkelmann H, Ringsdorf H, Wendorf JH (1978) Makromol Chem 179:273
9. Shibaev VP, Kostromin SG, Plate NA (1982) Eur Polym J 18:651
10. Davidson P, Levelut AM (1992) Liq Cryst 11:469
11. Kirste RG, Ohm HG (1985) Makromol Chem Rapid Commun 6:179
12. Keller P, Carvalko B, Cotton JP, Lambert M, Moussa F, Pepy G (1985) J Phys Lett 46:1065
13. Noirez L, Keller P, Davidson P, Hardouin F, Cotton JP (1988) J Phys 49:67
14. Vertogen G, de Jeu WH (1988) Thermotropic liquid crystals, fundamentals. Springer, Berlin
15. Cotton JP (1991) In: Lindner P, Zemb T (eds) Neutron, X-ray and light scattering. North-Holland, Amsterdam, p 3
16. Cotton JP, Hardouin F (1997) Prog Polym Sci 22:795
17. Freidzon YaS, Tsukruk VV, Boiko NI, Shibaev VP, Shilov VV, Lipatov YuS (1986) Polym Commun 27:190
18. Shibaev VP, Lam L (eds) (1994) Liquid crystalline and mesomorphic polymers. Springer, New York
19. Ostrovskii BI, Sulyanov SN, Boiko NI, Shibaev VP (1998) Liq Cryst 25:53
20. Mitchell GR, Davis FJ, Guo W, Cywinski R (1991) Polymer 32:1347
21. Hardouin F, Sigaud G, Achard MF, Brulet A, Cotton JP, Yoon DY, Percec V, Kawasumi M (1995) Macromolecules 28:5427
22. Noirez L, Boeffel C, Daoud-Aladine A (1998) Phys Rev Lett 80:1453
23. Boeffel C, Spiess HW, Hisgen B, Ringsdorf H, Ohm H, Kirste RG (1986) Makromol Chem Rapid Commun 7:777
24. Noirez L, Keller P, Cotton JP (1995) Liq Cryst 18:129
25. Renz W, Warner M (1986) Phys Rev Lett 56:1268
26. Kunchenko A, Svetogorsky DA (1986) J Phys 47:2015
27. Rieger J (1988) J Phys 49:1615
28. Bouwman WG, de Jeu WH (1994) Liq Cryst 16:863b
29. Ostrovskii BI, Sulyanov SN, Boiko NI, Shibaev VP, de Jeu WH (2001) Eur Phys J E 6:277
30. Cladis PE (1975) Phys Rev Lett 35:48
31. Prost J, Barois P (1983) J Chim Phys 80:53
32. Longa L, de Jeu WH (1983) Phys Rev A 28:2380
33. Li MH, Brulet A, Davidson P, Keller P, Cotton JP (1993) Phys Rev Lett 70:2297
34. D'Allest JF, Maissa P, ten Bosch A, Sixou P, Blumstein A, Blumstein RB, Teixera J, Noirez L (1988) Phys Rev Lett 61:2562
35. Li MH, Brulet A, Keller P, Strazielle C, Cotton JP (1993) Macromolecules 26:119
36. Li MH, Brulet A, Keller P, Cotton JP (1996) J Mol Struct 383:11
37. De Gennes PG (1982) In: Ciferri A, Krigbaum WR, Meyer RB (eds) Polymer liquid crystals. Academic, New York, p 115
38. Wang XJ, Warner M (1986) J Phys A 19:2215

39. Meyer RB (1982) In: Ciferri A, Krigbaum WR, Meyer RB (eds) Polymer liquid crystals. Academic, New York, p 133
40. Beyer P, Terentjev EM, Zentel R (2007) Macromol Rapid Commun 28:1485
41. Beyer P, Braun L, Zentel R (2007) Macromol Chem Phys 208:2439
42. Ren W, McMullan PJ, Guo H, Kumar S, Griffin AC (2008) Macromol Chem Phys 209:272
43. Sánchez-Ferrer A, Finkelmann H (2008) Macromolecules 41:970–980
44. Hessel F, Finkelmann H (1985) Polym Bull 14:375
45. Zhou QF, Li HM, Feng XD (1987) Macromolecules 20:233
46. Xie H, Hu T, Zhang X, Chen E, Zhou Q (2008) J Polym Sci A Polym Chem 46:7310
47. Lecommandoux S, Noirez L, Richard H, Achard MF, Strazielle C, Hardouin F (1996) J Phys II 6:1
48. Leube HF, Finkelmann H (1991) Makromol Chem 192:1314
49. Achard M-F, Lecommandoux S, Hardouin F (1995) Liq Cryst 19:581
50. Lecommandoux S, Noirez L, Achard M-F, Hardouin F (1997) J Phys II 7:1417
51. Lecommandoux S, Noirez L, Achard M-F, Hardouin F (2000) Macromolecules 33:67–72
52. Finkelmann H, Kock HJ, Rehage G (1981) Makromol Chem Rapid Commun 2:317
53. Zentel R, Reckert G, Reck B (1987) Liq Cryst 2:83
54. Zentel R, Schmidt GF, Meyer J, Benalia M (1987) Liq Cryst 2:651
55. Mitchell GR, Davis FJ, Ashman A (1987) Polymer 28:639
56. Finkelmann H (1984) Adv Polym Sci 60/61:99
57. Zentel R (1989) Angew Chem Adv Mater 101:1437
58. Barclay GG, Ober CK (1993) Prog Polym Sci 18:899
59. De Gennes PG (1979) Scaling concepts in polymer physics. Cornell University Press, Ithaca
60. Stauffer D, Aharony A (1992) Introduction to percolation theory, 2nd edn. Taylor & Francis, London
61. Castillo HE, Goldbart PM (1998) Phys Rev E 58:R24
62. Rubinstein M, Colby RH (2005) Polymer physics. Oxford University Press, Oxford
63. Ferry JD (1980) Viscoelastic properties of polymers. Wiley, New York
64. Verwey GC, Warner M, Terentjev EM (1996) J Phys II 6:1273
65. Abramchuk SS, Khokhlov AR (1987) Dokl Akad Nauk SSSR (Dokl Phys Chem) 297:385
66. Finkelmann H, Greve A, Warner M (2001) Eur J Phys E 5:281–293
67. Clarke SM, Tajbakhsh AR, Terentjev EM, Warner M (2001) Phys Rev Lett 86:4044
68. Wermter H, Finkelmann H (2001) e-Polymers 13:1
69. Gleim W, Finkelmann H (1987) Makromol Chem 188:1489
70. Greve A, Finkelmann H (2001) Macromol Chem Phys 202:2926
71. Kupfer J, Finkelmann H (1991) Makromol Chem Rapid Commun 12:717
72. Kupfer J, Finkelmann H (1994) Macromol Chem Phys 195:1353
73. Lacey D, Beattie HN, Mitchell GR, Pople JA (1998) J Mater Chem 8:53
74. Rogez D, Brömmel F, Finkelmann H, Martinoty P (2010) In: Abstracts of the 23rd international liquid crystal conference, Krakow, Poland, 11–16 July, p 323
75. Bladon P, Terentjev EM, Warner M (1993) Phys Rev E 47:R3838
76. Brand HR, Pleiner H, Martinoty P (2006) Soft Mater 2:182
77. De Gennes PG (1980) In: Helfrich W, Heppke G (eds) Liquid crystals of one- and two-dimensional order. Springer, New York, p 231
78. Kundler I, Finkelmann H (1998) Macromol Chem Phys 199:677
79. Golubovich L, Lubensky TC (1989) Phys Rev Lett 63:1082 (1989)
80. Warner M, Bladon P, Terentjev EM (1994) J Phys II 4:93
81. Biggins JS, Terentjev EM, Warner M (2008) Phys Rev E 78:041704
82. Petelin A, Čopič M (2009) Phys Rev Lett 103:077801
83. Menzel AM, Pleiner H, Brand HR (2009) Eur Phys J 30:371
84. Chaikin PM, Lubensky TC (1995) Principles of condensed matter physics. Cambridge University Press, Cambridge

85. Cordoyiannis G, Lebar A, Zalar V, Zumer S, Finkelmann H, Kutnjak Z (2007) Phys Rev Lett 99:197801
86. Kaufhold W, Finkelmann H, Brand HR (1991) Makromol Chem 192:2555
87. Disch S, Schmidt C, Finkelmann H (1994) Macromol Rapid Commun 15:303
88. Selinger JV, Jeon HG, Ratna BR (2002) Phys Rev Lett 89:225701
89. Lebar A, Kutnjak Z, Zumer S, Finkelmann H, Sanchez-Ferrer A, Zalar B (2005) Phys Rev Lett 94:197801
90. Cordoyiannis G, Lebar A, Rozic B, Zalar V, Kutnjak Z, Zumer S, Brommel F, Krause S, Finkelmann H (2009) Macromolecules 42:2069
91. Landau LD, Lifschitz EM, Pitaevskii LP (1980) Statistical physics. Pergamon, New York
92. Verwey GC, Warner M (1997) Macromolecules 30:4196
93. Petridis L, Terentjev EM (2006) Phys Rev E 74:051707
94. Lebar A et al. (2011) In: De Jeu WH (ed) Liquid crystal elastomers: materials and applications. Adv Polym Sci. Springer, Heidelberg, Berlin. doi: 10.1007/12_2010_103
95. Landau D (1937) Phys Z Sowjet 11:545
96. Peierls RE (1934) Helv Phys Acta 7(Suppl II):81
97. De Gennes PG, Prost J (1993) The physics of liquid crystals. Clarendon, Oxford
98. Caillé A (1972) C R Acad Sci B 247:891
99. Gunther L, Imry Y, Lajzerowicz J (1980) Phys Rev A 22:1733
100. Als-Nielsen J, Litster JD, Birgeneau RJ, Kaplan M, Safinya CR, Lindegaard-Andersen A, Mathiesen S (1980) Phys Rev B 22:312
101. Zisman AN, Nikiforov DV, Ostrovskii BI, Terentjev EM (1987) JETP Lett 45:238
102. Kaganer VM, Ostrovskii BI, de Jeu WH (1991) Phys Rev A 44:8158
103. Safinya CR, Roux D, Smith GS, Sinha SK, Dimon P, Clark NA, Bellocq AM (1986) Phys Rev 57:2718
104. Roux D, Safinya CR (1988) J Phys (France) 49:307
105. Wack DC, Webb WW (1989) Phys Rev A 40:1627
106. Nachaliel E, Keller EN, Davidov D, Boeffel C (1991) Phys Rev A 43:2897
107. Štěpánek P, Nallet F, Diat O, Almdal K, Panine P (2002) Macromol 35:7287
108. Dutta P, Sinha SK (1981) Phys Rev Lett 47:50
109. Blatter G, Feigelman MV, Geshkenbein VB, Larkin AI, Vinokur VM (1994) Rev Mod Phys 66:1125
110. Fisher DS, Fisher MPA, Huse DA (1991) Phys Rev B 43:130
111. Birgeneau RJ (1998) J Magn Magn Mater 177:1
112. Chan M, Mulders N, Reppy J (1996) Phys Today 49:30
113. Bellini T, Radzihovsky L, Toner J, Clark NA (2001) Science 294:1074
114. Leheny RL, Park S, Birgeneau RJ, Gallani JL, Garland CW, Iannacchione GS (2003) Phys Rev E 67:011708
115. Radzihovsky L, Toner J (1997) Phys Rev Lett 79:4214
116. Radzihovsky L, Toner J (1999) Phys Rev B 60:206
117. Park S, Leheny RL, Birgeneau RJ, Gallani JL, Garland CW, Iannacchione GS (2002) Phys Rev E 65:050703
118. Kutnjak Z, Kralj S, Lahajnar G, Zumer S (2003) Phys Rev E 68:021705
119. Liang D, Leheny RL (2007) Phys Rev E 75:31705
120. Clark NA, Bellini T, Malzbender RM, Thomas BN, Rappaport AG, Muzny CD, Schaefer DW, Hrubesh L (1993) Phys Rev Lett 71:3505
121. Krivoglaz M (1996) X-ray and neutron diffraction in non-ideal crystals. Springer, Berlin
122. Larkin AI (1970) Sov Phys JETP 31:784
123. Giamarchi T, LeDoussal P (1995) Phys Rev B 52:1242
124. Clegg PS, Birgeneau RJ, Park S, Garland CW, Iannacchione GS, Leheny RL, Neubert ME (2003) Phys Rev E 68:032706
125. Larochelle S, Ramazanoglu M, Birgeneau RJ (2006) Phys Rev E 73:060702
126. Ramazanoglu M, Larochelle S, Garland CW, Birgeneau RJ (2008) Phys Rev E 77:031702

127. Lambreva DM, Ostrovskii BI, Finkelmann H, de Jeu WH (2004) Phys Rev Lett 93:185702
128. Terentjev EM, Warner M, Lubensky TC (1995) Europhys Lett 30:343
129. Osborne MJ, Terentjev EM (2000) Phys Rev E 62:5101
130. Olmsted PD, Terentjev EM (1996) Phys Rev E 53:2444
131. Terentjev EM (1997) Macromol Symp 117:79
132. Witkowski LT, Terentjev EM (2009) Phys Rev E 80:051701
133. Fera A, Dolbnya IP, Optiz R, Ostrovskii BI, de Jeu WH (2001) Phys Rev E 63:020601
134. De Jeu WH, Ostrovskii BI, Shalaginov AN (2003) Rev Mod Phys 75:181–235
135. De Jeu WH, Komp A, Obraztsov EP, Ostrovskii BI, Finkelmann H (2009) Soft Matter 5:4922
136. Nishikawa E, Finkelmann H (1997) Macromol Chem Phys 198:2531–2549
137. Nishikawa E, Finkelmann H, Brand HR (1997) Macromol Rapid Commun 18:65–71
138. Wong GCL, de Jeu WH, Shao H, Liang KS, Zentel R (1997) Nature 389:576
139. Reibel J, Brehmer M, Zentel R, Decher G (1995) Adv Mater 7:849
140. Brodowsky HM, Boehnke U-C, Kremer F (1999) Langmuir 15:274
141. Stannarius R, Köhler R, Dietrich U, Lösche M, Tolksdorf C, Zentel R (2002) Phys Rev E 65:041707
142. Stannarius R, Aksenov V, Bläsing J, Krost A, Rössle M, Zentel R (2006) Phys Chem Chem Phys 8:2293
143. Stannarius R, Köhler R, Rössle M, Zentel R (2004) Liq Cryst 31:895
144. Aksenov V, Bläsing J, Stannarius R, Rössle M, Zentel R (2005) Liq Cryst 32:805
145. Schüring H, Stannarius R, Tolksdorf C, Zentel R (2001) Macromolecules 34:3962
146. Stannarius R, Schüring H, Tolksdorf C, Zentel R (2001) Mol Cryst Liq Cryst 364:305
147. Adams JM, Warner M (2005) Phys Rev E 71:021708
148. Nishikawa E, Finkelmann H (1999) Macromol Chem Phys 200:312
149. Clark NA, Meyer RB (1973) Appl Phys Lett 22:493
150. Bouchaud J-P (2008) In: Radons G, Sokolov IM, Klages R (eds) Anomalous transport: foundations and applications. Wiley, New York, p 327
151. Falus P, Borthwick MA, Narayanan S, Sandy AR, Mochrie SGJ (2006) Phys Rev Lett 97:066102
152. Warren BE, Averbach BL (1950) J Appl Phys 21:595
153. Williamson GK, Hall WH (1953) Acta Metall 1:22
154. Kaganer VM, Brandt O, Trampert A, Ploog KH (2005) Phys Rev B 72:045423
155. De Jeu WH, Obraztsov EP, Ostrovskii BI, Ren W, McMullan PJ, Griffin AC, Sánchez-Ferrer A, Finkelmann H (2007) Eur Phys J E 24:399
156. Langfort JI, Louer D, Scardi P (2000) J Appl Crystallogr 33:964
157. Li MH, Brulet A, Cotton JP, Davidson P, Strazielle C, Keller PJ (1994) J Phys II 4:1843
158. Vix A, Stocker W, Stamm M, Wilbert G, Zentel R, Rabe JP (1998) Macromolecules 31:9154
159. Komp A, Finkelmann H (2007) Macromol Rapid Commun 28:55
160. Ren W, McMullan PJ, Griffin AC (2008) Macromol Chem Phys 209:1896–1899

Adv Polym Sci (2012) 250: 235–236
DOI: 10.1007/12_2011_158

Published online: 23 September 2011

Erratum to: Order and Disorder in Liquid-Crystalline Elastomers

Wim H. de Jeu and Boris I. Ostrovskii

Caption Fig. 1 :
"main-chain (**a**, **b**) and side-chain (**c**, **d**)" should read "side-chain (**a**, **b**) and main-chain (**c**, **d**)"

Section 3.1, last paragraph:
"$c_0 \cong$ 1–4" should read "$c_0 \cong 0.25$".

Section 4.1, paragraph below eq. (6):
["However, for samples in the millimolar range…"]
"millimolar" should read "millimeter".

Section 5.2.3, second last paragraph line 14:
[If the value $\zeta \cong 50$ nm, characteristic of the low temperature state of E70/30, is divided by 3 …]
"divided by 3" should read "divided by $\sqrt{3}$"

The Online version of the original chapter can be found under
DOI 10.1007/12_2010_105

W.H. de Jeu (✉)
DWI at RWTH Aachen University, Forckenbeckstraße 50, D-52056 Aachen, Germany
e-mail: dejeu@dwi.rwth-aachen.de

B.I. Ostrovskii
Institute of Crystallography, Academy of Sciences of Russia, Leninsky prospect 59, 117333, Moscow, Russia

Index